Copyright

by

Jordan Douglas Clark

2013

The Dissertation Committee for Jordan Douglas Clark certifies that this is the approved version of the following dissertation:

Modeling of Transport Processes for the Reduction of Energy Use in Commercial Buildings

Committee:

Atila Novoselac, Supervisor

Richard Corsi

Jeffrey Siegel

Benny Freeman

Jason Woods

Modeling of Transport Processes for the Reduction of Energy Use in Commercial Buildings

by

Jordan Douglas Clark, B.E.; B.A.; M.S.E

Dissertation

Presented to the Faculty of the Graduate School of

The University of Texas at Austin

in Partial Fulfillment

of the Requirements

for the Degree of

Doctor of Philosophy

The University of Texas at Austin

December 2013

Acknowledgements

First I would like to thank my advisor, Dr. Atila Novoselac, for taking me on as a student in 2009 and supporting me throughout my graduate studies. Dr. Novoselac brings unparalleled energy and a wealth of knowledge to the world of building energy modeling and I am grateful to have worked with him.

Along with Dr. Novoselac, I owe a debt of gratitude to Dr. Jason Woods, Dr. Richard Corsi, Dr. Jeffrey Siegel, and Dr. Benny Freeman, for taking time out of their busy schedules to serve on my committee and bestowing upon me a chunk of their massive knowledge through classroom instruction, personal interactions, and review of my work. Other encyclopedic intellects with whom I have had the pleasure of working during my graduate studies include Dr. Neil Crain, who is indispensable to the operation of our research group, and Mr. Eric Kozubal, who is commanding the vanguard in the world of air-conditioning engineering, and was kind enough to let me tag along.

Ms. Dori Eubank and Ms. Kathy Rose have been pillars holding up the infrastructure of our department and research group for many years and have ensured that my graduate career went as smooth as could be hoped for.

Members of my research group and coworkers have provided amusing banter as well as essential advice over the last several years. It was a pleasure and sometimes a riot working with Brandon Boor, Elliot Gall, Priscilla Guerrero, Yirui Liang, Shichao Liu, Liangchung Lo, Luis Rivera and Cristian Wolleter at UT and Lesley Herrmann at NREL.

My wife Stephanie is probably the best hand I've ever been dealt. She brought me popcorn as I was writing this, and she has brought and, for some reason, continues to

bring me literal and figurative popcorn during all of life's crunch times. I owe her a lot of flowers. The only person who might compare is my amazing mother who is singly responsible for the formative portion of my education and continues to provide unwavering support and example.

My education would not have been possible without the generosity of the organizations who funded it. First, the American Society of Heating, Refrigeration and Air-Conditioning Engineers is a wonderful institution that funds world-class research and provides authoritative information which immediately impact the HVAC and refrigeration industries. The THRUST 2000 Foundation, and specifically Raymond Filmore Dawson Endowed Graduate Fellowship in Engineering, has been extremely generous in providing funding to engineering students at UT. The National Science Foundation, through its funding of innovative research, provides an opportunity for exploration of paths which would otherwise be unexplored. I would also like to thank the National Renewable Energy Laboratory and The University of Texas at Austin for partially funding my education and continuing to change the world with their top-notch research.

Modeling of Transport Processes for the Reduction of Energy Use in Commercial Buildings

Jordan Douglas Clark, Ph. D.

The University of Texas at Austin, 2013

Supervisor: Atila Novoselac

Buildings are responsible for over a third of the energy consumption in the United States annually. This energy consumption contributes to some of the most pressing problems facing our society. Modeling of buildings and their systems is an integral part of most strategies for reduction of energy use in buildings. Modeling allows for informed building designs, optimization of systems, and greater market acceptance of new energy-saving technologies. This work addresses two particular modeling applications concerned with reduction of energy usage in buildings: convective heat transfer modeling in perimeter zones, and liquid desiccant dehumidification modeling.

The first objective of this work is concerned with modeling convective transport in buildings and creation of inputs for energy modeling programs and passive pollutant removal calculations. This is accomplished through four investigations. In the first investigation, the influence of floor diffusers on convection heat transfer at perimeter zone windows in commercial buildings is measured. In the second, the impact of blinds on convection under a variety of circumstances is quantified. In the third, movement of air jets issuing from floor diffusers is predicted, and the effect of buoyancy on convective heat transfer at perimeter zone surfaces is analyzed. In the fourth investigation, convective mass transfer at indoor surfaces is investigated. Full scale experiments were conducted in support of these four investigations and semi-empirical correlations

consistent with theory are given to predict jet movement and convective transport under a variety of circumstances.

The second objective of this dissertation is concerned with modeling and analysis of liquid desiccant dehumidification systems and is pursued through three additional investigations. The first is concerned with modeling small-scale transport within the channels of a liquid desiccant absorber and regenerator. Physical and empirical models are developed which agree well with laboratory data. During the second investigation, a dynamic model of a liquid desiccant dehumidification system is developed and integrated into a full-building energy simulation. This is used to assess the potential applicability of the system in supermarkets in various climates. The models developed are used to optimize the system and develop a procedure to size components in the final investigation.

Table of Contents

List of Tables

List of Figures

Chapter 1: Introduction

Buildings are responsible for 41% of source energy consumption in the United States, of which 91% is generated with non-renewable sources (U.S. Department of Energy, 2012). Just under half of this is attributed to commercial buildings (U.S. Department of Energy, 2012). Engineers and researchers seeking to diminish these numbers must approach the problem from several directions, the most promising of which are improvement of building envelope and improvement of heating, ventilation, and air-conditioning (HVAC) systems.

These two approaches are complementary in that by improving the processes which occur at the envelope of a building, HVAC loads are reduced, and by improving HVAC systems, these loads are handled more efficiently. Specifically, improvements in building envelope design and reduction of internal loads have eliminated a large portion of sensible loads in buildings already. Latent loads, however, remain relatively constant. For this reason, improvements in the dehumidification aspect of HVAC systems are needed to offset these latent loads and complement improvements in building envelopes.

Accurate modeling of transport processes, both in the building and in HVAC systems, is an integral part of both these approaches to building energy reduction. This work attempts to move the state of the art of commercial building energy modeling forward through contributions to two subsets of building energy modeling science: indoor convection heat transfer modeling and liquid desiccant dehumidification modeling. The following paragraphs briefly introduce indoor convection modeling and then liquid desiccant systems.

1.1 Indoor Convection Modeling

Predicting heat transfer through building envelopes is an important part of any load calculation or building energy simulation and interior convection modeling is a crucial part of this prediction. Until recently, interior surfaces of perimeter walls of buildings were assumed to interact thermally with interior spaces either via natural convection only [Alamdari, Hammond, & Melo (1984), Khalifa (1989), and Awbi (1998)], or through relatively weak forced convection resulting from centrally located diffusers [Spitler, Pederson, & Fisher (1991), Fisher & Pederson (1997)]. This assumption held in buildings with massive structural walls along their perimeter in which heat transfer through the envelope was very slow. However, modern construction often employs relatively thin glass curtain walls that are heated or cooled with a jet from a nearby diffuser: either a ceiling slot diffuser directly above the wall or a floor register directly below, as in Figure 1.

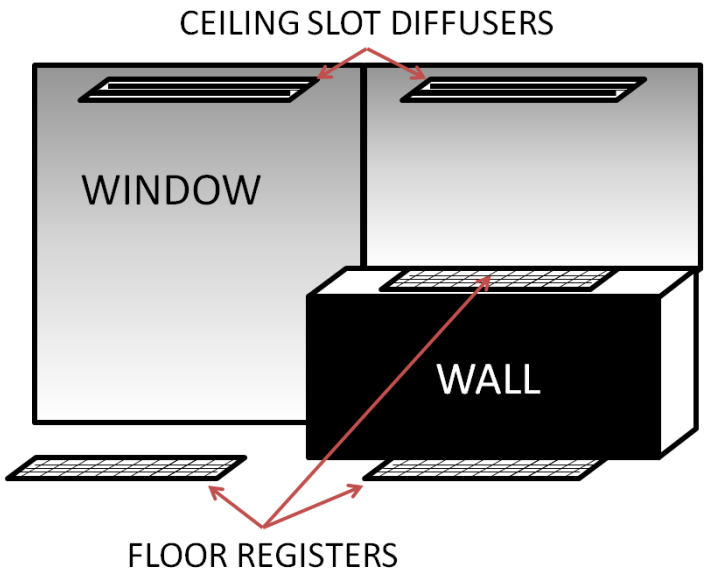

Figure 1. Depiction of diffuser layout in modern buildings with floor-to-ceiling glass windows

For energy modeling and load calculation, this presents a unique challenge in that both buoyancy and momentum forces may influence the movement of this jet, and the subsequent convection heat transfer at the perimeter wall or window. While a great deal of work has been done to understand radiation heat transfer through window assemblies and some work on natural convection heat transfer at interior surfaces of small window assemblies has been conducted, little extant work describes the variety of convection heat transfer processes that occur near walls and windows in sufficient detail. In order to accurately model energy flows in buildings and thus allow for optimization of systems and architectural elements, more work is needed in this area.

Another area in which indoor convection modeling is important is in calculations of pollutant emission and removal at indoor surfaces, either as part of multi-zone pollutant transport simulations, steady-state pollutant concentration calculations, or in design of some low-energy air cleaning strategies. Air quality models are even more sensitive to the accuracy of indoor convection models than are building energy simulations. This is especially the case for mass transfer-limited reactions, such as ozone decomposition at indoor surfaces such as ceiling tiles. Often analogies are used between heat and mass transfer which can leverage work on convection heat transfer modeling to understand mass transfer in indoor spaces.

1.2 LIQUID DESICCANT SYSTEM MODELING

Heat transfer through building envelopes, along with ventilation and infiltration, results in HVAC loads which must be dealt with in an efficient manner. Space cooling, dehumidification, and ventilation in buildings account for 8% of primary energy usage in the United States and over 19% of electricity consumption (U.S. Department of Energy,

2012). This is because the overwhelming majority of air conditioning is provided by electrically driven vapor-compression (VC) systems. These systems cool and dehumidify simultaneously by cooling air beyond its dewpoint in order to condense water out of the air, and then, in many applications, reheat the air to the supply condition.

Liquid desiccant systems have been gaining interest recently as a means of providing dehumidification without using VC overcooling and reheat. Several different types of benefits have been demonstrated. At a basic level, desiccant systems shift energy usage for dehumidification from electricity to cleaner and more efficient thermal sources, and eliminate or reduce the amount of hazardous refrigerants used (Lowenstein, 2008). Liquid desiccants have also been shown to reduce overall energy usage [(Burns, Mitchell, & Beckman, 1985), (Dai, Wang, Zhang, & Yu, 2001), (Bergero & Chiari, 2010), (Kim, Park, & Jeong, 2013), (Kozubal, Woods, Burch, Boranian, & Merrigan, 2011)]; shift load profiles and reduce peak power demand [(Kessling, Laevemann, & Peltzer, 1998), (Kozubal, Woods, Burch, Boranian, & Merrigan, 2011)]; provide more stable and deeper dehumidification of buildings (Lowenstein, 2008); remove pollutants and improve indoor air quality (Chung, Ghosh, Hines, & Novosel, 1993) and provide ancillary savings from things such as reduced energy usage for defrosting display cases in grocery stores.

1.2.1 Overview of Low Flow Liquid Desiccant Systems

Many different types of liquid desiccant systems have been proposed. A review of available technologies is given in Lowenstein (2008). Among these is the low flow liquid desiccant (LFLD) system which is described in detail in Lowenstein, Slayzak, & Kozubal (2006) and Lowenstein (2004). In its most basic form, it consists of a parallel

plate absorber, an interchange heat exchanger to exchange sensible energy between the strong hot desiccant stream and the weak cold one, and a regenerator to remove water from the weak desiccant. A cross section of the LFLD absorber or regenerator (Section A-A) is also depicted in Figure 2. It consists of a set of extruded CPVC plates with internal flutes through which water flows and external surfaces flocked with polyester flocking fibers to distribute the desiccant.

In the low flow system, desiccant and air flow rates are limited in order to prevent any carryover of desiccant droplets into the air stream. This is very undesirable in building applications as the corrosive desiccant (usually a salt solution) can damage ducts and downstream equipment if it is not removed with a high efficiency mist eliminator. This adds fan power costs and requires additional maintenance. Internal cooling or heating which is present in the LFLD absorber and regenerator allows for more efficient operation by counteracting the heat of absorption. The LFLD system is also currently being demonstrated in several retrofit commercial building applications throughout the United States.

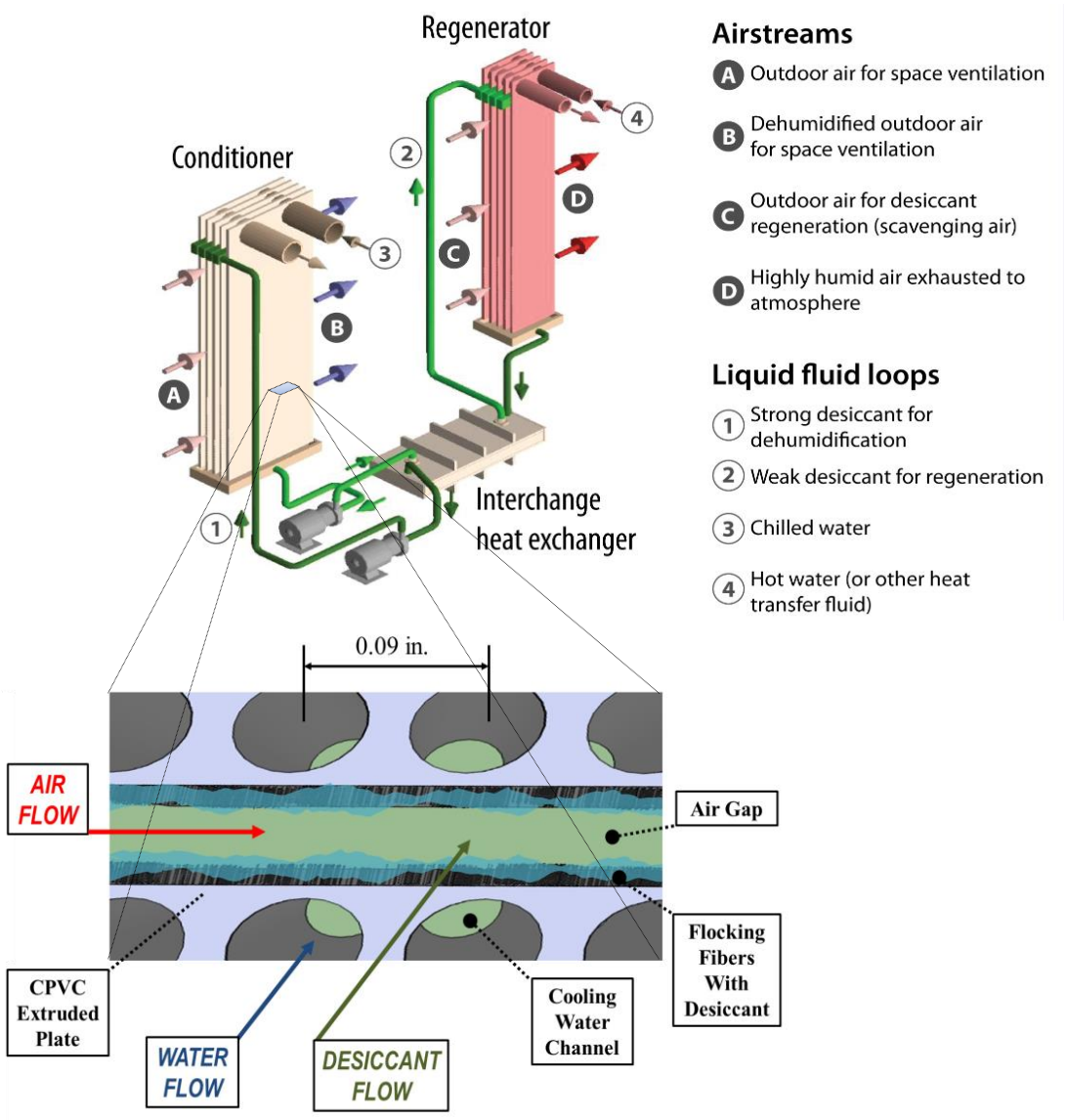

Figure 2. Low flow liquid desiccant system with cross-section of absorber

Many practical questions must be answered in order to design an LFLD system that is acceptable to the commercial buildings market. Modeling the processes within the absorber and regenerator and modeling the dynamic interactions of the different components are the first steps in doing so. This modeling will also allow for an accounting of the potential energy savings of the system in different climates.

1.3 Overview of Dissertation Structure

This dissertation seeks to advance the state of the art in the two sub-disciplines of the building energy modeling field just described. This is done through both experiments and simulations. Seven manuscripts resulted from the work done for this dissertation. These manuscripts are included in the appendices in the back of this dissertation and contain detailed information on the methods employed as well as detailed results. For specific information, the reader should refer to these appendices.

The following sections give an overview of the content in the appendices and highlight the major elements of the work. Section Two presents a detailed review of the state of the art of the two areas of building energy modeling with which this dissertation is concerned, in order to establish the motivation for this work. Section Three describes the major objectives of this dissertation and the investigations conducted in order to achieve them. Section Four gives a brief summary of the methods used in pursuit of these objectives, Section Five describes the major findings of this work, and Section Six concludes this dissertation. Appendices are included at the end.

Chapter 2: Literature Review

The following chapter presents existing research on the areas to be investigated in this work. The state of the art in interior convection modeling is first presented, followed by existing work on modeling liquid desiccant systems. More detailed information on existing research in these areas is available in the manuscripts located in the Appendices at the end of this work.

2.1 Interior Convection Modeling

Various researchers have demonstrated the importance of the model used for convection heat transfer from indoor surfaces on the accuracy of any building energy simulation. Waters (1980) compared existing computer models to actual building performance and found a strong dependence of the accuracy of the model on the indoor convection model used. Similarly, Alamdari, Hammond, & Melo (1984) found that for a certain case study in London, predicted energy consumption varied by as much as 18% depending on the convection coefficient employed. Lomas (1996) simulated a particular building using three different sets of published values for the assumed indoor convection coefficients, h, and found the choice of h to have an effect of as much as 27% on predicted heating demand in the building. Beausoleil-Morrison & Strachan (2001) also demonstrated the profound effect that proper convection modeling can have on building energy simulation.

2.1.1 Natural and Forced Convection Modeling

Different interior flow conditions and different building zones require different interior convection models. Numerous researchers have developed a library of convection coefficients which describe convection heat transfer due to temperature differences in room air [notably Alamdari, Hammond, & Melo (1984), Khalifa (1989), and Awbi & Hatton (1999)]. Awbi & Hatton (2000) also developed correlations for mixed (natural and forced) convection from interior surfaces. Further work has been done on convection resulting from mechanically induced flow fields. Spitler, Pederson, & Fisher (1991) developed convection correlations for situations in which large ventilation rates (>15 air changes per hour (ACH)) were employed. The results of their investigation suggested that at ventilation rates less than 15 ACH, ventilation rate is a more important parameter than either jet momentum or inlet velocity. Additional investigations by Fisher & Pederson (1997) and Goldstein & Novoselac (2010) confirmed that this was the case for all flow rates used in the current investigation (2-12 ACH). All three of these papers found that indoor convection can be modeled as a function of volumetric flow rate raised to an exponent of 0.8 ± 0.2, which corresponds to the exponential dependence expected in a turbulent forced convection situation. Exponential dependences of 0.5, in contrast, suggest laminar forced convection, while correlation with a temperature difference would suggest natural convection.

Fisher & Pederson (1997) extended the work of Spitler, Pederson, & Fisher (1991) into ventilation regimes characterized by ventilation rates below 12 ACH. They calculated convection heat transfer coefficients for various surfaces in an office-size environmental chamber with either a ceiling-mounted radial diffuser or a side-wall inlet.

Their work informed the current investigation in a few ways. First, they confirmed Spitler's assertion that inlet volumetric flow rate was the proper variable with which to correlate heat transfer models for commonly employed ventilation rates and the exponential dependence (0.8) held in lower ventilation rate regimes as well. Secondly, they found that the inlet temperature was the best reference temperature for their correlations.

Goldstein & Novoselac (2010) analyzed forced convection heat transfer along vertical surfaces near ceiling slot diffusers. They found, like previous researchers, that the convection heat transfer coefficient was relatively independent of room-supply air temperature difference and surface-supply temperature difference. They also found that inlet temperature and volumetric flow rate were the proper variables for correlating convection heat transfer results in the configuration studied.

2.1.2 Mixed Convection Modeling

Beausoleil-Morrison (2001) proposed a method for modeling the competing and assisting forces present in mixed convection situations which "blends" the two phenomena: forced and natural convection. This method entailed a generic interpolation between the two phenomena which did not take into account the flow fields responsible for convection. Awbi & Hatton (2000) also analyzed small scale mixed convection phenomena in wall jets in which the local velocity field was known. Kapoor & Jaluria (1993) analyzed buoyant downward-directed jets and their effect on convection. Very little has been done on directly measuring diffuser jets under buoyant conditions and resulting mixed convection.

2.1.3 Modeling the Effect of Blinds

Much effort has also been expended toward the goal of understanding the complex process whereby energy is transferred via natural convection heat transfer at a blind-window assembly. Collins (2004) conducted a numerical study of an isothermal flat plate adjacent to a set of Venetian blinds which were assumed to be irradiated by solar radiation with a constant flux. Shahid & Naylor (2005) numerically analyzed a double-pane window with an adjacent set of Venetian blinds. Many investigations of a sealed window cavity which houses an internal set of Venetian blinds have been conducted (Dalal, Naylor, & Roeleveld, 2009), (Avedissian & Naylor, 2008).

Experimental studies in the same vein have been conducted as well. Machin, Harrison, Naylor, & Oosthuizen (1998) conducted an experimental study of convection heat transfer from a small (0.38m×0.36m) window-blind assembly. Results were reported for one surface-air temperature difference (20°C) and four blind angles: -45°,0°, +45° and -90°. Flow visualization showed a cellular flow field between blinds, of the type expected in an enclosure. Machin, Harrison, Naylor, & Oosthuizen (1998) observed that heat transfer at the window surface in some instances was greater when covered with blinds than the similarity solution for a flat plate without blinds. Collins, Tasnim, & Wright (2008) validated their numerical study with an experimental evaluation of their results. The main limitation of the experimental setup was that it would be most valid for a small window (.2 m × .4 m) which was embedded into a wall cavity.

Recently, Wright, Collins, Kotey, & Barnaby (2009) have attempted to synthesize most of the existing knowledge on radiative and convective heat transfer through fenestration systems into one complete model. The model includes complicated radiative

heat transfer processes through systems several layers thick, and includes multiple surfaces within one system which transfer energy through convection. A full-scale floor-ceiling window, such as is present in much of contemporary commercial construction has not yet been analyzed. Forced convection in window-blind assemblies also has yet to be studied.

2.1.4 Wall Jets

Interior convection in newer buildings is often strongly affected by the behavior of a wall jet. In order to understand convection, proper modeling of this wall jet is often necessary. The following section looks at the current state of wall jet modeling for the different types of jets which may be present, organized by region of the jet.

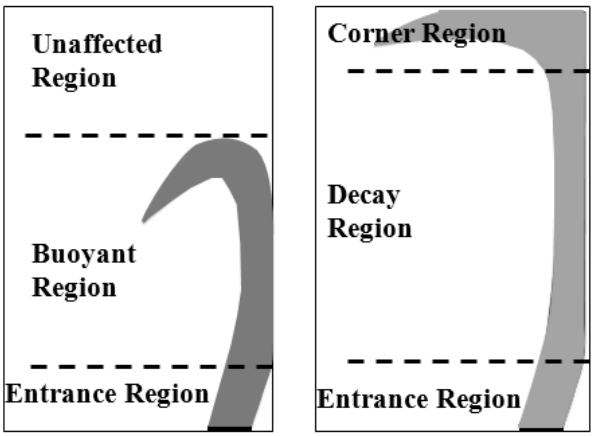

Figure 3. Schematic of (left) buoyant and (right) isothermal wall jets

2.1.4.1 Entrance Region

Both free jets and wall jets contain an entrance region in which the momentum supplied by the HVAC device dominates the flow field and the jet is relatively unaffected by either buoyancy, friction, or entrainment (He, Xu, & Jackson, 2002). It quickly begins

to interact with the quiescent fluid and either creates a fully developed free jet, or attaches to a nearby wall and becomes a fully developed wall jet.

The current investigation is of the offset wall jet, meaning the jet is free for a short period of time before it attaches to the wall. In the region between the diffuser and the wall (see Figure 3) a negative pressure is created by air entrainment into the passing jet. This pulls the jet toward the wall via the phenomenon known as the Coanda effect, until it eventually impinges on and attaches to the wall at some distance away from the diffuser. Nasr & Lai (1998) synthesized the data of many researchers on this phenomena into a best-fits empirical curve which relates the diffuser position relative to the wall (h), the width of the opening, D, and the point of reattachment, X_A. The relationship

Eq. (1) $$X_A/D = 2.632(h/D)^{0.851}$$

is shown to predict the reattachment length well for a variety of different configurations, including the various Reynolds numbers and idealized geometries analyzed in the current experiments, which were similar to those analyzed by Nozaki (1983).

2.1.4.2 Decay Region

Once a wall jet attaches to the wall, its velocity will begin to decay due to friction forces, entrainment of room air, and buoyant forces if they are present. Song, Soon, & Lee (2000) found that after a length of roughly 20 diffuser widths from the floor, the jet profile became similar to a non-offset jet and behaved similarly in the region beyond. When the entering jet is of the same temperature as the quiescent fluid (isothermal wall jet), it is well established (Rajaratnam, 1976) that the maximum velocity decays according to:

Eq. (2)
$$\frac{u_{\max}}{u_{inlet}} = C_1\left[\frac{D}{x + x_0}\right]^{0.5}$$

where u_{max} is the maximum vertical velocity at any horizontal plane in the jet,
u_{inlet} is the average jet velocity at the diffuser (m/s, fpm),
C_1 is an empirical constant, suggested as 2.43 (SI) for linear diffusers (Miller & Comings, 1960)
D is the short dimension of a two-dimensional diffuser (m, ft),
x is the vertical distance along the wall (m, ft), and
x_0 accounts for shape of the jet (m, ft).

This accepted model of isothermal jet decay is used to validate the experimental method used to measure non-isothermal jets in this dissertation.

2.1.4.3 Buoyant Region

The behavior of the decaying jet in the buoyant region is influenced strongly by the relationship between the temperatures of the jet and the quiescent air. The behavior of a buoyant attached plane jet has been studied by various researchers. Most relevant to the current investigation is the work of Goldman & Jaluria (1986) and Kapoor & Jaluria (1993). In the course of these two studies the authors correlated the distance a jet entering quiescent fluid of a different temperature would travel before reversing direction (jet penetration distance, $\delta_{p,}$ in Figure 4) to a convection regime parameter.

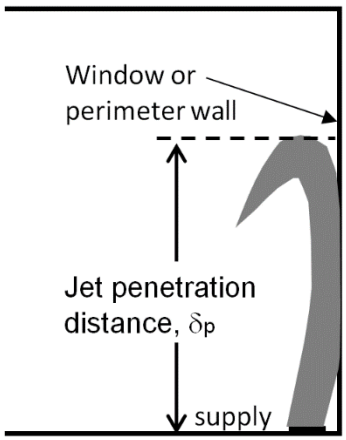

Figure 4. Definition of jet penetration distance

Jet penetration distance depends on the conditions in the room and at the jet inlet, and these research studies found that δ_p correlated well to the mixed convection parameter Gr/Re^2 called the Richardson number, Ri. The relationship is given as:

Eq. (3) $$\frac{\delta_p}{D} = 4.5\,[Ri]^{-0.402}$$

where $Ri = \frac{g\beta\Delta TD}{U^2}$
β is the coefficient of thermal expansion
and U is a reference velocity.

This equation assumes an inlet located immediately adjacent to an adiabatic wall. Furthermore, it assumes the inlet as one solid opening rather than an array of openings, such as in a floor grille. Other researchers such as He, Xu, & Jackson (2002) and Abdulhadi & Pederson (1971) have given slightly different and much more complex correlations, but each fall within 20% of the Goldman & Jaluria (1986) relation.

The velocity of the jet moving in the buoyant region has been mathematically described by Cao, Kurnitski, Ruponen, & Seppanen (2009) by adding the effect of buoyancy to the model for isothermal jet decay (Equation 2). They developed and validated the following equation:

Eq. (4)

$$u_{\max} = C_1 u_{inlet}\left(\frac{D}{x + x_0}\right)^{0.5} + \left(\frac{Kgx\Delta T}{T_{inlet}}\right)^{0.5}$$

where K is an additional empirical constant,
g is the acceleration due to gravity (m/s^2, ft/s^2),
T is temperature (^oC, ^oF), and
$\Delta T = T_{local} - T_{inlet}$.

With the jet penetration distance established according to Equation (3), a velocity profile between the inlet and δ_p can be calculated using Equation (4).

2.1.5 Convective Mass Transfer Modeling for Indoor Surfaces

Transport of species to indoor surfaces is usually given in the form of a space-averaged deposition velocity (Nazaroff, Gadgil, & Weschler, 1993). This model is usually used with a single value of deposition velocity for a single space, which implies either a static value or an appropriate time-averaging, and an insensitivity to various parameters such as type and operation of HVAC system, type of surfaces in the space, space temperatures, etc. Shortcomings of this model include its lack of a clear reference concentration and inability to account for different airflow patterns within a space. Improvements to the model have been proposed by Cano-Ruiz (1993) who among other improvements, suggested decoupling various components of transport by use of a more complex model. One potential challenge with the use of this convention is the identification of a proper driving force for transport between the air adjacent to the surface in question and the air in the bulk space. The classic model for flux across a film (Bird, Stewart, & Lightfoot, 2007) can be employed if the driving force across the film is known. However, in modeling of real spaces, this driving force is rarely known, and the

overall transport is often a function of fluid mechanics which are much more complex than a simple boundary layer.

Several groups have sought to refine the models of mass transfer to indoor surface through various means. Sparks (1991) attempted to give an idea of the magnitude of this influence through use of moth cakes (nearly pure paradichlorobenzene) in a small chamber or a test house and varying flow conditions in the space. The group of Morrison and colleagues has provided methods for determination of more refined models of transport of indoor pollutants. These include gravimetric methods Morrison (2003), which will be employed in the current study. Morrison & Wiseman (2006) used the method they had previously validated to quantify the effect of the temporal averaging of deposition velocities over long time periods during which central HVAC systems were cycling on and off and other perturbations in flow fields such as ceiling fans were running. Still, very little is known on the influence of forced convection on mass transfer from indoor surfaces. This knowledge is critical, as forced convection may be an order of magnitude more effective than natural convection.

Many of the challenges present in indoor-surface mass transfer modeling have also been dealt with by researchers modeling heat transfer at indoor surfaces. Spitler, Pederson, & Fisher (1991) developed convection correlations for situations in which large ventilation rates (>15 Air Changes per Hour (ACH)) were employed. The results of their investigation suggested that at ventilation rates greater than 15ACH, jet momentum and inlet velocity become relatively unimportant compared to ventilation rate. Additional investigations by Fisher & Pederson (1997) and Goldstein & Novoselac (2010) confirmed that this was the case for a variety of lower ventilation rates and geometries,

including all flow rates used in the current investigation. These three papers also concluded that the inlet temperature was the best reference temperature for their correlations. Lastly, they all three found that correlations of the form $h=C*V^{0.8}$ (where h is a transfer coefficient, C is an empirical constant, and V is volumetric flow rate) work in a variety of situations in which forced convection is present.

2.2 LIQUID DESICCANT SYSTEM MODELING

The previous section described the state of the art in modeling processes at building envelopes. Processes which occur within HVAC systems must be properly modeled as well in order to optimize commercial buildings and reduce their energy consumption. One type of system gaining interest for dehumidification of buildings is the liquid desiccant air conditioning system. Many researchers have demonstrated the potential for liquid desiccants to reduce energy consumption in commercial buildings. A great deal of work has been conducted in the modeling of small-scale process occurring within liquid desiccant absorbers and regenerators. Some work has also been done on modeling the interaction between various components of a liquid desiccant system. This work has led to better understanding of the advantages and shortcomings of liquid desiccant systems and means for optimization. The following section reviews the work done in these areas.

For the sake of brevity, the multitude of papers related to modeling well-understood processes inside adiabatic desiccant-air contactors are not reviewed here. Nor are the many papers concerning theoretical treatment of micro-scale transport phenomena in falling films. Nor are the many papers on absorption cooling systems. This work is concerned with modeling internally cooled or heated absorbers and regenerators and their

interaction in a system designed primarily to dehumidify air for building humidity control, and this literature review will be confined to these areas as well.

2.2.1 Advantages of Liquid Desiccant Systems

Many different advantages of liquid desiccant (LD) systems have been demonstrated. First, the most fundamental function of a liquid desiccant system is to shift energy consumption from the electrical input of the compressor in a vapor compression (VC) system to a thermal input in the regenerator of a LD system (Lowenstein, 2008). This allows for the use of waste heat, thermal energy generated on-site, solar thermal energy, etc., in place of electricity. Another advantage over VC systems is that desiccant systems in isolation do not require harmful refrigerants as do vapor compression systems, although they often must be combined with sensible cooling devices which may or may not involve the use of refrigerants. Lastly, because they dehumidify through contact with hygroscopic media rather than overcooling and reheat, desiccant systems can achieve dewpoints below the freezing point of water, which would cause ice build-up in conventional systems (Lowenstein, 2008).

Desiccant systems have also been shown to reduce overall energy usage, especially when combined with VC or indirect or direct evaporative (IE or DE) coolers. Dai, Wang, Zhang, & Yu (2001) showed that a combined VC/LD/DE system could produce a 20-30% reduction in energy usage, as well as a 10% increase in COP, and a smaller overall system. Bergero & Chiari, (2011) showed a 50% reduction in compressor electricity use with a hybrid VC/LD system. Kim, Park, & Jeong (2013) showed a 50% reduction in energy usage for the cooling season in South Korea with an IE/LD system combined with a solar heater for desiccant regeneration and operating in a 100% outdoor

air ventilation mode. Kinsara, Elsayed, & Al-Rabghi (1996) and (1997) showed a COP near that of a VC system for operation at high humidities and 2.5 times that of the VC system for operation at lower humidities. Kozubal, Woods, Burch, Boranian, & Merrigan (2011) showed a 40-80% reduction in yearly source cooling energy for an office building using an IE/LD system.

Desiccant systems have also been put forward as a way of using air-conditioning to help solve the perennial problem of shifting power demand to the times when supply is more plentiful. VC systems require electrical input at the time they are being used. The primary energy use in a desiccant system is heat needed for regeneration. Because heat needed for regeneration can be captured and stored when energy is plentiful or cheap and then used later when dehumidification loads are high, load shifting is possible. Kessling, Laevemann, & Peltzer (1998) demonstrated that even a system with a relatively small amount of desiccant contains substantial potential for storage. Kozubal, Woods, Burch, Boranian, & Merrigan (2011) showed that reduction of peak electricity demands of 80% are possible with an LD/IE system.

Ancillary benefits have also been demonstrated. For example, Chung, Ghosh, Hines, & Novosel (1993) state that contact of process air with salt solution is capable of removing harmful pollutants and improving indoor air quality. In some particular applications, particularly when sensible heat ratios are low, desiccant systems offer great advantages (Lowenstein, 2008). For example, Burns, Mitchell, & Beckman (1985) showed that a hybrid VC/LD systems can reduce air conditioning costs in a supermarket by 60% from the all-VC baseline. This is owed to the low SHR in supermarkets due to the presence of refrigeration equipment, which will be discussed later.

As was shown in previous studies, desiccant systems offer the potential for many advantages in buildings. In order for these to be realized, greater understanding of their operation and optimization of their components must be achieved.

2.2.2 Component Level Modeling

The first step in understanding liquid desiccant systems is the modeling of the small-scale phenomena which occurs within the main components of the system: the absorber (or conditioner) which dehumidifies the air and the regenerator which re-concentrates the desiccant (see Figure 2). The following sections describe the work done in modeling these two components.

2.2.2.1 Absorber Modeling

Numerous researchers have developed mathematical models to predict the performance of desiccant absorbers and regenerators. Packed-bed adiabatic spray-type absorbers have been studied for quite a while and their performance is well understood. More recently, researchers have developed models for internally cooled absorbers or regenerators [(Khan, 1998), (Kessling, Laevemann, & Peltzer, 1998), (Liu, Chang, & Jiang, 2009), (Mesquita, Harrison, & Thomey, 2006), (Park, Howell, Vliet, & Peterson, 1994), (Peng & Howell, 1981), (Pietruschka, Eicker, Huber, & Schumacher, 2006), (Qi, Lu, & Yang, 2013), (Rahamah, Elsayed, & Al-Najem, 1998), (Ren, Tu, & Wang, 2007), (Saman & Alizadeh, 2001), (Scalabrin & Scaltriti, 1988), (Woods & Kozubal, 2013), (Yin Y. , Zhang, Peng, & Li, 2009), (Zhang, Liu, & Jiang, 2012)]. These have been shown to perform better than adiabatic absorbers [(Pietruschka, Eicker, Huber, & Schumacher, 2006), (Liu, Chang, & Jiang, 2009)] or regenerators (Yin Y. , Zhang, Peng,

& Li, 2009). This is due to two differences between adiabatic and internally cooled systems. First, internally cooled systems maintain the desiccant at a lower temperature, which translates to a much lower equilibrium vapor pressure above the desiccant and thus a greater affinity for water absorption. Second, by removing the latent heat of absorption, internally cooled systems reduce the load that a secondary sensible system must meet, often through "free" cooling such as a cooling tower or other direct or indirect evaporative cooling device.

Different means of internal cooling or heating have been studied, including absorbers with integral indirect evaporative coolers [(Pietruschka, Eicker, Huber, & Schumacher, 2006), (Saman & Alizadeh, 2001), (Woods & Kozubal, 2013), (Kozubal, Woods, Burch, Boranian, & Merrigan, 2011)], plate fin tube absorbers [(Khan, 1998) (Park, Howell, Vliet, & Peterson, 1994), (Peng & Howell, 1981), (Mahmoud & Ball, 1992), (Zhang, Liu, & Jiang, 2012)] and internally cooled, falling film, flat plate absorbers [(Peng & Howell, 1981), (Park, Howell, Vliet, & Peterson, 1994), (Liu, Chang, & Jiang, 2009), (Ren, Tu, & Wang, 2007), (Woods & Kozubal, 2013)]. Advantages of IE-integrated systems include free cooling and often the lack of a need for a secondary sensible system such as a VC system. Advantages of an integral coil type system such as a plate fin tube system are lower cooling water temperatures and synergistic benefits from integration with a VC system, such as a simultaneous lowering of the desiccant vapor pressure and sensible cooling.

Assumptions used in the models vary by application but some general trends can be noticed. Nearly all employed assumptions of negligible heat transfer to surroundings, constant physical properties of the fluids, negligible diffusive transport in the direction of

flow, fully developed flow, and negligible shear at the solution-air interface. With a few exceptions, all component-level models are steady state. Diaz (2010) modeled a transient falling film absorber and showed that it reaches a steady condition after 2-3 minutes. This compared well with the experimental work in the same vein (Gandhidasan, Al-Farayedhi, & Antar, 2002). Peng & Pan (2009) modeled transient operation in a packed bed absorber with low flow rates and showed that even under these operating conditions, the system stabilized after five minutes, and most variables were within 10% of their steady state value after three minutes.

Some researchers have employed additional assumptions of constant heat and mass transfer coefficients [(Liu, Chang, & Jiang, 2009), (Ren, Tu, & Wang, 2007), (Scalabrin & Scaltriti, 1988), (Jain, Dhar, & Kaushik, 2000)]. Some make simplifying assumptions such as an isothermal plate [(Mesquita, Harrison, & Thomey, 2006), (Rahamah, Elsayed, & Al-Najem, 1998), (Mahmoud & Ball, 1992)], negligible plate heat transfer resistance [(Pietruschka, Eicker, Huber, & Schumacher, 2006), (Saman & Alizadeh, 2001), (Yin Y. , Zhang, Peng, & Li, 2009)] or negligible desiccant heat transfer resistance [(Rattner, Nagavarapu, Garimella, & Fuller, 2011), (Mesquita, Harrison, & Thomey, 2006)]. Liu, Jiang, & Qu (2007) assumed a constant desiccant concentration in the direction transverse to the direction of flow in a falling film absorber. The validity of these assumptions is usually justified by preliminary calculations and will vary from application to application.

One important assumption made in many models of internally cooled absorbers is the use of an empirical “wetted fraction” to account for uneven desiccant coverage of the surfaces at which mass transfer occurs [(Kessling, Laevemann, & Peltzer, 1998), (Peng

& Howell, 1981), (Pietruschka, Eicker, Huber, & Schumacher, 2006), (Ren, Tu, & Wang, 2007), (Yin Y. , Zhang, Peng, & Li, 2009), (Jain, Dhar, & Kaushik, 2000)]. The selection of the proper wetting fraction is often the goal of the modeling effort and has been shown to significantly affect the results. For example, Katejanekarn & Kumar (2008) showed that varying wetted fraction from 0.25 to 1 resulted in an evaporation rate three times greater. Kessling, Laevemann, & Peltzer (1998) found this to be one of the most important parameters in determining the performance and encouraged further research into improving it. Pietruschka, Eicker, Huber, & Schumacher (2006) suggested a wetted fraction of 0.6 or greater for efficient operation.

Systems modeled in existing literature differ somewhat from the system being modeled in this dissertation and the model created herein must be adjusted accordingly. The absorber modeled in this work includes thin polyester fiber wicking material (called flocking from here forward) attached to the air side of the plates to distribute desiccant more evenly and has been shown qualitatively to distribute desiccant over the entire surface of the plate, possibly preventing the need for an empirical "wetted fraction" parameter. The current system is also designed to operate at very low desiccant flow rates (ratios of air mass flow rate to desiccant mass flow rate of 6-25) and therefore the desiccant properties change more drastically within the absorber and cannot be assumed constant. As material properties for the desiccant being analyzed, a Lithium Chloride-Water solution, are well documented now, variable material properties may be easily included to increase accuracy. Lastly, the presence of the flocking could affect the flow of the desiccant or air.

2.2.2.2 Regenerator Modeling

The regenerator modeled herein as part of system-level optimization is also a parallel plate, internally heated heat-and-mass exchanger, similar to the absorber (see Figure 2). However, mainly because of the presence of greater temperature differences, processes inside the regenerator are more complex and cannot be modeled to the desired level of accuracy with the same approaches used in the absorber. This conclusion was also drawn by Andrusiak, Harrison, & Mesquita (2010) who opted for a purely empirical model of the regenerator, and Jain, Dhar, & Kaushik (2000) who found much better agreement in their absorber model than in that of the absorber. Rattner, Nagavarapu, Garimella, & Fuller (2011) found that air-gap membrane regenerator with similar geometry and temperatures to the regenerator being studied in the current work could not be adequately modeled without the inclusion of complicated radiation heat transfer effects.

2.2.3 Component-Level Variables Affecting Moisture Transfer Performance

The creation of models of LD system components has allowed for analyses of the impact of variables affecting component performance. In general, desiccant systems operate on the principle that lower desiccant temperatures and higher concentrations in the absorber lead to lower outlet humidities [(Yin Y. , Zhang, Wang, & Luo, 2008), (Saman & Alizadeh, 2001), (Katejanekarn & Kumar, 2008), (Rahamah, Elsayed, & Al-Najem, 1998)] and higher regeneration temperatures lead to more concentrated desiccants out of the regenerator, as shown by (Abdel-Salam, Ge, & Simonson, 2013). The following section describes some other general trends witnessed in the parametric analyses of components available in the literature. The effect of most variables is

presented as a moisture transfer effectiveness, which can be thought of as the amount of moisture transferred divided by the maximum amount that could be transferred in an infinitely large component with identical boundary conditions.

2.2.3.1 Air Flow Rate

The variable most often pointed to as having the greatest effect on absorber or absorber performance is the air flow rate. A lower air flow rate increases residence time in the component, while a higher air flow rate may increase transfer coefficients in some cases. Nearly all researchers who explicitly report the relationship between flow rate and report a decrease in moisture removal effectiveness with an increase in flow rate [(Yin Y. , Zhang, Peng, & Li, 2009), (Tu, Ren, Long-Ai, & Shao, 2009), (Liu, Jiang, & Qu, 2007), (Rahamah, Elsayed, & Al-Najem, 1998), (Katejanekarn & Kumar, 2008)]. This same phenomena is often presented in terms of one of several definitions of "number of transfer units" (NTUs), which is inversely proportional to air flow rate. Abdel-Salam, Ge, & Simonson (2013), Ge, Moghaddam, Namvar, Simonson, & Besant (2013) and (Saman & Alizadeh (2001) found removal effectiveness to increase with increased NTU's (number of transfer units, which is inversely proportional to flow rate), implying an inverse relationship between air flow rate and effectiveness. Katejanekarn & Kumar (2008) found that the air flow rate was much less important in the regenerator than in the absorber, likely owing to the fact that the scavenging air is not the fluid of interest in the regenerator and transfer rate was limited by the desiccant rather than the air flow. Saman & Alizadeh (2001) found an absolute maximum efficiency at an intermediate flow rate, but the flow rates they investigated included those high enough to induce a transition to turbulence. For the purposes of the current work, in which low flow conditions are

maintained to prevent desiccant carryover, it is safe to assume that absorber effectiveness will decrease with increased air flow rate and scavenging air flows should be set to the maximum for which entrainment does not occur.

2.2.3.2 Desiccant Flow Rate

Desiccant flow rate was also shown to effect performance of the absorber and regenerator. Katejanekarn & Kumar (2008) showed that varying desiccant flow rate over an order of magnitude in the absorber can increase moisture transfer effectiveness by 12%. Saman & Alizadeh (2001) showed that increasing desiccant flow rate increases effectiveness substantially up to a point, until the internal processes become limited by mass transfer rates and the desiccant can be considered to be at a constant concentration. Katejanekarn & Kumar (2008) also showed that in the regenerator, increasing desiccant flow rate increases the mass flux of moisture but can decrease the overall removal rate, and thus an optimum flow rate exists in this component.

2.2.3.3 Minor Variables

Other variables have been shown to have small or no effects on component moisture transfer performance. Liu, Chang, & Jiang (2009) showed that, as in the case of sensible heat exchangers, a counter-flow LD heat and mass exchanger is more effective than a cross-flow exchanger, which is in turn more effective than a parallel flow exchanger. Rahamah, Elsayed, & Al-Najem (1998) and Saman & Alizadeh (2001) showed that inlet air temperature has little to no effect on transfer effectiveness. Bergero & Chiari (2011) and Rahamah, Elsayed, & Al-Najem (1998) report a significant decrease in transfer effectiveness with an increase in inlet humidity. This is a general trend

observed in the current work as well, owing most likely to the simple need for more mass to be transferred when inlet conditions are more humid. Rattner, Nagavarapu, Garimella, & Fuller (2011) found that the aspect ratio of individual plates in an air-gap membrane regenerator had an insignificant effect on its performance. His setup included only two fluids, though; a separate cooling fluid was not included.

2.2.4 System Level Modeling

While a great deal of work has been conducted to understand the effect of different operating conditions and determine optimal configurations of components, much less has been done to optimize the interactions between components and develop optimal control strategies which take into account these dynamic interactions. Some work has been conducted to model the interaction of the many components of a liquid desiccant system [(Abdel-Salam, Ge, & Simonson, 2013), (Ahmed, Gandhidasan, & Al-Farayedhi, 1997), (Andrusiak, Harrison, & Mesquita, 2010), (Bergero & Chiari, 2010), (Bergero & Chiari, 2011), (Dai, Wang, Zhang, & Yu, 2001), (Katejanekarn & Kumar, 2008), (Kim, Park, & Jeong, 2013), (Kinsara, Elsayed, & Al-Rabghi, 1996) (Kinsara, Al-Rabghi, & Elsayed, 1997), (Tu, Ren, Long-Ai, & Shao, 2009), (Yamaguchi, Jeong, Saito, Miyauchi, & Harada, 2011), (Zhang, Liu, & Jiang, 2012)]. Nearly all of these model the absorber and regenerator as steady-state components and either model all other components as steady state as well, or include storage tanks for various fluids with continuously changing state variables. Nearly all boundary conditions are applied as either single conditions or discretely changing boundaries in a quasi-steady state system.

Types of systems modeled include hybrid vapor systems, including VC/LD systems [(Bergero & Chiari, 2010), (Bergero & Chiari, 2011), (Kinsara, Al-Rabghi, & Elsayed, 1997), (Kinsara, Elsayed, & Al-Rabghi, 1996), (Yamaguchi, Jeong, Saito, Miyauchi, & Harada, 2011)], and DE/LD systems [(Ahmed, Gandhidasan, & Al-Farayedhi, 1997), (Dai, Wang, Zhang, & Yu, 2001), (Kim, Park, & Jeong, 2013), (Tu, Ren, Long-Ai, & Shao, 2009), (Woods & Kozubal, 2013). LD systems have also been modeled to assess the viability of solar regeneration [(Ahmed, Gandhidasan, & Al-Farayedhi, 1997), (Andrusiak, Harrison, & Mesquita, 2010), (Katejanekarn & Kumar, 2008)].

The system models in most of these works were usually developed either to provide a comparison with field testing (Andrusiak, Harrison, & Mesquita, 2010), optimize systems [(Abdel-Salam, Ge, & Simonson, 2013), (Bergero & Chiari, 2010), (Bergero & Chiari, 2011), (Katejanekarn & Kumar, 2008), (Kinsara, Elsayed, & Al-Rabghi, 1996), (Tu, Ren, Long-Ai, & Shao, 2009), (Yamaguchi, Jeong, Saito, Miyauchi, & Harada, 2011)] or to compare the system with an alternative, such as a vapor compression system [(Ahmed, Gandhidasan, & Al-Farayedhi, 1997), (Bergero & Chiari, 2010), (Dai, Wang, Zhang, & Yu, 2001), (Kim, Park, & Jeong, 2013), (Kinsara, Elsayed, & Al-Rabghi, 1996)]. The interesting results of these investigations are reviewed below.

A few interesting interactions of components have been documented. Abdel-Salam, Ge, & Simonson (2013) reports that dehumidification efficiency (performance of the absorber) can be strongly predicted by just the temperature of the desiccant entering the regenerator. This information is used extensively in the current work. He also found that supply air temperature was not strongly affected by regeneration temperature.

Bergero & Chiari (2010) found similarly that supply humidity can be effectively regulated by modulating the flow rate of desiccant in the absorber and regenerator. Kim, Park, & Jeong (2013) found that supply humidity could be controlled by modulating overall desiccant flow rate in the system. Rattner, Nagavarapu, Garimella, & Fuller (2011) found that moisture removal rate increased in the absorber with a decrease in inlet concentration in the regenerator

2.2.5 Energy Efficiency in LD Systems

Component and system-level models have been used to determine the effect of certain variables on LD system energy usage. First and second law analyses have been conducted for this purpose. Energy efficiency of the system has, in general, been shown to increase when latent loads increase. Bergero & Chiari (2011) showed that power savings increase over a VC system with increases in latent loads. Kinsara, Al-Rabghi, & Elsayed (1997) showed a decrease in COP with an increase in sensible heat ratio. Zhang, Liu, & Jiang (2012) and Ahmed, Gandhidasan, & Al-Farayedhi (1997) show a decrease in COP with entering air humidity, but this is not compared with a VC system and for this reason may not be contradictory to the findings of Bergero & Chiari (2011) and Kinsara, Al-Rabghi, & Elsayed (1997).

The effect of other variables on energy efficiency has been investigated as well. Rattner, Nagavarapu, Garimella, & Fuller (2011) found a decrease in system COP with an increase in desiccant concentration into the regenerator and Tu, Ren, Long-Ai, & Shao (2009) corroborated this finding. Tu, Ren, Long-Ai, & Shao (2009) also found an increase in COP with increasing air/desiccant flow rate ratios, and with ambient air

temperature. Bergero & Chiari (2010) found that increasing the size of the regenerator for the same absorber resulted in a greater COP.

Some second law analysis on LD systems has been conducted as well. Tu, Ren, Long-Ai, & Shao (2009) found that 2nd Law efficiency decreased with desiccant temperature into the regenerator, increased with air/desiccant flow rate ratio into both the regenerator and absorber, increased with absorber inlet humidity up to relative humidity of 50%, at which point it leveled off, and was highest when scavenging air temperature was near the temperature of the desiccant in the regenerator. Wang, Li, & Zhao (2010) found that second law efficiency decreased with increasing desiccant temperature.

A few interesting general trends can be pulled from the previous observations. First, as expected, nearly all trends can be attributed to the size of gradients across which heat and mass transfer processes occur. It is well established that entropy generation, and thus loss of efficiency, is proportional to the size of the gradients across which transport occurs, and this is witnessed in nearly all the trends in the results described above. Next, some opportunity for control strategies are suggested by analysis of the trends, including modulation of controllable variables such as desiccant temperature and scavenging air temperature and flow rate.

2.2.6 Liquid Desiccant Systems in Grocery Stores

The ways in which liquid desiccant systems have benefitted offices and other buildings were reviewed above. Supermarkets, however, may offer more applicability for these systems than any other building type. The reason for this is three-fold and is discussed below.

First, energy use in supermarkets is driven primarily by refrigeration and HVAC comprises a significant portion as well. Estimates for the percentage of whole-building energy consumed by refrigeration range from 23% to 50% and by HVAC; 5%-10% [(Kosar & Dumitrescu, 2005), (Spyrou, Shanks, Cook, Pitcher, & Lee, 2013), (Tassou, Ge, Hadawey, & Marriott, 2011)]. HVAC and refrigeration play complementary roles in supermarkets as is discussed further below.

The second way in which supermarkets differ from other building types is that supermarket space and supply conditions are different from an office building or other retail building, mainly due to the presence of large quantities of refrigeration equipment in the space. Refrigerators and freezers are strong heat sinks and provide the majority of the sensible cooling in supermarkets during the cooling season (Munters, 2005) while adding heating loads in the heating season. This causes desirable supply conditions to be much warmer than in other building types and reduces the sensible heat ratio.

Recommendations exist for keeping space conditions at dry bulb temperatures comparable to offices or other building types [75°F (Munters, 2005), 66-77°F (Spyrou, Shanks, Cook, Pitcher, & Lee, 2013), Point P in Figure 5] but somewhat drier. However, in reality building owners will not provide reheat required to maintain space conditions at this point during the cooling season, and spaces are much cooler (Point C in Figure 5). Because of the low sensible loads and low sensible heat ratio (depicted in lines J-C and L-P in Figure 5), space are colder in area with refrigerators and comfort is sacrificed.

Besides differing sensible conditions, drier conditions are more desirable in supermarkets than in other building types as well, especially in zones with freezers or refrigeration equipment. Munters (2005) recommends a 53°F dewpoint in the space and a

45-50°F supply dewpoint to maintain drier conditions. ASHRAE recommends a space condition less than 55% RH for proper refrigerated display case operation. This is due to the fact that refrigerator compressors work more efficiently in drier conditions and the need for heating energy for defrost and defogging of display cases is reduced. Numerous researchers have found a 3-21% reduction in compressor energy use with a 20% RH reduction in the; a 4-6% reduction in defrost energy and a 15-25% reduction in anti-sweat energy space [(Farmarzi, Sweetser, & Henninger, 2000) (Howell & Adams, 1991) (Henderson & Khattar, 1999) (Kosar & Dumitrescu, 2005)].

Because of these facets of supermarket operation, desiccant dehumidification is particularly well-suited for this application. Desiccant system operation and supermarket building operation are complementary in many ways, as shown in Figure 5. A typical vapor compression system process for an office is shown process A-B-C in Figure 5. A-B is accomplished by contact with cooling coils operating well below the dewpoint of the air. B-C is accomplished partially with free (Green) reheat from condenser coils and partially with a secondary device. Larger sensible heat ratios in offices lead to a space line similar to C-D. Red lines depict active processes which must be paid for directly, while green lines depict passive process. For a supermarket cooled and dehumidified by a vapor compression, a similar process occurs (A-Q-J in the system, J-C in the space). However, for this process, the deeper dehumidification consumes much more energy and the space condition met without additional reheat is colder than recommended.

Adiabatic desiccant processes must involve pre-cooling and multi-stage operation in order to meet the desired humidity levels when outdoor enthalpy levels are high (depicted as process A-E-F-G-H-L in Figure 5). Internally-cooled desiccant processes,

however, are great candidates for control of supermarkets as the passive process in an internally cooled desiccant absorber (A-K) is capable of bringing air very near to the desired supply condition (L), which in turn allows for a more comfortable space condition (point P).

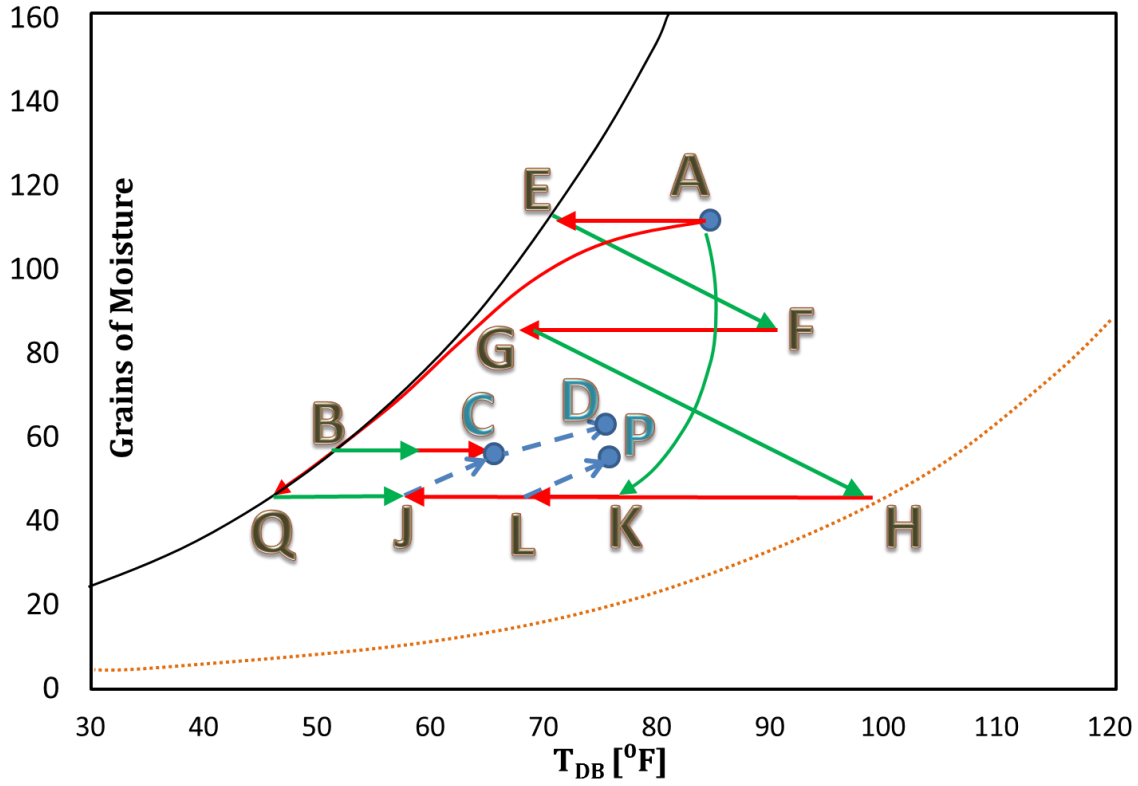

Figure 5. System and space processes in vapor compression and desiccant systems depicted in a psychrometric chart

For the reasons discussed above, desiccant systems have been shown to reduce energy use significantly in supermarkets. Lazzarin (2006) showed a possible 26-63% reduction in source energy use for a hybrid VC/LD system over a VC system for a single day in July. Burns showed a 50-70% reduction in air conditioning energy for a hybrid solid desiccant/VC/solar-regenerator system. Capazzoli (2006) showed an 11-17%

yearly electricity reduction and a 5-13% reduction in operating costs attributed to AC for 3 sites in Italy over the course of a year. To the authors' knowledge, however, savings possible with an internally cooled, low-flow liquid desiccant system have not been quantified. Furthermore, interaction of the many systems within a grocery store with the desiccant system has not been conducted to any level of detail. This work seeks to fill that gap.

Chapter 3: Specific Research Objectives

Chapter two identified a few areas in the modeling of transport processes in commercial buildings which may be improved with additional research. It also pointed to a few areas of this subject which may be exploited to understand how best to reduce energy used in the air conditioning of commercial buildings. For these reasons, this dissertation pursues two primary research objectives through the course of 7 supporting investigations. These objectives and their corresponding investigations are described below.

3.1 Research Objectives and Supporting Investigations

1) Improve the accuracy of existing models of convective transport in commercial buildings through measurements of convective heat transfer in perimeter zones under a variety of conditions and convective mass transfer at ceiling tiles. Objective 1 was fulfilled through three investigations and extended with an ancillary investigation:

    1a. This investigation quantified convective heat transfer occurring in perimeter zones of commercial buildings when a floor register is present near an external wall or window. This is accomplished through full scale experiments. Convection was expected to correlate to supply flow rate and have an exponential dependence on flow rate suggesting forced convection. These measurements were used to develop models consistent with existing theory which can be used to predict perimeter heat transfer under a variety of flow rates and thermal conditions.

1b. The second investigation measured convective heat transfer along perimeter zone windows with blinds which are cooled or heated by jets from a ceiling slot diffuser or floor register. The experiments done in this investigation were done in collaboration with another University of Texas student, Kate Goldstein, and a visiting researcher, Leen Peeters. Qualitative understanding of the effect of several variables on heat transfer was gained. Correlations were developed which more accurately predict heat transfer along windows with blinds.

1c. The final investigation for Objective 1 measured the movement of buoyant jets issuing from floor registers in order to more accurately map jets entering perimeter zone spaces and refine heat transfer models developed in Investigation 1a. The effect of buoyancy was expected to be significant when weak jets enter spaces of a much different temperature, and the effect of buoyancy on convection in these situations was expected to explain discrepancies seen in Investigation 1a and convective heat transfer research done by others.

1d. This ancillary investigation measured convective mass transfer in commercial building spaces and uses the method of developing correlations for heat transfer used in Investigations 1a-c to more accurately model mass transfer in commercial spaces as well. Convective mass transfer is expected to be analogous to heat transfer and allow for similar modeling techniques.

2) Develop a method for modeling transport processes in low flow liquid desiccant air conditioning systems. Then use this process to analyze, design, and optimize these systems and quantify energy savings which can be achieved with their implementation in commercial buildings. This objective was fulfilled through 3 investigations:

   2a. The first investigation for Objective 2 identified a process for modeling the small-scale heat and mass transfer processes which occur within the channels of an internally cooled low flow liquid desiccant flat plate absorber. A purely physical model of the absorber and an empirical model of the regenerator were developed.

   2b. The second investigation integrated the models developed in Investigation 2a into a model of the entire liquid desiccant system which was coupled with a building energy simulation of a typical supermarket. This model was used to quantify the potential cost effectiveness and energy savings of LFLD retrofits in supermarkets across America. A detailed error analysis was conducted to improve confidence in these results. Operation of the building software used to quantify savings was done by Lesley Herrmann, an employee at the National Renewable Energy Laboratory (NREL), and modeling assumptions were decided upon in collaboration with NREL employees Michael Deru, Ian Doebber, and Lesley Herrmann.

   2c. The models developed in Investigations 2a and 2b were used to develop procedures for sizing liquid desiccant systems and components and optimize component performance. It was expected that component sizing

and optimization will differ greatly from sensible heat exchanger methods, such as NTU-effectiveness, owing to material limitations, mass transfer, and the addition of a third fluid stream.

The models developed in these investigations contribute to the reduction of energy usage in commercial buildings in two distinct but complementary ways. Interior convection models are developed which have been integrated into widely available energy simulation and load calculation programs. These allow for more accurate whole-building energy simulations and load calculations. These can be used to better understand the interaction of the multitude of processes which occur within commercial buildings, and to optimize the buildings as a whole. Liquid desiccant models contribute directly to more efficient operation and design of internally cooled low flow liquid desiccant systems. Building simulations provide justification for liquid desiccant system retrofits which can lead to large HVAC energy savings in supermarkets across the country. Final and complete results of the seven investigations are presented in seven manuscripts which are included in Appendices A-G.

3.2 CORRESPONDENCE BETWEEN OBJECTIVES AND APPENDICES

Objective 1 is fulfilled with information contained in: Appendix A: "Experiment-Based Convection Heat Transfer Correlations near Floor Registers (RP-1416)", which has been accepted by *HVAC&R Research*; Appendix B: "Experimental Study of Convective Heat Transfer from Windows with Venetian Blinds", which is published in *Building and Environment*; and Appendix C: "Flow and Mixed Convection Heat Transfer in Buoyant Jets from Floor Registers", published in *Energy and Buildings*; and extended

by Appendix D: “Modeling the Effect of HVAC Operation on Transport of Gaseous Species to Indoor Surfaces” presented at the ASHRAE 2013 Annual Conference. Objective 2 is fulfilled with the information presented in Appendix E: “Validated Modeling of an Internally Cooled/Heated Low-Flow Liquid Desiccant Absorber and Regenerator for Building Dehumidification”; Appendix F: “Detailed Assessment of the Energy- and Cost-Effectiveness of Low-Flow Liquid Desiccant System Retrofits in Supermarkets in the United States ”; and Appendix G: “The Effects of Component-Level and System-Level Variables on the Operation and Performance of Low Flow Liquid Desiccant Systems”. All three papers in support of Objective 2 are under review at the time of writing.

Chapter 4: Methodology

This section describes the methods used in the investigations reported in this dissertation. The environmental chambers used for Investigations 1a-1d are first described, followed by the methods used in these investigations. Next, the modeling assumptions and methods used in the remaining three Investigations (2a-2c) are described.

4.1 EXPERIMENTAL METHODS

The basic research tools for the first four Investigations were experiments in a full scale test room. The experiments were conducted in the Center for Energy and Environmental Resources (CEER) at the University of Texas at Austin. This section provides a description of the experimental setup used, the methods employed in the experiments, methods and assumptions made in calculation of radiative and convective transport, and the method used for the formulation of the experimental results.

4.1.1 Test Room Set-up

Experiments for Investigations 1a-1d were conducted in a large, full scale test room/environmental chamber at the CEER. The environmental chamber has interior dimensions of 4.5 m× 5.5 m × 2.7 m high. For experiments analyzing forced convection from surfaces near a ceiling slot diffuser, a 0.3 m deep suspended ceiling was built into the chamber. The ceiling was sealed on its bottom surface to prevent air infiltration between the space proper and the plenum above the ceiling. The suspended ceiling housed an insulated flexible duct along its length leading to two diffuser boxes and two

ceiling double-slot diffusers, 1.2 m long each, spaced 0.5 m apart (Figure 6). For floor register experiments, the suspended ceiling was removed, and instead, the duct was placed in a 0.3m high raised floor. The plenum beneath the floor was sealed and the duct attached to diffuser boxes were fitted with two standard, 1.2 m long grille registers with 0° pitch.

The chamber itself has a dedicated and modifiable control system capable of supplying air between 6 and 50°C. The chamber also contains hydronic cooling coils embedded into one wall capable of simulating a cold surface, such as occurs during the winter in perimeter zones. Thin electrical resistance heaters are placed on walls and floor to simulate internal loads and conduct natural convection investigations.

The chamber walls, floor and ceiling were divided into 14 sections as shown in Figure 6. Short-wave solar radiation transmitted through the window and internal loads such as computers and occupants were also simulated with electrical resistance heaters on the floor and portions of the side walls, respectively. In calculating the radiation heat transfer during the course of the experiments, each section was assumed to be isothermal and the temperature of the surface was given as the average of at least two temperature measurements on the surface.

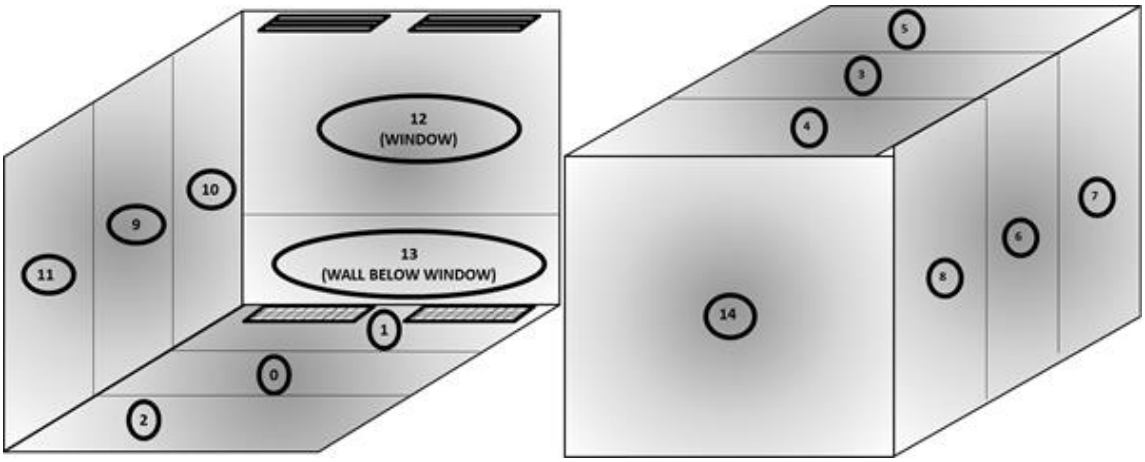

Figure 6. Schematic of chamber characteristic surfaces with wall, window, and diffuser location

One wall of the environmental chamber was designated the "window" of the chamber (See Figure 6) and was heated with thin electrical resistance heaters to simulate a pane of glass absorbing long wave solar radiation. For the winter condition, the window was cooled with hydronic cooling coils to simulate losses to the exterior environment.

For Investigation 1d (measurement of mass transfer coefficients), high sidewall diffuser experiments were conducted in the environmental chamber described above, in order to simulate a geometry in which they would be used. A 0.5m x 4cm (20in x 1.6in) high sidewall diffuser was installed with its horizontal centerline 3 cm (1.2in) below the ceiling, centered on one of the short walls. Fourteen samples were distributed throughout the chamber in a random pattern on each surface: Four were placed on the ceiling; three on the wall housing the diffuser and the one being hit directly by it, two on the floor and two on the other walls. Isothermal conditions were maintained in the chamber at all times and the samples were assumed to be at the temperature of the average of four sensors distributed throughout the chamber.

Radial ceiling diffuser experiments were conducted in a 2.4m (7.9ft) cubic chamber with insulated and sealed walls, but no dedicated temperature control system. Four samples were distributed randomly on the ceiling, two on each of the walls and two on the floor. A 2ft x 2ft (0.6m x 0.6m) 4-way square cone diffuser was installed in a drop ceiling, centered on the ceiling. Isothermal conditions were again maintained and the samples were assumed to be at the temperature of the supply, which was virtually equal to both the room temperature and the temperature of the surroundings.

4.1.2 Instrumentation

During the selection of the measurement instrumentation, focus was placed on increasing the accuracy of instrumentation which measured the variables which had the largest impact on the uncertainty of the results. Table 1 shows the instruments used and accuracy.

Variable	Instrument Used	Accuracy	Comments
Supply and Return Volume Flow Rate	EBTRON GT Type A 116	5% of measured	Verified with duct bluster
Interior Surface Temperature	Omega 44033 thermistors	±0.1°C	Additional uncertainty introduced in averaging and radiation calc.
Supply Temperature	Omega 44033 thermistors	±0.1°C	
Electric Power	Brand Electronic Power Meter	3% of measured	
Exterior Air and Room Surface Temperature	Omega 44033 thermistors	±0.1°C	
Surface Emissivity	Measured by Oak Ridge National Laboratories	Assumed to be exact	Sensitivity analysis shown to negligibly affect final calculation
Conductive Losses through wall	ITI GHT-1C Flux meter	1% of measured	Used for calculation of UA value of chamber
Hydronic Coils Flow Rate	Omega FTB-9500	2% of measured	
Hydronic Coils Temperature	Encapsulated Omega 44033 thermistors	±0.17°C	

Table 1. Instruments Used and Accuracy

4.1.3 Convective Heat Flux Calculation Procedure

The calculation of convective heat flux was accomplished by performing an energy balance at the window or wall surface as described by Equation (5):

Eq. (5) $$\dot{Q}_{gen} + \dot{Q}_{convection} + \dot{Q}_{radiation} = 0$$

where $\dot{Q}_{gen}$ is the energy dissipated by the resistance heaters (W);
$\dot{Q}_{convection}$ is the convective heat flux (W) and
$\dot{Q}_{radiation}$ is the radiative heat flux (W).

Since the heat flux generated at the surface is known from the amount of energy sent to the surface, and the radiation heat transfer is calculated as described below, $\dot{Q}_{convection}$ can be calculated. Once $\dot{Q}_{convection}$ is known, h (convective heat transfer coefficient) is calculated according to Equation 6, given the measured air-surface temperature difference and the area of the surface:

Eq. (6) $$Q_{convection} = A_{surface}\, h\, (T_{surface} - T_{air})$$

where A is the surface area in question (m^2), and
T is temperature (K).

Once several particular values of h are calculated for particular ventilation rates and room-surface temperature differences, they are correlated together into an equation as a function of either temperature difference (natural convection), or flow rate (forced convection). The air temperature, to which Equation (6) refers, changes with the situation being analyzed. In natural convection experiments, it refers to the bulk air temperature. In forced convection experiments, it refers to the inlet temperature at the diffuser. These are the temperatures driving convection heat transfer from the surface.

To properly determine the radiative component of heat transfer from the window surface, view factors between various surfaces were calculated. All view factors used in radiation calculations were calculated with a Monte Carlo simulation created by Dr. Atila Novoselac. View factors between surfaces change with the angle at which blinds are set, and thus a new Monte Carlo simulation was conducted for each blind angle. The geometry of the enclosure, including the blinds, was drawn with AutoCAD for each experiment. This drawing was then imported into Sinda/Fluint RadCAD and a calculation for the view factors between each surface was performed by running a Monte Carlo simulation with two million rays. With this number of rays, an accuracy of 0.5 % was achieved for the view factors. These view factors were then imported into a program developed by the researchers and radiation heat transfer between each surface in the experiment was calculated. Emissivities of surfaces were determined by Oak Ridge National Laboratories. Emissivities used in the radiation calculation were 0.89 for electric heaters, 0.87 for paper, 0.9 for the blinds, 0.84 for tape, and 0.2 for aluminum and stainless steel.

To provide correlations which are readily usable by energy analysts, a few modifications to the traditional form of correlations were made. First, correlations are given which relate heat transfer at a surface to the difference between the surface temperature, and either the bulk room temperature (natural convection) or the supply inlet temperature (forced convection). Secondly, forced convection correlations are given as a function of supply volumetric flow rate. This convention is adopted from Spitler et al. (1991). All heat transfer correlations are given in dimensional form so as not to imply a generality that does not exist and point to their empirical nature.

4.1.4 Jet Measurements

For Investigation 1c, measurements of diffuser jet properties were taken. Penetration distances, defined as the height the jet reaches in the room before reversing direction (see Figure 4), are ascertained via flow visualization using isothermal pulverized chalk dust (Regin S201P Powder "Smoke", 0.7 micron peak particles) inserted horizontally into the diffuser jet. Particle size distribution was established using a TSI 3321 aerodynamic particle sizer and found to be within the size range typically assumed to follow streamlines when placed in moving air (< 1 micron). The penetration distance is established by flow visualization and a tape measure and it is assumed that the recorded distance had a precision of ± 5cm. This penetration distance was then verified by analyzing data on jet velocities taken with omnidirectional hotwire anemometers along the wall and extrapolating to the point where the vertical jet velocity would be zero, corresponding to another estimate of the penetration distance. These two methods were compared and found to be in good agreement, as is shown below in the results section. Local jet velocities are measured with anemometers.

4.1.5 Mass Transfer Measurements

Mass transfer measurements for Investigation 1d were conducted with the naphthalene sublimation technique (Mendes, 1991). All data is analyzed by assuming transport from naphthalene samples to the bulk space. Total mass transfer from the samples was quantified using gravimetric methods. Naphthalene is used as the species of interest in these experiments, owing to its high volatility, and inexpensiveness. Naphthalene plates (9cm x 9cm, 3.5in x 3.5in) are constructed by melting commonly available moth balls (99.9% naphthalene) onto aluminum sheets. These sheets are

weighed, and then affixed to the surface of interest with a Velcro-type adhesive in a controlled environmental chamber. Once a certain amount of time has elapsed (usually 1-3 days), the sample is removed, and weighed again. The difference in mass between the two measurements is the amount of naphthalene that was volatilized during the experiment. This quantity divided by the time elapsed and then by the area of the sample is the mass flux. Samples are left in the chamber under a certain set of circumstances for a minimum of a day each to minimize time-dependent effects and ensure a greater degree of precision. With this convention and the precision of the balance (electric balance with a precision of 0.1g) the measured mass transfer rate had a precision of roughly 1%. Additional error may be present from the spatial averaging convention and the measurement of the surface roughness, described below.

The driving concentration difference also needed to be quantified precisely. Conservative calculations confirmed that the bulk concentration in the room, even under conditions of high mass transfer rates and large amounts of naphthalene present, never reached beyond 1% of the equilibrium concentrations. The supply air was filtered through an activated carbon filter and also had a naphthalene concentration of virtually zero. Therefore, it was assumed that the reference concentration was zero in the space for all situations analyzed. The surface concentration was assumed to be the concentration in equilibrium with the vapor pressure of the solid at the temperature of the solid.

On solidification, the naphthalene samples were observed to form a fuzzy surface, which meant the surface area available for sublimation was not simply the 2-dimensional, or projected, surface area. To quantify the actual available area, three samples were analyzed with a non-contact profilometer. Details of the profilometer can be found in

Yao et al. (2008) . The ratio of the actual surface area to the two-dimensional surface area of each of the three samples was averaged and this ratio was assumed to be the ratio for all samples tested. The standard deviation for the three ratios was less than 6% of the average value, suggesting a fairly consistent surface for various samples.

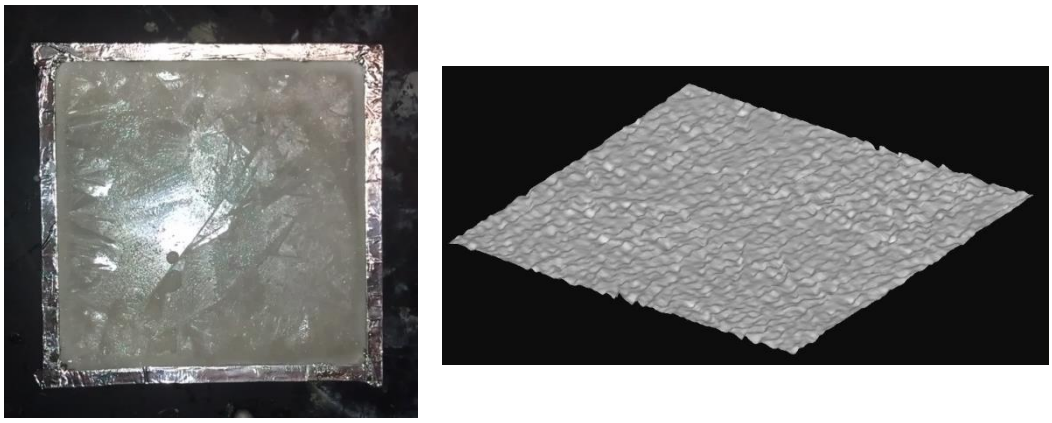

Figure 7. (Left) Photograph of typical naphthalene sample used in all experiments. (Right) Profilometer-generated image of surface roughness of naphthalene sample. Image represents 20mm x 20mm (0.79in x 0.79in) section of surface.

Additional uncertainty in mass transfer rate measurements arises from the spatial averaging process. Often jets only partially covered surfaces and the sample points in the path of the jet were averaged with those not in the path. This introduces additional error but was necessary in order to provide a level of resolution that would be usable in multi-zone transport simulations or other calculations. Also, published diffusion coefficients for naphthalene span a large range and thus this additional uncertainty is present in the final calculations.

4.1.6 Quality Control and Uncertainty Analysis

For experimental investigations (Investigation 1a-1d), measures were taken to minimize error in experimental design, experiment execution, and data processing. The uncertainty in the measured and processed data for all developed correlations was investigated in detail. Also, substantial effort has been dedicated to the design of experimental set-ups to ensure the robustness of the newly developed convection correlations and their applicability to a wide range of possible situations. A set of control measures was introduced to minimize the systematic or specific errors in the correlation development procedure. The following subsections briefly describe these control measures.

Whenever possible, experiments were conducted for situations in which well-established correlations already exist. For this purpose we conducted both heat transfer and mass transfer experiments for the development of correlations for natural convection at vertical surfaces in a confined space. The agreement between experimentally measured coefficients and the previously developed correlation was good, and the details of this test are presented in the appendices.

Bulk room air temperatures within the chamber were maintained at or near the temperature immediately outside the chamber to minimize any conductive losses through the chamber walls. This, combined with maintaining the same pressure in the chamber as in the surrounding environment, provided for very good thermal insulation and air tightness of the chamber and a precise mass and energy balance. Nonetheless, very small losses through the insulated walls were calculated to account for conductive losses. The

energy balance was checked for each experiment. If the balance was satisfied, energy supplied to the chamber would equal energy removed according to:

Eq. (7) $$\dot{Q}_{gen} - \dot{m}c_p(T_{air\ inlet} - T_{air\ outlet}) - \dot{Q}_{conduction\ losses} = X \rightarrow 0$$

where m is the mass flow rate of air (kg/s) and
c_p is the specific heat capacity of air (J/kgK).

The normalized energy balance was calculated by:

Eq. (8) $$Balance = X/\dot{Q}_{internal\ sources}$$

where $Q_{internal\ sources}$ indicates the power released in the chamber by the electrical heaters or absorbed by hydronic cooling panels. In experiments where the difference was greater than 10%, it was determined that the steady state condition in the chamber had not been reached and the experiments were discarded and/or repeated.

With the systematic error minimized as described in the text above, care was taken to precisely evaluate the uncertainty associated with each reported value. Uncertainty is given as a function of the imprecision inherent in all measured variables used to calculate a reported value. With the uncertainty in each measurement calculated, the effect on the final value calculated is determined based on the general uncertainty.

4.2 Modeling Methods and Assumptions

For Investigations 2a-2c, modeling of the low flow liquid desiccant (LFLD) system and its effect on building performance was conducted in three phases: 1) component-level modeling of the heat and mass transfer processes occurring within the absorber and regenerator, using physical and empirical modeling techniques with a solver developed for this purpose; 2) system-level modeling of the dynamic interaction of the various components of the LDAC system (see Figure 8), performed in the Dymola environment, and 3) building-level modeling of a typical grocery store retrofitted with the LDAC system, performed in EnergyPlus. The following briefly describe the modeling approach for each of these phases. For more details on the component- and system-level procedures, refer to the appendices.

4.2.1 Component-level Modeling

The absorber was modeled with a purely physical approach. The following assumptions were used in the physical modeling of the exchangers:

1. Steady state operation is employed nearly uniformly in the modeling of liquid desiccant heat and mass exchangers and is used here as well, as the boundary conditions of a typical system change much more slowly than the internal state variables.
2. A resistance-in-series model was used for modeling heat transfer between the three fluids.
3. Lewis-Whitman two-film theory with a single value for the Henry's constant was used for mass transfer modeling. Actual Henry's constant values vary by ±5% over the range of likely operating conditions and ±9% over the entire

range of conditions that could ever be expected even at extreme operating conditions.

4. Laminar developing flow transfer coefficients for both heat and mass transfer (Bejan, 2004) from the bulk air to the air-desiccant interface, assuming a smooth surface, no shear the interface, and constant temperature within each cell at the interface and no fluid-fluid interaction. A fully developed assumption is often used, but preliminary calculations showed that this assumption added appreciable error in the LFLD model.
5. Developing flow falling film transfer coefficients for mass transfer modeling in the desiccant film, taken from Grossman (1982).
6. Estimations of heat transfer resistance in the desiccant film showed that the heat transfer resistance in the desiccant was less than 1% of the overall resistance and justified neglect of this resistance.
7. The flocking on the plate surface uniformly distributed the desiccant over the plate surface (as was qualitatively verified in the laboratory) but negligibly affected heat and mass transfer within the desiccant layer. Neglecting the effect of the flocking on transport is justified by Lund & Knowles (2001) which shows a less than 5% effect on Nusselt number under the operating conditions of the LFLD system.
8. The desiccant-plate interface was assumed to be impermeable to moisture transfer.

9. Conduction shape factors were used to model thermal conductance between the desiccant-plate interface and the water-plate interface. These were calculated with the correlation given in Ganzevles & Gled (1997).
10. Conduction and diffusion were assumed to occur in one dimension only (perpendicular to the plates) as is uniformly done in absorber modeling, justified by the much quicker rate of advection in this direction than diffusion.
11. Heat transfer coefficients describing heat transfer from the plate-water interface to the bulk water were taken from fully-developed correlations for laminar pipe flow. This resistance was estimated at 2-3% of the overall heat transfer resistance; thus, any error in this assumption should be negligible.
12. All desiccant properties were assumed to be functions of the temperature and concentration in each cell and were taken from Conde (2009) except for enthalpy, which was calculated with a correlation provided by AIL Research, manufacturer of the LFLD system.

Half of a single plate, one desiccant film, and half of the adjacent air gap was modeled. The plate was divided into 8 equally sized elements in each and the mass and energy conservation equations were solved in each element. Increasing grid resolution beyond this point was shown to negligibly affect the results (<1% change in relevant quantities). Residuals were calculated for energy conservation equations on the three fluids and mass conservation on the desiccant and air in each cell. Five corresponding state variables were adjusted at each iteration: three fluid temperatures and desiccant and air concentrations. A Newton solver was used to adjust state variables in each cell until normalized residuals were below 10^{-7}, at which time energy balances were accurate

within 0.015% and mass balances within machine precision. For most inlet conditions, solutions converged in fewer than 10 iterations, which took roughly 2 minutes.

4.2.2 System-level Modeling:

The performance maps of the conditioner and regenerator were then input into a system level model containing all other necessary components using the Dymola environment (see Figure 8). Dymola is a user interface and solver for work done with the Modelica modeling language. Modelica is an object-oriented acausal modeling language created for system modeling (Tiller, 2001). Other components of the LFLD system were either created by the author for the purposes of this study (labeled "JDC" below), taken from the Modelica Standard Library (labeled "MSL"), or taken from the open source Modelica Buildings Library ("MBL") created by the Simulations Research Group at Lawrence Berkeley Laboratory, and have been previously validated. Components were chosen and sized to reflect the components that have been used in field demonstrations of the system and those which will likely be used in future installations. Some components were considered to operate at steady state, given the time scales of the changes in their associated state variables. These include the components developed in Investigation 2a and are labeled (SS) below. Dynamic components are labeled (D).

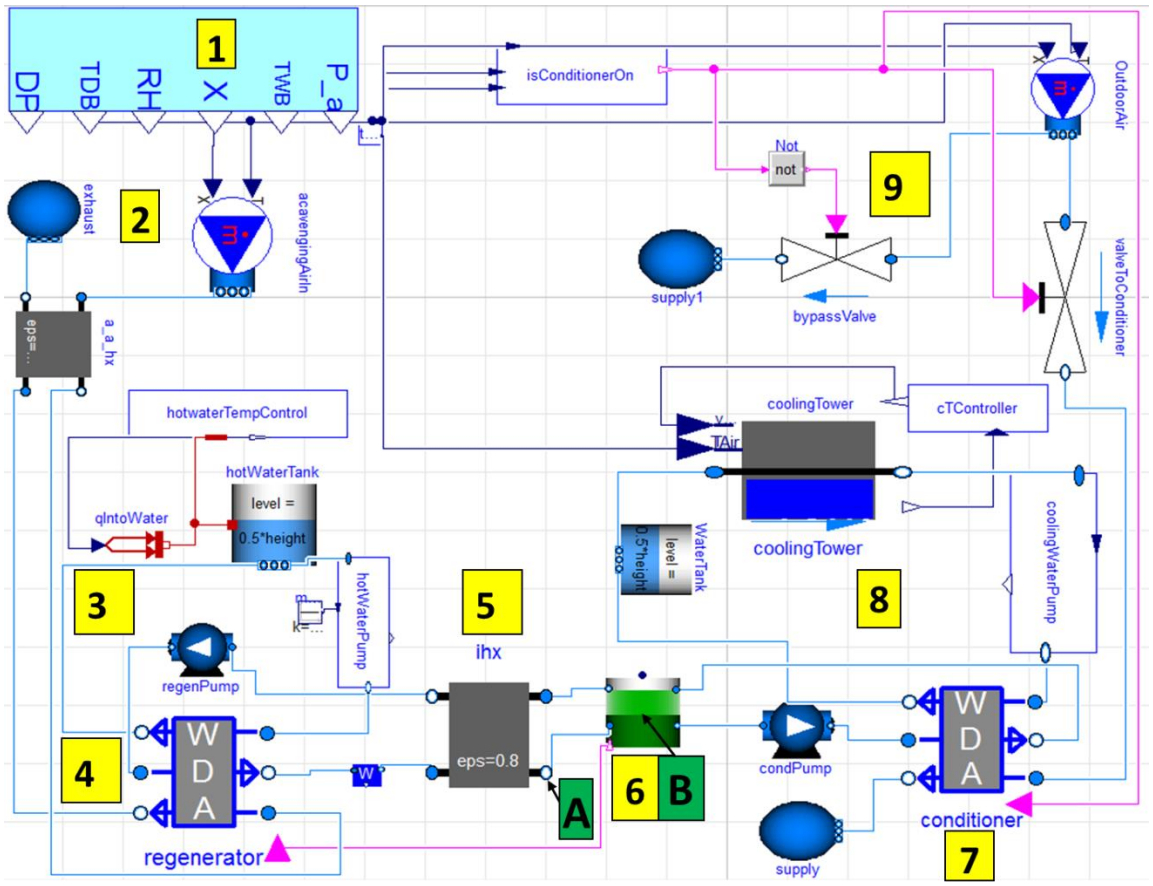

Figure 8. Schematic of LFLD system-level model

A schematic of the system level model is provide in Figure 8, which is a screen shot of the Dymola GUI during the work done for Investigation 2b. Inputs and assumptions for each component of the model are described in the following. The schematic is explained by beginning at the upper left corner and proceeding in a counter-clockwise direction.

1. Starting from the upper left corner of the schematic, Typical Meteorological Year 3 (TMY3, (Wilcox & Marion, 2008)) weather data is represented by the light blue box. TMY3 data is given at hourly intervals and the software interpolates

between these points linearly to give fully dynamic boundary conditions. (JDC) (D)

2. Directly below, a constant flow rate scavenging air input is modeled. The air is pre-heated with an air-to-air heat exchanger with a constant effectiveness of 0.55. This effectiveness was chosen so as to prevent condensation in the heat exchanger at the worst operating conditions. (JDC) (SS)
3. Directly below the air-air heat exchanger is the hot water loop which supplies heating water to the regenerator. This includes a 110kW constant-rate heat input (MBL)(SS), a hot water storage tank (MSL)(D) with a capacity of 0.25 m^3, and a controller (JDC), which maintains the temperature of the hot water between 80°C and 93°C. The boiler efficiency is assumed to be 0.82. The pump (MSL)(SS) is modeled as a constant-flow rate device. The small tank (D) is assumed to insulated well enough to prevent appreciable heat transfer to the environment.
4. The regenerator (JDC)(SS) is shown below which treats the three fluid streams (Water, Desiccant, and Air labeled with letters W, D, and A). Lab data exists from experiments done by other researchers for the regenerator over the entire expected range of operating conditions and an empirical correlation of the lab data was used as an input to the system level model. Firm limits on the inlet variables and operating conditions are placed in the system-level model so as to ensure extrapolation is never done for the empirical model.
5. To the right of the regenerator is an interchange heat exchanger (MBL)(SS), which exchanges sensible heat only between weak and strong desiccant streams with an assumed constant effectiveness of 0.8.

6. To the right of this is a model of a completely stratified small desiccant tank (or sump) (JDC)(D). In this model, the strong (bottom) and weak (top) desiccant regions are completely separate; with the one exception that weak desiccant is allowed to be pulled into the strong tank if the conditioner is running at a higher flow rate than the regenerator. This captures the stratification that occurs in the field due to density differences between weak and strong desiccant. This and the cooling and heating water reservoirs are the only elements whose operation is fully transient. Desiccant concentration and temperatures in the tanks are calculated continuously by application of energy and mass balances on the tank volumes.
7. In the bottom right corner is the absorber (JDC)(SS), also called conditioner or dehumidifier). The absorber used for this work is the parallel-plate low-flow liquid desiccant absorber patented by Lowenstein (2004). Its operation and performance in the laboratory is described in Lowenstein et al. (2006). A first-principles physical model validated with laboratory data is implemented in the current work via polynomial mapping of outlet variables to inlet variables. Air flow rate in the absorber was set to ensure maximum removal. Desiccant and water flow rates in the conditioner are set to the maximum allowable by material limitations.
8. Above the absorber is the cooling water loop. This includes a model of a York cooling tower (MBL)(SS) with a variable speed fan. The cooling tower is sized to provide a 3.9° C approach at design conditions and a 5.6° C range. Cooling tower performance is given by a performance map of the York cooling tower. A

controller (JDC) adjusts fan speed to one of three speeds according to delivered water temperature; natural convection operation of the cooling tower is also modeled when the fan is off. At design conditions, desired water temperature is set to be 3.89° C above the site's design dew point temperature for all sites. The pump (MSL)(D) is modeled as a constant-flow rate device.

9. The upper right corner of the schematic represents the constant supply air flow (MSL)(SS) of the LDAC. Outdoor air is delivered directly to the conditioner when the conditioner is in operation. When the LDAC conditioner is shut off, outdoor air is sent through a bypass valve to either a secondary sensible device or directly to the building (neither of which are modeled as part of this phase).
10. (not shown) A NEW class was implemented for the Lithium Chloride solution used as the liquid desiccant in this system which extends the Partial Medium model included in the Modelica Standard Library. This model implements all properties contained in Conde (2009) with two exceptions: specific heat capacity is modeled as constant value rather than a function of temperature, which results in less than 5% discrepancy at the extremes of the operating range, and density is modeled as a function of concentration only (not temperature) resulting in negligible discrepancy with the Conde (2009) relations. Specific enthalpy is also modeled with correlations developed by AIL Research.

In building simulations (Investigation 2b), the LFLD system was bypassed when the ambient dry-bulb temperature was less than 41°F or relative humidity was less than 15%. The conditioner fan and pump did not operate during this time. The regenerator shut off when desiccant concentration reached 0.42 kg of salt per kg of solution. Control

strategies implemented in the system-level and building-level modeling represent the likely mode of operation, rather than those which create space conditions identical to the baseline model. For this reason, space DB and RH often differ slightly between the baseline and the LDAC models as they would in an actual retrofit situation. In nearly all situations, this leads to a more comfortable situation in the LDAC model, in addition to the energy and cost savings presented below.

4.2.3 Building-level Modeling

For Investigation 2b, Output values for the processed air conditions (dry-bulb and wet-bulb temperatures) of the system-level model were fed into the EnergyPlus building model using the Energy Management System (EMS) by Lesley Hermann, an employee at the National Renewable Energy Laboratory. The processed air temperatures replaced the outdoor air node temperatures for the roof top units (RTUs) serving the produce and the sales zones. The reheat coils and humidistats were removed, as the LDAC provide all of the latent cooling. Modeling assumptions for this phase were determined through a collaboration with NREL employees Lesley Herrmann, Michael Deru, Ian Doebber, and Eric Kozubal.

Six representative cities expected to benefit most from LFLD retrofits were tested: Miami, Houston, Atlanta, Baltimore, Chicago, and Minneapolis. These are all classified as "humid" climates and span the range of yearly dry bulb temperature characteristics in the continental United States.

A representative supermarket retrofitted with an LFLD system addition upstream of the existing VC system was modeled. A variation of the "new construction"

supermarket reference building model for EnergyPlus version 8.0 was used as the starting point for model development. This model was previously created by others based on 2003 Commercial Buildings Energy Consumption Survey (CBECS) data and additional research carried out by the National Renewable Energy Laboratory and Pacific Northwest National Laboratory and serves as an accepted standard building with which to compare new technologies (Deru, et al., 2011); other inputs refer to ASHRAE Standards 90.1and 62.1. The following sections describe the building in more detail.

The supermarket model is a 45,000-ft^2 (4,186-m^2), single story, six-zone building and includes a sales floor (56% of floor area), bakery (5%), deli (5%), produce section (17%), dry storage area (15%), and office space(2%). Envelope construction and fenestration comply with ASHRAE Standard 90.1-2004 for each humid climate subcategory (ASHRAE, 2004). The produce and sales floor include 1,064 linear ft (324 linear m) of refrigerated cases; walk-in freezers are located in the dry storage area. There are a total of four racks, each including four compressors.

In the baseline building model, each zone is equipped with a unitary packaged roof top unit, which includes an electric cooling coil and a gas heating coil. Humidity is controlled by cooling the zone supply air past saturation. Reheat energy is provided by an electric coil also included in the unitary packaged system that serves each zone. Building loads are typical of a building of this end use. Outdoor air flow and exhaust rates were calculated based on ASHRAE 62.1-2007 requirements (ASHRAE, 2007); outdoor air supply and exhaust is operated during occupied hours (06:00 to 22:00). Two zones, the deli and the bakery, have exhaust requirements for cooking equipment. About 70% of the makeup air for the deli and bakery is transferred from the sales zone; the

remainder is brought in through the unitary systems that serve the deli and the bakery. (This makeup air is an addition to the ventilation air provided by the unitary systems.)

Energy and economic assessments of the LDAC were conducted by combining model results with pricing data. Utility tariffs used were based on the average national monthly rates from January 2010 through September 2012 for electricity (EIA 2013a) and from January 2010 through July 2012 for natural gas (EIA 2013b). This strategy rather than referring to last year's average is used to account for price volatility.

4.2.3.1 Uncertainty Analysis for Investigation 2b

Uncertainty is often not quantified for whole-building energy simulations, as the number of inputs is great enough to make this a very difficult task. However, in this study a few inputs were not known very precisely and yet had a disproportionate effect on final outputs and for this reason an attempt was made to bound the uncertainty in the model.

Uncertainty in the model outputs was quantified by perturbing the input values of the five inputs having the greatest effect on model outputs: case runtime fraction (analogous to the size of the refrigeration cases and thus the sensible cooling done by the refrigeration systems); latent heat ratio in three different types of refrigerator cases (relative amount of latent/sensible cooling done by refrigerators); and infiltration rate. These five inputs were perturbed to a best estimate for ± two standard deviations and their individual effect on the output variables quantified. Assumed average values and values at plus and minus two standard deviations for these four quantities are given in Table 2. It was assumed that uncertainty due to other inputs would be dwarfed by the

uncertainty dude to these inputs and thus final uncertainties calculated through standard error propagation on these 5 inputs can be taken as total uncertainty in the model.

Perturbation was done for the climate with the greatest energy savings (the hottest climate) in the baseline model and that with the least energy savings (the coldest climate). It is assumed that uncertainty in the other climates can be interpolated from these, as this was the case for the average values calculated. Ranges given on the output variables in the results section are calculated by standard error propagation analysis on these four variables and should be considered a ±two standard deviation range on the output variables.

Variable	**Low**	**Baseline**	**High**
Case runtime fraction	0.6	0.75	0.9
Latent Heat Ratio			
Open Refrigerator	0.15	0.3	0.33
Freezer w/ Doors	0.05	0.12	0.30
Coffins	0.05	0.1	0.030
Infiltration rate	-50% of baseline		+ 50% of baseline

Table 2. Variables Perturbed to Quantify Uncertainty

Chapter 5: Summary of Research Findings

Chapter 3 laid out the specific research objectives pursued in this work and Chapter 4 explained the methods used to achieve these objectives. This chapter presents the major findings and implications of each investigation, organized by the objective toward which the investigation was aimed. Detailed information on methodology used in the investigations and detailed results may be found in Appendices A-G.

5.1 Objective 1: Improve the Accuracy of Existing Models of Convective Transport in Perimeter zones.

Fulfillment of Objective 1 required three investigations into modeling heat transfer in perimeter zones and one ancillary investigation into modeling mass transfer in commercial buildings. Models of convection heat transfer in perimeter zones of commercial buildings were developed in these investigations as part of this dissertation have been implemented in simulation and load calculation software such as Energy Plus and the ASHRAE Load Toolkit and are currently improving the accuracy of thousands of building design calculations. The following sections highlight the most interesting results of these investigations. More detailed results may be found in Appendices A-D. Methods used to arrive at the results presented in these sections are found in Chapter 4 and in Appendices A-E.

5.1.1 Investigation 1a: Modeling Forced Convection Heat Transfer at Bare Surfaces near Floor Registers

Several goals were accomplished during this investigation. Convection correlations were developed which add refinement and accuracy to load calculations and energy simulations while maintaining consistency with theory. A few general trends can be noticed in the results, which are discussed below. More detailed information is available in Appendix A.

In the first phase of this investigation, the experimental method was validated. Comparison of the natural convection results with previous research and natural convection theory showed a close agreement, thus validating the experimental method used for this dissertation. This method may be used for rapid measurements of convective heat transfer in the future, and does not require detailed measurement of small-scale phenomena, as do other methods used to measure convection.

The next major phase of this investigation involved measuring forced convection heat transfer at perimeter zone windows. One major objective was to relate convection to variables which are known by designers at the beginning phases of a building design, and known by load calculation and energy simulation programs during the course of the simulation. Previous research by others had suggested correlating convection to volumetric flow rate of the supply air yielded repeatable results which could be understood when compared with extant theory.

Specifically, several researchers found an exponential dependence of 0.8 on the flow rate, which agrees with forced convection flat plate theory, as well as forced convection in many other situations. The investigation done as part of this dissertation,

however, suggested a linear dependence on flow rate when a cold jet was issuing from the floor diffusers into relatively warmer room. The linear dependence contrasts with previous work by others that showed indoor convection usually could be modeled as a function of volumetric flow rate to an exponent of 0.8 [(Goldstein & Novoselac, 2010), (Fisher & Pederson, 1997)], and flat plate turbulent convection theory which predicts convection as a function of velocity to a power of 0.8 (Bejan, 2004).

This discrepancy is due to the effects of buoyancy slowing down the jet at lower flow rates in this investigation and thus reducing convection, which is examined further in Investigation 1c. While the phenomenon is not inherently linear, the juxtaposition of buoyancy and momentum effects results in a dependence that seems to be linear. Previous research had investigated convection in buildings due to either much higher flow rates, much stronger jets, or jets whose temperatures were such that any buoyancy forces which were present would act in the same direction as momentum forces. As the lower flow rates at which buoyancy was an issue are not often realized in practice, a correlation with an exponential dependence of 0.8 which only is valid at large flow rates could be used as well as the linear correlation. While correlations developed in this phase of the investigation were repeatable and within the precision usually required for load calculation and energy simulation, the buoyancy issue suggested an interesting path for further research.

Heat transfer from a warm jet issuing from a floor register was also analyzed in this Investigation. Heating condition results are shown to conform better to the exponential dependence on volumetric flow rate (exponent = 0.8) that was found in previous research on indoor convection. One should also note that the magnitude of the

convection coefficients developed for the heating condition in this investigation is roughly 50% higher than those for the cooling condition, suggesting buoyancy significantly affected the jets in one or both of the conditions. While there is a small but noticeable difference in the two values of supply-room temperature difference analyzed, the correlation presented should provide for more accurate load calculations and energy models than currently used conventions.

The last question that needed to be answered in this investigation was whether other variables needed to be included in the functional form of the correlations for convection. Sensitivity analyses were done to understand the effects of wall temperature, window size, window geometry and room temperature. Window size and geometry were found to appreciably change the correlations from the floor-to-ceiling window baseline, and new correlations were developed for this situation. Window temperature was found to have negligible effects. Supply-room air temperature difference was found to have appreciable effects at lower flow rates and this phenomenon was further investigated in Investigation 1c. Graphs showing this dependency are located in Appendix A.

5.1.1.1 Summary of Work Done in Investigation 1a

In all, ten correlations, given in Table 3, were developed to predict convection heat transfer in a variety of circumstances, using only knowledge available to the designer in the first phases of a building design, or to a load calculation or energy simulation program. These correlations are a major improvement over existing methods of modeling convection in buildings for a few reasons. First, the values for convection coefficient generated by this work are an order of magnitude greater than natural convection values which are often used and 2-3 times as great as forced convection

values developed for centrally located diffusers (Fisher and Pederson correlations (1997) predict a correlation of 0.0032 $V^{0.8}$ in all cases). For these reasons, they offer much better accuracy in indoor convection modeling, which has been shown to have a large effect on the accuracy of whole building energy simulations [(Alamdari, Hammond, & Melo, 1984) (Lomas, 1996) (Waters, 1980)]. Second, these correlations are consistent with the physics of the problem and forced convection theory. The magnitude of the values generated in this investigation are similar to those predicted by flat plate convection theory, with a free stream velocity of 0-1.5 m/s, which is the range in which most velocities measured in this work fell.

Configuration	HVAC Regime	Domain	Correlation
Floor-Ceiling Window	Cooling	$(\dot{V}/L) \le 160 m^3/hr \cdot m$ $(\dot{V}/L) \le 29 cfm/ft$	$h = 0.032(\dot{V}/L) - 0.33(SI)$ $h = 0.022(\dot{V}/L) - 0.22(IP)$
Floor-Ceiling Window	Heating	$(\dot{V}/L) \le 160 m^3/hr \cdot m$ $(\dot{V}/L) \le 29 cfm/ft$	$h = 0.12(\dot{V}/L)^{0.8}(SI)$ $h = 0.082(\dot{V}/L)^{0.8}(IP)$
Half-Window	Cooling, Low Flow Rates	$(\dot{V}/L) \le 120 m^3/hr \cdot m$ $(\dot{V}/L) \le 22 cfm/ft$	Window: $h = 2.12\,\Delta T^{0.33}(SI)$ $h = 0.031\,\Delta T^{0.33}(IP)$ Wall: Dependent on geometry
Half-Window	Cooling, Large Flow Rates	$(\dot{V}/L) > 120 m^3/hr \cdot m$ $(\dot{V}/L) > 22 cfm/ft$	Window: $h = 0.056(\dot{V}/L)^{0.8}(SI)$ $h = 0.038(\dot{V}/L)^{0.8}(IP)$ Wall: Dependent on geometry
Extruded Wall Below Window	Cooling	$(\dot{V}/L) \le 160 m^3/hr \cdot m$ $(\dot{V}/L) \le 29 cfm/ft$	Window: $h = 0.051(\dot{V}/L)^{0.8}(SI)$ $h = 0.035(\dot{V}/L)^{0.8}(IP)$ Wall: Dependent on geometry

Table 3. Correlations of convective heat transfer developed in Investigation 1

Lastly, these correlations allow for a much more refined calculation of convection in perimeter zones: one that is dependent on window geometry, diffuser type, flow rate, etc. This contrasts with existing methods which employ either a single value for all forced convection situations, or a correlation based only on air exchange rate.

Correlations cover the flow, thermal, and geometrical situations likely to be covered in practice. These correlations, along with those of (Goldstein & Novoselac, 2010) and those developed in subsequent Investigations of this dissertation, cover the vast majority of situations found in perimeter zones of buildings being constructed today.

It should be noted that these correlations are developed for a particular geometry and diffuser layout and type that was deemed to be the most prevalent in commercial construction today. Changes in diffuser layouts, manufacturer, and diffuser type are sure to affect the results developed herein. Linear floor diffusers with similar layouts will result in heat transfer characteristics very similar to those developed herein.

The correlations resulting from these investigations have been implemented in the ASHRAE Load Toolkit software and partially implemented in the building energy simulation software EnergyPlus. They are currently improving the accuracy of load calculations and energy simulations across the world.

5.1.2 Investigation 1b: Modeling the Effect of Venetian Blinds on Convection Heat Transfer in Perimeter Zones

Venetian blinds can significantly affect heat transfer in building envelopes. The effect of Venetian blinds on convection heat transfer at perimeter walls was analyzed experimentally in Investigation 1b. In this section, major results of the investigation are presented. More detailed information on experimental methods and more detailed results are given in Appendix B.

5.1.2.1 Natural Convection

Natural convection in a window-blind assembly was analyzed first for a floor-to-ceiling window. The results show that when blinds are present, convection at the window surface is best described by a correlation of the form of

Eq. (9) $$h = C\,(T_{surface} - T_{room})^{1/4}$$

while Investigation 1a. had shown the bare window case results correlate better to an equation of the form :

Eq. (10) $$h = C\,(T_{surface} - T_{room})^{1/3}$$

As correlations for laminar flow are typically given in the form of Equation (9) and those for turbulent flow in the form of Equation (10), these results suggest different near-window flow characters for situations in which blinds are present and those in which they are absent.

One conjecture as to the reason for this is that when the blinds are present, the distance between the window surface and the nearest tip of the blinds is such that the boundary layer is never able to grow past a certain thickness, and thus eddies cannot develop and the flow never reaches turbulence (Figure 9). This conjecture is given some credence by flat plate natural convection theory which predicts a boundary layer with a thickness of the order 2cm for laminar flow and a transition to turbulent flow occurring on the wall in all situations analyzed (Bejan, 2004). This phenomenon would not be captured in an experimental setup shorter than roughly 1.5 m, as the boundary later would not have sufficient length to develop in this small setup.

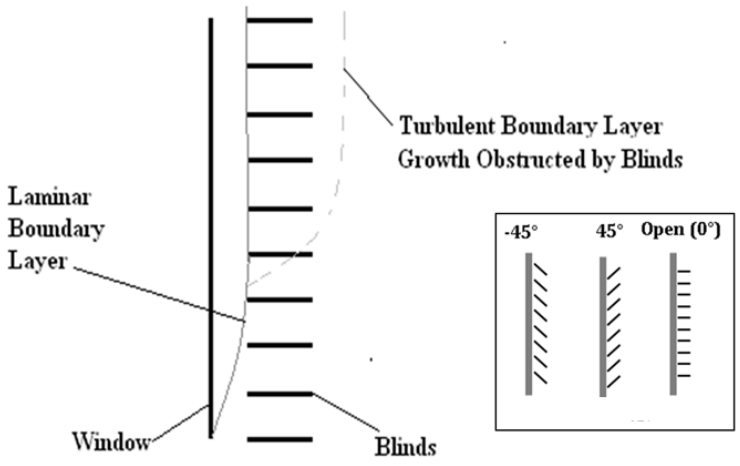

Figure 9. Boundary layer obstruction by blinds with the schematic of jet entrainment as a function of blind angle

Blind angle was also shown to affect the magnitude of natural convection by as much as 25% in Investigation 1b. The variation of the effectiveness of heat transfer with blind angle is most likely due to the variation in the ease of entrainment of room air into the gap between the blinds and the window surface, and thus the mass flow rate of air in the gap (Figure 9). At an angle of -45°, blinds are oriented nearly parallel with the natural direction of entrainment into the boundary layer, and thus entrainment is relatively easy. At a blind angle of +45°, blinds act as a barrier to the entrainment, which would naturally occur if blinds were not present.

5.1.2.2 Forced Convection

Forced convection often arises when diffusers are located near exterior windows. When a ceiling slot diffuser was used to cool the window, the presence of blinds was shown to reduce convection heat transfer by approximately 40% from the bare window situation for a floor-to-ceiling window and by 30% for a half-wall window. Blind angle

was again shown to have a significant effect on convection, as much as 40%, owing to the phenomena discussed in the previous section. When a floor register jet cools or heats the window, heat transfer is hindered up to 45% by the presence of the blinds and blind angle can affect convection by up to 30%.

Again, a few sensitivity studies were conducted to determine whether the inclusion of other variables in the functional form of the correlations was warranted. The results show that the temperature difference between the supply air and room air had a negligible effect on the convective heat transfer, suggesting the forced mode of convection is dominant at all flow rates. As expected, the convection coefficients are consistently higher for the situation in which only half the wall is a window (see Figure 1). This is due to the convention of using the supply temperature as a reference. In the case of the full-height window, the jet has a chance to heat up or cool down as it moves along the window, thus rendering the local temperature difference at lower portions of the window smaller, and affecting convective heat transfer accordingly. While the physical heat transfer mechanism is unchanged, the average heat transfer for the entire window surface as a function of supply temperature is relatively smaller for the full-height window. This is due to the actual local temperature difference, the driving force behind the convective heat transfer, is smaller at lower portions of the window.

Another sensitivity study was conducted to investigate the difference between the heating and cooling conditions. Theoretically, a warm jet issuing downward into a relatively cool room could experience buoyancy forces due to the room air-jet air temperature difference that acted contrary to the momentum forces of the jet. Ultimately, the sensitivity study showed that convection heat transfer in the heating or

cooling conditions were virtually identical. This suggests that the jet momentum is sufficiently larger than the buoyancy forces as to render the buoyancy effects negligible. This phenomenon is investigated further in Investigation 1c.

5.1.2.3 Summary of Work Done in Investigation 1b.

In all, 11 correlations were developed which describe convection under many situations at exterior windows when blinds are present. Correlations are robust for the two most common diffuser types used to condition large perimeter windows and are sensitive to blind angle. While many additional refinements, such as the inclusion of variations of diffuser layout and the addition of several manufacturer's diffusers could add resolution to these correlations, these correlations offer a vast improvement over existing correlations for blind-window assemblies, which were limited to natural convection in small-scale setups.

Configuration	Surface	Convection Correlation h [W/m^{2}K]
Natural convection with blinds		
Floor-to-Ceiling Window	Window	$h = 1.89\Delta T^{0.25}$ *(blinds -45°)* $h = 1.67\Delta T^{0.25}$ *(blinds 0°)* $h = 1.48\Delta T^{0.25}$ *(blinds 45°)*
	Blinds	$h = 2.0\Delta T^{0.33}$
Ceiling slot diffusers heating and cooling		
Floor-to-Ceiling Window	Window	$h = c \cdot (\dot{V} / L)^{0.8}$ *c= 0.063 (blinds 0° or closed)* *c=0.079 (blinds at 45°)*
	Blinds	$h = 0.060(\dot{V} / L)^{0.8}$ *(bl. closed)* $h = 0.030(\dot{V} / L)^{0.8}$ *(blinds open)*
Half-Window	Window	$h = c \cdot (\dot{V} / L)^{0.8}$ *c=0.080 +4.93E-4β -4.34E-6β^2 -6.06E-8β^3* *β - blind angle: 0for open +90 for closed*
	Blinds	$h = c \cdot (\dot{V} / L)^{0.8}$ *c=0.040 +1.72E-4β -3.29E-6β^2 -1.22E-8β^3* *β- blind angle: 0 for open +90 for closed*
Floor registers		
Floor-to-Ceiling Window	Window	$h = c \cdot (\dot{V} / L)^{0.8}$ *c=0.052 +1.561E-4β -4.867E* *-7β□^{2}+1.30E-8β^3* *β - blind angle: 0 for open +90 for closed*
Half-Window	Window	$h = 0.042(\dot{V} / L)^{0.8}$

Table 4. Summary of correlations developed in Investigation 1b. Note: All temperatures (ΔT) are given in degrees Celsius and the normalized flow rate (V/L) is in m^3 per hour of supply air per meter of perimeter wall.

This was the first study to investigate forced convection in blind-window assemblies and show the effect of blinds can be profound and should be included in any load calculation or energy simulation in order to ensure accuracy. This was also the first study to investigate natural convection in a full scale setup. A few phenomena were observed which could not be observed in a smaller setup, such as the retardation of the development of a turbulent boundary layer by the blinds. While the level of refinement given herein in regards to blind angle is not likely to find its way into energy modeling

software soon, it does suggest a dynamic control strategy, when used in conjunction with existing radiation heat transfer models.

5.1.3 Investigation 1c: Modeling Buoyant Floor Jet Movement and its Effect on Heat Transfer

The issue of buoyancy affecting diffuser jets and thus convection in perimeter zones was raised in the previous two investigations. To understand this phenomenon and model its effect on jet movement and heat transfer in perimeter zones, a three-step investigation was proposed: determine the effect of buoyancy on jet penetration, determine the effect on decay of jet velocity along the wall, and then correlate this to heat transfer along the wall. Resulting models allow for accurate jet mapping in perimeter zones and improve the accuracy of heat transfer models developed in previous investigations. They also explain discrepancies seen in previous investigations done in this work and in work by other researchers. The following paragraphs present the major results of each of these steps. More detailed information is available in Appendix C.

5.1.3.1 Modeling Buoyant Jet Movement

In order to predict jet movement, the penetration of a floor jet into the room was first correlated to the mixed convection parameter, *Ri*. This parameter is defined as

Eq. (11) $$Ri = \frac{g\beta\Delta TD}{U^2}$$

Where g is acceleration due to gravity [m/s^2];
β is the coefficient of thermal expansion[1/K],
ΔT is characteristic temperature difference [K];
D is characteristic length [m] and
U is a reference velocity [m/s].

is a ratio of the buoyancy forces experienced by the jet to the momentum forces present and was shown to be the most important parameter in determining jet penetration into the space. The exponential dependence on *Ri* was found to be either -0.45 or -0.5, depending

on the measurement method employed. This exponential dependence compares well with previous work analyzing penetration of hot jets from open slots pointing downward which showed an exponential dependence with exponent equal to -0.41 (Goldman & Jaluria, 1986). The flow visualization ("smoke") method and the anemometer data method were shown to be in reasonable agreement.

Once the distance the jet travelled into a room was modeled, the manner in which the jet decays along the wall was also investigated. The experimental setup was first validated by comparing it to existing theory on decay of isothermal wall jets and found to be sufficient. The velocity decay of buoyant jets was then investigated. The effect of buoyant forces was analyzed by plotting the decay of the maximum jet velocity along the wall, as shown in Figure 10. The velocities plotted are normalized by the face velocity at the register, v_{face}. The linear fit predicts a small entrance region (roughly $x/\delta_{penetration}$= 0.1) in which the maximum jet velocity does not yet decay. After the center of the jet begins to decay (after the entrance region), the jet velocity decays in a nearly linear fashion until it reverses course at its penetration distance. This is consistent with jet theory, and caused by the fact that the center of the jet has not started to interact with its environment until the end of this region. Although the linear fit does not capture some features of the detailed jet movement, such as a more rapid decay near the end of the jet, and although there is an appreciable degree of scatter in this data, its effect on the final variables of interest, convective heat transfer along the wall and overall jet mapping, is minimal. The points in this figure cover the variety of situations likely to be encountered in practice and show that the velocity of the jet along the wall can be predicted with just two equations.

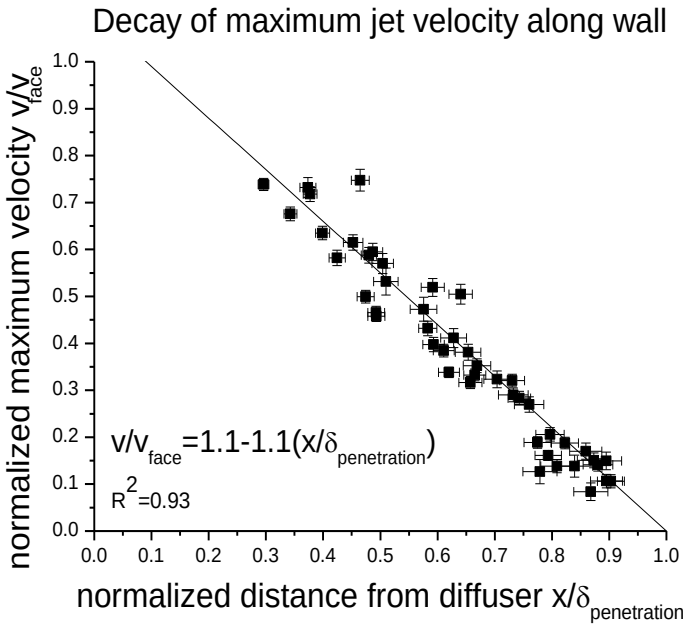

Figure 10. Plot of decay of jet velocity along length of wall with linear fit.

5.1.3.2 Heat Transfer Resulting from Buoyant Jet

With the decay of the maximum jet velocity along the wall known, the heat transfer correlations previously developed were reformulated by correlating convection to wall-averaged maximum jet velocity. A vast improvement of previous methods was gained, as shown in Figure 11. This represents a much more accurate model for heat transfer at vertical surfaces near diffusers than that previously used.

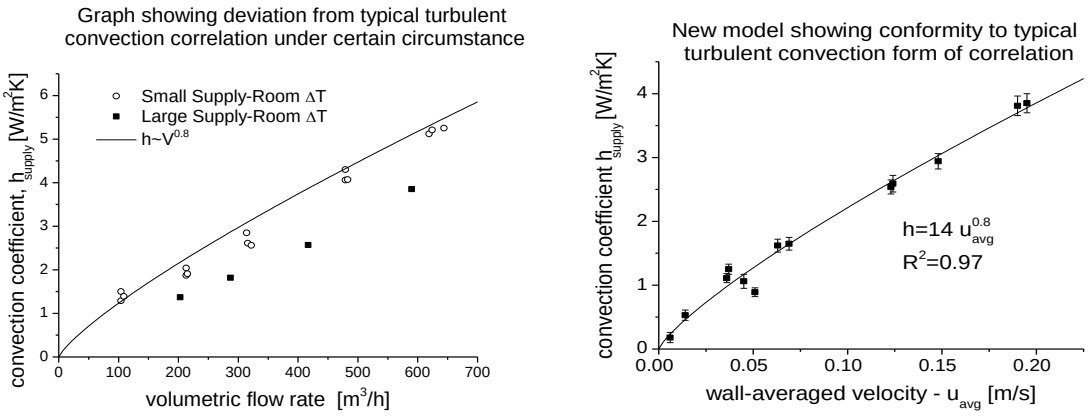

Figure 11. a) (Left) Previous formulation showing large deviation (black dots) from model correlated to total flow rate along length of 4.5m wall with 2-1.2m floor registers
b) (Right) Reformulation of previous convection heat transfer data with new information on jet penetration and decay

The remaining question that this study sought to answer was why the discrepancy shown in Figure 11a did not show up during investigations of the heating condition (supply air temperature greater than room air temperature) but did during investigations of the cooling condition. The answer to this question is demonstrated in Figure 12 below. Typical operation of HVAC systems in the heating condition fall into the left-most region of the graph (shown in hatched in horizontal lines in Figure 12), corresponding to a regime in which buoyancy forces are dominated by momentum forces. This is due to three causes: the fact that internal loads such as people and electronics assist the HVAC system in maintaining set temperature during the heating condition while opposing it during the cooling condition, the fact that supply temperature-room temperature differences are less during the heating condition than those during the cooling condition, and the fact that the jet from the large-effective area floor register is relatively weaker than that from the ceiling slot diffuser with smaller effective area. Typical cooling

condition operation is shown in hatched in diagonal lines in Figure 12 and occupies a region of the graph in which both buoyancy and momentum forces are important in determining jet movement.

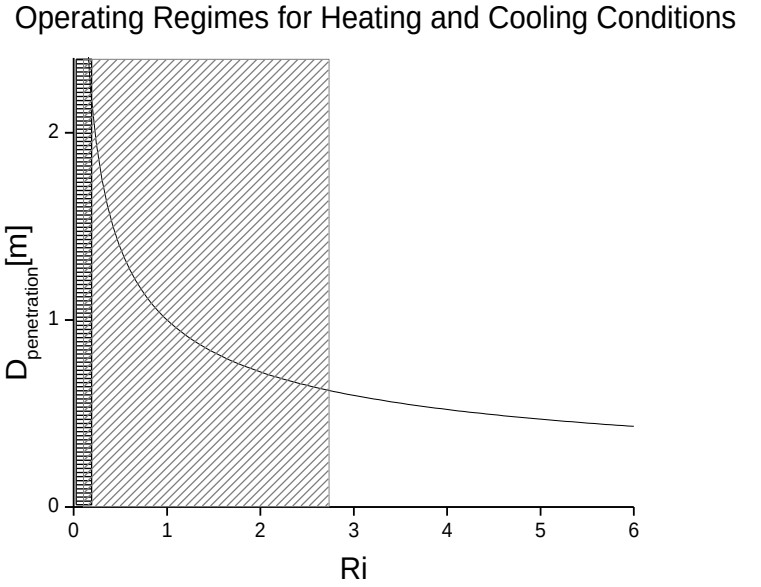

Figure 12. Typical operating regimes for heating with ceiling slot diffusers (hatched in horizontal lines) and cooling with floor registers (hatched in diagonal lines) conditions. Cooling region corresponds to 12°C supply-room temperature difference and air exchange rates of 2-10ACH. Heating regime area corresponds to 5°C temperature difference and 2-10ACH. All values of Ri use room height, 2.4m, as characteristic length.

The information gained during this investigation advances the state of the art in modeling transport phenomena in commercial buildings in three distinct ways. First, mapping of buoyant jets from floor registers can be done in a much more precise way. Current practice advocates simply increasing flow rates by a certain percentage when buoyancy forces act against the jet in order to ensure momentum dominates. The correlations given in this investigation allow for more informed design strategies. Secondly, heat transfer correlations for situations in which buoyancy forces are

significant are improved substantially, as shown above. Lastly, the situations under which buoyancy forces must be considered were identified, which will allow for more precise operation and design.

5.1.4 Investigation 1d: Modeling Mass Transfer to Ceiling Tiles in Commercial Buildings

The knowledge gained in modeling heat transfer at indoor surfaces in the first three investigations was leveraged to model mass transfer to ceiling tiles in commercial buildings under a variety of conditions. The measurements taken in this investigation demonstrate the effect HVAC operation can have on the boundary layer component of mass transfer. This effect is not usually included in existing models. They also served to suggest bounds on the magnitudes of mass transfer coefficients that can be expected in indoor environments, including those resulting from forced convection near diffusers. The major findings of these measurements are presented below and more detailed information is available in Appendix D.

Natural convection experiments were first conducted to validate the naphthalene sublimation technique used. This comparison was somewhat inconclusive, owing to a large degree of uncertainty resulting from the wide range of published diffusion coefficients for naphthalene (Keumnam, 1992). Nonetheless, the results of the natural convection experiments were well within an order of magnitude of the theoretical correlations, and showed very good agreement at lower temperature differences.

Next, a high sidewall diffuser was analyzed. This type of diffuser creates a very strong jet with a great deal of entrainment and high jet velocities, which were expected to result in high mass transfer coefficients. Results are given in Figure 13. A few observations can be were made. First, data for the ceiling and the wall opposite the diffuser appeared to follow an exponential dependence on flow rate greater than 0.8. Exponential dependences of convective transport on characteristic velocity greater than

0.8 arise in impinging jet situations, which is present to some degree on these surfaces. The effect of spatial averaging likely played a role in the deviation from the expected dependence as well. Correlations for all surfaces had exponential dependences between 0.6 and 1 and magnitudes of convective mass transfer coefficient between 0.05 and 0.45 cm/s.

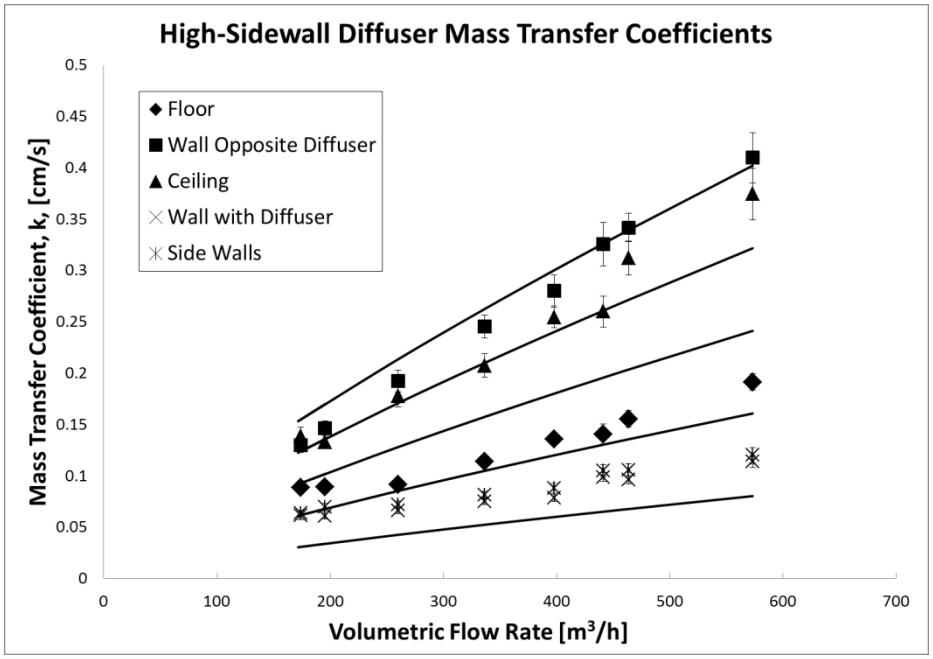

Figure 13. Mass transfer results for high sidewall diffuser. Lines are equally spaced lines with correlation form $k=C*V^{0.8}$

Lastly, a radial square ceiling cone diffuser was analyzed. This diffuser distributes air in a much different manner, with a much weaker, low velocity jet which is attached to the ceiling before it falls into the space. Mass transfer due to this jet was expected to show a lower bound on forced convection in indoor spaces. The coefficients measured for this diffuser were roughly a factor of four less than those for the high-sidewall diffuser. Furthermore, ceiling mass transfer coefficients conformed more closely to an exponential dependence on flow rate of 0.5, suggesting the laminar mode of

forced convection was dominant. Furthermore, it was noticed that a lower bound may be present around 0.05cm/s, which may be thought of as a good assumption for the boundary layer component of mass transfer in room in which the HVAC system is either not in operation or has a negligible effect on the surface of interest.

5.1.4.1 Summary of Work Done in Investigation 1d

In summary, the measurements taken during this investigation, summarized in Table 5, showed that HVAC operation can have the effect of changing convective mass transfer coefficients by an order of magnitude over expected operating conditions and thus should be included in any simulation of transport in indoor environments. In the forced convection mode alone, results showed that diffuser type could have the effect of changing mass transfer coefficients by a factor of more than 5 over expected operating conditions and also altering the mode of forced convection present.

***k* [cm/s]**	***Low***	***High***
Natural Convection	0.01	0.07
Radial Ceiling	0.08	0.12
High Sidewall	0.25	0.45

Table 5. Summary of ranges of mass transfer coefficients in cm/s under normal operating conditions measured in Investigation 1d.

This work represents an appreciable benefit in terms of accuracy over existing models which employ a static value for the mass transfer coefficient. It should be noted that in modeling mass transfer in indoor environments, convective transport is often even more important to the accuracy of the overall calculation than it is in modeling heat transfer. While convective heat transfer resistances are often components in a large series of resistances which dictate the overall process, mass transfer to indoor surfaces is often

linearly proportional to the boundary layer component of the mass transfer resistance. This is especially true in convection-limited reactions, such as decomposition of ozone at indoor surfaces. These measurements focus on this resistance and offer a better understanding of the values it may assume under different conditions.

5.2 Objective 2: Modeling Liquid Desiccant Air Conditioning Systems

The theory used in modeling large-scale phenomena in commercial buildings in the first four investigations applies to the modeling of smaller scale phenomena in building systems as well. This is the objective of the second phase of this dissertation: modeling transport occurring in liquid desiccant systems and using these models to optimize systems and quantify energy savings potential. This is accomplished through three investigations. The results of these investigations lend insight into the modeling of low flow liquid desiccant components; allow for an optimized system, both at the component and system level; and enable a quantification the energy and cost savings available in different building types with the integration of low-flow liquid desiccant systems into building HVAC systems.

The following sections present the most interesting findings from these three investigations. More information on methods used in creation of these results can be found in Chapter 4 and in Appendices E-G. More detailed results are also found in the appendices.

5.2.1 Investigation 2a: Modeling of a Low-Flow Liquid Desiccant Absorber

The main objective of this investigation was the creation of numerical models of the physical processes within a low-flow liquid desiccant absorber which would accurately predict the operation of these components under all the circumstances expected in practice. The models created in this investigation advance the understanding of the processes in flat-plate liquid desiccant heat and mass exchangers. They also allow for component optimization, and when combined in a system-level model will allow for system optimization and evaluation of the applicability of such systems in commercial

buildings. These abilities contribute to the reduction of energy usage in commercial buildings.

5.2.1.1 Absorber

A purely physical model capturing the small scale processes occurring within the channels was developed for the absorber, as described in Chapter Four. The numerical model was compared against laboratory data previously measured by others to assess its validity. The modeled moisture removal rate in the absorber compared well with the 32 lab conditions tested as shown in Figure 14.

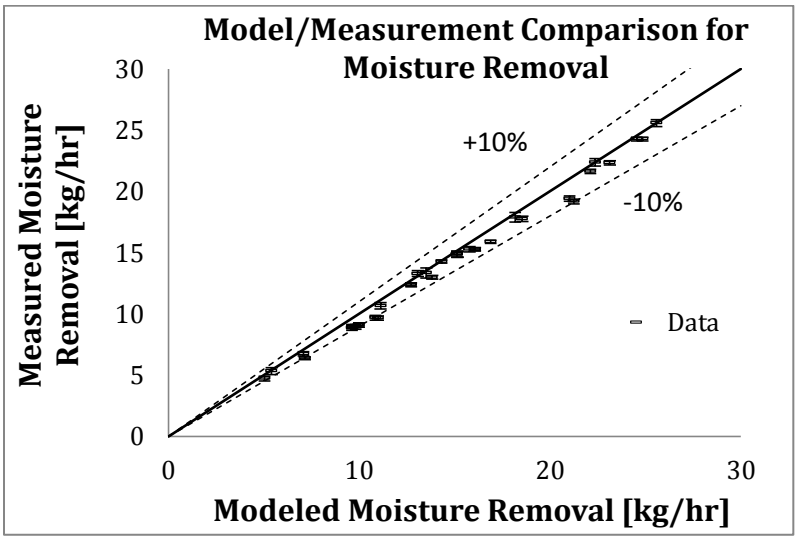

Figure 14. Comparison of conditioner model and laboratory data showing good agreement. Error bars reflect precision of chilled mirrors used to measure removal rate in process air stream.

Temperature of the fluid streams, however, could not be measured immediately at the boundary of the modeled domain because of practical limitations such as presence of the sump and the water distribution header (see Figure 2). The modeled domain included only the plates as the processes within them could be precisely defined. For this reason

some heat transfer occurred between the fluids and the ambient before the temperature measurement point. This led to a discrepancy between the modeled and measured temperatures of the fluid which increased with temperature difference between exiting fluid and the ambient in the laboratory.

For this reason, a lumped empirical heat transfer coefficient between the exiting fluid (in the desiccant sump at the bottom of the absorber in the case of the desiccant or the water distribution header at the top of the absorber in the case of the water) and the ambient air in the lab during measurements needed to be assumed to account for these losses. These adjustments changed the modeled outlet fluid temperatures by an average of 2.3°C in the relatively hot desiccant, an average of 0.6°C in the exiting water and an average of 0.2°C in the leaving air. Instruments used to measure the temperature of the three fluids were accurate to 0.3°C, 0.3°C, and 0.4°C at two standard deviations for the desiccant, water, and air, respectively. These adjustments account for heat transfer which does occur in reality. The adjustments have very little bearing on the analyses that have been conducted with this model, but were necessary to completely capture the operation of the absorber. When the heat transfer coefficient mentioned previously was employed, modeled exit temperatures matched well with measured temperatures.

5.2.1.2 Regenerator

As expected, the regenerator modeling presented more challenges than the absorber. Previous researchers [(Andrusiak, Harrison, & Mesquita, 2010), (Jain, Dhar, & Kaushik, 2000)] had found this to be the case as well. For this reason, and because of the fact that the regenerator is being phased out in field demonstrations an empirical

correlation of the regenerator performance made from the laboratory data was used for all subsequent modeling and new designs for the regenerator are being pursued. This model consists of five equations relating outlet variables to inlet variables which predict performance over the range of conditions expected with an average coefficient of determination (R^2) of 0.98.

5.2.1.3 Summary of Results of Investigation 2a.

Numerical models were developed which predict the performance of a low flow liquid desiccant absorber and regenerator. Prediction of moisture removal in the absorber was accomplished with purely physical descriptions (no empirical constants). This has not been done before to the author's knowledge, owing to the fact that most systems contain uneven wetting of the contact surface and thus require an empirical "wetted fraction". The presence of flocking, a wicking material designed to distribute the desiccant over the entire plate in the low flow system, likely allowed for removal of this empiricism. Empirical constants were needed for prediction of fluid outlet temperatures, owing to the difficulties in measuring precisely at the edge of the modeled domain. Modeling of the regenerator proved more difficult.

The modeling efforts also led to insights into the real world operation of the low flow liquid desiccant absorber and regenerator. First, the lack of a need for an empirical wetted fraction to account for uneven distribution of desiccant corroborated anecdotal evidence that flocking on the plate surface successfully distributed desiccant over the entire plate as intended. The regenerator was observed in the field to be underperforming and modeling work done herein showed this as well. Because of these observations, the modeling outputs, and weak performance of the regenerator in the field, a new design is

being pursued for the regenerator and has replaced the design modeled herein in at least one existing real world demonstration of this technology, a building in New Jersey (Kozubal, Herrmann, Deru, Lowenstein, & Clark, Under Review).

5.2.2 Investigation 2b: Assessment of Potential Energy Savings of Low Flow Liquid Desiccant System Retrofits in Supermarkets

The component level models created during Investigation 2a were integrated into a system level model of an entire low-flow liquid desiccant system. Detailed explanation of the modeling assumptions and additional models used is available in Chapter 4 and Appendix F. This system-level model was then used to assess the potential savings available when and Low Flow Liquid Desiccant (LFLD) system is installed upstream of an existing vapor compresson (VC) system in supermarkets across the United States. The LFLD is sized to handle all of the latent loads for the supermarket. Figure 15 shows a schematic of the modeled system and the fluid loops. The savings potentials are assessed through comparison with a baseline model, in which all sensible and latent loads are handled by the VC system.

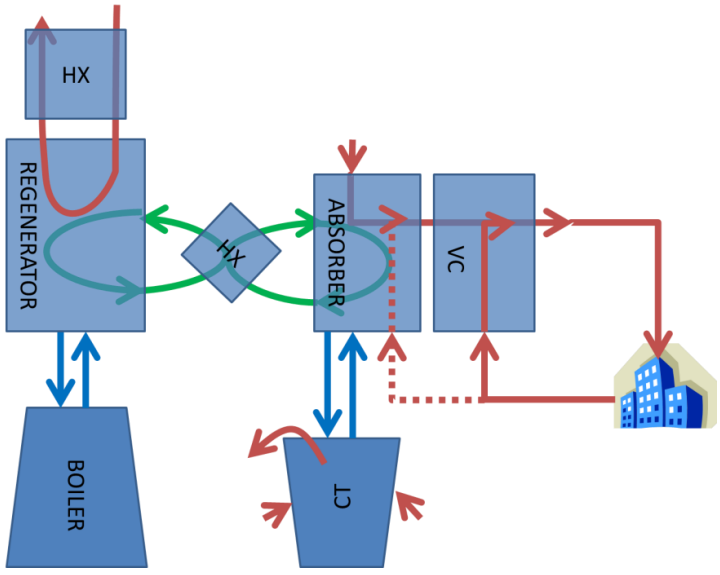

Figure 15. Schematic of system modeled in Investigation 2c. Air paths are shown in red; desiccant paths in green; water paths in blue. Dotted red line shows another possible mode for LFLD operation (treating recirculation air). CT is cooling tower; HX is heat exchanger; VC is vapor compression system.

To the author's knowledge, this study is by far the most in-depth and detailed study of the multitude of complex and important interactions between refrigeration systems in supermarkets and desiccant-based HVAC systems. Important considerations were identified which have profound effects on the accuracy and precision of this type of simulation. The simulations show the energy and cost savings achievable in various locations through LFLD system additions. This section presents overall results from the simulations and a brief discussion of the uncertainties in the model. More detailed information is available in Appendix F.

5.2.2.1 HVAC Energy Savings Available with Low Flow Liquid Desiccant Additions

Figure 16 shows cooling energy use calculated in the baseline and retrofit models. Cooling energy is greatly reduced as a result of the elimination of the need for overcooling with the vapor compression system. This is done by removing the latent load from the ventilation air upstream of the VC system, which now only handles sensible loads. Reheat energy is completely eliminated. The majority of the compressor electricity is shifted to thermal sources with the addition of the new LFLD system. It should be noted that this energy often may be available in the form of solar thermal energy or waste heat. Heating and fan energy savings are within the uncertainty of the model outputs. While some small benefit may be gained by adding complicated control strategies which take advantage of the latent heat of vaporization generated in the LDAC conditioner during the heating season, this was not modeled in this work and thus heating savings are minimal.

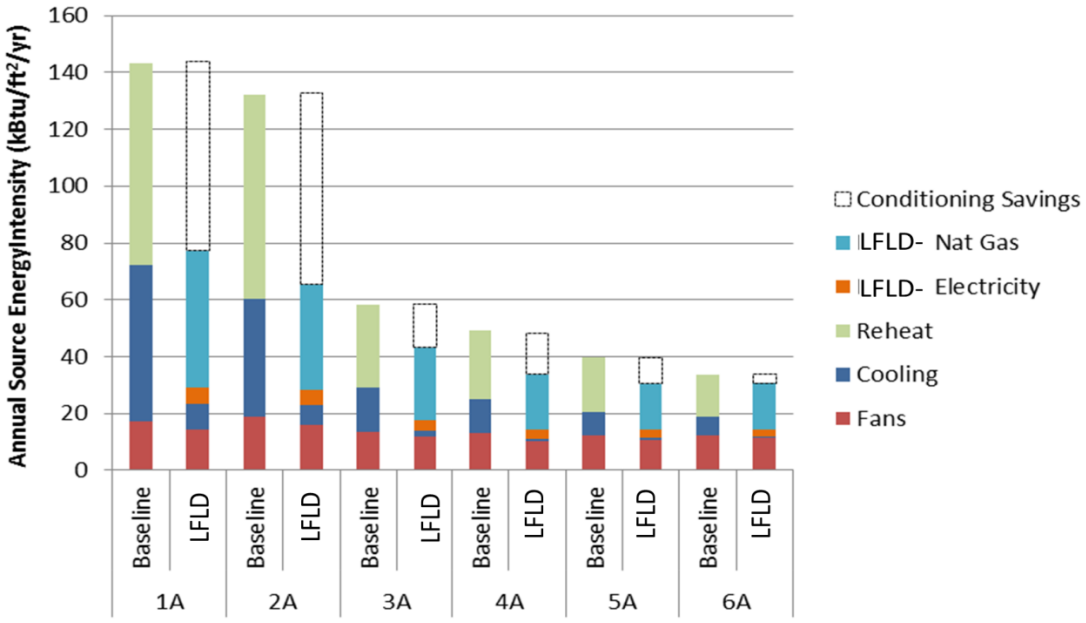

Figure 16. HVAC energy use with baseline (DX only) and LFLD retrofit

5.2.2.2 Refrigeration Energy Savings Available with Low Flow Liquid Desiccant Additions

Table 6 shows the refrigeration savings demonstrated in this study. Overall refrigeration energy savings as a percentage of baseline energy usage are small, but often significant in the whole-building energy consumption because of the large portion of building energy dedicated to refrigeration. Significant savings are demonstrated for the defrost and anti-sweat functions of the refrigerator. The defrost heaters remove frost buildup on display cases by heating and melting it, while the anti-frost heaters or anti-sweat heaters remove condensation from glass doors, also by providing electrical resistance heating. These savings are comparable to those demonstrated in previous studies [(Farmarzi, Sweetser, & Henninger, 2000) (Howell & Adams, 1991) (Henderson & Khattar, 1999) (Kosar & Dumitrescu, 2005)].

City	Climate	Zone	Defrost	Anti-sweat Heater	Compressor	Condenser Fan	Total Refrigeration
Miami	**Hot-Humid**	**1A**	12%	6%	-1%	-1%	~ 0%
Houston	**Hot-Humid**	**2A**	14%	7%	0%	0%	1%
Atlanta	**Mixed-Humid**	**3A**	17%	8%	1%	3%	2%
Baltimore	**Mixed-Humid**	**4A**	15%	7%	3%	11%	4%
Chicago	**Cold-Humid**	**5A**	17%	8%	1%	4%	2%
Minneapolis	**Cold-Humid**	**6A**	16%	6%	1%	4%	2%

Table 6. Refrigerator Energy Savings by Function in Baseline and Retrofit Models

5.2.2.3 Total Energy Savings

Table 7 shows a summary of the relative performance of the LFLD system as modeled. As expected, the highest source energy savings are seen in the hot humid climate zones (1A and 2A). The model shows whole building energy savings with the LFLD retrofit across all humid climates, suggesting the LFLD is most applicable in climates with large latent loads. Ranges given for values in Miami and Minneapolis represent a ±two standard deviation range calculated with the perturbation analysis discussed in Chapter 4. Uncertainty as a portion of building energy savings is significant and is discussed further below.

Energy Savings (kBtu/ft²)	1A	2A	3A	4A	5A	6A
Total Electricity	113 [41 to 197]	108	49	16	32	22 [10 to 46]
Total Natural Gas	-48 [-48 to -46]	-36	-20	-26	-16	-16 [-16 to -16]
Source Energy Savings	66 [3 to 156]	72	32	28	16	5.2 [-4.5 to 30]
	8% [0% to 20%]	9%	4%	4%	2%	1% [-1% to 5%]

Table 7. Normalized Annual Source End Use Energy (kBtu/ft^2/yr)

5.2.2.4 Cost Savings

Table 8 shows the yearly cost savings achievable with an LFLD retrofit. Two distinct benefits are gained. First, reduction in overall energy expenditure, shown in Table 7 reduces overall cost. Second, shift in energy usage from electricity to natural gas also results in some benefit. Cost savings in Miami and Houston are 5% of total building energy costs for the year. This is achieved completely with natural gas, rather than taking advantage of any "free" heating for regeneration on site such as solar thermal or waste heat. Colder climates such as Chicago and Minneapolis show energy savings of only 1% of building energy costs.

Yearly Cost Savings ($1000/yr)	1A Miami, FL	2A Houston, TX	3A Atlanta, GA	4A Baltimore, MD	5A Chicago, IL	6A Minneapolis, MN
Electricity Cost	46 [21 to 80]	39.9	19.2	18.1	12.0	8 [5 to 18]
Natural Gas Cost	-17 [-17 to -17]	-13.0	-8.9	-7.2	-5.8	-6 [-6 to -6]
Total Energy Cost	29 [4 to 63]	26.9	10.3	11.0	6.3	2.6 [-1 to 12.1]

Table 8. Cost savings available with liquid desiccant retrofits

5.2.2.5 Uncertainty Analysis

As can be seen above in Tables 7 and 8, overall uncertainty as compared to energy savings is considerable. For climates with small savings, total uncertainty in energy usage at two standard deviations is equal to or greater than total building energy savings. The analysis found that around 60% of this uncertainty is attributable to the input for latent heat ratio (LHR) in the refrigeration systems and the majority of the rest is attributable to the uncertainty in infiltration rate. The other perturbed variables had little effect on overall uncertainty.

While infiltration will always be difficult to know precisely, latent heat ratio is a quantity that should be relatively predictable. However, there is only one instance (Farmarzi, Sweetser, & Henninger, 2000) where this quantity was actually measured, to the author's knowledge, and this used equipment and assumed operating patterns that cannot be assumed general for all supermarkets. The input for LHR strongly affects the current simulations in three ways. First, increasing the amount of dehumidification done by the refrigerators (proportional to LHR) removes latent load on the HVAC system and causes the LFLD to be relatively less beneficial, and vice versa. Secondly, decreasing sensible cooling done by the refrigerator (inversely proportional to LHR) increases the sensible load on the HVAC system and causes the VC system to be more useful and the LFLD to be relatively less useful. Furthermore, increasing LHR on the refrigerator increases the overall dehumidification capacity of the (HVAC + Refrigeration) system and allows for lower space humidity levels, which in turn reduces overall refrigerator energy usage. More research is needed in this area to provide for more accurate simulations of supermarkets.

5.2.2.6 Summary of Results of Investigation 2b.

Overall applicability of the LDAC for a particular climate can be understood as one of four situations:

- In hot, humid climates, baseline cooling energy is dominated by latent loads, including a large penalty for reheat (over 40% of HVAC energy). In these climates, the LFLD is particularly well-suited. Refrigeration savings are small. Because such a great quantity of energy usage is shifted from electricity to gas in these climates, large cost savings are achievable: roughly 5% of the yearly energy cost expenditure of the whole building.
- In mixed, humid climates such as 3A and 4A, reheat still comprises over 20% of total HVAC energy usage and this is completely eliminated by the LFLD. Again, cooling and dehumidification savings are great enough to offset additional energy expenditure for desiccant regeneration and HVAC savings of over 10% are achievable. Additional refrigeration savings are similar to hot humid climates and contribute to a whole-building energy savings of 3-4% and cost savings of 2-3%.
- Cold, humid climates such as 5A and 6A are less applicable for the LDAC as the sensible heating dominates the HVAC energy expenditure. The LDAC retrofitted system was, however, shown to minimally improve energy usage and costs.

- The LFLD system is not expected to provide a cost or energy benefit in marine or dry climates where most of the cooling need is sensible.

Overall, the LFLD showed significant potential, especially in humid climates, although perturbation of model inputs had a significant effect on results, particularly in the case of latent heat ratio. However, even when this is taken into account, when control strategies are optimized and alternative thermal sources included, the LFLD system promises to greatly reduce supermarket energy usage and provide substantial cost savings in many climates.

5.2.3 Investigation 2c: Design and Optimization of Low Flow Liquid Desiccant Components and System

With the models developed in Investigations 2a and 2b, the effect of design parameters could be determined and operating conditions optimized to provide for a compact, effective and efficient system. Selection of auxiliary components was also made possible through analysis of the modeling outputs. To the author's knowledge, no detailed design guidance for LFLD systems exists, and dynamic interaction of components of any desiccant system has rarely been investigated, owing to inadequate software. This investigation provides for manufacture and selection of an efficient, effective and compact system.

5.2.3.1 Component Level Optimization

The main thrust of the component optimization phase was to improve the removal effectiveness of the absorber. Simple correlations were established between controllable variables and removal effectiveness. In general, inlet air conditions (temperature and humidity) were weaker predictors of removal effectiveness than controllable factors such as geometry and flow rates, and performance decreased slightly with entering air humidity.

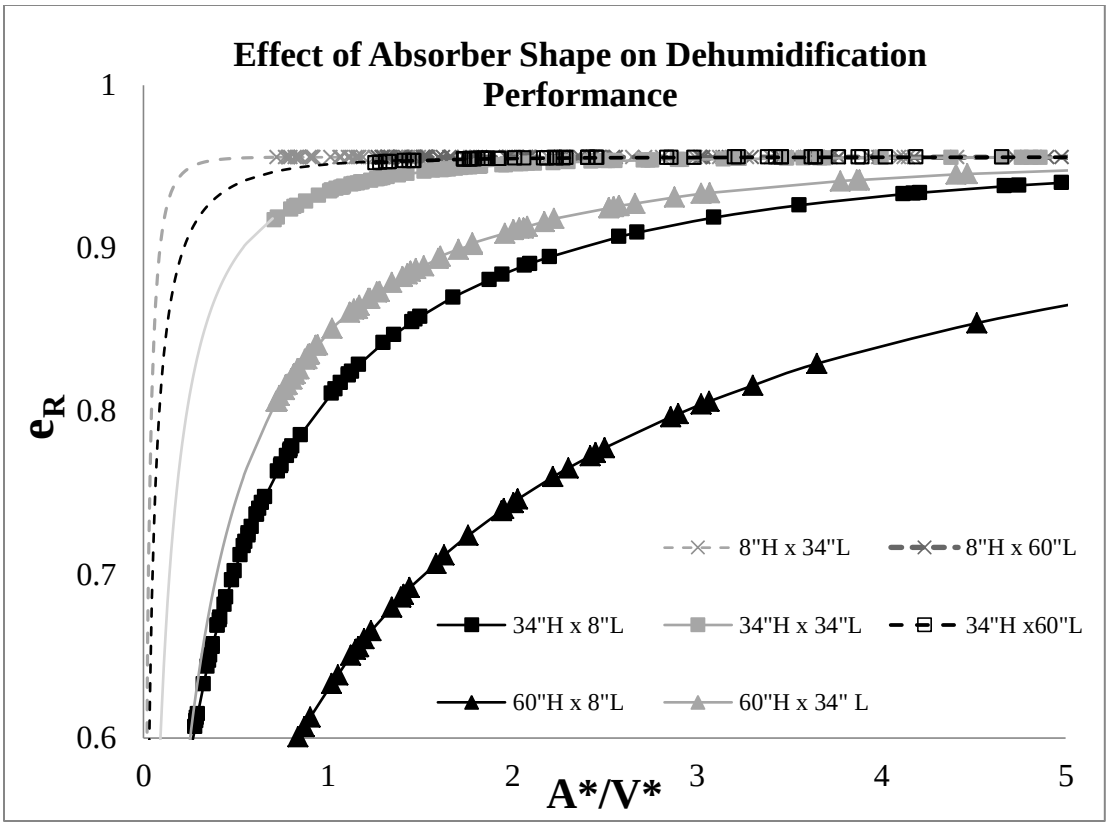

Figure 17. Graph showing the effect of absorber shape and air flow rate on performance at design conditions.

Performance of the LFLD was found to be very sensitive to the shape of the absorber and the air flow rate through it, as shown in Figure 17. Figure 17 shows the relationship between the removal effectiveness, defined as

Eq. (12) $$\varepsilon_R = \frac{(\omega_{inlet} - \omega_{outlet})}{(\omega_{inlet} - \omega_{eq,desiccant})}$$

and absorber shape and size. All points in Figure 17 refer to an absorber handling 4,000 cfm of air. Variables A* and V* are plate surface area normalized by the area of a cubic absorber and velocity normalized by the maximum allowable velocity, respectively. This

parameter may be thought of as analogous to the number of transfer units (NTU) parameter traditionally used to describe sensible heat exchangers.

Among the reasons for this sensitivity are changes in residence time, changes in concentration drop in the desiccant, and changes in water residence time and thus water temperature. A process is suggested in Appendix G for selecting an LFLD absorber to ensure maximum effectiveness within the space and fan power constraints of a particular application. It was shown that changes in the shape of the system, with the same amount of material or the same fan power, could have substantial effects on the effectiveness of the system.

Cooling water flow rate and temperature were also found to have a substantial effect on the performance of the absorber, as shown in Figure 18. Performance decreased rather quickly for entering water temperatures of greater than 25-30°C or for flow rates less than about half of the maximum allowable flow rate. These are attributable to the lack of the cooling fluid's ability to perform its function because of either insufficient driving force for heat transfer or insufficient capacity in the case of low flow rates. When the absorber is operating properly, the cooling water maintains the desiccant temperature, and thus its equilibrium vapor pressure, at a level low enough to allow for adequate moisture transfer from the process air stream. As equilibrium vapor pressure is an exponential function of desiccant temperature, small changes in cooling water temperature may have profound effects on dehumidification performance.

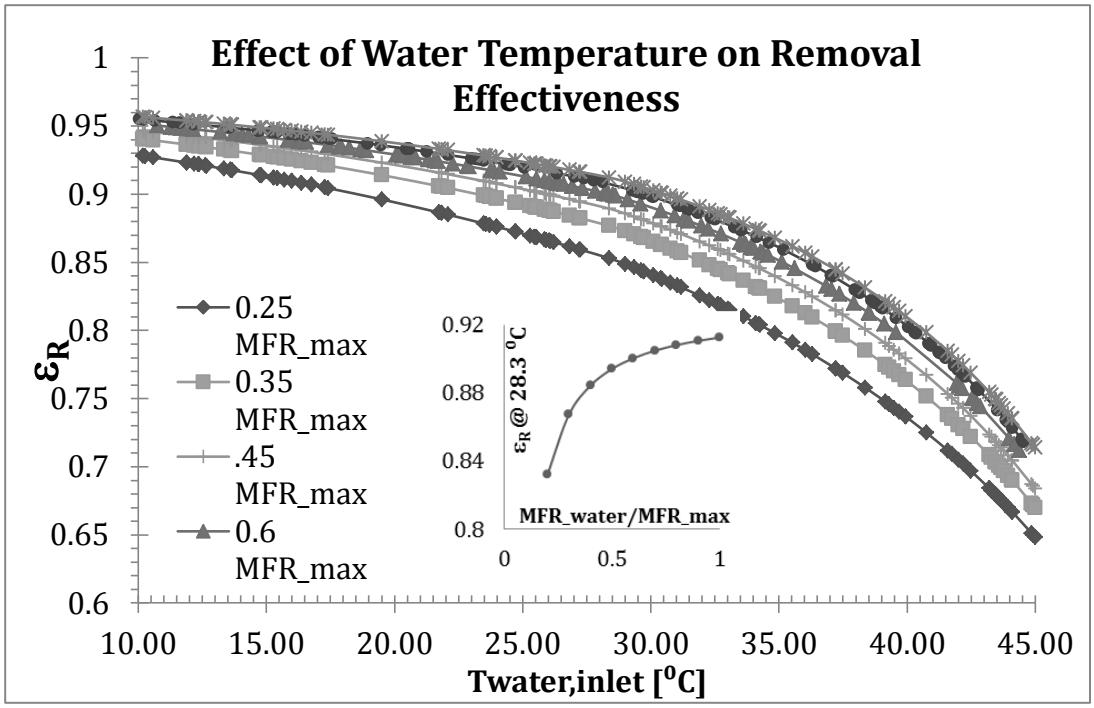

Figure 18. Graph showing relationship between entering cooling water temperature, cooling water flow rate, and absorber performance

This information was used to determine under what conditions a cooling tower could be replaced with an air-to-water heat exchanger, thus removing the cooling tower and its required maintenance from the system. An analysis at design conditions yielded a few interesting results, shown in Table 9. First, the driest air achievable, with a humidity ratio of 0.0045 $kg_{water}/kg_{dry\ air,}$ was only achievable with a cooling tower sized for the greatest flow rate possible, in order to minimize water temperature change across the absorber. However, if a slightly less effective absorber (ω_{out}=0.0057 $kg_{water}/kg_{dry\ air}$) were acceptable, the cooling of the water could be achieved with a cooling tower at low water flow rates (and thus reduced pumping costs and lower internal pressures). An outlet humidity ratio of 0.0071 $kg_{water}/kg_{dry\ air}$ at design conditions can be achieved with mid-

range heat exchanger at the highest flow rates and an excellent heat exchanger at 80% of the maximum flow rate. Given the desirability of elimination of the cooling tower, the additional cost of a good heat exchanger and the added fan power (which will likely be more than compensated for by the reduced pumping power), will often be worth the expense. It should be noted also that a very effective heat exchanger with a high mass flow rate would likely be very large, and thus the least effective system acceptable would be selected if doing so was deemed more desirable than keeping a cooling tower.

Desired Humidity Ratio	$\dot{m}_{water}/\dot{m}_{max}$	Inlet Water Temperature Needed [^{0}C]	Modeled Outlet Temperature [^{0}C]	Inlet Water Temperature [^{0}C] Achievable With:				
				Cooling Tower	Air-Water Heat Exchanger with Water-Side Effectiveness of:			
					0.25	*0.3*	*0.35*	*0.4*
0.0071	0.6	33.0	36.6	28.2	34.6	34.2	33.8	33.4
0.0071	0.7	33.7	36.5	28.7	34.5	34.1	33.7	33.3
0.0071	0.8	34.2	36.4	29.2	34.4	34.0	33.7	33.3
0.0071	0.9	34.5	36.3	29.7	34.4	34.0	33.6	33.2
0.0071	1.0	34.7	36.2	30.0	34.3	33.9	33.5	33.1
0.0057	0.6	28.5	33.6	26.3	32.3	32.1	31.8	31.6
0.0057	0.7	29.6	33.9	26.8	32.5	32.3	32.0	31.7
0.0057	0.8	30.4	34.0	27.2	32.7	32.4	32.1	31.8
0.0057	0.9	30.8	34.0	27.6	32.6	32.3	32.1	31.8
0.0057	1.0	30.8	33.7	27.8	32.4	32.1	31.9	31.6
0.0045	0.6	23.0	29.1		29.0	29.0	28.9	28.9
0.0045	0.7	24.5	29.6		29.3	29.2	29.2	29.1
0.0045	0.8	25.6	30.0	25.6	29.6	29.5	29.4	29.4
0.0045	0.9	26.4	30.2	26.0	29.8	29.7	29.6	29.5
0.0045	1.0	26.9	30.3	26.3	29.8	29.7	29.7	29.6

Table 9. Assessment of capability of two water-cooling devices to meet load requirements. Light gray shading on inlet water temperatures indicates a mode of operation which delivers sufficient cooling. Dark gray indicates a mode which cannot deliver the necessary water temperatures.

5.2.3.2 System Level Optimization and Design

System level efficiency measures were also made possible by the models developed. These include proper sizing of equipment, selection of system components for greatest energy efficiency, downsizing of the system, and provision for an acceptable amount of system cycling.

Regenerator selection was first investigated. The results showed that there is a direct relationship between regenerator size and system removal efficiency, but an inverse relationship between regenerator size and regeneration effectiveness, although regeneration efficiency changed only 10% over the interesting range. For some applications, such as in grocery stores, energy savings within the building continue to increase as humidity decreases and thus the largest regenerator which does not cause crystallization would be selected. In other applications, a greater supply humidity would be acceptable in favor of regeneration energy savings, and the regenerator would be sized to produce this humidity at design conditions. This investigation points to a strategy for determining the optimum regenerator size in various applications.

The relationship between the amount of heating water and desiccant in the system and system performance were also analyzed. The primary concerns in this exercise were preventing excessive cycling of the regenerator or boiler, preventing crystallization of the desiccant system and delivering desired humidity levels. At the same time, overall system size should be minimized to allow for a smaller packaged unit and market acceptance. The analysis of the relationship between the amounts heating water and desiccant and system performance showed that the amount of desiccant in the system greatly affects the operation of the system, while the water tank size does not. Changing the amount of

water in the system only changed the period of the fluctuation in the water temperature and only changed the temperature itself minimally. Similarly, desiccant concentrations in the tank also changed slightly for all cases analyzed. Variations in total regeneration energy for the period were less than 1% as the same amount of water was removed and the RSHI is dictated by the regenerator design. If a small system were desired, a system designer would chose the least amount of desiccant which gave an acceptable cycling period, and then implement a tankless water heater in order to reduce overall system size.

5.2.4 Summary of Results of Investigation 2c

In the course of this investigation, guidance was given on design, selection and optimization of various components of the LFLD system. Many improvements and optimizations to the low flow liquid desiccant system have been suggested. Result show that simpler methods for correlating system variables to performance, such as the NTU-effectiveness method, are not sufficient for a three fluid system with unique constraints. Methods were put forward to improve and optimize such as a system and it was shown that some of the larger components of the system, the cooling tower and any hot water storage device, could be eliminated if desired. Sizing of system components was shown to require considerations of several interactions between systems. With the improvements suggested herein, the LFLD system may move closer to a state in which large market acceptance is possible.

Chapter 6: Conclusions

Seven investigations were conducted for this dissertation, each contributing to the reduction of energy use in commercial buildings through modeling of transport processes. A greater understanding of the methods which need to be employed in modeling these processes was gained. The models generated in this dissertation can be and have been included in larger building models in order to more precisely and accurately predict the many interactions within a building. Lastly, models developed herein can be used to reduce the amount of energy used in a building, both by directly affecting the efficiency of HVAC systems and by allowing for a better optimization of the building as whole.

This dissertation improves the state of the art of indoor convection modeling. More than twenty new correlations were developed to predict convection heat transfer in building perimeter zones. This set of correlations allows for a more refined process of modeling heat transfer in buildings. Two diffuser types that are prevalent in commercial construction can now be specifically accounted for, where previously no such distinction exited. The convective component of heat transfer through windows with Venetian blinds can also be accounted for as a function of HVAC operation and blind angle, where existing models used single static values for this component. Other refinements such as accounting for the presence of window sills and small walls below windows are also offered.

The correlations generated as part of this dissertation are currently improving the accuracy of thousands of building energy simulations worldwide, through their inclusion in widely used load calculation and energy modeling software. This is done through their allowance for an accounting of forced convection which is sensitive to HVAC operation and diffuser type. Previous models were developed as a function of air exchange rate only or as natural convection. The improvements in accuracy of convection models that

are gained as a result of this work will have a substantial effect on the accuracy of the whole building simulation, as has been shown by several previous researchers.

The models of convective heat transfer presented herein also more closely relate to the physics of the situation occurring at glass curtain walls, which is a factor strongly affecting the overall building simulation. All of the correlations presented herein take into account the position of the diffuser jet relative to the window, rather than assuming convection is only a function of air exchange rate regardless of diffuser type. Some of the correlations presented herein take into account the movement of the diffuser jet along the wall and its interaction with the air in the space and the wall or window itself. Buoyancy effects are accounted for in a mechanistic way, which had never been done in previous convection models. Forced convection is modeled as a function of volumetric flow rate to an exponent of around 0.8 for turbulent forced convection and 0.5 for laminar forced convection, corresponding to exponential dependencies on characteristic velocity that are found through solution of the Navier-Stokes equations.

The heat transfer correlations developed herein are applicable in any buildings in which large glazing areas are present which are heated or cooled by nearby linear diffusers. As this practice is done almost exclusively in perimeter zones of commercial buildings, this is the situation in which they will be most applicable. Different diffuser types and layouts will lead to heat transfer situations that vary from the situations studied herein.

Lessons learned in the modeling of convective heat transfer were applied to the modeling of convective mass transfer as well. Previous models of convective mass transfer did not take into account the operation of the HVAC system, but rather assumed a static value; often a single value for the entire room. By providing a better understanding of the effects of HVAC operation on the magnitude of the boundary layer component of convective mass transfer, large gains in accuracy can be realized, despite

the uncertainty and scatter in the calculated data. The boundary layer component of transport was shown to vary over an entire order of magnitude depending on HVAC operation; an effect that is not captured in previously existing models. For forced convection alone, the magnitude of mass transfer coefficients varied by roughly a factor of 4. The data presented in this section of the work can allow for both more accurate multi-zone building transport simulations and more accurate estimations of the efficacy of passive removal strategies which employ decomposition of harmful pollutants at ceiling tiles.

Many of the general principles and theoretical underpinnings used in the modeling of the large scale processes in buildings were similarly applied to the modeling of small scale phenomena within a particular building HVAC system: a low flow liquid desiccant dehumidification system. The models generated in this phase of the work allow for accurate simulations of buildings which employ low flow liquid desiccant (LFLD) dehumidification systems, provide tools that can be used to optimize the systems themselves, and give methods for design and sizing of the system components and choice of a system operation which provides effective and efficient dehumidification of commercial buildings. The systems explored herein are most applicable in supermarket applications and in high-latent load climates and building types.

Modeling of the small scale phenomena occurring within the channels of an LFLD absorber offered instructive lessons in the modeling of this type of system and confirmed qualitative observations of actual component performance that had been made previously in the laboratory. The good comparison between the absorber model and measured data despite the use of a wetted fraction parameter suggested the flocking material used to distribute desiccant on the plates was successfully distributing the desiccant over the entire surface of the plate, as it had been intended to do. This allowed for a purely physical model of the processes in the LFLD absorber when the proper

information was included in the model. The lack of agreement between the modeled and measured regenerator data confirmed that the regenerator in its current form was operating below its potential and new regenerator designs should be pursued. An empirical model was nonetheless offered which can be used to predict measured performance well until a new regenerator design is finalized.

Development of component level models allowed for a system level model to be made which predicted the dynamic interaction of the many system components over time when the system was subjected to changing boundary conditions. This model was integrated into a full building energy simulation that was used to predict cost and energy savings possible in supermarkets across the United States. To the author's knowledge, this series of simulations was by far the most detailed and accurate accounting of the potential of desiccant systems to reduce energy usage in supermarkets. A detailed error analysis was also conducted, which is rarely done in whole-building simulations, in an attempt to bound the uncertainty and lend more credence to the simulation results. This error analysis identified weaknesses in existing data sets used to predict supermarket energy consumption and a temporary means of dealing with these weaknesses.

Results of the simulations showed that substantial energy and cost savings are likely achievable in grocery stores in hot and humid climates with LFLD retrofits. Cooling energy savings in the most applicable supermarkets was around 40% and this led to cost savings of around $30,000 a year for a supermarket requiring 6800 m^3/hr (4,000 cfm) of ventilation, a whole-building energy reduction of around 9% of total energy expenditure, and elimination of the wasteful overcool-and-reheat strategy. LFLD systems were shown to be applicable in other humid climates as well, with 10-40% cooling energy savings calculated in all type A climates in the United States and $10,000-11,000 savings in mixed humid climates.

Lastly, the analyses done with the models of the LFLD gave a better understand the operation of the components and system and provided methods for design and optimization. Distinctions were made between this system and other heat exchangers in regards to appropriate formulations of system performance based on controllable system variables. It was shown that some of the more expensive and larger components may be removed from the system entirely under certain conditions, thus possibly increasing market acceptance and allowing for more rapid deployment.

Future work in these areas can take several directions. Improvement of regenerator design through modeling can drastically improve operation of desiccant systems. Optimization of components in order to make the system smaller and less complex can lead to greater market acceptance. Liquid desiccant systems can also be optimized to perform secondary functions such as improvement of indoor air quality. Dynamic system modeling can be used to gain large advantages from controls and from shifting loads to times when energy is cheaper or more readily available.

Through these seven investigations, the state of the art of modeling buildings and their systems was improved in several distinct but complementary ways. The models developed herein and the understanding gained through their development and use provide for more accurate and precise building energy models. Through the inclusion of these models in many present and future simulations of buildings and building systems, efficiencies can be realized which reduce the amount of energy attributed to commercial building operation.

Appendices

Appendix A: Experiment-Based Convection Heat Transfer Correlations near Floor Registers (RP-1416)

Jordan Clark *Student Member ASHRAE*

Atila Novoselac, Ph.D. *Member ASHRAE*

ABSTRACT

Accurate modeling of energy flows in buildings is necessary for proper load calculation and simulation of building energy use. Easy-to-use design tools are needed for predicting heat transfer processes in a building. One process which has been studied little is forced convection at the interior surfaces of window assemblies, which is present in the majority of newly constructed commercial buildings. To this end, energy flows associated with a specific HVAC configuration- a floor register near an external wall and/or window- are analyzed experimentally and described with accepted theory. A 60 m^3 (2119 ft^3) environmental chamber with precisely controlled interior conditions and electrical resistance heating panels is employed to study heat transfer at the interior surfaces of a building's envelope. Convection heat transfer processes for various inlet conditions, surface temperatures, and window sizes are examined. Results show that convection at window and wall surfaces is highly dependent on supply temperature and flow rate, moderately dependent on room-supply air temperature difference, and weakly dependent on surface-supply air temperature difference. Simplified models of convection heat transfer for external walls and windows are proposed for easy implementation in load calculation tools and energy modeling software.

INTRODUCTION

Predicting heat transfer through building envelopes is an important part of any load calculation or building energy simulation. Interior convection modeling is a crucial part of this prediction. Contemporary building designs often include large windows or glass curtain walls. Modeling convection heat transfer at the interior surfaces of these windows becomes more important in these types of buildings as conduction through the thin windows is rapid and thus heat transfer to the space is often governed by interior convection. While a great deal of work has been done to understand radiation heat transfer through window assemblies and some work on natural convection heat transfer at interior surfaces of small window assemblies has been conducted, little extant work describes the variety of convection heat transfer processes that occur near walls and windows in sufficient detail. In order to accurately model energy flows in buildings and thus allow for optimization of systems and architectural elements, more work is needed in this area.

The present study addresses this need through the course of 93 experiments, in which interior convection heat transfer at perimeter walls and window surfaces under conditions of both buoyant flow and pressure-driven flow is investigated. Existing literature on the topics of indoor convection modeling is first reviewed. Objectives and hypotheses of the current investigation are then presented. Experimental method is described and results are given.

EXISTING LITERATURE

Various researchers have studied convection heat transfer at interior surfaces and flow patterns in interior spaces. The following section reviews relevant research on indoor convection modeling.

Indoor Convection Modeling

Since air can be considered a transparent media in regard to radiation heat transfer, and is a very poor conductor, convection heat transfer is virtually the sole mode by which the temperature of indoor air is ultimately affected. Various researchers have demonstrated the effect of the selection of a model for convection heat transfer from indoor surfaces on the accuracy of any building energy simulation. Waters (1980) compared existing computer models to actual building performance and found a strong dependence of the accuracy of the model on the indoor convection model used. Similarly, Alamdari et al. (1984) found that for a certain case study in London, predicted energy consumption varied by as much as 18% depending on the convection coefficient employed. Lomas (1985) simulated a particular building using three different sets of published values for the assumed indoor convection coefficients, h, and found the choice of h to have an effect of as much as 27% on predicted heating demand in the building. Beausoleil-Morrison (2001) also demonstrated the profound effect that proper convection modeling can have on building energy simulation.

Numerous researchers have developed a library of convection coefficients which describe convection heat transfer due to temperature differences in room air: notably Alamdari et al. (1984), Khalifa (1989), and Awbi (1998). Awbi and Hatton (2000) also developed correlations for mixed (natural and forced) convection from interior surfaces. Further work has been done on convection resulting from mechanically induced flow

fields. Spitler et al. (1991) developed convection correlations for situations in which large ventilation rates (>15 air changes per hour (ACH)) were employed. The results of their investigation suggested that at ventilation rates less than 15 ACH, ventilation rate is a more important parameter than either jet momentum or inlet velocity. Additional investigations by Fisher and Pederson (1997) and Goldstein and Novoselac (2010) confirmed that this was the case for all flow rates used in the current investigation (2-12 ACH). All three of these papers found that indoor convection can be modeled as a function of volumetric flow rate raised to an exponent of 0.8.

Fisher and Pederson (1997) extended Spitler's work into ventilation regimes characterized by ventilation rates below 12 ACH. They calculated convection heat transfer coefficients for various surfaces in an office-size environmental chamber with either a ceiling-mounted radial diffuser or a side-wall inlet. Their work informed the current investigation in a few ways. First, they confirmed Spitler's assertion that inlet volumetric flow rate was the proper variable with which to correlate heat transfer models for commonly employed ventilation rates and the exponential dependence (0.8) held in lower ventilation rate regimes as well. Secondly, they found that the inlet temperature was the best reference temperature for their correlations.

Goldstein and Novoselac (2010) analyzed forced convection heat transfer along vertical surfaces near ceiling slot diffusers. They found, like previous researchers, that the convection heat transfer coefficient was relatively independent of room-supply air temperature difference and surface-supply temperature difference. They also found that inlet temperature and volumetric flow rate were the proper variables for correlating convection heat transfer results in the configuration studied.

Beausoleil-Morrison (2001) analyzed mixed convection and proposed a method for modeling the competing and assisting forces present in mixed convection situations which "blends" the two phenomena: forced and natural convection.

In currently used energy modeling and load calculation software, such as the ASHRAE Load Toolkit, forced convection in perimeter zones is modeled either with a single value for the convection coefficient which is insensitive to diffuser type and flow rate, or a natural convection assumption is used. This work aims to provide correlations for forced convection specifically for perimeter zones conditioned by floor registers along their outer walls or windows, and give correlations which are sensitive to the volumetric flow rate supplied to the room.

OBJECTIVES AND HYPOTHESES

The objectives of the current experiments are as follows:

1. **Quantitatively predict convection heat transfer at window and wall surfaces near floor diffusers for the situations most commonly encountered in practice.** The scope of this work is limited to one representative diffuser layout and room height which was deemed to be the most common situation in commercial construction after extensive consultation with industry professionals. Resources did not permit an in-depth quantitative analysis of the effects of variation of specific diffuser type, size, layout, etc., but the situation analyzed is a common one and the correlations developed should be applicable with an acceptable degree of error for load calculation and energy simulation.
2. **Present these findings in a form that is readily integrated into load calculation and energy simulation tools.** Because load calculation and energy modeling

software do not access detailed information about flow fields and temperature fields in room, convection correlations developed in this project needed to be developed as a function of only a few variables: namely volumetric flow rate or air exchange rate, diffuser type, set point temperature, supply temperature, and a single window or wall temperature. Previous work by other authors (Spitler et al. (1991) and Fisher and Pederson (1997)) shows that modeling convection as only a function of volumetric flow rate and surface-supply temperature difference provides correlations with an acceptable degree of error in the intended application (load calculation or energy modeling). Goldstein and Novoselac (2010) also found that when describing convection in perimeter zones with ceiling slot diffusers, variables such as jet momentum, slight variations in diffuser location, and room-supply temperature difference did not need to be included in correlations to keep uncertainty under an acceptable level. This work follows the conventions used in these three works.

Two hypotheses were made prior to the investigation. The first is that, in order to accurately predict thermal loads, window surfaces near floor diffusers must be treated as a situation distinct from other surfaces in regards to convection heat transfer. This means that existing convection models for either forced or natural convection at interior surfaces will need to be augmented and modified in order to capture the behavior of jets issuing from floor registers near windows. The second is that convection heat transfer at windows can be described by a function of three variables: supply temperature, window temperature, and supply velocity, which was found to be the case in earlier work for different diffusers, as discussed above.

METHODOLOGY

All experiments conducted in the course of this investigation were performed at the Center for Energy and Environmental Resources (CEER) at the University of Texas at Austin. Experiments were conducted in a large environmental chamber with interior dimensions of 4.5 m×5.5 m×2.7 m high (14.8 ft×18.0 ft×8.9 ft). U-values of the chamber walls are 0.2 W/m^{2}K (.035 BTU/hft^2°F). More detailed information on the environmental chamber, as well as detailed information on preliminary sensitivity analyses, can be found in Goldstein and Novoselac (2010). For the purpose of the current experiments, a 0.3 m (1ft) deep raised floor was built into the chamber floor. The floor was sealed on its top surface to prevent air infiltration between the space proper and the plenum under the floor. The raised floor housed an insulated flexible duct along its length leading to two diffuser boxes separated by 0.5m (1.6 ft) and standard CT-PP-0 1.22m × 10.2cm (4ft × 4in) grille registers with 0° pitch. The diffusers were located 10cm (4in) from the wall, parallel to and centered on the wall.

The experimental setup was first validated by using it to calculate natural convection correlations. Convection correlations were calculated using an energy balance at the wall or window surface, and then correlated to the proper governing variable (wall-room temperature difference for natural convection and average velocity near the wall for forced convection). Much more detailed information about the calculation procedure, instruments used, correlation of final results, sensitivity of parameters, and the quantification of experimental uncertainty is available in Goldstein and Novoselac (2010), in which the same experimental chamber and methods were employed. As

established natural convection correlations are available in the literature, matching values calculated with the current setup confirmed the accuracy of the current methodology.

During the course of the investigation, several different window configurations, HVAC regimes, and flow rates were tested. Window configurations analyzed were: A) a floor-to-ceiling window, B) a 1.3m high window above a coplanar wall, and C) a 1.3 m high window above a wall protruding into the space. These are displayed in Figure A1 below. Windows heated by long-wave radiation were simulated with electrical resistance heating panels as further described in Goldstein and Novoselac (2010).

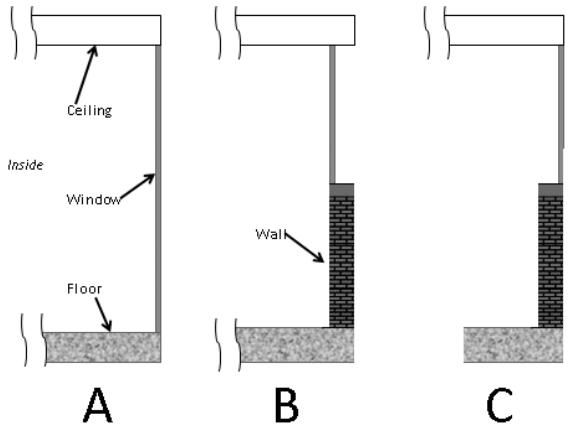

Figure A1. Three different window configurations analyzed. Configuration A is a floor-to ceiling window, Configuration B is a window with interior surface coplanar with the interior wall surface, and Configuration C is a window with interior face recessed into the wall.

Set point temperature was maintained at 23ºC (73 ºF) during all experiments. Supply temperature varied by experiment, but was maintained in the range of 7-21 ºC (45-70 ºF). Constant heat fluxes were sent to electrical resistance panels on the walls which maintained wall and window temperatures in the range of 24-32 ºC (75-90 ºF) for

the cooling condition experiments. For heating condition experiments, a nearly constant-temperature boundary condition was maintained at the window surface through the use of hydronic panels. Temperatures of the walls were maintained at 14-22 ºC (57-72 ºF). Other walls of the chamber were near set point temperature throughout experiments, with deviations of 1-2 ºC (2-4 ºF) witnessed due to radiative heat transfer with the window.

The following experimental matrix (Table A1) categorizes the experiments by the configuration analyzed, HVAC regime tested, and ventilation rates (ACH) at which the experiments were conducted. In the HVAC regime column, cooling signifies the summer condition in which supply air is cooler than room air. Very large ΔT corresponds to a supply-return air temperature difference of 16±1°C (29°F); large ΔT to 12±1°C (22°F); medium ΔT to 8±1°C (14°F)**;** small ΔT to 4±1°C (7.2°F); and very small ΔT to 2±1°C (3.6°F).

Configuration	HVAC regime	Ventilation rates
A. Floor-to-ceiling window	Cooling: Very Small ΔT, Small ΔT, Medium ΔT, Large ΔT, Very Large ΔT Heating: Small ΔT, Large ΔT	0-135m^3/h// meter of perimeter wall (0-79cfm/ft)
B. Half window	Cooling: Large ΔT	40-135m^3/h// meter of perimeter wall(24-79cfm/ft)
C. Extruded wall/sill	Cooling: Small ΔT, Large ΔT	40-135m^3/h// meter of perimeter (24-79cfm/ft)wall

Table A1. Experimental Matrix

RESULTS

The following section presents and analyzes the results of the experimental validation and correlation development phases of the study.

Validation of Experimental Setup

As a baseline case and as a verification of experimental accuracy, a floor-to-ceiling window with associated flow fields created by only air temperature differences was simulated in the chamber. The convection coefficients associated with this configuration are given in Figure A2 below. In Figure A2 and others to follow, "h_{room}" designates a convection coefficient developed with the bulk room temperature as the reference temperature. Similarly "h_{supply}" uses the supply temperature as a reference. T_{room} refers to the bulk room temperature and T_{supply} to the supply temperature. Figure A2 provides comparison of the natural convection coefficients measured in the current experiments with those previously developed by Awbi and. Hatton (1999). The small (<10%) difference can be explained by the fact that the reference temperature used by Awbi and Hatton was the temperature 10cm from the wall, while the current experiment used the bulk room temperature. When the same convention is used, the resulting correlations are coincident. However, as the current investigation seeks to develop correlations that are

easily included in load calculation and energy simulation programs, this correlation is not

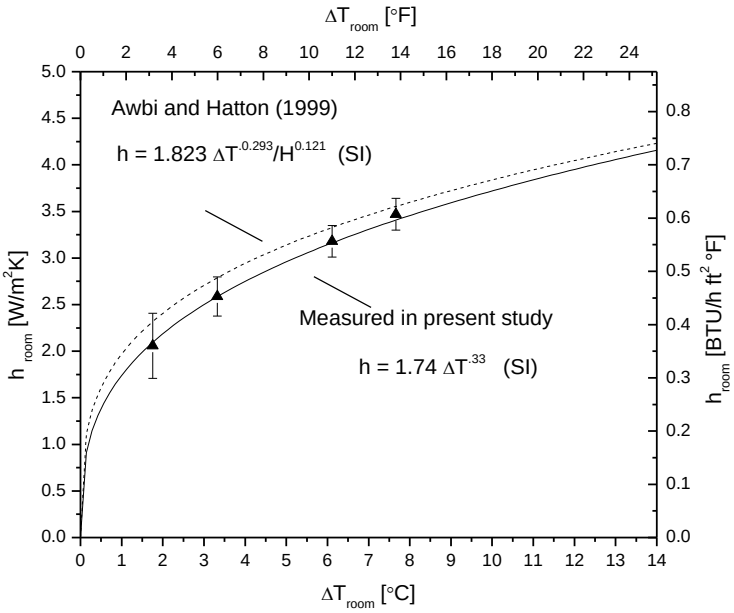

given.

Figure A2. Results of natural convection experiments for floor-to-ceiling window

Forced Convection Heat Transfer: Cooling Condition

The set of experiments conducted to analyze forced convection in window assemblies are the core of the current work. The results are given in the following sections.

The simplest configuration analyzed was that of a floor-to-ceiling window being cooled or heated by the jet from an adjacent floor register. The first situation analyzed was that of a floor register being used to provide space cooling. This situation presented a unique modeling challenge in that since a cold jet was entering a relatively warm space, it was required to overcome the negative buoyant force exerted on it, and it was not known previously how this would affect heat transfer at the window surface. Results for

various supply-room air temperature differences are given in Figure A3 and show that the average convection heat transfer coefficient for the full window surface varies nearly linearly with volumetric flow rate.

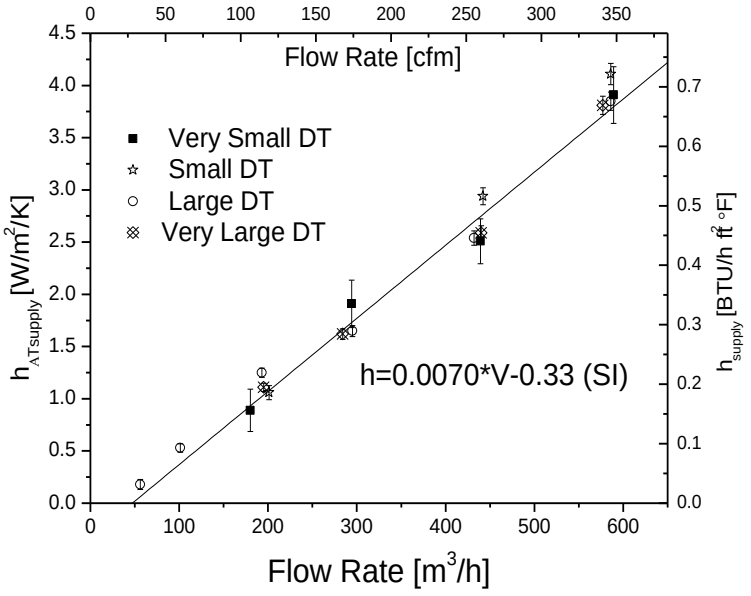

Figure A3. Results of forced convection experiments for floor-to-ceiling window correlated to volumetric flow rate

The linear dependence shown in Figure A3 contrasts with previous work that showed indoor convection usually could be modeled as a function of volumetric flow rate to an exponent of 0.8 (Goldstein and Novoselac 2010, Fisher and Pederson 1997), and flat plate turbulent convection theory which predicts convection as a function of velocity to a power of 0.8. This discrepancy is due to the effects of buoyancy slowing down the jet at lower flow rates and thus reducing convection. Since inclusion of competing buoyancy and momentum effects in the correlations being developed in this study would require information on local velocities and temperature differences, which contradicts the

objectives of this work, they will not be discussed further. The given correlation should be sufficient for load calculation and energy modeling applications. While the correlation would give negative values for very low flow rates, these flow rates are never found in practice. As can be seen from Figure A3, it is robust for a wide range of supply-room temperature differences, although it admittedly does not directly include this difference in the correlation and it does not follow directly from the physics of the problem.

Forced Convection: Heating

Heat transfer from a warm jet issuing from a floor register was also analyzed for a floor-to-ceiling window. Results from the heating condition experiments are shown in Figure A4. Heating condition results are shown to conform better to the exponential dependence on volumetric flow rate (0.8) that was found in previous research on indoor convection. One should also note that the magnitude of the convection coefficients developed for the heating condition is roughly 50% higher than those for the cooling condition, suggesting buoyancy significantly affected the jets in one or both of the conditions. While there is a small but noticeable difference in the two values of supply-room temperature difference analyzed, the correlation presented should provide for more accurate load calculations and energy models than currently used conventions. .

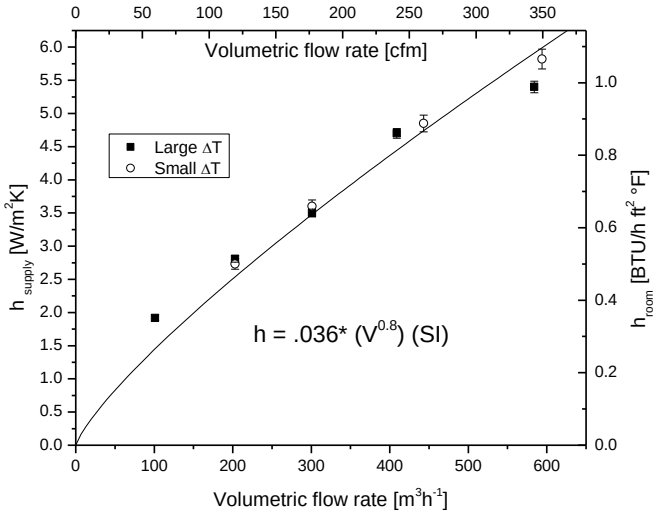

Figure A4. Heat transfer results for heating condition at floor-to-ceiling window surface

Coplanar Wall

Another configuration present in many commercial buildings today is that of a small wall with a coplanar large window above it (Configuration B in Figure A1). In this case, the change in radiative and conductive properties at the lower surface affects the convective heat transfer from the overall surface. In the situation in which a small wall is located below a window, and its inner surface is flush with the window, it would be expected that flow patterns along the wall would be only minimally affected by the energy supplied to the flow by the bottom surfaces, and depend primarily on supply and room conditions. This hypothesis was tested and the results for both the wall surface and the window are presented below.

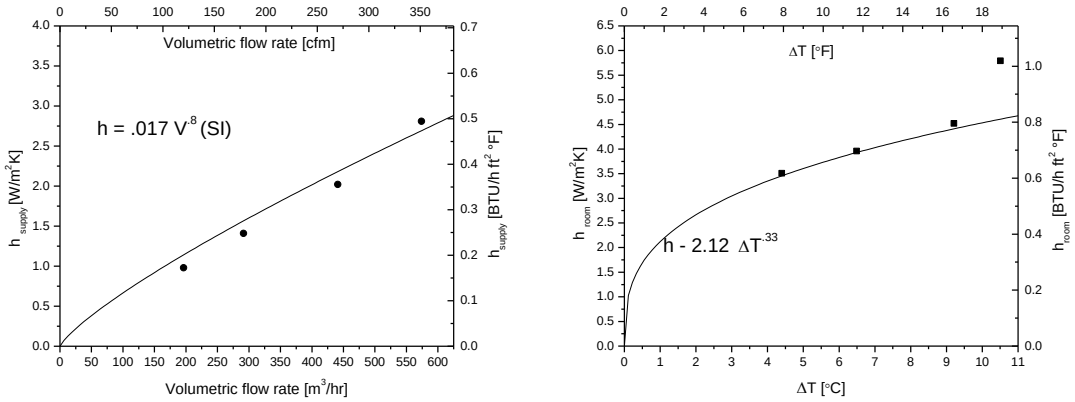

Figure A5. Heat transfer from window surface above coplanar wall correlated to both temperature difference (right) and volumetric flow rate. (left).

Figure A5 shows that for the purposes of predicting heat transfer from the window surface with a noticeable degree of error, a function of the form expected for turbulent forced convection can be employed. However, a correlation of the form corresponding to natural convection more accurately captures the heat transfer process for low (<500 m^3/hr, <300 cfm) flow rates. All experiments used to generate Figure A5 were conducted with a relatively large (~12°C, 21.6°F) temperature difference between the supply and room air. Looking at Figure A5, a logical conclusion to be drawn is that the jet issuing from the diffuser fails to reach the window surfaces except for the largest ventilation rate. Under conditions used in these tests, the window surface is likely being cooled by natural convection only for all ventilation rates tested below 12ACH.

Convection coefficients were also calculated for the wall surface. Figure A6 shows the results correlated to the volumetric flow rate. As can be seen, results correlate to a function of the form $h = C\dot{V}^n$ where n is slightly larger than one. This coincides roughly with heat transfer results from previous studies (e.g. Song et al. 2000) of offset

jets in the impingement region, although no more definitive explication of results can be given without further understanding of the mechanisms involved.

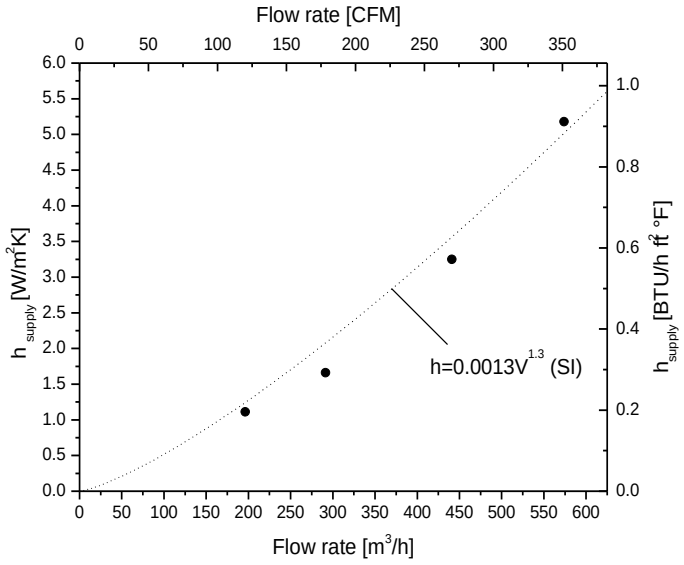

Figure A6. Heat transfer from wall surface below coplanar window correlated to volumetric flow rate

Experiments were conducted to test whether the horizontal position of the window surface relative to the wall below it affected the heat transfer from either surface. In this case, an extruded wall which protruded 9 cm (3.5 in) beyond the plane of the window was simulated below the heated window. As can be seen from Figure A7, the heat transfer from the window surface correlates fairly well to the volumetric flow rate. The right-hand figure in Figure A7 shows heat transfer coefficients do not correlate well to temperature difference, suggesting forced convection is dominant. It should be noted

that, as expected, the constant in the correlations $h = C\dot{V}^{0.8}$ is slightly smaller than the situation in which the window is flush with the wall surface. This is expected, as some loss of energy is likely to occur when the jet briefly detaches from the wall at the sill of the window and causes an eddy to form in the window-sill corner. Wall results again correlate to volumetric flow rate to a power greater than one, as seen previously.

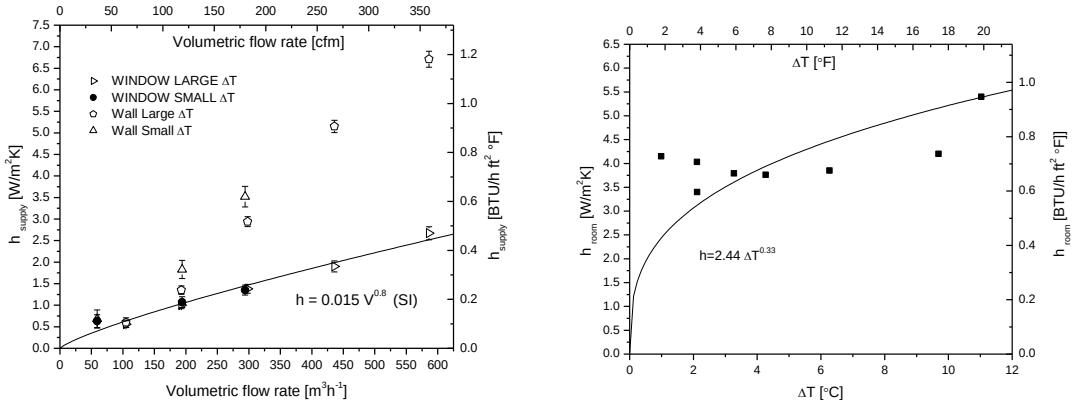

Figure A7. Heat transfer results at both wall and window surfaces for extruded wall configuration correlated to volumetric flow rate (left) and for window only correlated to wall-room temperature difference (right) for comparison with Figure A5.

Summary of Correlations

The correlations developed for various configurations are given in Table A2. In order to allow for use in perimeter zone rooms with depths (measured normal to the window surface) different than the environmental chamber used in the experiments, correlations are given as a function of volumetric flow rate divided by the length (L) of the window or external wall shown in Figure A8 (for experimental set-up used in this study L was 4.5m or 15ft). This should not be understood as a normalization resulting in

general correlations, but rather as a means to ensure implementation into load calculations of different sized rooms is possible. A precedent in this regard was set in previous work on forced convection modeling. Convection coefficients are given in [W/m^{2}K] for SI correlations and [Btu/h·ft2·°F] for IP correlations. The letters A, B, and C refer to Figure A1.

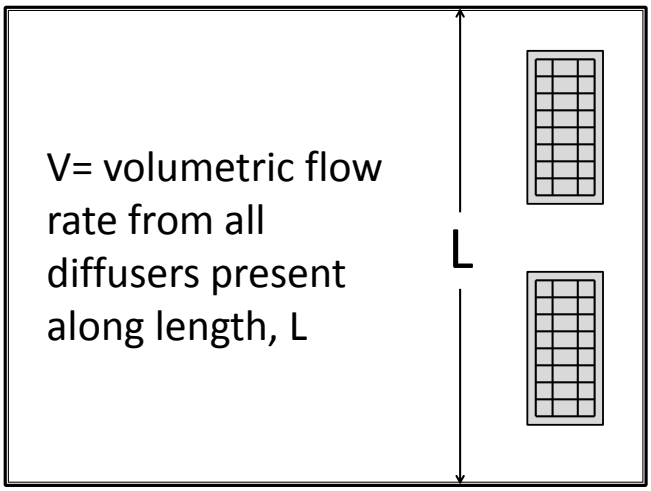

Figure A8. Schematic of a perimeter zone room and its corresponding definitions for V and L which are used in Table A2.

Configuration	HVAC Regime	Domain	Correlation
Floor-Ceiling Window (A)	Cooling	$(\dot{V}/L) \le 160 m^3/hr \cdot m$ $(\dot{V}/L) \le 29 cfm/ft$	$h = 0.032(\dot{V}/L) - 0.33(SI)$ $h = 0.022(\dot{V}/L) - 0.22(IP)$
Floor-Ceiling Window (A)	Heating	$(\dot{V}/L) \le 160 m^3/hr \cdot m$ $(\dot{V}/L) \le 29 cfm/ft$	$h = 0.12(\dot{V}/L)^{0.8}(SI)$ $h = 0.082(\dot{V}/L)^{0.8}(IP)$
Half-Window (B)	Cooling, Low Flow Rates	$(\dot{V}/L) \le 120 m^3/hr \cdot m$ $(\dot{V}/L) \le 22 cfm/ft$	Window: $h = 2.12\,\Delta T^{0.33}(SI)$ $h = 0.031\,\Delta T^{0.33}(IP)$ Wall: Dependent on geometry
Half-Window (B)	Cooling, Large Flow Rates	$(\dot{V}/L) > 120 m^3/hr \cdot m$ $(\dot{V}/L) > 22 cfm/ft$	Window: $h = 0.056(\dot{V}/L)^{0.8}(SI)$ $h = 0.038(\dot{V}/L)^{0.8}(IP)$ Wall: Dependent on geometry
Extruded Wall Below Window (C)	Cooling	$(\dot{V}/L) \le 160 m^3/hr \cdot m$ $(\dot{V}/L) \le 29 cfm/ft$	Window: $h = 0.051(\dot{V}/L)^{0.8}(SI)$ $h = 0.035(\dot{V}/L)^{0.8}(IP)$ Wall: Dependent on geometry

Table A2: Summary of correlations

Implementation of Developed Correlations into Load Calculation Software

One challenge that is anticipated in using the correlations presented herein is the lack of knowledge of some of the variables necessary for using the correlations directly, e.g wall and window position, wall geometry, and operating regime. The further refinement of the correlations to account for buoyant effects, mentioned above, requires even more knowledge of the situation, including diffuser geometry. In the situation where correlations are used to calculate cooling loads or conduct energy modeling of new buildings these parameters are not known. For this reason, one correlation is given presently that can be used for all forced convection situations in perimeter zone with floor

registers, including walls and windows, when no further information is known. The correlation is:

$$h = 0.082\left(\dot{V} / L\right)^{0.8}(SI)$$
$$h = 0.055\left(\dot{V} / L\right)^{0.8}(IP) \quad (1)$$

where L is the horizontal length of the perimeter wall or window in question and $\dot{V}$ Is the total volumetric flow rate from all diffusers present along this length. This correlation is a best fit of the combined results of the floor register experiments contained in this paper, and is shown in Figure A9. Results show an accuracy definded by a ratio between residual sum of squares and total sum of sqares ($1\text{-}R^2$) of ±45%. This correlation should only be used when no further information is known. It should be noted that despite the large degree of scatter and uncertainty in the correlation, this still represents an improvement to currently used models, such as single-value models or a natural convection assumption.

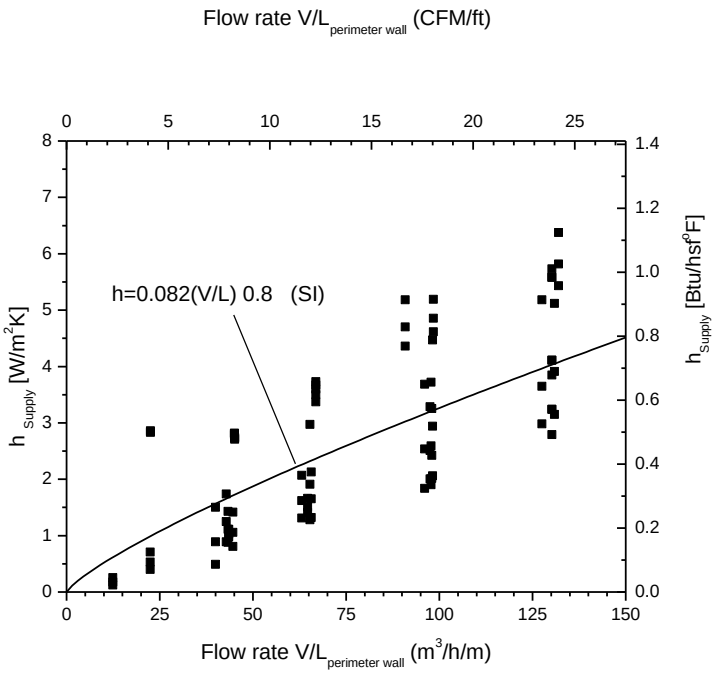

Figure A9. Convection correlation based on all experiments conducted with floor registers (excluding experiments with blinds)

Furthermore, when compared with analogous results from experiments with a ceiling slot diffuser near a perimeter wall, taken from Goldstein and Novoselac (2010), the results match up well as shown in Figure A10. Goldstein and Novoselac did extensive analysis of the effect of various parameters, such as diffuser type (single or double slit), diffuser location (distance from the perimeter wall), window location and size, operating regime (heating/cooling), wall geometry (different sill sizes). All results from Goldstein and Novoselac's study with ceiling diffusers are contained in Figure A10. Figure A10 shows that the generalized correlation presented in Equation (1) has an accuracy similar to the analogous floor diffuser correlation. Therefore one may use

Equation (1) for any forced convection situation on perimeter walls or windows, when more detailed knowledge of the building is not known.

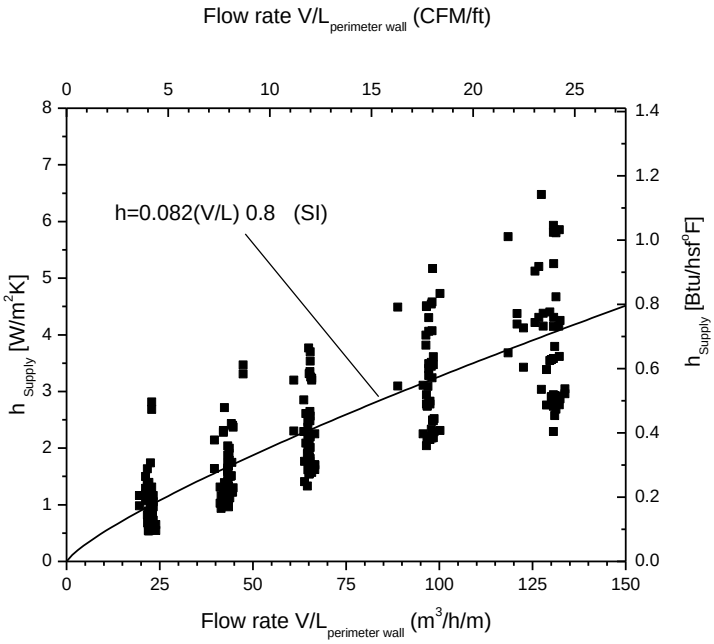

Figure A10. Combination of ceiling slot diffuser results with fit of all data (Goldstein and Novoselac 2010)

While the scatter in data in Figures A9 and A10 may seem large when compared to specific correlations presented in Figures A2–A7, or the one presented by Goldstein and Novoselac, the resulting overall uncertainty in the final load calculation is on the order of that caused by lack of precision in various other input parameters, such as exterior convection coefficient, weather variables, occupancy, etc. Furthermore, this generalized correlation for perimeter walls with floor registers or ceiling diffusers is still far more accurate in this particular situation than using convection correlations developed for natural convection (i.e. Awbi and Hatton, 1999) or forced convection

correlations developed for use with ceiling diffuser (Fisher and Pederson, 1997), as is currently done. With this correlation and those given previously, the designer should have flexibility in the level of resolution which he or she can employ, based on how much information of the situation he or she has and the level of accuracy desired.

Discussion and Conclusion

In the course of this investigation, convection correlations were developed for heat transfer due to jets from floor registers, under three different window geometries. Simple models were put forth for prediction of heat transfer at perimeter walls which can be used when all information about a building is not known. These models take as their input only the volumetric flow rate, the general type of diffuser in the room, the window or wall temperature, and the set point temperature. All of this information is available to a designer calculating heating or cooling loads or to an energy simulation software package. The analysis admittedly lacks a full accounting of the physical processes which occur, such as buoyant effects on the jet, local driving temperature differences, etc., but it does so in order to be easily integrated into the applications for which it was intended. When warranted, separate correlations are given for heating and cooling conditions, but the supply-room temperature difference is not included directly in the functional form of the correlations as its inclusion would only minimally improve the accuracy of the correlations and require more information, some of which may not be available. The analysis was also limited to one representative diffuser layout. Care was taken to consult practitioners in order to determine the most representative setup, but deviation from the correlations given herein will certainly occur for very different setups. Further research which accounts for additional phenomena, such as the effects of blinds on heat transfer at

windows and the effect of buoyancy on diffuser jets, could improve the models given herein.

ACKNOWLEDGMENTS

This research is funded by the American Society of Heating, Refrigerating and Air-Conditioning Engineers and Jordan Clark is partially supported by a National Science Foundation (NSF) IGERT traineeship in Indoor Environmental Science and Engineering (Award DGE-0549428). The authors thank the members of the RP-1416 Project Monitoring Subcommittee for their useful suggestions and advice and Dr. Leen Peeters from the University of Brussels for her help with experiments.

REFERENCES

Alamdari, F., G.P. Hammond, and C. Melo. "Appropriate calculation methods for convective heat transfer from building surfaces." *Proc. 1st U.K.: National Conference on Heat Transfer*, no. 2 (1984): 1201-1211.

Awbi, H.B. "Calculation of convective heat transfer coefficients of room surfaces for natural convection." *Energy and Buildings*, 1998: 219-227.

Awbi, H.B. and Hatton, A. "Natural convection from heated room surfaces."*Energy and Buildings* no.30 (1999): 233–244.

Beausoleil-Morrison, Ian. "An algorithm for calculating convection coefficients for internal building surfaces for the case of mixed flow in rooms." *Energy and Buildings*, no. 33 (2001): 351-361.

Beausoleil-Morrison, Ian, and Paul Strachan. "On the significance of modeling internal convection in dynamic whole-building simulation programs." *ASHRAE Transactions*, 2001: 929-939.

Fisher, D.E., and C.O. Pederson. "Convective heat transfer in building energy and thermal load calculations." *ASHRAE Transactions* 103, no. 2 (1997): 137-148.

Goldstein, K. and A. Novoselac. “Convective Heat Transfer in Rooms with Ceiling Slot Diffusers (RP-1416)” *HVAC&R Research*16, no. 5 (2010): 629-655

Khalifa, A.J.N. *Heat transfer processes in buildings.*Ph.D Thesis, Cardiff, U.K.: University of Wales College of Cardiff, 1989.

Lomas, Kevin J. "The U.K. applicability study: an evaluation of thermal simulation programs for solar passive house design." *Building and Environment* 31, no. 3 (1996): 197-206.

Song, Heung Bok, Hyun Yoon Soon, and DaeHee Lee. "Flow and heat transfer characteristics of a two-dimensional oblique wall attaching offset jet." *International Journal of Heat and Mass Transfer*, no. 43 (2000): 2395-2404.

Spitler, J.D., C.O. Pederson, and D.E. Fisher. "Interior convective heat transfer in buildings with large ventilative flow rates." *AHSRAE Transactions* 97, no. 1 (1991): 505-515.

Waters, J.R. "The experimental verification of a computerised thermal model for buildings." *Building Services Engineering Research and Technology* 1, no. 2 (1980): 76-82.

Appendix B: Experimental Study of Convective Heat Transfer from Windows with Venetian Blinds

Jordan Clark, Leen Peeters, and Atila Novoselac

A**bstract**

To provide for more detailed and accurate load calculations and energy simulation of buildings, the effect of blinds on convection heat transfer at interior window surfaces was analyzed. Based on full-scale experiments in an office-size chamber for various diffuser locations, window geometry, and blind angles, the study provides convective heat transfer models for natural convection, forced convection due to a ceiling slot diffuser, and forced convection due to a floor register. Results are given in the form of correlations which relate either supply volumetric flow rate or room-surface temperature difference to convection heat transfer at both window and exterior wall surfaces. Results show that heat transfer is dependent on supply flow rate, blind angle, diffuser location and window configuration. Results are compared against previously reported data and show that convection in cases with blinds follows the same form as often arises in turbulent forced convection situations, but differs appreciably in magnitude from previously given models for bare windows. These results should allow for more accurate simulation of energy use in buildings and contribute to the construction of more energy efficient buildings.

1. INTRODUCTION

As load calculation and energy simulation methods become more accurate, more detailed models must be created to include the effects of different architectural

components and systems in the calculations. Heat transfer processes in window assemblies strongly influence the overall thermal load in a space, and this area offers ground for additional research. While heat transfer at bare window surfaces, and in small isolated window-blind assemblies has been analyzed, little full-scale work on floor-to ceiling windows with blinds, which exist in a large portion of commercial construction today, currently can be found in the literature. To this end, experiments were conducted to determine the effect of blinds on heat transfer through windows under a variety of thermal conditions and geometries.

Many researchers have investigated convection heat transfer at indoor surfaces. Among these, Waters [1], Alamdari et al. [2] and Lomas [3] have demonstrated the importance of selecting a proper model for indoor convection in accurately performing load calculations. Correlations pertaining to natural convection heat transfer at interior surfaces have been developed [2,4,5], while others [6-8] have analyzed forced convection from interior surfaces. Additional researchers [9-10] have created correlations for situations which could not be properly classified as either forced or natural convection.

Much effort has also been expended toward the goal of understanding the complex process whereby energy is transferred via natural convection heat transfer at a blind-window assembly. Collins et al. [11] conducted a numerical study of an isothermal flat plate adjacent to a set of Venetian blinds which were assumed to be irradiated by solar radiation with a constant flux. Shahid and Naylor [12] numerically analyzed a double-pane window with an adjacent set of Venetian blinds. Many investigations of a sealed window cavity which houses an internal set of Venetian blinds have been conducted [e.g.13-15].

Experimental studies in the same vein have been conducted as well. Machin et al. [16] performed an experimental study of convection heat transfer from a small (0.38m×0.36m) window-blind assembly. Results were reported for one surface-air temperature difference (20°C) and four blind angles: -45°,0°, +45° and -90°. Flow visualization showed a cellular flow field between blinds, of the type expected in an enclosure. Machin et al. [16] observed that heat transfer at the window surface in some instances was greater when covered with blinds than the similarity solution for a flat plate without blinds. Collins et al. [11] validated their numerical study with an experimental evaluation of their results. The main limitation of the experimental setup was that it would be most valid for a small window (.2 m × .4 m) which was embedded into a wall cavity. Cuevas et al. [17] recently studied natural convection at window surfaces with blinds in a small-scale setup.

Recently, Wright et al. [18] have attempted to synthesize most of the existing knowledge on radiative and convective heat transfer through fenestration systems into one complete model. The model includes complicated radiative heat transfer processes through systems several layers thick, and includes multiple surfaces within one system which transfer energy through convection. A full-scale floor-ceiling window, such as is present in much of contemporary commercial construction has not yet been analyzed. Forced convection in window-blind assemblies also has yet to be studied. The objective of the presented study is to bridge some of the gaps in the knowledge about convective heat transfer at complex surfaces such as windows with Venetian blinds.

The specific objectives of the present study are to (1) determine whether existing correlations for natural convection at windows covered with blinds, which were

developed for small windows, are applicable to floor-to-ceiling windows and (2) develop new correlations describing forced convection in the same situation. The two basic hypotheses investigated in this study are (A) floor-to-ceiling windows will experience heat transfer that is appreciably different from a small window under buoyant flow conditions due to the larger length scales inherent in the process, and (B) forced convection at windows with blinds will be less effective than the bare window situation

The following sections describe the experimental methodology used to analyze convection in blind-window assemblies. Results of these experiments are then given and compared with existing work. Models for predicting convection in these situations are given and their applicability is discussed.

2. METHODOLOGY

The basic research tools for the investigation described in this paper were experiments in a full scale test room. The experiments were conducted in the Center for Energy and Environmental Resources (CEER) at the University of Texas at Austin. This section provides a description of the experimental setup used, the methods employed in the experiments, methods and assumptions made in calculation of radiative and convective heat transfer, and the method used for the formulation of the experimental results.

2.1 Test room set-up

Experiments were conducted in a full scale test room / environmental chamber at the CEER. The environmental chamber has interior dimensions of 4.5 m× 5.5 m × 2.7 m high. U-values of the chamber walls are 0.2 W/m^2K. For experiments analyzing forced

convection from surfaces near a ceiling slot diffuser, a 0.3 m deep drop ceiling was built into the chamber. The ceiling was sealed on its bottom surface to prevent air infiltration between the space proper and the plenum above the ceiling. The drop ceiling housed an insulated flexible duct along its length leading to two diffuser boxes and two ceiling double-slot diffusers (Titus ML 39), 1.2 m long each, spaced 0.5 m apart. For floor register experiments, the ceiling was removed, and the duct placed in a 0.3m high raised floor. The plenum beneath the floor was sealed and the duct attached to diffuser boxes were fitted with two standard, 1.2 m long grille registers with 0° pitch (Titus CT-PP-0).

The chamber itself has a dedicated and modifiable control system capable of supplying air between 6 and 50°C, with a relative humidity between 2% and 99%. Flow rates corresponding to ventilation rates between 0 and 15 air changes per hour (ACH) are achievable. The chamber contains supply and return fans capable of maintaining a pressure of 0 ± 0.5 Pa gage in the chamber. Flow rate measurements were calibrated prior to commencement of the experiments and found to be accurate within 5%. The chamber also contains hydronic cooling coils embedded into one wall capable of simulating a winter condition. Thin electrical resistance heaters are placed on walls and floor to simulated internal loads and conduct natural convection investigations.

The chamber walls, floor and ceiling were divided into 14 sections as shown in Figure B1. Short-wave solar radiation transmitted through the window and internal loads such as computers and occupants were also simulated with electrical resistance heaters on the floor and portions of the side walls, respectively. In calculating the radiation heat transfer during the course of the experiments, each section was assumed to be isothermal

and the temperature of the surface was given as the average of at least two temperature measurements on the surface.

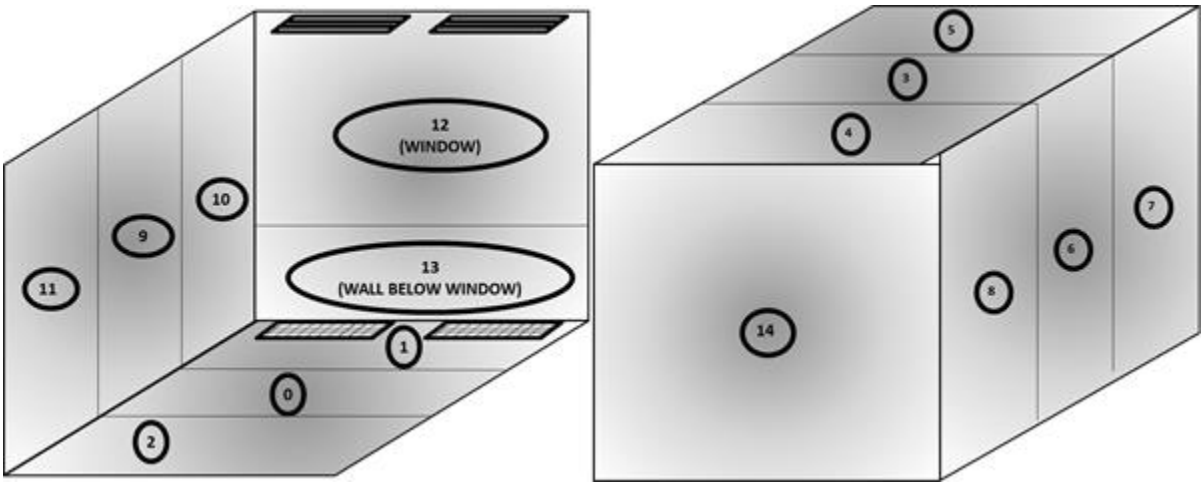

Figure B1. Schematic of chamber characteristic surfaces with wall, window, and diffuser location

One wall of the environmental chamber was designated the "window" of the chamber (See Figure B1) and was heated with thin electrical resistance heaters to simulate a pane of glass absorbing long wave solar radiation. For the winter condition, the window was cooled with hydronic cooling coils to simulate losses to the exterior environment. Two window configurations were analyzed, corresponding to the two most common window configurations found in typical contemporary commercial construction. A depiction is shown in Figure B2. "Configuration A" was that of a floor-ceiling window. "Configuration B" was comprised of a 1.03 m high wall below a 1.37 m high window in the same plane. Thin electrical resistance heaters simulating the heated wall

were taped continuously to the chamber surface and then additionally taped continuously to each other to avoid any air movement between the heaters and the wall.

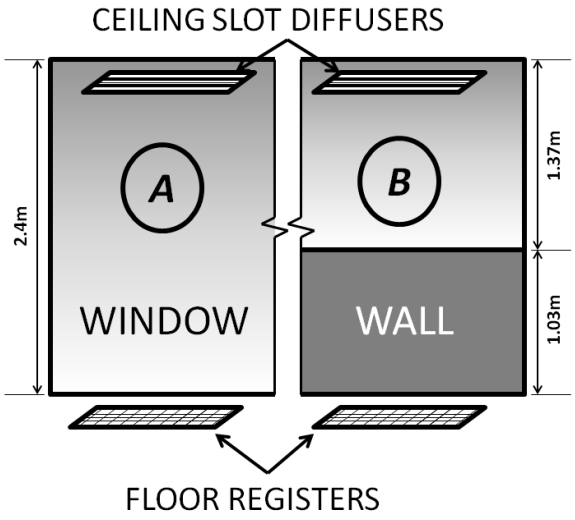

Figure B2. Distinction between two analyzed configurations. Configuration A is a floor-to-ceiling window while configuration B is a window above a small wall.

The specific configuration of the wall designated the "window" changed based on the particular situation being analyzed. In experiments simulating Configuration A, equal heat fluxes were sent to all portions of the wall. In Configurations B, a flux corresponding to only conduction heat transfer through the wall was sent to the "wall" portion, and a larger flux simulating the absorbed long-wave solar radiation was sent to the window. Standard commercial Venetian blinds, 2.5 cm wide and spaced at 2.2 cm vertically, were placed 2.5 cm from the window surface, which is the standard distance of installation in commercial construction.

2.2 Instrumentation

During the selection of the measurement instrumentation, focus was placed on increasing the accuracy of instrumentation which measured the variables which had the largest impact on the uncertainty of the results. The following describes the equipment used.

Electrical power sent to the resistance heaters was measured with a power meter, accurate to 3% of the measured value. For the calculation of conductive losses through the wall an ITI GHT-1C-(210) electric power meter was used, calibrated to an accuracy of 1% of the measured value. Temperatures of all surfaces were measured with Omega 44033 thermistors accurate to ±0.1°C. The temperature of each of the surfaces was taken to be the average of at least two thermistor readings. When blinds were employed, six dedicated thermistors were attached to the blinds' surfaces. These temperatures were averaged to give one temperature, which was assumed to be the isothermal temperature of all blinds. Supply air, return air, and center-of-room air temperatures were also measured and included in the calculations.

Additional measurements and calculations were performed to verify the accuracy of the measured results, but not used directly to calculate convection correlations. These included calibration of the flow rate readings, which was accomplished with a duct blaster accurate to 5%. Also, general knowledge of flow fields near the wall was gained through the use of omni-directional anemometers accurate to 0.02m/s. A summary of the equipment used and associated uncertainties are given in Table B1.

Variable	Instrument Used	Accuracy	Comments
Supply and Return Volume Flow Rate	EBTRON GT Type A 116	5% of measured	Verified with duct bluster
Interior Surface Temperature	Omega 44033 thermistors	±0.1°C	Additional uncertainty introduced in averaging and radiation calc.
Supply Temperature	Omega 44033 thermistors	±0.1°C	
Electric Power	Brand Electronic Power Meter	3% of measured	
Exterior Air and Room Surface Temperature	Omega 44033 thermistors	±0.1°C	
Surface Emissivity	Measured by Oak Ridge National Laboratories	Assumed to be exact	Sensitivity analysis shown to negligibly affect final calculation
Conductive Losses through wall	ITI GHT-1C Flux meter	1% of measured	Used for calculation of UA value of chamber
Hydronic Coils Flow Rate	Omega FTB-9500	2% of measured	
Hydronic Coils Temperature	Encapsulated Omega 44033 thermistors	±0.17°C	

Table B1. Instruments Used and Accuracy

2.3 Calculation procedure

The calculation of convective heat flux, was accomplished by performing an energy balance at the window or wall surface as described by Equation (1):

$$\dot{Q}_{gen} + \dot{Q}_{convection} + \dot{Q}_{radiation} = 0 \qquad (1)$$

where $\dot{Q}_{gen}$ is the energy dissipated by the resistance heaters (W), $\dot{Q}_{convection}$ is the convective heat flux (W) and $\dot{Q}_{radiation}$ is the radiative heat flux (W).

Since the heat flux generated at the surface is known from the amount of energy sent to the surface, and the radiation heat transfer is calculated as described below, $\dot{Q}_{convection}$ can be calculated. Once $\dot{Q}_{convection}$ is known, h (convective heat transfer coefficient) is calculated according to Equation 2, given the measured air-surface temperature difference and the area of the surface:

$$Q_{convection} = A_{surface}\, h\, (T_{surface} - T_{air}) \qquad (2)$$

where A is the surface area in question (m^2), and T is temperature (K).

Once several particular values of h are calculated for particular ventilation rates and room-surface temperature differences, they are correlated together into an equation as a function of either temperature difference (natural convection), or flow rate (forced convection). The air temperature, to which Equation (2) refers, changes with the situation being analyzed. In natural convection experiments, it refers to the bulk air temperature. In forced convection experiments, it refers to the inlet temperature at the diffuser. These are the temperatures driving convection heat transfer from the surface.

To properly determine the radiative component of heat transfer from the window surface, view factors between various surfaces were calculated. All view factors used in radiation calculations were calculated with a Monte Carlo simulation. View factors

between surfaces change with the angle at which blinds are set, and thus a new Monte Carlo simulation was conducted for each blind angle. The geometry of the enclosure, including the blinds, was drawn with AutoCAD for each experiment. This drawing was then imported into Sinda/Fluint RadCAD and a calculation for the view factors between each surface was performed by running a Monte Carlo simulation with two million rays. With this number of rays, an accuracy of 0.5 % was achieved for the view factors. These view factors were then imported into a program developed by the researchers and radiation heat transfer between each surface in the experiment was calculated. Emissivities of surfaces were determined by Oak Ridge National Laboratories. Emissivities used in the radiation calculation were 0.89 for electric heaters, 0.87 for paper, 0.9 for the blinds, 0.84 for tape, and 0.2 for aluminum and stainless steel. For more information on the radiation calculation please refer to reference [8].

To provide correlations which are readily usable by energy analysts, a few modifications to the traditional form of correlations were made. First, correlations are given which relate heat transfer at a surface to the difference between the surface temperature, and either the bulk room temperature (natural convection) or the supply inlet temperature (forced convection). Secondly, forced convection correlations are given as a function of supply volumetric flow rate. This convention is adopted from Spitler et al. [6].

2.4 Quality Control and Uncertainty Analysis

Measures were taken to minimize error in experimental design, experiment execution, and data processing. The uncertainty in the measured and processed data for

all developed correlations was investigated in detail. Also, substantial effort has been dedicated to the design of experimental set-ups to ensure the robustness of the newly developed convection correlations and their applicability to a wide range of possible situations. A set of control measures was introduced to minimize the systematic or specific errors in the correlation development procedure. The following subsections briefly describe these control measures.

In the first phase of the project, a group of experiments was repeated to identify faulty sensors. For each experiment, multiple temperature and velocity sensors switched positions in the chamber. In addition, air flow rate was measured in the supply and return air ducts to prevent the failure of an experiment due to a faulty flow measurement. Furthermore, the symmetry in the experimental setup and comparison of temperatures and heat fluxes at the symmetric surfaces was used to check if there was any discrepancy in the experimental results. For example, very similar values of measured variables on surfaces of side walls improve the reliability of meshed values.

To test the whole correlation development process, experiments were conducted for an environment in which well-established correlations already exist. For this purpose we mimicked experiments for the development of correlations for natural convection at vertical surfaces in a confined space [5]. The agreement between experimentally measured coefficients and the previously developed correlation was good, and the details of this test are presented in the results section of this report.

Bulk room air temperatures within the chamber were maintained at or near the temperature immediately outside the chamber to minimize any conductive losses through the chamber walls. This, combined with maintaining the same pressure in the chamber as

in the surrounding environment, provided for very good thermal insulation and air tightness of the chamber and a precise mass and energy balance. Nonetheless, very small losses through the insulated walls were calculated to account for conductive losses. The energy balance was checked for each experiment. If the balance was satisfied, energy supplied to the chamber would equal energy removed according to:

$$\dot{Q}_{gen} - \dot{m}c_p(T_{air\ inlet} - T_{air\ outlet}) - \dot{Q}_{conduction\ losses} = X \rightarrow 0 \qquad (3)$$

where m is the mass flow rate of air (kg/s) and c_p is the specific heat capacity of air (J/kgK). The normalized energy balance was calculated by:

$$Balance = X/\dot{Q}_{internal\ sources} \qquad (4)$$

where $Q_{internal\ sources}$ indicates the power released in the chamber by the electrical heaters or absorbed by hydronic cooling panels. In experiments where the difference was greater than 10%, it was determined that the steady state condition in the chamber had not been reached and the experiments were discarded and/or repeated.

With the systematic error minimized as described in the text above, care was taken to precisely evaluate the uncertainty associated with each reported value. Uncertainty is given as a function of the imprecision inherent in all measured variables used to calculate a reported value. With the uncertainty in each measurement calculated, the effect on the final value calculated is determined based on the general uncertainty theory given in ASHRAE Engineering Analysis of Experimental Data [19]. As the convection coefficient is derived from the convective heat flux ($q_{surface\_convective}$) and reference temperature difference (ΔT: surface – supply air or surface – room air) the uncertainty in the convection coefficient is calculated based on:

$$\delta h = h\sqrt{\left(\frac{\delta Q_{surface\_convective}}{Q_{surface\_convective}}\right)^2 + \left(\frac{\delta \Delta T}{\Delta T}\right)^2} \quad (5)$$

The uncertainty in temperature difference is calculated by uncertainty in surface ($\delta T_{surface}$) and air (δT_{air}) temperature:

$$\delta \Delta T = \sqrt{(\delta T_{surface})^2 + (\delta T_{air})^2} \quad (6)$$

The uncertainty in the specific convective heat flux for a given surface ($Q_{surface\_convective}$) consists of the uncertainties in the heat fluxes used for its calculation:

$$\delta Q_{surface\_convective} = \sqrt{(\delta Q_{surface\_total})^2 + (\delta Q_{surface\_radiative})^2 + (\delta Q_{wall\_loss})^2} \quad (7)$$

where $Q_{surface\_total}$ is the uncertainty in an electric heat flux measurement for surfaces where electric heaters controlled the surface temperature. For surfaces where the hydronic system is used, the uncertainty in total heat flux was calculated with an equation similar to equation (6) based on the uncertainty in the water flow measurement and supply-return water temperature difference. Losses were calculated based on the U value of the chamber walls and the surface outdoor air temperature difference. The corresponding uncertainty Q_{wall_loss} is calculated based on the measured Q_{wall_loss} and the uncertainty in these two temperatures.

Due to the complex long wave radiation heat exchange between indoor surfaces, calculation of radiative heat flux is computationally very intensive and the calculation of the uncertainty in $Q_{surface\_radiative}$ is correspondingly intensive. The uncertainty calculation of $Q_{surface\_radiative}$ for each surface was built into the program code developed for the radiative heat flux calculation. The uncertainty in radiative heat flux for specific surfaces is based on view factors and includes uncertainties in radiative heat flux in-between this

specific surface and all outer characteristic surfaces in the test chamber. These were calculated based on uncertainties in surface temperatures and uncertainty in surface emissivity coefficients.

2.5 Experimental matrix

During the course of the investigation, several different window configurations, HVAC regimes, and flow rates were tested. The following experimental matrix (Table B2) categorizes the experiments by the configuration analyzed, HVAC regime tested, ventilation rates (ACH) at which the experiments were conducted, and the different blind angles which were tested. In the HVAC regime column, cooling signifies the summer condition in which supply air is cooler than room air. Large ΔT corresponds to a supply-return air temperature difference of 12±1°C; medium ΔT to 8±1°C; and small ΔT to 4±1°C. Room set point was maintained at 23°C for all experiments.

Configuration	**HVAC regime**	**Ventilation Rates**	**Blind Angle**
Configuration A, Natural Convection	Cooling Small, Medium, and Large ΔT	NA	-45°,0°,45°
Configuration A, Ceiling Diffuser	Cooling Large ΔT	2, 12 ACH	0°,45°,80°
Configuration B, Ceiling Diffuser	Cooling and Heating Small, Medium, Large ΔT	2-12 ACH	-80°,-45°,0°,45°,80°
Configuration A, Floor Register	Cooling Large ΔT	2-12 ACH	-80°,-45°,0°,45°,80°
Configuration B, Floor Register	Cooling Large ΔT	2-12 ACH	-80°,-45°,0°,45°,80°

Table B2. Experimental Matrix

3. RESULTS AND DISCUSSION

In this section, results of the various sets of experiments are presented. Results of natural convection experiments are presented first, followed by ceiling slot diffuser results, and then floor register results.

3.1 Natural Convection

Window Surface

An experimental analysis of the phenomenon of natural convection in a window-blind assembly was conducted for a floor-to-ceiling window with blinds. Results are correlated to the temperature difference between the window and the bulk room air (defined as the average of 8 sensors spread throughout the interior of the chamber) or between the blinds and the bulk room air, according to which surface the correlation describes. The results are given in the following paragraphs. In Figure B3 and others to follow, "h_{room}" designates a convection coefficient developed with the bulk room temperature as the reference temperature. Similarly "h_{supply}" uses the supply temperature as a reference. T_{room} refers to the bulk room temperature and T_{supply} to the supply temperature.

Convection coefficients which describe heat transfer at the window surface under natural convection conditions are given in Figure B3. The results show that when blinds are present, convection at the window surface is best described by a correlation of the form of

$$h = C\,(T_{surface} - T_{room})^{1/4} \qquad (8)$$

while the bare window case results correlate better to an equation of the form :

$$h = C\,(T_{surface} - T_{room})^{1/3} \qquad (9)$$

As correlations for laminar flow are typically given in the form of Equation (8) and those for turbulent flow in the form of Equation (9), these results suggest different near-window flow characters for situations in which blinds are present and those in which they are absent.

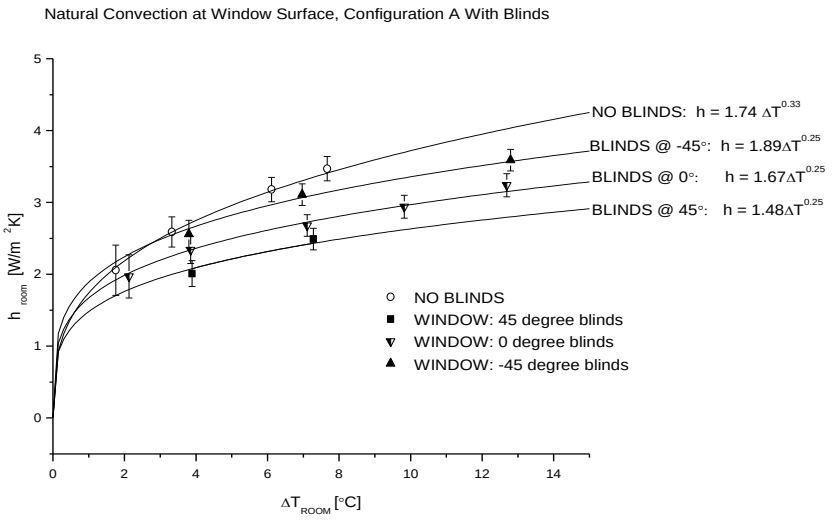

Figure B3. Natural convection coefficient at window surface for configuration A with and without blinds

One conjecture as to the reason for this is that when the blinds are present, the distance between the window surface and the nearest tip of the blinds is such that the boundary layer is never able to grow past a certain thickness, and thus eddies cannot develop and the flow never reaches turbulence (Figure B4). This conjecture is given some credence by flat plate natural convection theory which predicts a boundary layer with a thickness of the order 2cm for laminar flow and a transition to turbulent flow occurring on the wall in all situations analyzed [19]. This phenomenon would not be captured in an experimental setup shorter than roughly 1.5 m.

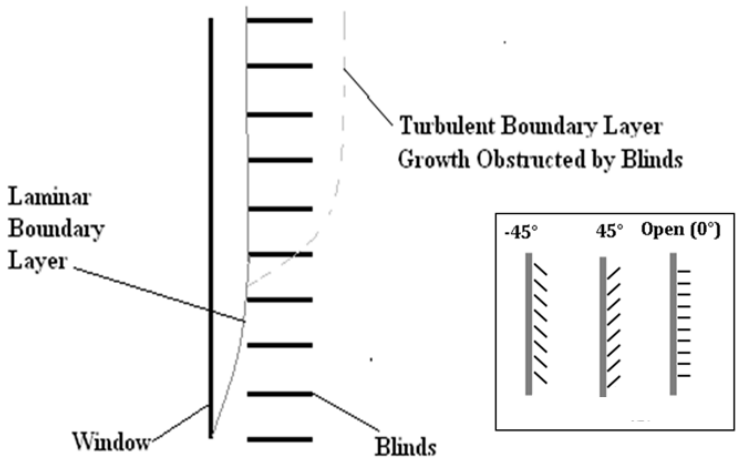

Figures B4. Boundary layer obstruction by blinds with the schematic of jet entrainment as a function of blind angle

The variation of the effectiveness of heat transfer with blind angle is most likely due to the variation in the ease of entrainment of room air into the gap between the blinds and the window surface, and thus the mass flow rate of air in the gap (Figure B4). At an angle of -45°, blinds are oriented nearly parallel with the natural direction of entrainment into the boundary layer, and thus entrainment is relatively easy. At a blind angle of +45°, blinds act as a barrier to the entrainment, which would naturally occur if blinds were not present. It should be noted that for blind angles of more than 45°, or less than -45°, the trend witnessed in the analyzed range would most likely not continue, as the path for entrainment through the blinds would become smaller and eventually reach zero, preventing entrainment altogether and significantly dampening the effectiveness of heat transfer at the window.

The current investigation can be employed to validate the approach put forth in ASHRAE RP-1311 [18]. The natural convection correlations suggested by Wright et al.

[18] are presented in Figure B5 in graphical form. The correlations assume the user has selected a convection coefficient of 3.5 W/m^2-K to describe heat transfer under natural convection conditions from a bare wall or window surface. As can be seen, correlations are given as a function of the distance between the glass and the shading layer, which in the case of the current investigation are the Venetian blinds. In the current investigation, blind-glass spacing is maintained at 25 mm. From the correlation given in the current investigation, a no-blinds convection coefficient of 3.5 W/m^2-K.

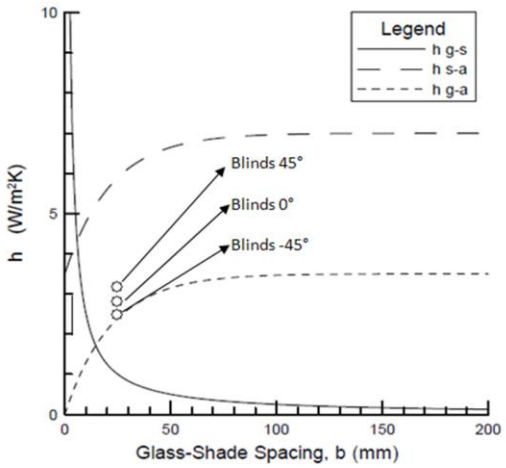

Figure B5. Comparison of results from this study with the results previously obtained by Wright et al. [18] (Model given in Wright et al. (2009) with superimposed experimental results from this study)

corresponds to a temperature difference of 8.1 °C. Points are plotted for this temperature difference, using the current correlations, superimposed on the graph depicting the correlations of Wright et al. [18] In Figure B5, h g-a (dotted line) describes heat transfer between the glass and the room air.

Results in Figure B5 show that current results are in relatively good agreement with the Wright et al. model, albeit slightly higher, likely because of the different experimental

setup. Results of the current investigation also vary with blind angle, as the Wright et al. [18] model does not. This trend is further demonstrated by Figure B6, which shows all results for the Configuration A, with convection coefficients scaled to compare them to a baseline h_c value of 3.5 W/m²K. As can be seen from the two figures, an allowance for change in the model due to blind angle would represent an improvement to the Wright et al. [18] model.

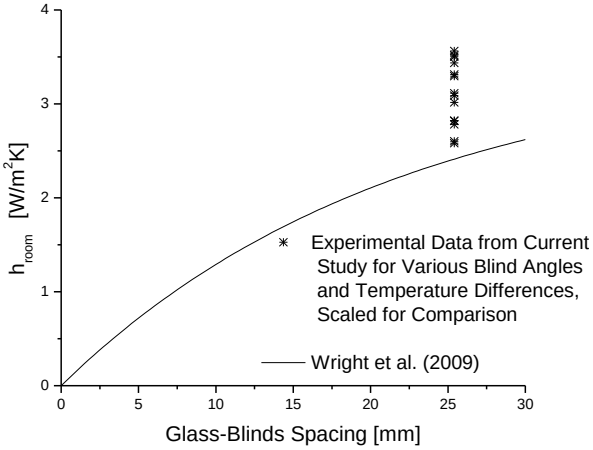

Figure B6. Comparison of results at all blind angles tested with Wright et al. [18] model (all results plotted are for Configuration A in Figure B2)

Blind Surfaces

Natural convection heat transfer at the blind surfaces was also analyzed and convection coefficients specifically for the blinds were calculated. Figure B7 shows the large degree of error inherent in the calculation precludes any definitive conclusion being drawn from the results. As the blinds used were not heated, the temperature difference between the blinds and ambient air was often very small, resulting in the accuracy of the thermistors

becoming relatively important. Future experiments with heated blinds will likely produce results with less uncertainty.

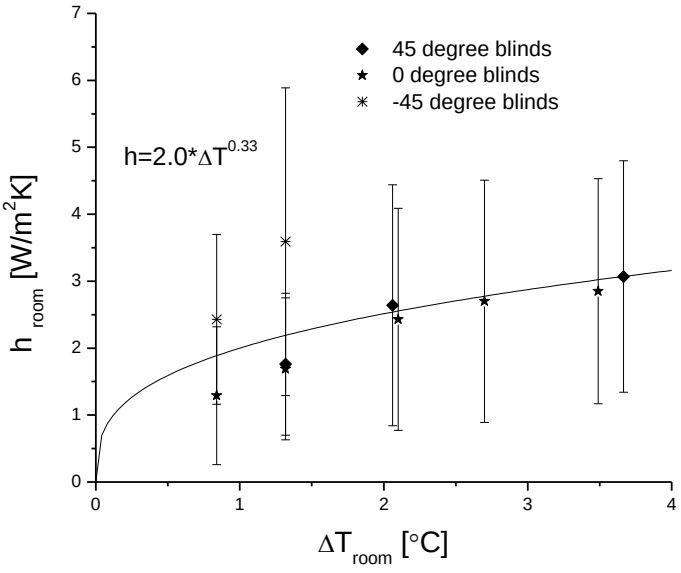

Figure B7. Natural convection coefficient at blind surfaces for Configuration A. ΔT_{room} refers to the difference between the average blind surface temperature and the average bulk room temperature. Solid line is a best-fits correlation with an exponent of 0.33 for the data.

These results can also be qualitatively compared with the model given in Wright et al. [18] to describe the effect of blind angle on convection heat transfer at the shading surface (Figure B8). It should be noted that data from the current experiment contains a large degree of error, as correlations are based on a small temperature difference between blinds and room air, thus inflating the significance of the ±0.1°C precision of the thermistors used. The comparison shows very good agreement between experimental data and the Wright et al. [18] model for blind angles of 0 and -45 degrees. However, the Wright et al. [18] model could be improved by including the effect of the blinds at 45

degrees blocking the flow into the assembly and decreasing the effectiveness of heat transfer at the blind surfaces.

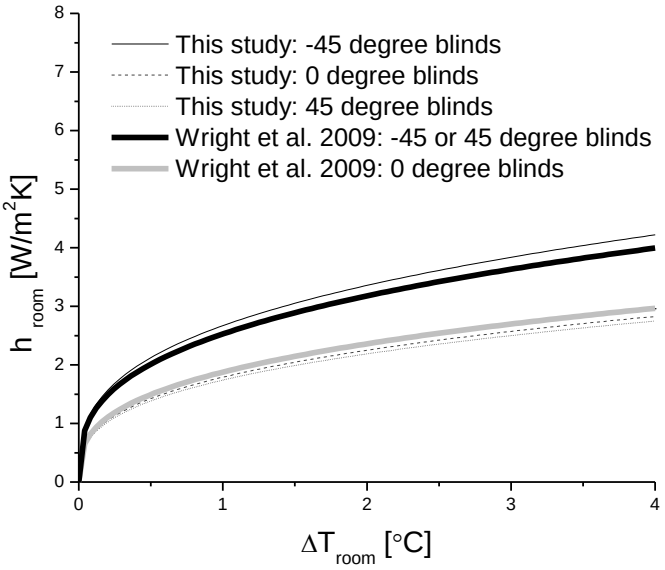

Figure B8. Comparison of Wright [18] model for convection at blind surfaces with experimental results

4.2 Forced Convection with Ceiling Slot Diffusers

This section presents the results of experiments run with a ceiling slot diffuser. It shows the results for the window surface in the form of comparisons with the bare window case, for various configurations. These results are followed by results for blind surfaces given as a function of blind angle.

Window Surface

The first comparison made in the ceiling slot diffuser experiments is between the situations in which blinds were present and fully open (0°) and that in which they were absent. The results are shown as a function of volumetric flow rate in Figure B9. Figure

B9a shows that in Configuration A, blinds reduce convection heat transfer by approximately 40%. Figure B9b shows that the open blinds have the effect of reducing convective heat transfer by roughly 30% at all flow rates in Configuration B.

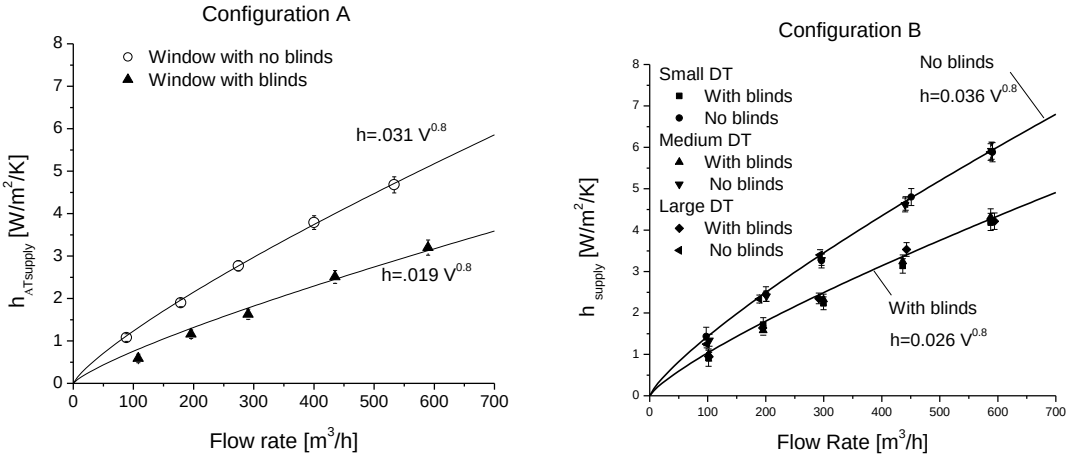

Figures B9. Comparison of convection coefficient for window surface with no blinds versus window surface with blinds for configuration A (left graph) and B (right graph) with ceiling diffusers. Blinds are at zero degrees for both geometries: A and B.

Another important observation to notice in Figure B9 is the tight clustering of points for each flow rate representing different temperature differences. These results show that the temperature difference has a negligible effect on the convective heat transfer. This suggests that the forced mode of convection is dominant at all flow rates. This implies that separate models need not be generated to account for the possible competing effects of buoyancy caused by the heated air and the downward supply momentum. This phenomenon was witnessed for the bare-window configuration as well, which was analyzed by Goldstein and Novoselac [8].

The next parameter studied was the effect of the angle at which the blinds were set. As can be seen in Figure B10, blind angle can affect the overall convective heat transfer by

as much as 40%. The blind angle at which convection was observed to be the greatest was positive 45°. In this situation the blinds are oriented roughly parallel with the direction of the bulk momentum of the jet, and as such impede jet momentum to a lesser degree than angles in which the jet and the blinds are perpendicular and thus the jet is retarded most effectively by the blinds.

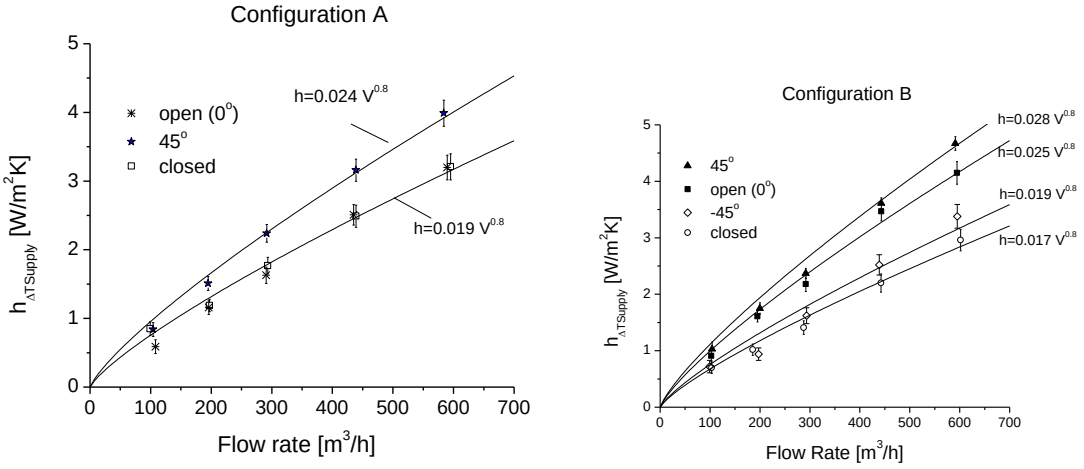

Figure B10. Effect of blind orientation on convection heat transfer at window surface for Configuration A (left graph) and B (right graph) with ceiling diffusers

Two sensitivity studies were conducted in order to determine if other relevant parameters were potentially influential enough to warrant further research. The first looked at the effect of the surface-air temperature difference as mentioned previously, which was embedded into the experiments quantifying the effect of blind presence (Figure B9b). This showed that for the ceiling slot diffuser experiments, temperature difference affected heat transfer very little. The second sensitivity study conducted was on the relationship between the heating and the cooling condition. Theoretically, a warm jet issuing downward into a relatively cool room could experience buoyancy forces due to the room air-jet air temperature difference that acted contrary to the momentum forces of the jet.

Ultimately, the sensitivity study showed that convection heat transfer in the heating or cooling conditions were virtually identical. This suggests again that the jet momentum is sufficiently larger than the buoyancy forces as to render the buoyancy effects negligible. Since the final purpose of this project was to provide for more accurate calculation of cooling and heating loads in energy modeling software, an additional effort was introduced to quantify the effect of the size of the window. The two most common configurations found in commercial buildings are that of floor-to-ceiling windows and that of a 1.37m window with a small wall beneath it. These situations were each simulated as explained previously and the results are contained in Figure B11. The "half window" situation corresponds to Configuration B.

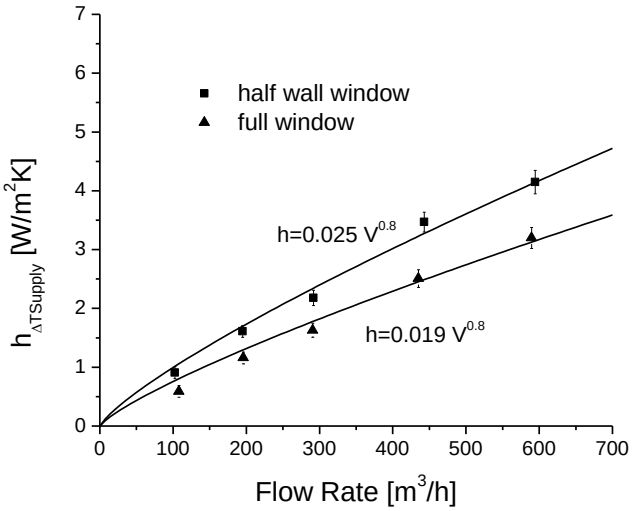

Figure B11. Impact of window height on convection heat transfer at window surface near ceiling slot diffuser for the configuration with open blinds

As expected, the convection coefficients are consistently higher for the situation in which only half the wall is a window. This is due to the convention of using the supply temperature as a reference. In the case of the full-height window, the jet has a chance to

heat up or cool down as it moves along the window, thus rendering the local temperature difference at lower portions of the window smaller, and affecting convective heat transfer accordingly. While the physical heat transfer mechanism is unchanged, the average heat transfer for the entire window surface as a function of supply temperature is relatively smaller for the full-height window. This is due to the actual local temperature difference, the driving force behind the convective heat transfer, is smaller at lower portions of the window.

Blind Surfaces

Correlations were also developed for blind surfaces. Results are given in Figure B12 for both configurations. As fluid movement near blind surfaces is complex, characterized by recirculating flow between the blinds and entrainment from both sides of the blinds, no attempt is made to make a strong connection between results and theory. Results indicate that the jet results in correlations similar to those for turbulent forced convection heat transfer at blinds surfaces and correlations are given in the form typically used, $h=CV^{0.8}$.

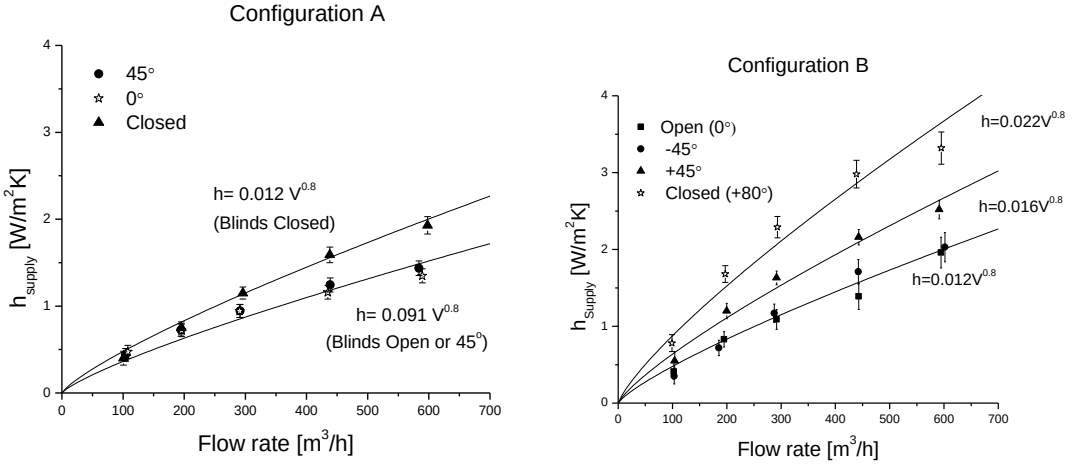

Figure B12. Impact of blind orientation on convection heat transfer at blind surfaces for Configuration A (left graph) and B (right graph) with ceiling diffusers

For configuration B, in which the jet moving along the relatively short height of window results in a strong correlation between h and blind angle (β), a relationship between blind angle and heat transfer can be given in the form of an equation for the constant C in the correlation $h=C\dot{V}^{0.8}$, as shown in Figure B13. Comparison of the coefficient C for blind and window surfaces show opposite trends. Unlike the correlation for windows, blind surface convection is greatest when the jet is presented with a smooth surface to move along (i.e. the blinds-closed situation). When blinds are open, jet approach the blinds at larger angle and less of the blind surface is

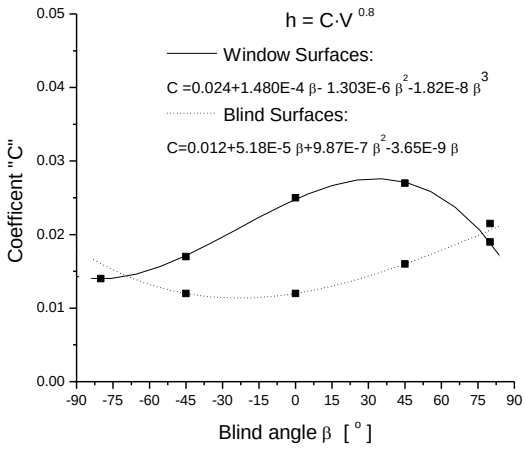

Figure B13. Effect of blind angle on convection coefficient for window and blind surfaces in Configuration B with a ceiling diffuser (blind angle is defined in Figure B4)

exposed to the strong jet flow; thus the convective heat transfer is less intensive. Increased convection coefficient at the blinds means a reduced convection coefficient at the windows.

4.3 Forced Convection with Floor Registers

Convection heat transfer at a window surface near a floor register was analyzed as well. Experiments were conducted for several blind angles. The results for configuration

A are displayed in Figure B14. Comparison of results for configurations with and without blinds (Figure B14, left graph) shows that heat transfer is hindered up to 45% by the presence of the blinds and that the effect of blinds is somewhat dependent on blind angle. Also, the results indicate a small dependency on blind angle. The right graph in Figure B14 show this dependency and compare it with the dependency for the ceiling diffuser. The variable C for the configuration with the floor register has the reverse profile of the variable C for the ceiling slot diffuser. This reverse profile is due to the jet direction relative to the blinds. With a ceiling diffuser the maximum value of C (which indicates maximum convection at the window) is at 45° since this angle enables maximum air flow through the blinds; with a floor register the jet approaches from the opposite direction and thus the maximum flow through the blinds occurs at an angle of-45°.

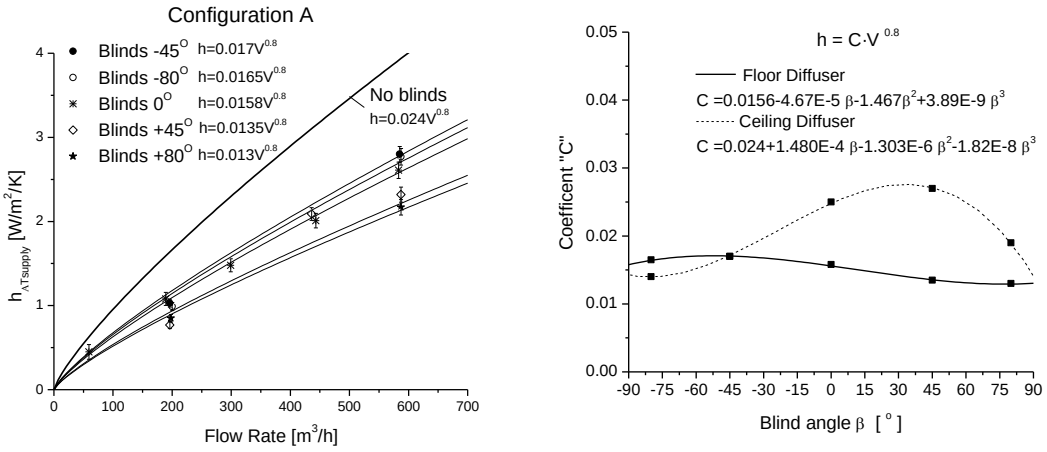

Figure B14. Forced convection coefficient at window surface for Configuration A with floor registers (left graph) with the impact of blind angle (right graph)

Results for Configuration B are presented in Figure B15 and, like for Configuration A, blinds reduce convection coefficients at window surfaces by approximately 35%. When analyzing the impact of blind angle in this configuration, the results show a large degree of scattering, and therefore no correlations predicting the dependency on blind angle were derived. This scattering of results for Configuration B is likely due to the lesser strength of the floor jet. Under these circumstances, the effect of the obstructions (blinds) becomes more pronounced. However, the correlation for the window surface with blinds in Configuration B should be able to be employed in load calculation applications with an acceptable degree of uncertainty for most of engineering applications.

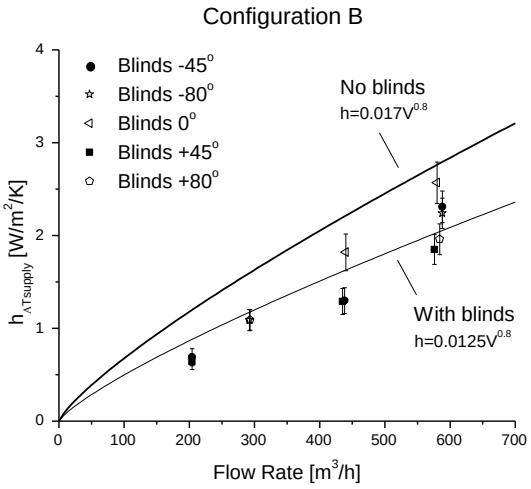

Figure B15. Forced convection coefficient at window surface for configuration B with floor registers

The convection coefficients measured at blind surfaces for Configurations A and B with floor registers are not shown in this study because of the large degree scattering and uncertainty.

5. SUMMARY

Through the course of more than 100 experiments, convection heat transfer at window surfaces was characterized for different window geometries, diffuser locations, and HVAC operating regimes. In general, it was found that blind presence strongly affects forced convection at window surfaces, as does window geometry and supply conditions. HVAC regime (i.e. heating condition or cooling condition) was found to be nearly irrelevant, as was surface-air temperature difference.

Results are summarized in Table B3 below. For the purpose of providing correlations which can be adopted and used by industry professionals and energy modeling programs, all correlations are given in terms of the total volumetric flow rate along the length of the wall in question normalized by the length of the wall, $\left(\dot{V}/L\right)$. This convention will introduce a source of uncertainty into the correlations, as the correlations were developed for a certain layout (2-1.2m long registers per 4.5m of wall length). However, this convention will allow the results to be readily used and represents an improvement over previous assumptions, such as natural convection or a single value of *h* in a perimeter zone. Results show that improvements should be made to existing models of natural convection in window-blind assemblies to account for larger geometries and different blind angles. In situations where forced convection is present, new correlations are given.

Configuration	Surface	Convection Correlation h [W/m^{2}K]
Natural convection with blinds		
A	Window	$h = 1.89\Delta T^{0.25}$ *(blinds -45°)* $h = 1.67\Delta T^{0.25}$ *(blinds 0°)* $h = 1.48\Delta T^{0.25}$ *(blinds 45°)*
	Blinds	$h = 2.0\Delta T^{0.33}$
Ceiling slot diffusers heating and cooling		
A	Window	$h = c \cdot (\dot{V}/L)^{0.8}$ *c= 0.063 (blinds 0° or closed)* *c=0.079 (blinds at 45°)*
	Blinds	$h = 0.060(\dot{V}/L)^{0.8}$ *(bl. closed)* $h = 0.030(\dot{V}/L)^{0.8}$ *(blinds open)*
B	Window	$h = c \cdot (\dot{V}/L)^{0.8}$ *c=0.080 +4.93E-4β -4.34E-6β^2 -6.06E-8β^3* *β - blind angle: 0for open +90 for closed*
	Blinds	$h = c \cdot (\dot{V}/L)^{0.8}$ *c=0.040 +1.72E-4β -3.29E-6β^2 -1.22E-8β^3* *β- blind angle: 0 for open +90 for closed*
Floor registers		
A	Window	$h = c \cdot (\dot{V}/L)^{0.8}$ *c=0.052 +1.561E-4β -4.867E* *-7β□^{2}+1.30E-8β^3* *β - blind angle: 0 for open +90 for closed*
B	Window	$h = 0.042(\dot{V}/L)^{0.8}$

Table B3. Summary of results **Note:** All temperatures *(ΔT)* are given in degrees Celsius and the normalized flow rate (*V/L*) is in m^3 per hour of supply air per meter of perimeter wall.

There are several limitations to this study. While this study analyses convection at window and blind surfaces for diffuser positioning in perimeter zones (50-70% of perimeter zone length covered by diffusers) which was deemed to be the most representative of what is installed in commercial construction currently, the investigation could be extended to other diffuser types and layouts. Other diffuser types and spacings

of floor registers or ceiling slot diffusers are likely to affect the applicability of the correlations. Larger or more complex window configurations, such as a 12-foot high floor-to-ceiling window, an angled window, or a bay window, would certainly experience heat transfer differently than the situation analyzed and would require individual analysis. Blinds analyzed were also chosen because of their prevalence, but other types such as vertical blinds will produce different heat transfer characteristics. Lastly, while a 25mm gap between blind and window surface was determined to be the standard gap in the vast majority of commercial construction, variation of the distance between blind and window may produce a more refined model that may be desirable for a specific application.

Acknowledgements

This project was funded by the American Society of Heating, Ventilation, and Refrigeration Engineers (ASHRAE) RP 1416, a National Science Foundation Integrated Graduate Engineering Research Traineeship (NSF IGERT) in Indoor Environmental Science and Engineering, grant# nDGE-0549428, and a University of Texas Engineering Thrust Fellowship.

References

[1] Waters, J.R. "The experimental verification of a computerised thermal model for buildings." *Building Services Engineering Research and Technology* 1, no. 2 (1980): 76-82.

[2] Alamdari, F., G.P. Hammond, and C. Melo. "Appropriate calculation methods for convective heat transfer from building surfaces." *Proc. 1st U.K.: National Conference on Heat Transfer*, no. 2 (1984): 1201-1211.

[3] Lomas, Kevin J. "The U.K. applicability study: an evaluation of thermal simulation programs for solar passive house design." *Building and Environment* 31, no. 3 (1996): 197-206.

[4] Khalifa, A.J.N. *Heat transfer processes in buildings.* Ph.D Thesis, Cardiff, U.K.: University of Wales College of Cardiff, 1989.

[5] Awbi, Hazim B. "Calculation of convective heat transfer coefficients of room surfaces for natural convection." *Energy and Buildings*, 1998: 219-227.

[6] Spitler, J.D., C.O. Pederson, and D.E. Fisher. "Interior convective heat transfer in buildings

with large ventilative flow rates." *AHSRAE Transactions* 97, no. 1 (1991): 505-515.

[7] Fisher, D.E., and C.O. Pederson. "Convective heat transfer in building energy and thermal load calculations." *ASHRAE Transactions* 103, no. 2 (1997): 137-148.

[8] Goldstein K. and Novoselac A.,"Convective Heat Transfer in Rooms With Ceiling Slot Diffusers (RP-1416)". HVAC&R Research Journal16,2010: 629-655.

[9] Beausoleil-Morrison, Ian. "An algorithm for calculating convection coefficients for internal building surfaces for the case of mixed flow in rooms." *Energy and Buildings*, no. 33 (2001): 351-361.

[10] Novoselac A., Burley J., and Srebric J.,"Development of New and Validation of Existing Convection Correlations for Rooms with Displacement Ventilation Systems". Energy and Buildings, 38,2006:, 163-173.

[11]Collins, M., S.J. Harrison, D. Naylor, and P.H. Oosthuizen. "Heat transfer from an isothermal vertical surface with adjacent heated horizontal louvers: validation." *Journal of Heat Transfer* 124, no. 6 (2002): 1078-1087.

[12] Shahid, and Naylor. "Energy performance assessment of a window with a horizontal Venetian blind." (Energy and Buildings) 37, no. 8 (2005).

[13] Dalal, R., Naylor D., and Roeleveld D., "A CFD study of convection in a double glazed window with an enclosed pleated blind". Energy and Buildings 41, 2009: 1256-1262.

[14] Avedissian, T., and D. Naylor. "Free convective heat transfer in an enclosure with an internal louvered blind." *International Journal of Heat and Mass Transfer* 51, no. 1-5 (2008): 283-293 .

[15] Collins, Mike, Syeda Tasnim, and John Wright. "Determination of convective heat transfer for fenestration with between-the-glass louvered shades." *International Journal of Heat and Mass Transfer* 51, no. 11-12 (2008): 2742-2751 .

[16] Machin, A.D., S.J. Harrison, D. Naylor, and P.H. Oosthuizen. "Experimental Study of Free Convection at an Indoor Glazing Surface with a Venetian Blind." *HVAC&R Research* 4,

[17] Cuevas, Cristian, Adelqui Fissore and Nestor Fonseca. "Natural convection at an indoor glazing surface with different window blinds" *Energy and Buildings* 42, no. 10 (2010): 1685-1691.

[18] Wright, John L., Michael R. Collins, Nathan A. Kotey, and Charles S. Barnaby. *Improving cooling load calculations for fenestration with shading devices.* Atlanta, GA: ASHRAE, 2009.

[19] ASHRAE. *Engineering Analysis of Experimental Data. Guideline-2.* Atlanta: ASHRAE, 2000.

[20] Bejan A. 2004. Convection Heat Transfer. New York: John Wiley & Sons.

Appendix C: Flow and mixed convection heat transfer in buoyant jets from floor registers

Jordan Clark **Atila Novoselac, Ph.D.**

Abstract:

As models of energy movement in buildings and tools for load calculation become more refined, more accurate descriptions of fluid mechanics and heat transfer in perimeter zones are needed. New construction which includes glass curtain walls around perimeter zones presents a unique challenge. A mixed convection regime may be present which precludes the use of existing models developed for purely forced convection. In order to study flow and heat transfer in these situations, environmental conditions are precisely controlled in a test room to simulate situations that may occur in perimeter zones of buildings with glass curtain walls. Diffuser jets issuing from floor registers were shown to exhibit behavior not accounted for in existing heat transfer models. Results show that the movement of the jet issuing from floor registers is highly dependent on the mixed convection parameter Gr/Re^2 or Richardson number. Models are put forth to predict the movement of these jets, and the resulting heat transfer at walls or windows. When the effect of buoyancy forces is accounted for, models conform to a form used previously for turbulent forced convection. Three distinct flow regimes are identified and prescriptions are put forth for ensuring proper thermal control and accurate energy models.

1. Introduction

Until recently, interior surfaces of perimeter walls of buildings were assumed to interact thermally with interior spaces via natural convection only. This assumption held in buildings with massive structural walls along their perimeter in which heat transfer through the envelope was very slow. However, modern construction often employs relatively thin glass curtain walls that are heated or cooled with a jet from a nearby diffuser; either a ceiling slot diffuser directly above the wall or a floor register directly below. In terms of energy modeling and load calculation, this presents a unique challenge in that both buoyancy and momentum forces may influence the movement of this jet, and the subsequent convection heat transfer at the perimeter wall or window. Previous work by the authors includes an empirical study of heat transfer at exterior walls and windows under forced convection situations. (Clark and Novoselac, Under Review) Sensitivity studies to determine the domain of applicability of the forced convection models developed showed that in three of the four regimes analyzed (cooling from above with linear ceiling slot diffuser, heating from below with floor register, and heating from above with ceiling slot diffusers) heat transfer at the wall or window conformed to the well-known form for turbulent forced convection ($Nu=C*Re^{0.8}$). Furthermore, the correlations were insensitive to supply air-room air temperature difference. However, when cold air was supplied from floor registers below, convection at the wall or windown showed a strong deviation from this model and supply-room temperature difference affected the resulting heat transfer. This work attempts to explain this difference, model the movement of the jet along the wall, and provide refined models of heat transfer resulting from this movement.

2. Literature Review: Mixed convection

When a vertical wall jet is of the same temperature as the quiescent fluid, it is well established [1] that the maximum velocity decays according to:

$$\frac{u_{\max}}{u_{inlet}} = C_1\left[\frac{D}{x + x_0}\right]^{0.5} \qquad (1)$$

where u_{max} is the maximum vertical velocity component at any horizontal plane in the jet,

u_{inlet} is the average jet velocity at the diffuser [m/s],C_1 is an empirical constant,

D is the characteristic length of the opening [m],

x is the vertical distance along the wall [m], and

x_0 accounts for shape of the jet [m].

The behavior of a buoyant jet is influenced strongly by the relationship between the temperatures of the jet and the quiescent air. Most relevant to the current investigation is the work of Goldman and Jaluria [2] and Kapoor and Jaluria [3]. In the course of these two studies the authors correlated the distance a hot jet entering a colder quiescent fluid from above would travel before reversing direction (jet penetration distance $\delta_{p,}$ in Figure C1) to the mixed convection parameter Gr/Re^2 called the Richardson number, Ri.

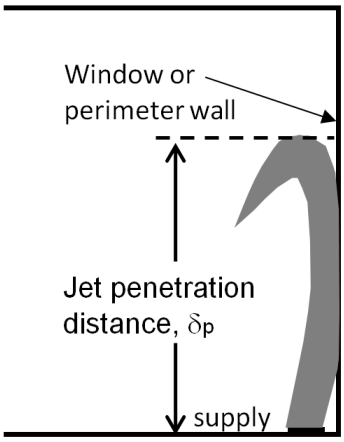

Figure C1. Definition of jet penetration distance

The relationship given by Goldman and Jaluria [2] is:

$$\frac{\delta_p}{D} = 4.5\,[Ri]^{-0.402} \qquad (2)$$

and Ri is defined as:

$$Ri = \frac{g\beta\Delta TD}{U^2} \qquad (3)$$

where β is the coefficient of thermal expansion[1/K], and U is a reference velocity [m/s]. This equation assumes an infinitely long inlet located immediately adjacent to an adiabatic wall. Furthermore, it assumes the inlet as one solid opening rather than an array of openings, such as in a floor grille. Other researchers such as He [4] and Abdulhadi and Pederson [5] have given slightly different and much more complex correlations, but each fall within 20% of the Goldman and Jaluria [2] relation.

Kapoor and Jaluria [3] assumed that any natural convection heat transfer in the region beyond the jet penetration distance was negligible in comparison to the forced convection heat transfer in the region of the wall affected by the jet. This assumption was justified by their calculations of local convection coefficients in the region beyond the jet penetration, which were found to be near zero. This could be explained by the fact

that the slight negative pressure created behind the downward moving jet cancels the natural tendency of the air to move upward as a result of buoyant fluid motion caused by natural convection. The velocity of a jet moving in the buoyant region has been mathematically described for radial ceiling diffusers by Cao et al. [6] by adding the effect of buoyancy to the model for isothermal jet decay (Equation 1). They developed and validated the following equation:

$$u_{\max} = C_1 u_{inlet}\left(\frac{D}{x + x_0}\right)^{0.5} + \left(\frac{Kgx\Delta T}{T_{inlet}}\right)^{0.5} \qquad (4)$$

where K is an additional empirical constant, g is the acceleration due to gravity [m/s^2], T is temperature [^{o}C], and

$\Delta T = T_{local} - T_{inlet}$.

Attempts at predicting convective heat transfer at interior walls have been put forth which aim to describe convective heat transfer without recourse to detailed knowledge of the flow fields involved. Churchill and Usagi [7] proposed a method of "blending" any two phenomena into one correlation, where the process in question behaved like either of the two phenomena in the limits of its domain. The correlation is given as:

$$Y = (X^a + Z^a)^{1/a} \qquad (5)$$

where Y is the process in question, X and Z are the two limiting behaviors, and a is a somewhat arbitrary "blending coefficient". Alamdari and Hammond [8], Beausoleil-Morrison [9]and Novoselac et al. [10] showed that this method could be fruitfully applied to indoor convection heat transfer processes in which two phenomena competed or assisted in creating the process in question. In assisting phenomena, the blending of the two was accomplished with the Churchill and Usagi [7] equation, where in competing

phenomena such as a downward jet along a warm vertical wall, an altered form could be used, i.e.:

$$h_{mixed,\ opposing} = \left| (h_{forced})^a - (h_{natural})^a \right|^{1/a.} \quad (6)$$

The current study offers an alternative method of describing the phenomenon of mixed convection. It studies the deviation from the typical turbulent flow correlation for heat exchange between jets and surfaces, and describes jet behavior in a manner that allows it to be included in refined convective heat transfer models. Specifically, it (1) predicts diffuser jet movement along a vertical surface for a variety of HVAC operation regimes and room conditions, and (2) correlates convective heat transfer to relevant variables in a way that is consistent with accepted theory. Basic hypotheses for this work are: (a) the interplay between momentum and buoyancy effects is responsible for the deviation from the typical turbulent forced convection correlation, (b) under some situations, the jet will not reach the ceiling and this behavior can be predicted from supply conditions and room temperature (c) once the buoyancy effects are included in the description of the jet movement, heat transfer will correlate as expected with jet velocity.

The study provides empirical models for jet penetration into indoor spaces from floor diffusers jet profile change along the wall. It also provides refined models of convective heat transfer between these jets and vertical room surfaces. The following sections describe the experimental and analytical methods used to create these models, presents the results of the experiments, and discusses the implementation of the models.

3. Methodology

Dimensional analysis of the variables that may affect the penetration of a buoyant jet shows that jet penetration along the wall is a function of one variable, $Ri=Gr/Re^2$. Experiments were thus run at several different values of this variable to determine the effect of this parameter on the penetration of the jet into the room.

Experiments were conducted in a large environmental chamber at the Center for Energy and Environmental Resources (CEER) of the University of Texas at Austin. The environmental chamber has interior dimensions of 4.5m×5.5m×2.7m and the indoor environment is controlled by a dedicated and modifiable HVAC system capable of supplying air between 6°C and 50°C, with a relative humidity in the range from 25% to 70% . A schematic of the control system is given in Figure C2. Flow rates corresponding to ventilation rates between 0 and 15 ACH are studied. The chamber contains a push-pull delivery system capable of maintaining a pressure of 0±0.5 Pa in the chamber.

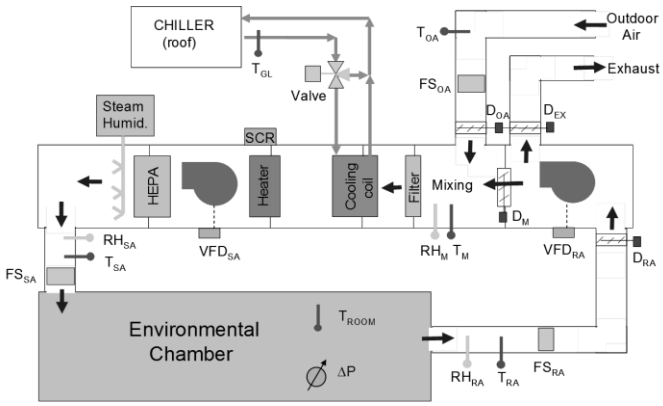

Figure C2. Schematic of control system for environmental chamber

Flow rate measurements were calibrated prior to the commencement of the experiments and were found to be accurate to within 5%. U-values of the chamber walls

are 0.2 W/m^2K. For the purpose of the current experiments, a 0.3m deep raised floor was built into the chamber. The floor was sealed on its top surface to prevent air infiltration between the space proper and the plenum created in the installation. The plenum houses an insulated flexible duct along its length leading to two diffuser boxes and a Titius CT-PP-0 1.22m × 0.10m grille registers with 0° pitch installed 23cm from the wall. The two diffusers were responsible for cooling a wall 4.5 m long. This was deemed to be the most representative setup for standard installation in new buildings, but variations in diffuser layout may lead to deviation from the behavior witnessed.

Penetration distances, defined as the height the jet reaches in the room before reversing direction (see Figure C1), are ascertained via flow visualization using isothermal pulverized chalk dust (Regin S201P Powder "Smoke", 0.7 micron peak particles) inserted horizontally into the diffuser jet. Particle size distribution was established using a TSI 3321 aerodynamic particle sizer. The penetration distance is established by flow visualization and a tape mesure and it is assumed that the recorded distance had a precision of ± 5cm. This penetration distance was then verified by analyzing data on jet velocities taken with omnidirectional hotwire anemometers along the wall and extraploating to the point where the vertical jet velocity would be zero, corresponding to another estimate of the penetration distance. These two methods were compared and found to be in good agreement, as is shown below in the results section.

Temperatures of were measured with OMEGA 4403 thermistors accurate to ±0.1˚C. Jet velocities along the wall were measured with omni-directional hot-wire anemometers accurate to ±0.02m/s. Eight anemometers were placed side by side in a horizontal plane next to the wall to capture the jet profile in the near-wall region. The maximum output of

these anemometers was assumed to be the maximum jet velocity at this height. Heights were varied to measure the decay of the maximum velocity along the wall.

All experiments were first allowed to run for 24 hours until a steady state condition was achieved. Data was recorded when the chamber was deemed to have reached steady state with regards to flow fields and energy exchanges. Temperature was recorded every twenty seconds throughout the process and flow data was recorded for the last 10 minutes of the experiment at ten second intervals. The arrival at steady state was determined by observation of the temperature sensor data. When only small oscillations around a certain value were witnessed for each sensor, rather than an ongoing trend in a certain direction, the system was deemed to be at steady state.

Additional quality control was also ensured by comparison with previously published data, including the work of Goldman and Jaluria [2] for the jet penetration, and the Rajaratnam [1] model for isothermal jet decay. A thorough analysis of the parameters which affect convection heat transfer along the wall (e.g. diffuser distance from wall, wall-room temperature difference, diffuser outlet momentum) was previously conducted and can be found in Goldstein and Novoselac[11]. One parameter which may affect the applicability of the results is the number of floor registers installed per length of room. As mentioned, as representative a setup as possible was analyzed. All velocity measurements were made at the center of the diffuser jet to avoid measuring the portion of the jet at its short ends interacting with room air. Wall temperature-room temperature difference was shown to have no appreciable effect on results within the range expected in normal operation.

Convection heat transfer which was analyzed in previous work (Clark and Novoselac, under review), assuming an isothermal turbulent jet, is analyzed again with the new understanding of the effect of buoyant forces on the jet. Instead of correlating heat transfer to volumetric flow rate, as was done in previous work and shown to be lacking, heat transfer is this time correlated to the average maximum jet velocity along the length of the wall, *H*, defined as

$$u_{avg} = \frac{1}{H}\int_0^H u_{\max}(z)dz \qquad (7)$$

Jet velocity above the penetration distance is assumed to be zero, as is justified by visual inspection of the flow during flow vizualization and analysis of the anemometer data.

A fit of the form derived for turbulent flow over flat plates,

$$Nu = C * Re^{0.8} \qquad (8)$$

where *c* is a constant and

V is a reference velocity [m/s],

is fit through the data. This correlation takes into account the difference in jet movement along the wall when buoyancy forces are present and signficant. A new model for convective heat transfer at vertical surfaces near diffusers is put forward and validated with existing data. This model takes as its input supply parameters which are usually know to a designer and as its output gives a refined and accurate prediction of heat transfer at perimeter zone walls heated and cooled by floor register jets.

Uncertainty is given as a function of the imprecision inherent in all measured variable used to calculate a reported value. With the uncertainty in each measurement calculated, the effect on the final value calculated is determined based on the general uncertainty theory given in ASHRAE Engineering Analysis of Experimental Data [12].

$$\delta\phi = \sqrt{\sum_i^n \ (\delta u_i \frac{d\phi}{du_i})^2} \qquad (9)$$

where $\delta\phi$ is the uncertainty in the considered value,

n is the number of parameters used in the equation for calculation of considered value,

δu_i is the uncertainty in the particular parameter and

$\frac{d\phi}{du_i}$ is the change in the considered value with a unit change of the parameter in question.

4. Results

In examining the effect of buoyancy on diffuser jets and the resulting heat transfer at nearby surfaces, a three-step investigation was proposed: determine the effect of buoyancy on jet penetration, determine the effect on decay of jet velocity along the wall, and then correlate this to heat transfer along the wall. The following shows the results of each of these investigations.

4.1 Jet Penetration

Figure C3 below shows the relationship between the mixed convection parameter *Ri* and the jet penetration into the room. The exponential dependence compares well with previous work analyzing penetration of hot jets from open slots pointing downward which showed an exponential dependence with exponent equal to -0.41 [2]. The flow vizualization ("smoke") method and the anemometer data method were shown to be in reasonable agreement. One can speak of three roughly defined regions in this graph: a region at the left of the graph in which buoyancy forces are weak compared to

momentum forces and the jet reaches the ceiling or beyond if unobstructed, a region to the right of the graph where buoyancy forces dominate and flow rate is relatively unimportant, and a middle range where the interplay of the two forces determines the jet penetration. This result is interesting as the assumption implicit in selecting HVAC equipment and operation is often that the system will be operating in the left-most region, which is not always the case.

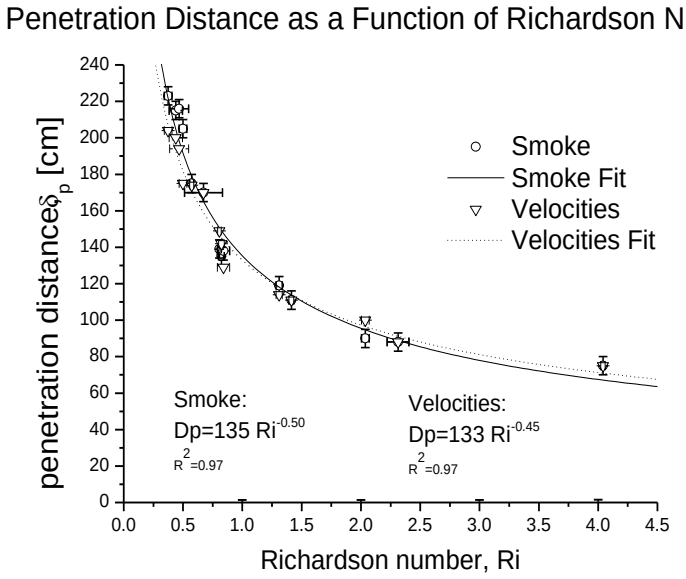

Figure C3. Results of jet penetration experiments showing variation of penetration distance with mixed convection parameter, *Ri*, by two different methods.

4.2 Jet Profile Decay

Also of interest is the manner in which the jet decays along the wall. Flow fields along the wall were recorded for two situations: an isothermal jet and a buoyant jet. The experimental setup was first validated by comparing it to existring theory on decay of wall jets [1]. Rajaratnam [1] models the decay as :

$$\frac{v_{max}}{v_{inlet}} = C_1 \left(\frac{D}{x+x_0}\right)^{0.5} \qquad (10)$$

where C_1 is an empirical constant,

and x_0 [m] accounts for shape of the jet.

For the isothermal jet, this equation was found to predict recorded flow fields to an acceptable degree of accuracy, with constants C_1=0.617 and x_0= 0.04228 m. Recorded velocities along the wall are shown with this model in Figure C4 below for two typical volumetric flow rates.

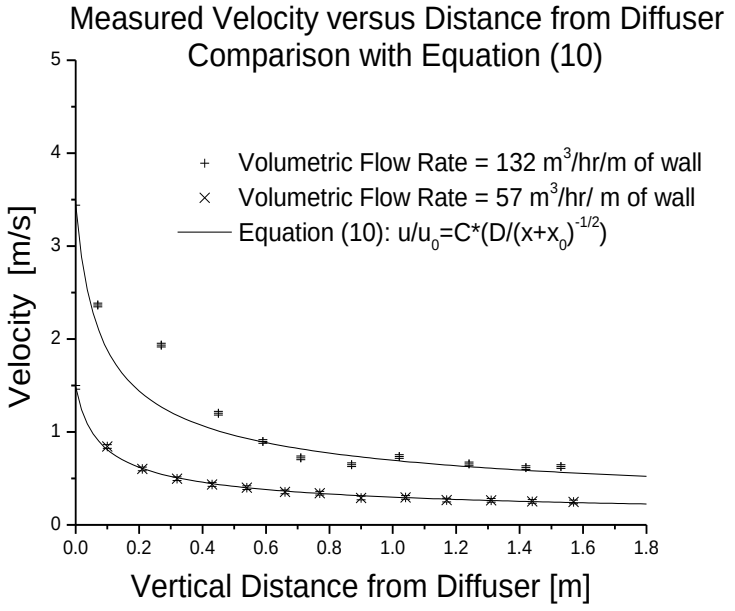

Figure C4. Comparison of theory with measured velocities in isothermal jet. Two flow rates tested report in flow rate per unit legth of perimeter wall.

The effect of buoyant forces is analyzed by plotting the decay of the maximum jet velocity along the wall in Figure C5. One can see that after the center of the jet begins to decay (after the entrance region), the jet velocity decays in a nearly linear fashion until

it reverses course at its penetration distance. One should notice that the linear fit predicts a small entrance region (roughly $x/\delta_{penetration}= 0.1$) in which the maximum jet velocity does not yet decay. This is consistent with jet theory, and caused by the fact that the center of the jet has not started to interact with its environment until the end of this region. Although there is an appreciable degree of scatter in this data, it's effect on the final variable of interest, convective heat transfer along the wall, is minimal.

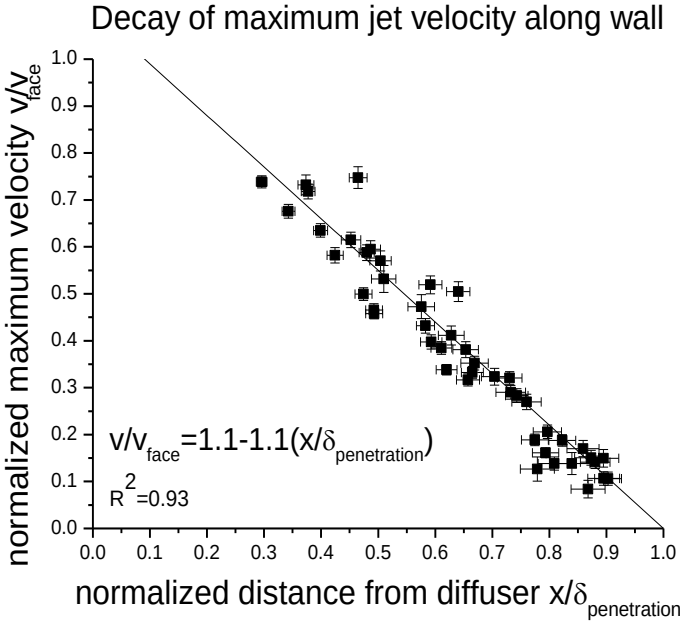

Figure C5. Plot of decay of jet velocity along length of wall with linear fit.

With this information, the heat transfer correlations previously developed can be reformulated with the wall-averaged maximum jet velocity on the x-axis and convection coefficient on the y-axis. Following the convention of Kapoor and Jaluria [3], and justified by their experiments and current experiments, the air velocity near the wall above the height at which the jet had reversed direction was taken to be zero. With this convention, heat transfer results were correlated to average maximum velocity and are

shown to correlate well displayed in Figure C6. This represents a much more accurate model for heat transfer at vertical surfaces near diffusers than that previously used.

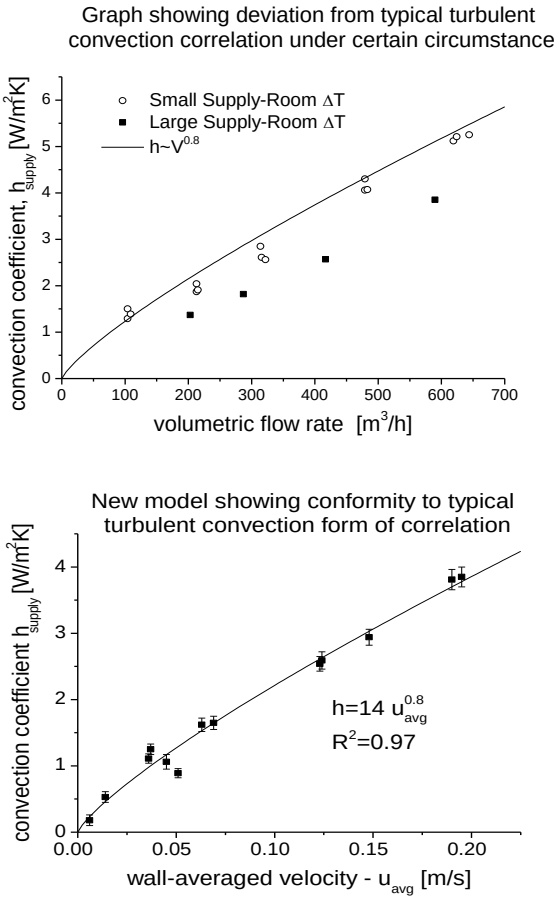

Figure C6. a) (Left) Previous formulation showing large deviation from model correlated to total flow rate along length of 4.5m wall with 2-1.2m floor registers b) (Right) Reformulation of previous convection heat transfer data with new information on jet penetration and decay

The remaining question that this study sought to answer was why the discrepancy shown in Figure C6a did not show up during investigations of the heating condition (supply air temperature greater than room air temperature) but did during investigations

of the cooling condition. The answer to this question is demonstrated in Figure C7 below. Typical operation of HVAC systems in the heating condition fall into the left-most region of the graph (shown in hatched in horizontal lines in Figure C7), corresponding to a regime in which buoyancy forces are dominated by momentum forces. This is due to three causes: the fact that internal loads such as people and electronics assist the HVAC system in mainting set temperature during the heating condition while opposing it during the cooling condition, the fact that supply temperature-room temperature differences are less during the heating condition than those during the cooling condition, and the fact that the jet from the large-effective area floor register is relatively weaker than that from the ceiling slot diffuser with smaller effective area. Typical cooling condition operation is shown in hatched in diagonal lines in Figure C7 and occupies a region of the graph in which both buoyancy and momentum forces are important in determining jet movement

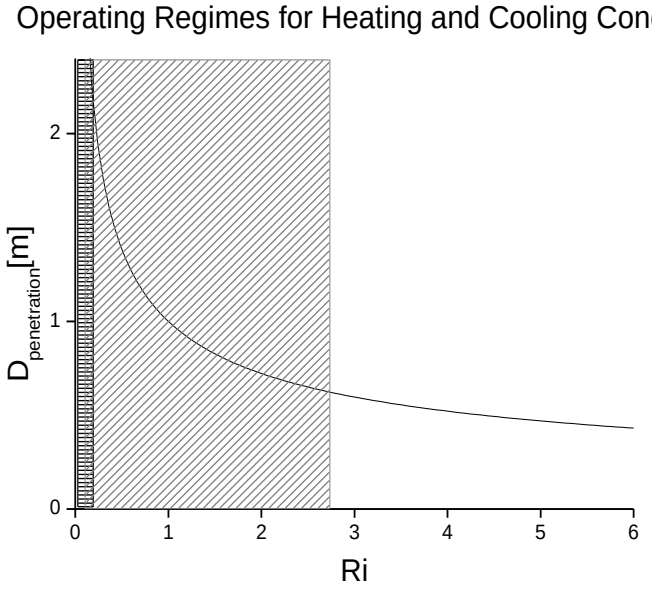

Figure C7. Typical operating regimes heating (hatched in horizontal lines) and cooling (hatched in diagonal lines) conditions (Graph shown without numerical values for clarity) Cooling region corresponds to 12°C supply-room temperature difference and air exchange rates of 2-10ACH. Heating regime area corresponds to 5°C temperature difference and 2-10ACH. All values of Ri use room height, 2.4m, as characteristic length.

5. Discussion

A method has been put forward for more accurately modeling heat transfer at exterior walls. This method requires knowledge of only the variables which a designer likely has at his or her disposal: face velocity at the inlet, room temperature, and supply temperature. With this knowledge, one can determine the penetration distance for the diffuser analyzed, and with this knowledge, calculate the decay of the maximum velocity along the wall. Once the decay is know, heat transfer at the wall can be related to the average wall velocity given in Equation 7.

While variations in the behavior documented here are likely to occur for different diffusers and installations, a representative geometry has been analyzed, and a method put forth for describing other geometries/setups. Further refinement could be gained by analyzing other diffuser types, and installations, in a similar manner. In addition to the increased precision in heat transfer calculations, this information may be valuable to a diffuser manufacturer or designer when considering air distribution, thermal comfort, or window performance.

6. Summary and future work

The behavior of floor register jets subject to buoyancy forces has been described and models have been put forth which allow for the effect of these buoyancy forces to be included in energy models and load calculations. A means for predicting the penetration of the jet into the room has also been put forward. At least two different operating regimes were identified, one in which buoyancy forces must be taken into consideration and one where this is unnecessary. While effort was taken to analyze the most representative diffuser and layout, additional refinement may be made for diffuser types and layouts not analyzed herein.

Acknowledgements

This project was funded by ASHRAE Research Project-1416: Development of Internal Surface Convection Correlations for Energy and Load Calculation Methods, and a National Science Foundation Integrative Graduate Education Research Traineeship in Indoor Environmental Science grant.

References

[1] Rajaratnam, N., Turbulent Jets. Elsevier, Amsterdam, 1976.

[2] Goldman, Daniel, and Yogesh Jaluria, Effect of buoyancy on the flow in free and wall jets, Journal of Fluid Mechanics 166 (1986): 41-56.

[3] Kapoor, Kamlesh, and Jaluria, Yogesh, Penetrative convection of a plane turbulent wall jet in a two-layer thermally stable environment: a problem in enclosure fires, International Journal of Heat and Mass Transfer 36, no. 1 (1993)155-167.

[4] He, S., Z. Xu, and J.D. Jackson, An experimental investigation of buoyancy-opposed wall jet flow, International Journal of Heat and Fluid Flow 23 (2002) 487-496.

[5] Abdulhadi, R., and C.O. Pederson, The behavior of a downward-directed heated wall jet, ASHRAE Transactions, (1971) 222-229.

[6] Cao, Guangyu, Jarek Kurnitski, Mika Ruponen, and Olli Seppanen, Experimental investigation and modeling of the attached plane jet velocity development characteristics in the transition process in a room, HVAC&R Research 15, no. 3 (2009) 489-508.

[7] Churchill, S.W., and R. Usagi, A general expression for the correlation of rates of transfer and other phenomena, AIChE Journal 18, no. 6 (1972) 1121-1128.

[8] Alamdari, F., G.P. Hammond, and C. Melo, Appropriate calculation methods for convective heat transfer from building surfaces, Proc. 1st U.K.: National Conference on Heat Transfer, no. 2 (1984) 1201-1211.

[9] Beausoleil-Morrison, Ian, An algorithm for calculating convection coefficients for internal building surfaces for the case of mixed flow in rooms, Energy and Buildings, no. 33(2001): 351-361.

[10] Novoselac A., Burley J., and Srebric J., Development of New and Validation of Existing Convection Correlations for Rooms with Displacement Ventilation Systems, Energy and Buildings, 38, (2006), 163-173.

[11] Goldstein, K. and A. Novoselac, Convective Heat Transfer in Rooms with Ceiling Slot Diffusers (RP-1416), HVAC&R Research 16, no. 5 (2010) 629-655

[12] ASHRAE, Engineering Analysis of Experimental Data. Guideline-2, ASHRAE, Atlanta, 2000.

Appendix D: Modeling the Effect of HVAC Operation on Transport of Gaseous Species to Indoor Surfaces

Jordan D Clark **Atila Novoselac, PhD**

ABSTRACT

Proper calculation of indoor mass transfer coefficients is essential for determination of human exposure to indoor pollutants and design of some removal strategies. Transport of species to indoor surfaces is traditionally given in the form of a space-averaged deposition velocity. Shortcomings of this model include its lack of a clear reference concentration and inability to account for different airflow patterns within a space. This work presents a method for calculating and modeling mass transfer to individual indoor surfaces and supports the approach put forth with full-scale experiments in an environmental chamber for flow situations typically found in indoor spaces.

Mass transfer to surfaces is often modeled as a two-step process in which the first step includes the boundary layer portion of transport and the second term quantifies surface phenomena. In this study, experiments are conducted in a 60m^3 walk-in environmental chamber to determine the boundary layer component of transport to indoor surfaces. The term of interest, k*, is determined using the naphthalene sublimation technique. Naphthalene plates are constructed by melting commonly available moth balls (99.9% naphthalene) onto aluminum sheets. These sheets are then weighed, and then affixed to the surface of interest with a Velcro-type adhesive in the environmental chamber. Surface area of the samples is quantified using a non-contact profilometer. Film theory is used in conjunction with published values of vapor pressures for pure naphthalene to determine the mass transfer coefficient.*

The experimental methods are first validated by comparing experimental results with natural convection theory for convective mass transfer on a vertical flat plate. Results were found to be reasonably close to theory. Next, forced convection is analyzed in the same manner. Results show that forced convection

correlations may be correlated to the volumetric flow rate, V*, issuing from the diffuser. When this convention is used, correlations conform roughly to the form* $v_t = C*V^{0.8}$. *This is consistent with flat plate forced convection theory and also with previous work on modeling heat transfer to indoor surfaces. What results is a refinement of existing mass transfer models which responds to changes in HVAC operation. This model may provide for more accurate estimates of exposure to indoor pollutants, and also may be used to design for passive removal strategies, such as removal of gaseous pollutants at indoor surfaces such as ceiling tiles.*

INTRODUCTION

Humans spend approximately 90% of their lives in indoor environments and for this reason, a large portion of a person's exposure to hazardous pollutants occurs indoors. Many researchers have studied indoor pollutants and created methods for modeling and controlling the movement and presence of pollutants in indoor environments. The motivation for the current study issues from two distinct areas of study related to the indoor environment. The first is accurate modeling of indoor environments. Many models exist which account for the various means by which indoor pollutant concentrations are altered in indoor environments, such as deposition, reaction, generation, etc. To the authors' knowledge, however, none of these models include the effect of HVAC operation. When reactive surfaces exist near diffusers, as is the case with some ceiling tiles near commonly used ceiling diffusers, the effect of HVAC operation may be significant. Secondly, a few researchers are beginning to investigate ways in which indoor pollutant concentrations may be controlled without the use of any additional energy. These strategies include taking advantage of boundary layer transport in diffuser supply jets to bring pollutants to reactive materials (Passive Removal Materials or PRM's) nearby where they are decomposed or deposited. Design of this type of strategy and quantification of its effects requires intimate

knowledge of boundary layer transport near diffusers.

PREVIOUS RESEARCH

Transport of species to indoor surfaces is usually given in the form of a space-averaged deposition velocity (Nazaroff et al. 1993). This model is usually used with a single value of deposition velocity for a single space, which implies either a static value or an appropriate time-averaging, and an insensitivity to various parameters such as type and operation of HVAC system, type of surfaces in the space, space temperatures, etc. Shortcomings of this model include its lack of a clear reference concentration and inability to account for different airflow patterns within a space. Improvements to the model have been proposed by Cano-Ruiz et al. (1993) who among other improvements, suggested decoupling various components of transport by use of a more complex model. One potential challenge with the use of this convention is the identification of a proper driving force for transport between the air adjacent to the surface in question and the air in the bulk space. The classic model for flux across a film (Bird et al. 2007) can be employed if the driving force across the film is known. However, in modeling of real spaces, this driving force is rarely known, and the overall transport is often a function of fluid mechanics which are much more complex than a simple boundary layer.

Several groups have sought to refine the models of mass transfer to indoor surface through various means. Sparks et al. (1996) attempted to give an idea of the magnitude of this influence through use of moth cakes (nearly pure paradichlorobenzene) in a small chamber or a test house and varying flow conditions in the space. The group of Morrison and colleagues has provided methods for determination of more refined models of transport of indoor pollutants. These include gravimetric methods (Morrison et al. 2003), which will

be employed in the current study. In 2006, the group of Morrison et al. used the method they had previously validated to quantify the effect of the temporal averaging of deposition velocities over long time periods during which central HVAC systems were cycling on and off and other perturbations in flow fields such as ceiling fans were running.

Many of the challenges present in indoor-surface mass transfer modeling have also been dealt with by researchers modeling heat transfer at indoor surfaces. Spitler et al. (1991) developed convection correlations for situations in which large ventilation rates (>15 Air Changes per Hour (ACH)) were employed. The results of their investigation suggested that at ventilation rates greater than 15ACH, jet momentum and inlet velocity become relatively unimportant compared to ventilation rate. Additional investigations by Fisher and Pederson (1997) and Goldstein and Novoselac (2010) and Clark and Novoselac (2012) confirmed that this was the case for a variety of lower ventilation rates and geometries, including all flow rates used in the current investigation. These three papers also concluded that the inlet temperature was the best reference temperature for their correlations. Lastly, they all three found that correlations of the form $h=C*V^{0.8}$ work in a variety of situations in which forced convection is present.

OBJECTIVES AND HYPOTHESES

This work aims to accomplish the following objectives:

1. Demonstrate that the naphthalene sublimation technique (Mendes 1991) is capable of quantifying mass transfer to indoor surfaces by comparison of experiments with natural convection theory
2. Use the validated technique to quantify forced convection mass transfer for two diffuser layouts.

We expect the forced convection correlations to conform to a model of the form $k=C*V^{0.8}$, as was previously found in similar heat transfer experiments. We also expect supply concentration and volumetric supply flow rate to be suitable variables for correlation of the results.

EXPERIMENTAL AND ANALYTICAL METHODS

All data is analyzed by assuming transport from the naphthalene samples to the bulk space according to the model:

$$N=kA(C_{surface}-C_{ref})$$

where N is the total rate of mass transfer of naphthalene [g/s, lb/s],

$C_{surface}$ is the air concentration just above the surface [g/m^3, lb/ft^3],

C_{ref} is the air concentration responsible for mass transfer across the boundary layer [g/m^3, lb/ft^3],

A is the area of the sample in contact with the air [m^2, ft^2], and

k is the mass transfer coefficient [m/s, ft/s].

Each term in this equation presented unique challenges. The first term, N, was quantified using gravimetric methods. Naphthalene is used as the species of interest in these experiments, owing to its high volatility, and inexpensiveness. Naphthalene plates (9cm x 9cm, 3.5in x 3.5in) are constructed by melting commonly available moth balls (99.9% naphthalene) onto aluminum sheets as shown in in Figure D1. These sheets are weighed, and then affixed to the surface of interest with a Velcro-type adhesive in a controlled environmental chamber. Once a certain amount of time has elapsed (usually 1-3 days), the sample is removed, and weighed again. The difference in mass between the two

measurements is the amount of naphthalene that was volatilized during the experiment. This quantity divided by the time elapsed and then by the area of the sample is the mass flux. Samples are left in the chamber under a certain set of circumstances for a minimum of a day each to minimize time-dependent effects and ensure a greater degree of precision. With this convention and the precision of the balance (electric balance with a precision of 0.1g, 2.2e-4lb) the quantity *N* had an uncertainty of roughly 1%.

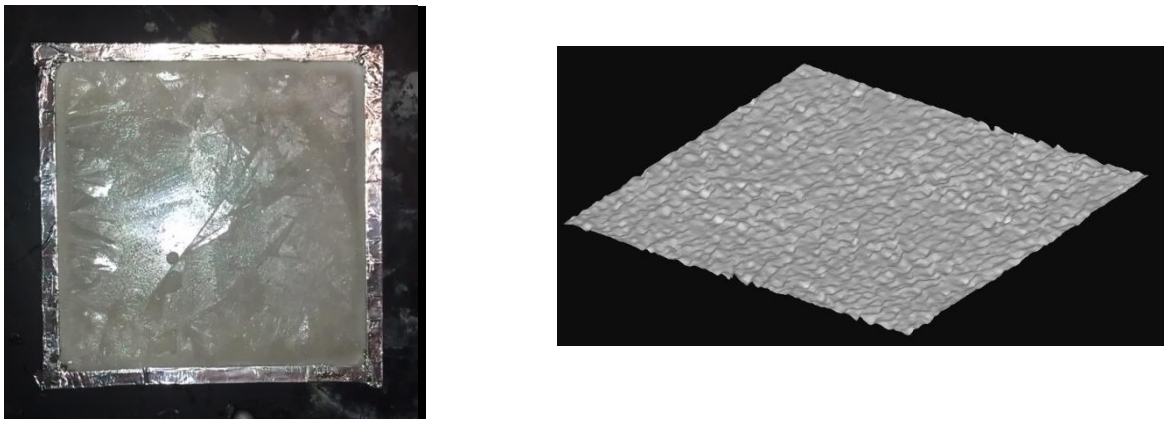

Figure D1. (Left) Photograph of typical naphthalene sample used in all experiments. (Right) Profilometer-generated image of surface roughness of naphthalene sample. Image represents 20mm x 20mm (0.79in x 0.79in) section of surface.

The driving concentration difference also needed to be quantified precisely. Conservative calculations confirmed that the bulk concentration in the room, even under conditions of high mass transfer rates and large amounts of naphthalene present, never reached beyond 1% of the equilibrium concentrations. The supply air was filtered through an activated carbon filter and also had a naphthalene concentration of virtually zero. Therefore, it was assumed that the reference concentration was zero in the space for all situations analyzed. The surface concentration was assumed to be the concentration in

equilibrium with the vapor pressure of the solid at the temperature of the solid.

The last challenge was in separating the two terms k and A once the other terms were known. On solidification, the naphthalene samples were observed to form a fuzzy surface (see Figure D1), which meant the surface area available for sublimation was not simply the 2-dimensional, or projected, surface area. To quantify the actual available area, three samples were analyzed with a non-contact profilometer (details of the profilometer can be found in Yao et al. (2008)) The ratio of the actual surface area to the two-dimensional surface area of each of the three samples was averaged and this ratio was assumed to be the ratio for all samples tested. The standard deviation for the three ratios was less than 6% of the average value, suggesting a fairly consistent surface for various samples.

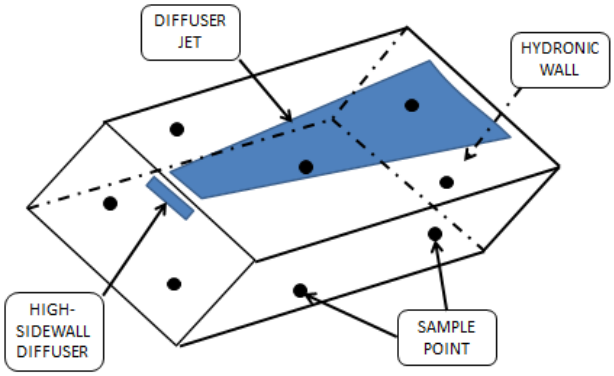

Figure D2. Schematic of large chamber, high-sidewall location, approximate diffuser jet from high-sidewall diffuser, and typical arrangement of sampling points.

Three sets of experiments were conducted: natural convection experiments, radial square ceiling diffuser experiments and high-sidewall diffuser experiments. Natural convection experiments were conducted in a well-insulated 4.5m x 5.5m x 2.4 m (14.8ft x 18ftx 7.9ft)environmental chamber with a dedicated complete HVAC system. The back wall

of the chamber contains a hydronic heating/cooling system which can create a hot/cold surface on the interior of the chamber. The chamber's HVAC system maintained a set point temperature in the space of 23ºC (73ºF). Natural convection results are presented in terms of a wall-room temperature difference. The wall temperature was taken as an average of 8 randomly distributed thermistors (accurate to 0.1ºC, 0.2ºF) on the heated wall. Room temperature was taken as the average of four thermistors spaced equally in the interior of the space and was very close (±0.4ºC, 0.7ºF) to the set point temperature for all experiments. Temperatures of the naphthalene samples were measured with a calibrated infrared thermometer with a precision of 0.1ºC (0.2ºF) so as to not disturb the samples.

High sidewall diffuser experiments were conducted in the same environmental chamber as the natural convection experiments, in order to simulate a geometry in which they would be used. A 0.5m x 4cm (20in x 1.6in) high sidewall diffuser was installed with its horizontal centerline 3 cm (1.2in) below the ceiling, centered on one of the short walls. Fourteen samples were distributed throughout the chamber in a random pattern on each surface: Four were placed on the ceiling; three on the wall housing the diffuser and the one being hit directly by it, two on the floor and two on the other walls. Isothermal conditions were maintained in the chamber at all times and the samples were assumed to be at the temperature of the average of four sensors distributed throughout the chamber.

Radial ceiling diffuser experiments were conducted in a 2.4m (7.9ft) cubic chamber with insulated and sealed walls, but no dedicated temperature control system. Four samples were distributed randomly on the ceiling, two on each of the walls and two on the floor. A 2ft x 2ft (0.6m x 0.6m) 4-way square cone diffuser was installed in a drop ceiling, centered on the ceiling. Isothermal conditions were again maintained and the samples were assumed to be at the temperature of the supply, which was virtually equal to both the room temperature and

the temperature of the surroundings.

RESULTS

Results are first presented for the natural convection experiments conducted to validate the naphthalene sublimation technique for application in modeling mass transfer to indoor surfaces. Results are shown in Figure D3 below. Experimental results are shown as a solid black range and theoretical correlations, based on analogy with heat transfer (Bird), are shown as dashed lines. Theoretical and experimental Sherwood numbers are calculated with the range of diffusion coefficients which have been published for naphthalene (Keumnam et al.1992), which results in a range of Sherwood numbers for each temperature difference, both in the theoretical prediction (which is a weak function of diffusion coefficient) and in the experimental data. Since theoretical correlations are given in dimensionless form, the diffusion coefficient enters directly into the calculation of the Sherwood number for experimental data in order to compare. In reality, simply the mass transfer coefficient was calculated and the experimental uncertainty is much less. Nonetheless, Figure D3 shows that the results of the natural convection experiments were well within an order of magnitude of the theoretical correlations, and showed very good agreement at lower temperature differences.

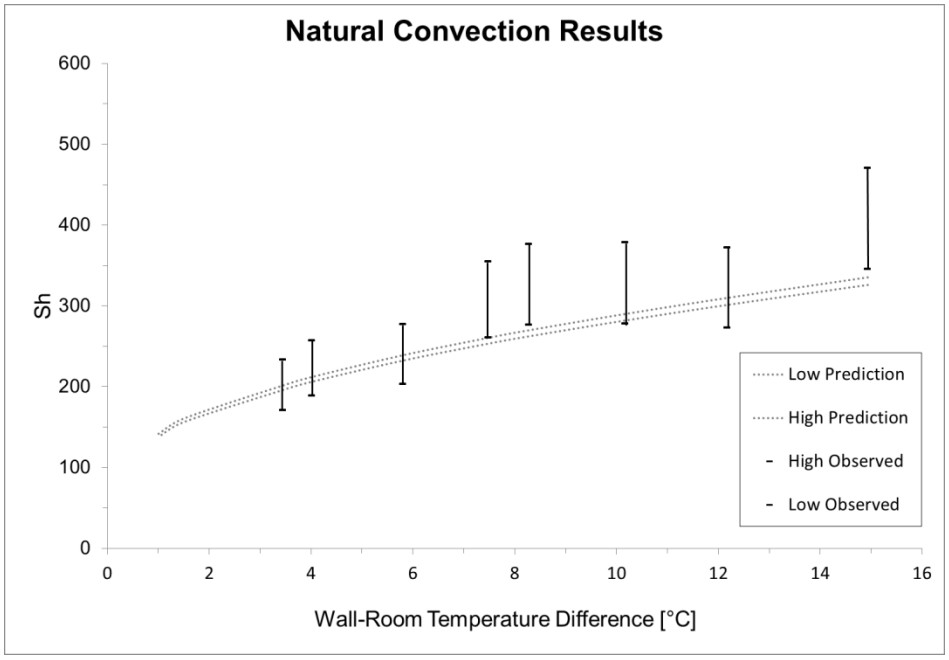

Figure D3. Natural convection theory and experimental results used for validation of naphthalene sublimation technique.

Next, results are presented for the high-sidewall diffuser in Figure D4. Also shown in Figure D4 are equally spaced lines depicting correlations of the form $k=C*V^{0.8}$. A few observations can be made when looking at Figure D4. First, data for the ceiling and the wall opposite the diffuser appear to follow a trend which has an exponential dependence on flow rate of greater than 0.8. Exponential dependences of convective transport on characteristic velocity greater than 0.8 arise in impinging jet situations, which is present to some degree on these surfaces. The effect of spatial averaging likely played a role in the deviation from the expected dependence as well. One should also note that mass transfer at the wall opposite the diffuser appears to be greater than on the ceiling, despite the diffuser being located on the ceiling send a jet along the ceiling surface. This is almost certainly due to the averaging process, which averaged samples which weren't in the diffuser jet with ones which were. This convention is adopted to simplify the modeling process.

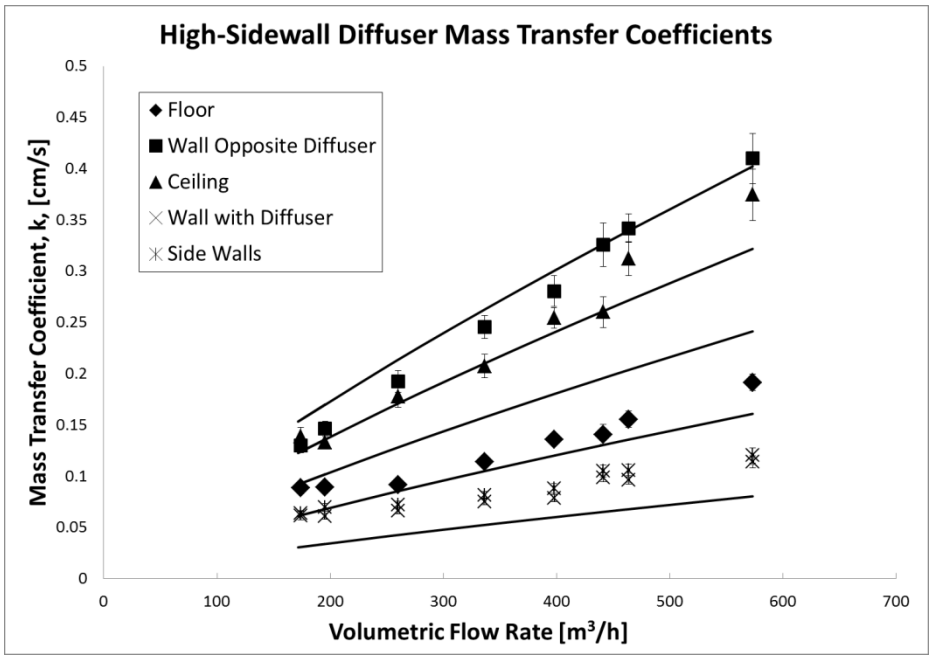

Figure D4. Forced convection results for all surfaces in large chamber during high-sidewall diffuser experiments

Lastly, in Figure D5, the results of the forced convection experiments employing a radial square ceiling cone diffuser are displayed. A few more observations can be made from Figure D5. First, the correlations for the ceiling are roughly a factor of four less than those for the high-sidewall diffuser. This is due to the nature of the different jets issuing from the two diffusers. While the high-sidewall diffuser issues a high-velocity jet which ensures air distribution by entraining a great deal of room air from below, the radial ceiling diffuser has a much lesser face velocity and distributes air by spreading across the ceiling and then falling into the room. Figure D5 is shown, as was Figure D4, with lines depicting an exponential dependence of 0.8. It is clear that no strong statements can be made about the exponential dependence of mass transfer in this situation. Furthermore, one notices to the left side of the figure and in the Floor data that a lower bound may be present around 0.05cm/s

(0.002ft/s). This may be thought of as a good assumption for the boundary layer component of mass transfer in room in which the HVAC system is either not in operation or has a negligible effect on the surface of interest.

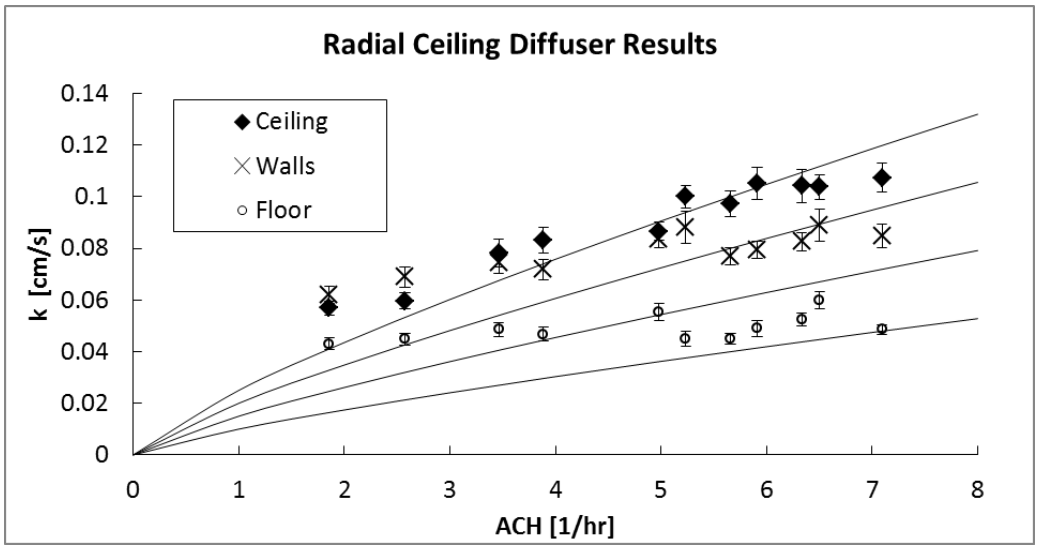

Figure D5. Forced convection results for radial ceiling diffuser

CONCLUSION AND FUTURE WORK

Through the course of several full-scale experiments, the boundary layer component of mass transfer to indoor surfaces in a few situations was calculated. Natural convection experiments showed that the naphthalene sublimation technique produced results with an acceptable deviation from theory. Forced convection experiments explored mass transfer under flow conditions caused by two different ceiling diffusers. The results of these experiments can be paired with predictions of surface phenomena to more accurately model room air pollutant concentrations and possibly be may be used in design and analysis of passive removal strategies. Forced convection did not conform nicely to an exponential dependence of 0.8 as has been the case in previous work on heat transfer, likely because of the averaging process and the possible presence of impinging jets on some surfaces. Forced

convection mass transfer was found to differ by a factor of 4 for the two diffusers analyzed. Lastly, a lower bound of 0.05cm/s (0.002ft/s) was suggested as a result of the forced convection experiments.

Future work will quantify mass transfer under other diffuser layouts and attempt to validate the model put forth herein by pairing boundary layer transport measurements with measurements of reaction probability on ceiling tiles and comparing them with full-scale experiments. Potential issues include the definition of a proper driving force for mass transfer. A comparison of previous heat transfer work for indoor surfaces with this work will be interesting as well, as some information may be gathered on the appropriateness of an analogy, which could be used to model mass transfer in many more situations.

REFERENCES

Bird, R. Byron, Warren E. Stewart, and Edwin N. Lightfoot. *Transport Phenomena.* New York: John Wiley and Sons, 2007.

Cano-Ruiz, et al. "Removal of reactive gases at indoor surfaces combining mass transport and surface kinetics." *Atmospheric Environment*, 1993: 2039-2050.

Clark, et al. "Experimental study of convective heat transfer from windows with Venetian blinds" *Building and Environment,* 59, (2013): 690-700

Colomina, M. et al. "Vapour pressures and enthalpies of sublimation of naphthalene and benzoic acid." *The Journal of Chemical Thermodynamics* 14, 8, (1982):779-784

Fisher, D.E., and C.O. Pederson. "Convective heat transfer in building energy and thermal load calculations." *ASHRAE Transactions* 103, no. 2 (1997): 137-148.

Goldstein, K. and A. Novoselac. "Convective Heat Transfer in Rooms with Ceiling Slot Diffusers (RP-1416)" *HVAC&R Research* 16, no. 5 (2010): 629-655

Keumnam, Cho, et al. "Measurement of the diffusion coefficient of naphthalene into air, *International Journal of Heat and Mass Transfer,* 35, 4, (1992): 957-966

Mendes, P.R. "The naphthalene sublimation technique." *Experimental Thermal and Fluid Science*, 4, 5, September (1991): 510-523

Morrison, et al. "Rapid measurements of indoor mass transfer coefficients." *Atmospheric Environment*, 2003: 5611-5619.

Morrison, GC, and DJ Wiseman. "Temporal considerations in the measurements of indoor mass transfer coefficients." *Atmospheric Environment*, 2006: 3389-3395.

Nazaroff, Gadgil, and Weschler. "Critique of the use of deposition velocity in modeling indoor air quality." In *Modeling of indoor air quality and exposure*, 81-104. Philadelphia, PA: ASTM, 1993.

Sparks, L. E. "Exposure version 2, a computer model for analyzing the effects of indoor air pollutant sources on individual exposure" EPA-600/8/91/013 (NTIS PB91-201095) (1991)

Spitler, J.D., C.O. Pederson, and D.E. Fisher. "Interior convective heat transfer in buildings with large ventilative flow rates." *AHSRAE Transactions* 97, no. 1 (1991): 505-515.

Yao, et al. "Evaluating fabric fuzziness using laser range sensing." *Optical Engineering* 47,1 (2008)

Appendix E: Validated Modeling of an Internally Cooled/Heated Low-Flow Liquid Desiccant Absorber and Regenerator for Building Dehumidification

Jordan D. Clark, Jason Woods, Eric Kozubal

Abstract

Air conditioning and dehumidification comprise a substantial part of the United States' energy use. Liquid desiccant dehumidification systems are gaining interest for commercial building applications because of their ability to reduce this energy usage. The absorber of an internally cooled, flocked-plate, low-flow liquid desiccant system is modeled. A purely physical model of the absorber is developed which compares well with previously collected laboratory data. The model does not include an empirical "wetted fraction" as has been used in the past. The model corroborates previous work which shows flocking on sparsely flocked plates need not be considered when thermal conductivity is low and suggests the flocking is distributing the desiccant well as had been observed qualitatively. Although a similar device is used for the regenerator, the physical model developed does not produce outputs consistent with measured data, as has been seen in previous work. Instead of the physical model, an empirical model is given to predict regenerator performance. These models can be used to predict system performance under various operating conditions and optimize components.

Introduction

Space cooling and ventilation in buildings account for 8% of primary energy usage in the United States and over 19% of electricity consumption (U.S. Department of Energy, 2012). The overwhelming majority of air conditioning is provided by electrically driven vapor compression systems which dehumidify by cooling air beyond its dewpoint in order to condense water out of the air and then reheat the air to bring it to the supply condition. Liquid desiccant systems have been gaining interest recently as a means of providing dehumidification without using vapor compression overcooling and reheat. Several different types of benefits have been demonstrated, including: a shift in energy usage for dehumidification from electricity to more efficient thermal sources; elimination of hazardous refrigerants; reduction in overall energy usage by eliminating the overcool-reheat cycle which occurs in vapor compression systems; a shift in load profiles and a reduction in peak power demand; and more stable and deeper dehumidification of buildings which can result in cost benefits from better indoor air quality as well as ancillary savings from things such as reduced energy usage for defrosting display cases in grocery stores.

1.1.1 Overview of LFLDA

Many different types of liquid desiccant systems have been proposed. A review of available technologies is given in (Lowenstein, 2008). Among these is the Low Flow Liquid Desiccant (LFLD) system which is described in detail in (Lowenstein, Slayzak, & Kozubal, 2006) and (Lowenstein, 2004). The LFLD prototype was developed by AIL Research and is shown in Figure E1. It consists of a parallel plate absorber, an interchange heat exchanger to transfer sensible energy between the strong hot desiccant

stream and the weak cold one, and a parallel plate regenerator to remove water from the weak desiccant. The present work is concerned with the operation of the absorber and regenerator. A lithium chloride solution is used as the desiccant for all of this work.

A cross section of the LFLD absorber or regenerator is also depicted at the bottom of Figure E1. These components consist of a set of extruded CPVC plates with internal flutes through which cooling water flows and external surfaces flocked with polyester flocking fibers to distribute the desiccant. Desiccant flow is perpendicular to air flow and water flow is anti-parallel to the desiccant flow in the process air entrance region and parallel to it in the process air exit region. Process air flows between adjacent flocked surfaces. Flocking allows for better distribution of desiccant on the plate surface.

Flow rates of the three fluids are bounded by material limitations and operating conditions. Water flow rates are limited by the pressure limitations of the CPVC plates. Desiccant and air flow rates are limited in order to prevent any carryover of desiccant droplets into the air stream. Carryover involves the entrainment of small droplets of desiccant into the process air stream. This is very undesirable in building applications as the corrosive desiccant (usually a salt solution) can damage ducts and downstream equipment if it is not removed with a high efficiency mist eliminator. This adds fan power costs and requires additional maintenance. Desiccant and air flow are arranged in cross-flow for the same reason. (Lowenstein, Slayzak, & Kozubal, 2006) showed that with these arrangements and limitations, no desiccant was entrained into the airstream, eliminating the need for a droplet filter downstream. Internal cooling/heating which is present in the LFLD exchangers allows for more efficient operation by counteracting the

heat of absorption/desorption. The LFLD is also currently being demonstrated in several retrofit commercial building applications throughout the United States.

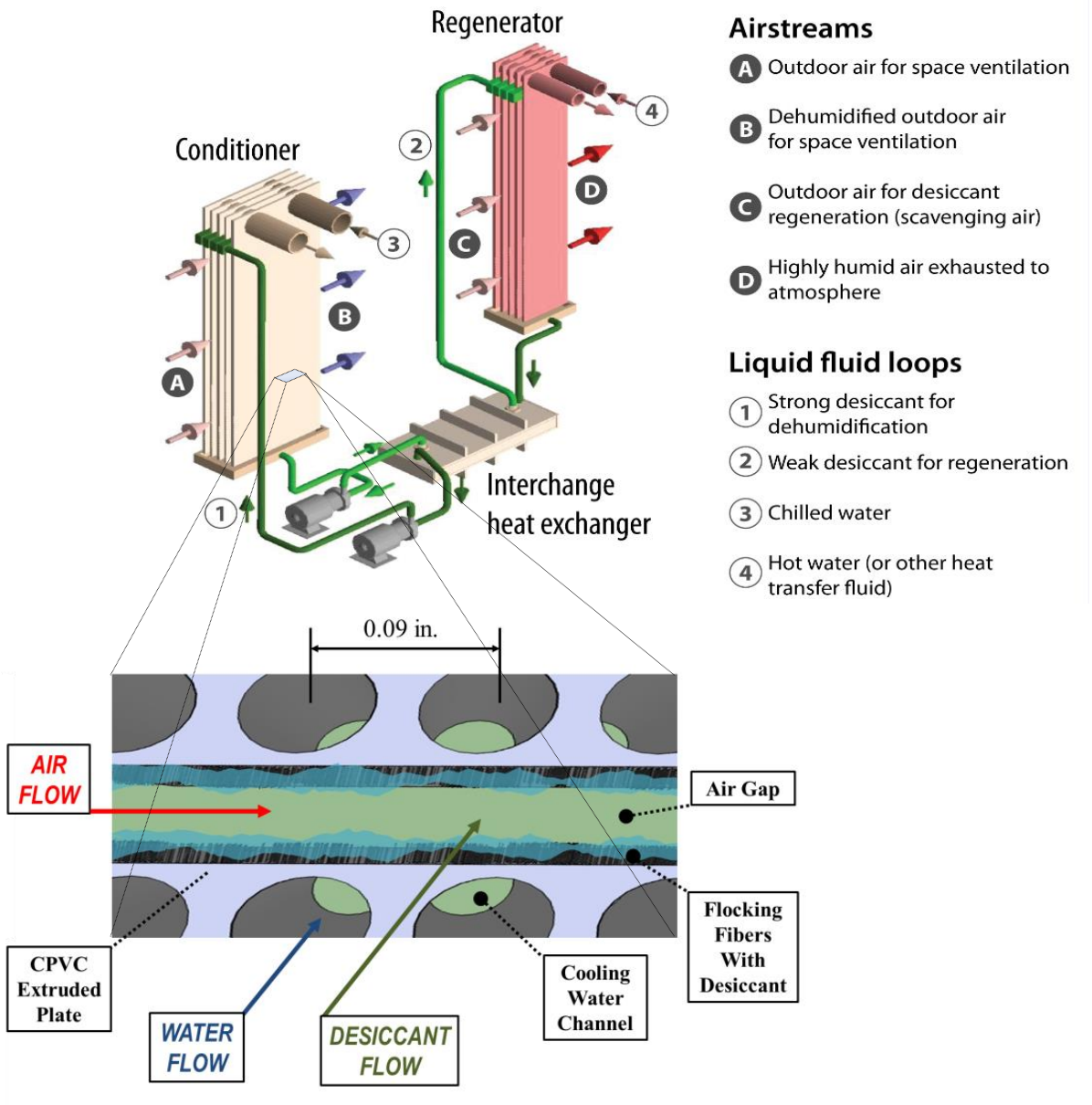

Figure E1. Depiction of low flow liquid desiccant system with section view magnification of water plate, air channel and desiccant film. Credit for system photo to AIL Research.

1.2 Previous research in modeling internally cooled liquid desiccant absorbers

Numerous researchers have developed mathematical models to predict the performance of desiccant absorbers and regenerators, (exchangers). Packed-bed and spray-type adiabatic exchangers have been studied for quite a while and their performance is well understood. More recently, researchers have developed models for internally cooled/heated exchangers (Khan, 1998), (Kessling, Laevemann, & Peltzer, 1998), (Liu, Chang, & Jiang, 2009), (Mesquita, Harrison, & Thomey, 2006), (Park, Howell, Vliet, & Peterson, 1994), (Peng & Howell, 1981), (Pietruschka, Eicker, Huber, & Schumacher, 2006), (Qi, Lu, & Yang, 2013), (Rahamah, Elsayed, & Al-Najem, 1998), (Ren, Tu, & Wang, 2007), (Saman & Alizadeh, 2001), (Scalabrin & Scaltriti, 1988), (Woods & Kozubal, 2013), (Yin Y. , Zhang, Peng, & Li, 2009), (Zhang, Liu, & Jiang, 2012). These have been shown to perform better than adiabatic exchangers (Pietruschka, Eicker, Huber, & Schumacher, 2006), (Liu, Chang, & Jiang, 2009) or regenerators (Yin Y. , Zhang, Peng, & Li, 2009). This is due to two differences between adiabatic and internally cooled/heated systems. First, internally cooled (or heated) systems reduce the change in desiccant temperature across the device, which translates to a much lower (or higher) equilibrium vapor pressure above the desiccant and thus a greater affinity for water absorption (or desorption). Second, by removing the latent heat of absorption, internally cooled systems reduce the load that a secondary sensible system must meet, often through "free" cooling such as a cooling tower or other direct or indirect evaporative cooling device.

Different means of internal cooling or heating have been studied, including absorbers with integral indirect evaporative coolers (Pietruschka, Eicker, Huber, & Schumacher, 2006), (Saman & Alizadeh, 2001), (Woods & Kozubal, 2013), (Kozubal,

Woods, Burch, Boranian, & Merrigan, 2011), plate fin tube absorbers (Khan, 1998) (Park, Howell, Vliet, & Peterson, 1994), (Peng & Howell, 1981), (Mahmoud & Ball, 1992), (Zhang, Liu, & Jiang, 2012) and internally cooled, falling film, flat plate absorbers (Peng & Howell, 1981), (Park, Howell, Vliet, & Peterson, 1994), (Liu, Chang, & Jiang, 2009), (Ren, Tu, & Wang, 2007), (Woods & Kozubal, 2013). Advantages of IE-integrated systems include free cooling and often the lack of a need for a secondary sensible system such as a VC system. Advantages of an integral coil type system such as a plate fin tube system are lower cooling water temperatures and synergistic benefits from integration with a VC system, such as a simultaneous lowering of the desiccant vapor pressure and sensible cooling.

Assumptions used in the models vary by application but some general trends can be noticed. Nearly all employed assumptions of negligible heat transfer to surroundings, constant physical properties of the fluids, negligible diffusive transport in the direction of flow, fully developed flow, and negligible shear at the solution-air interface. With a few exceptions, all component-level models are steady state. (Diaz, 2010) modeled a transient falling film absorber and showed that it reaches a steady condition after 2-3 minutes. This compared well with the experimental work in the same vein done by (Gandhidasan, Al-Farayedhi, & Antar, 2002). (Peng & Pan, 2009) modeled transient operation in a packed bed absorber with low flow rates and showed that even under these operating conditions, the system stabilized after five minutes, and most variables were within 10% of their steady state value after three minutes.

Some researchers have employed additional assumptions of constant heat and mass transfer coefficients (Liu, Chang, & Jiang, 2009), (Ren, Tu, & Wang, 2007),

(Scalabrin & Scaltriti, 1988), (Jain, Dhar, & Kaushik, 2000). Some make simplifying assumptions such as an isothermal plate (Mesquita, Harrison, & Thomey, 2006), (Rahamah, Elsayed, & Al-Najem, 1998), (Mahmoud & Ball, 1992), negligible plate heat transfer resistance (Pietruschka, Eicker, Huber, & Schumacher, 2006), (Saman & Alizadeh, 2001), (Yin Y. , Zhang, Peng, & Li, 2009) or negligible desiccant heat transfer resistance (Rattner, Nagavarapu, Garimella, & Fuller, 2011), (Mesquita, Harrison, & Thomey, 2006). (Liu, Jiang, & Qu, 2007) assumed a constant desiccant concentration in the direction transverse to the direction of flow in a falling film absorber. The validity of these assumptions is usually justified by preliminary calculations and will vary from application to application.

One important assumption made in many models of exchangers is the use of an empirical "wetted fraction" to account for uneven desiccant coverage of the surfaces at which mass transfer occurs (Kessling, Laevemann, & Peltzer, 1998), (Peng & Howell, 1981), (Pietruschka, Eicker, Huber, & Schumacher, 2006), (Ren, Tu, & Wang, 2007), (Yin Y. , Zhang, Peng, & Li, 2009), (Jain, Dhar, & Kaushik, 2000). The selection of the proper wetting fraction is often the goal of the modeling effort and has been shown to significantly affect the results. For example, (Katejanekarn & Kumar, 2008) showed that varying wetted fraction from 0.25 to 1 resulted in an evaporation rate three times greater. (Kessling, Laevemann, & Peltzer, 1998) found this to be one of the most important parameters in determining the performance and encouraged further research into improving it. (Pietruschka, Eicker, Huber, & Schumacher, 2006) suggested a wetted fraction of 0.6 or greater for efficient operation.

Specifically in the regenerator modeling, the literature points to some potential pitfalls. (Andrusiak, Harrison, & Mesquita, 2010) found that the large temperature differences in the regenerator led to situations that were not easily modeled with purely physical models and opted for a purely empirical model of the regenerator. (Jain, Dhar, & Kaushik, 2000) found much better agreement in their absorber model than in that of the conditioner. (Rattner, Nagavarapu, Garimella, & Fuller, 2011) found that air-gap membrane distillation system with similar geometry and temperatures to the regenerator being studied in the current work could not be adequately modeled without the inclusion of complicated radiation heat transfer effects. Their system included nearby membranes with large temperature differences in close proximity to each other, however.

Systems modeled in existing literature differ somewhat from the system being modeled in the current work and the model created herein must be adjusted accordingly. The exchangers modeled in this work include flocking to distribute desiccant more evenly. This has been shown qualitatively to distribute desiccant over the entire surface of the plate, possibly preventing the need for an empirical "wetted fraction" parameter. The current system is also designed to operate at very low desiccant flow rates (ratios of air mass flow rate to desiccant mass flow rate of 6-25) and therefore the desiccant properties can change more drastically within the exchanger and cannot be assumed constant. This may lead to large temperature differences within the system as well which may lead to buoyancy forces being appreciable. As material properties for the desiccant being analyzed, a Lithium Chloride-water solution, are well documented now, variable material properties may be easily included to increase accuracy. Lastly, the presence of the flocking could affect the flow of the desiccant or air.

Objectives

The objectives of the current work are to develop a model of the absorber and of the regenerator which can be used to predict performance at all expected operating conditions, and validate this model with previously measured laboratory data.

General modeling assumptions and procedure

The following assumptions were used in the physical modeling of the exchangers:

1. Steady state operation is employed nearly uniformly in the modeling of liquid desiccant heat and mass exchangers and is used here as well, as the boundary conditions of a typical system change much more slowly than the internal state variables.
2. A resistance-in-series model was used for modeling heat transfer between the three fluids
3. Lewis-Whitman two-film theory with a single value for the Henry's constant was used for mass transfer modeling. Actual Henry's constant values vary by ±5% over the range of likely operating conditions and ±9% over the entire range of conditions that could ever be expected even at extreme operating conditions.
4. Laminar developing flow transfer coefficients for both heat and mass transfer (Bejan, 2004) from the bulk air to the air-desiccant interface, assuming a smooth surface, no shear the interface, and constant temperature within each cell at the interface and no fluid-fluid interaction. A fully developed assumption is often used, but preliminary calculations showed that this assumption added appreciable error in the LFLD model.

5. Developing flow falling film transfer coefficients for mass transfer modeling in the desiccant film, taken from (Grossman, 1982)
6. Estimations of heat transfer resistance in the desiccant film showed that the heat transfer resistance in the desiccant was less than 1% of the overall resistance and justified neglect of this resistance.
7. The flocking on the plate surface uniformly distributed the desiccant over the plate surface (as was qualitatively verified in the laboratory) but negligibly affected heat and mass transfer within the desiccant layer. Neglecting the effect of the flocking on transport is justified by which shows a less than 5% effect on Nusselt number under the operating conditions of the LFLD system.
8. The desiccant-plate interface was assumed to be impermeable to moisture transfer.
9. Conduction shape factors were used to model thermal conductance between the desiccant-plate interface and the water-plate interface. These were calculated with the correlation given in (Lund & Knowles, 2001).
10. Conduction and diffusion were assumed to occur in one dimension only (perpendicular to the plates) as is uniformly done in absorber modeling, justified by the much quicker rate of advection in this direction than diffusion.
11. Heat transfer coefficients describing heat transfer from the plate-water interface to the bulk water were taken from fully-developed correlations for laminar pipe flow. This resistance was estimated at 2-3% of the overall heat transfer resistance; thus, any error in this assumption should be negligible.

12. All desiccant properties were assumed to be functions of the temperature and concentration in each cell and were taken from (Conde, 2009) except for enthalpy, which was calculated with a correlation provided by AIL Research.

Half of a single plate, one desiccant film, and half of the adjacent air gap was modeled. The plate was divided into 8 equally sized elements in each direction for absorber modeling and 16 for regenerator modeling and the mass and energy conservation equations were solved in each element. Increasing grid resolution beyond this point was shown to negligibly affect the results (<1% change in relevant quantities). Residuals were calculated for energy conservation equations on the three fluids and mass conservation on the desiccant and air in each cell. Five corresponding state variables were adjusted at each iteration: three fluid temperatures and desiccant and air concentrations. A Newton solver was used to adjust state variables in each cell until normalized residuals were below 10^{-7}, at which time energy balances were accurate within 0.015% and mass balances within machine precision. For most inlet conditions, solutions converged in fewer than 10 iterations, which took roughly 2 minutes per condition modeled.

Absorber Empirical Constants and Agreement

The numerical model was compared against laboratory data previously measured at the National Renewable Energy Laboratory in Golden, CO to assess its validity. A description of the experimental setup is given in (Lowenstein, Slayzak, & Kozubal, 2006). The laboratory conditions used for comparison are given in Table E1 for the conditioner and Table E2 for the regenerator. With the stated assumptions and methods employed, the modeled moisture removal rate in the absorber compared well with the 32

lab conditions tested as shown in Figure E2. Prediction of mass transfer/moisture removal in the absorber was accomplished with purely physical descriptions (no empirical constants).

Table E1. Experimental data for LFLD absorber used to validate model

RUN #	$P_{ambient}$ (Pa)	L_{Plate} (in)	W_{Plate} (in)	# Plates	$T_{Water,In}$ (deg C)	MFR_{Water} (kg/hr)	$T_{Air,In}$ (deg C)	MFR_{Air} (kg/hr)	$\omega_{Air,In}$ (kg/kg)	$T_{Desiccant,In}$ (deg C)	$MFR_{Desiccant}$ (kg/hr)	$C_{Desiccant}$ (kg/kg soln)
1	82890	48	12	42	27.9	3381	30.0	1692	0.0133	38.4	131	0.375
2	**81928**	**48**	**12**	**42**	**28.0**	**3374**	**30.0**	**1672**	**0.0165**	**39.7**	**141**	**0.365**
3	81915	48	12	42	26.0	3383	30.0	1683	0.0233	39.1	133	0.360
4	**81965**	**48**	**12**	**42**	**27.2**	**3378**	**30.0**	**1676**	**0.0164**	**38.6**	**285**	**0.365**
5	81836	48	12	42	25.6	3385	30.0	1683	0.0233	39.9	281	0.370
6	**81715**	**48**	**12**	**42**	**27.5**	**3385**	**30.0**	**1663**	**0.0164**	**37.8**	**399**	**0.365**
7	81903	48	12	42	25.2	3386	30.0	1686	0.0233	40.2	424	0.365
8	**81862**	**48**	**12**	**42**	**27.2**	**2259**	**30.0**	**1680**	**0.0164**	**36.8**	**276**	**0.355**
9	81900	48	12	42	28.1	3382	30.0	1679	0.0165	37.0	275	0.355
10	**81839**	**48**	**12**	**42**	**28.2**	**4509**	**30.0**	**1679**	**0.0164**	**36.9**	**276**	**0.355**
11	81488	48	12	42	27.5	3391	30.0	1673	0.0165	40.1	138	0.400
12	**81496**	**48**	**12**	**42**	**25.4**	**3391**	**29.9**	**1680**	**0.0233**	**43.0**	**151**	**0.400**
13	81464	48	12	42	26.8	3391	30.0	1675	0.0164	40.4	277	0.400
14	**81482**	**48**	**12**	**42**	**25.1**	**3385**	**30.0**	**1682**	**0.0233**	**42.7**	**279**	**0.395**
15	82241	48	12	42	26.5	3384	30.0	1683	0.0165	44.7	74	0.440
16	**82200**	**48**	**12**	**42**	**26.1**	**3381**	**30.0**	**1683**	**0.0165**	**44.2**	**147**	**0.440**
17	81599	48	12	42	24.9	3381	30.1	1684	0.0232	45.5	146	0.435
18	**82107**	**48**	**12**	**42**	**28.4**	**3388**	**30.0**	**1683**	**0.0097**	**39.3**	**276**	**0.440**
19	82137	48	12	42	26.2	3378	30.0	1692	0.0164	44.5	283	0.440
20	**81599**	**48**	**12**	**42**	**24.9**	**3381**	**30.1**	**1684**	**0.0232**	**45.5**	**147**	**0.440**
21	81928	48	12	42	28.0	3374	30.0	1672	0.0165	39.7	141	0.365
22	**81488**	**48**	**12**	**42**	**27.5**	**3391**	**30.0**	**1673**	**0.0165**	**40.1**	**138**	**0.400**
23	82200	48	12	42	26.1	3381	30.0	1683	0.0165	44.2	147	0.440
24	**82925**	**48**	**12**	**42**	**27.7**	**3379**	**30.0**	**2262**	**0.0162**	**35.0**	**141**	**0.363**
25	82890	48	12	42	25.2	3368	30.2	2287	0.0233	37.1	141	0.363
26	**82896**	**48**	**12**	**42**	**27.0**	**3374**	**30.0**	**3430**	**0.0164**	**34.5**	**136**	**0.363**
27	82265	48	12	42	28.9	3376	30.0	2254	0.0098	34.3	135	0.403
28	**81938**	**48**	**12**	**42**	**26.7**	**3375**	**30.0**	**2260**	**0.0165**	**38.2**	**142**	**0.400**
29	82427	48	12	42	24.2	3367	30.0	2275	0.0233	38.6	138	0.395
30	**81907**	**48**	**12**	**42**	**26.5**	**3377**	**30.0**	**2256**	**0.0164**	**38.3**	**67**	**0.400**
31	81938	48	12	42	26.7	3375	30.0	2260	0.0165	38.2	142	0.400
32	**81852**	**48**	**12**	**42**	**26.5**	**3373**	**30.0**	**2258**	**0.0164**	**39.4**	**210**	**0.398**

P: Pressure; T: Temperature; MFR: mass flow rate; C: Concentration; ω: humidity ratio

Table E2. Experimental data for LFLD regenerator

RUN	$P_{ambient}$	L_{Plate}	W_{Plate}	# $_{Plates}$	$T_{Water,\,in}$	MFR_{Water}	$T_{Air,\,in}$	MFR_{Air}	$\omega_{Air,in}$	$T_{Desiccant,\,in}$	$MFR_{Desiccant}$	$C_{desiccant,\,in}$
	(Pa)	(inches)	(inches)		(deg C)	(kg/hr)	(deg C)	(kg/hr)	(kg/kg)	(deg C)	(kg/hr)	(kg/kg soln)
1	82451	24	6.5	21	93.00	1356.9	30.00	221	0.016434	63.21	54.1	0.343
2	82584	24	6.5	21	93.02	1352.8	30.00	221	0.016370	65.33	81.9	0.360
3	81884	24	6.5	21	93.06	1361.3	30.00	221	0.016257	66.66	82.1	0.365
4	82468	24	6.5	21	92.99	1363.1	30.00	221	0.016418	65.66	82.0	0.363
5	82420	24	6.5	21	93.03	1343.2	30.00	221	0.016395	65.61	110.2	0.375
6	81395	24	6.5	21	82.20	1360.3	30.00	221	0.016435	53.02	26.8	0.318
7	82984	24	6.5	21	82.20	1367.9	30.00	221	0.016491	56.70	54.7	0.355
8	81333	24	6.5	21	82.21	1354.7	30.00	221	0.016414	58.36	63.1	0.363
9	82629	24	6.5	21	82.20	1367.8	30.00	221	0.016520	59.99	82.8	0.373
10	81708	24	6.5	21	71.12	1375.9	30.00	221	0.016343	50.56	35.8	0.363
11	82892	24	6.5	21	71.16	1362.8	30.00	221	0.016400	53.06	55.6	0.380
12	81289	24	6.5	21	71.05	1362.5	30.00	221	0.016390	49.98	55.7	0.380
13	82548	24	6.5	21	93.00	902.2	30.00	221	0.016362	64.90	82.4	0.370
14	82584	24	6.5	21	93.02	1352.8	30.00	221	0.016370	65.33	81.9	0.360
15	81884	24	6.5	21	93.06	1361.3	30.00	221	0.016257	66.66	82.1	0.365
16	82468	24	6.5	21	92.99	1363.1	30.00	221	0.016418	65.66	82.0	0.363
17	82520	24	6.5	21	93.00	1817.6	30.00	221	0.016471	65.47	82.1	0.365
18	82584	24	6.5	21	93.02	1352.8	30.00	221	0.016370	65.33	81.9	0.360
19	82468	24	6.5	21	92.99	1363.1	30.00	221	0.016418	65.66	82.0	0.363
20	81884	24	6.5	21	93.06	1361.3	30.00	221	0.016257	66.66	82.1	0.365
21	81881	24	6.5	21	93.00	1351.7	42.16	221	0.016542	67.22	81.9	0.363
22	81967	24	6.5	21	93.00	1357.2	56.42	221	0.016383	66.54	81.9	0.360
23	82016	24	6.5	21	93.00	1350.9	30.00	287	0.016392	64.69	81.9	0.360
24	82027	24	6.5	21	92.99	1345.5	40.90	287	0.016296	64.46	82.0	0.360
25	82060	24	6.5	21	92.98	1339.2	54.61	287	0.016424	65.84	81.8	0.358
26	81027	24	6.5	21	93.06	1347.5	30.00	354	0.016371	65.69	81.9	0.360
27	81042	24	6.5	21	92.96	1349.4	39.90	354	0.016571	65.79	81.9	0.360
28	81026	24	6.5	21	92.99	1357.6	53.09	354	0.016297	66.53	81.7	0.358
29	81066	24	6.5	21	93.03	1358.8	29.99	221	0.016207	64.28	80.2	0.323
30	81101	24	6.5	21	93.00	1351.6	41.18	221	0.016444	63.68	80.0	0.318
31	81135	24	6.5	21	93.00	1347.7	54.20	221	0.016392	63.76	79.7	0.313
32	81551	24	6.5	21	93.01	1348.2	30.00	221	0.016399	65.76	84.1	0.405
33	81734	24	6.5	21	93.03	1347.9	42.68	221	0.016422	65.47	84.0	0.403
34	81727	24	6.5	21	93.01	1356.4	57.45	221	0.016246	66.03	84.0	0.403
35	82654	24	6.5	21	93.00	1374.5	30.00	221	0.009829	66.23	81.6	0.355
36	82584	24	6.5	21	93.02	1352.8	30.00	221	0.016370	65.33	81.9	0.360
37	81884	24	6.5	21	93.06	1361.3	30.00	221	0.016257	66.66	82.1	0.365
38	82468	24	6.5	21	92.99	1363.1	30.00	221	0.016418	65.66	82.0	0.363
39	82547	24	6.5	21	93.00	1367.4	30.00	221	0.023572	65.74	82.1	0.365
40	81333	24	6.5	21	82.21	1354.7	30.00	221	0.016414	58.36	63.1	0.363
41	81341	24	6.5	21	82.20	1350.4	40.24	221	0.016390	58.57	63.0	0.360
42	81326	24	6.5	21	82.18	1346.2	52.40	221	0.016381	59.39	62.9	0.358
43	81708	24	6.5	21	71.12	1375.9	30.00	221	0.016343	50.56	35.8	0.363
44	81777	24	6.5	21	71.08	1366.9	38.67	221	0.016439	51.00	35.8	0.360
45	81812	24	6.5	21	71.08	1364.8	48.95	221	0.016459	50.56	35.7	0.358

P: Pressure; T: Temperature; MFR: mass flow rate; C: Concentration; ω: humidity ratio

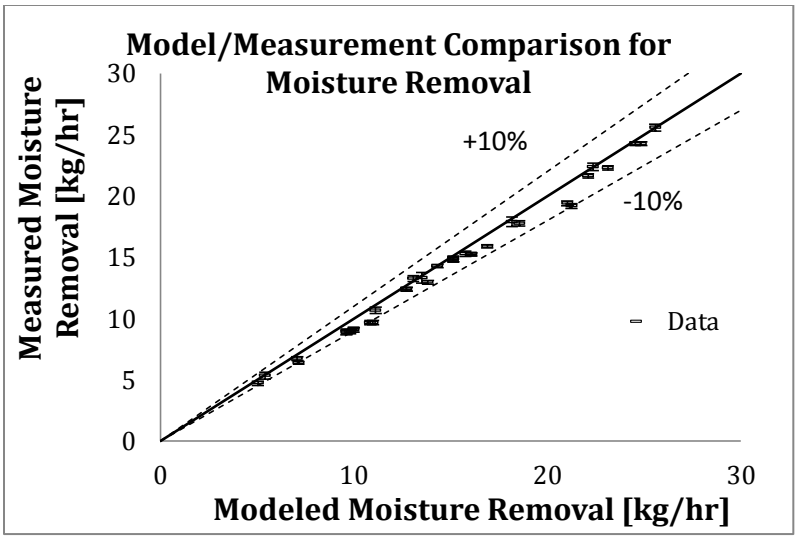

Figure E2. Comparison of conditioner model and laboratory data showing good agreement. Error bars reflect precision of chilled mirrors used to measure removal rate in process air stream.

However, temperature of the fluid streams could not be measured immediately at the boundary of the modeled domain because of practical limitations such as presence of the sump and the water distribution header. For this reason some heat transfer occurred between the fluids and the ambient before the temperature measurement point. This led to a discrepancy between the modeled and measured temperatures of the fluid which increased with temperature difference between exiting fluid and the ambient in the laboratory. Figure E3 shows this discrepancy for each of the three fluids. The vertical dashed line represents the ambient conditions in the space.

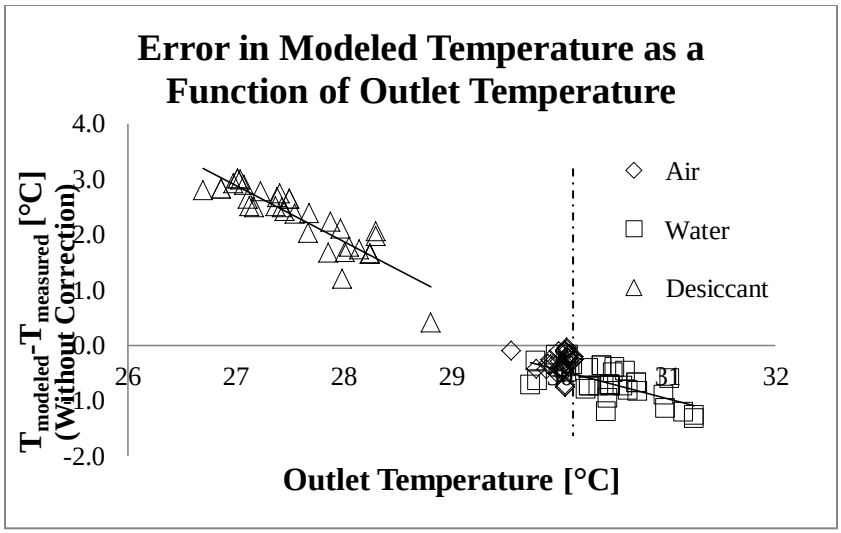

Figure E3. Discrepancy between measured and modeled temperature in three fluids of the absorber.

An empirical heat transfer coefficient between the exiting fluid and the ambient, h in Equation 1, was thus assumed to account for these losses.

Eq. (1)

$$\dot{m}_{\text{fluid}}(T_{\text{fluid,model}\textbf{(edge of domain)}}-T_{\text{fluid,model}\textbf{(measuring point)}})=h(T_{\text{fluid, model}\textbf{(edge of domain)}}-T_{\text{ambient}})$$

The value h was chosen so as to minimize the root mean squared discrepancy between modeled and measured temperatures for the 32 laboratory conditions tested. These adjustments changed the modeled outlet fluid temperatures by an average of 2.3°C in the relatively hot desiccant, an average 0.6°C in the exiting water temperature and an average of 0.2°C change in the leaving air temperature. Instruments used to measure the temperature of the three fluids were accurate to 0.3°C, 0.3°C, and 0.4°C for the desiccant, water, and air, respectively. These adjustments correspond to physical processes which

do occur in reality and have very little bearing on the analyses that have been conducted with this model, but were necessary to completely capture the operation of the absorber.

When the heat transfer coefficient mentioned previously was employed, modeled exit temperatures matched well with measured temperatures as shown in Figure E4. The error bars in Figure E4 represent the bounds of the precision of the measuring instruments.

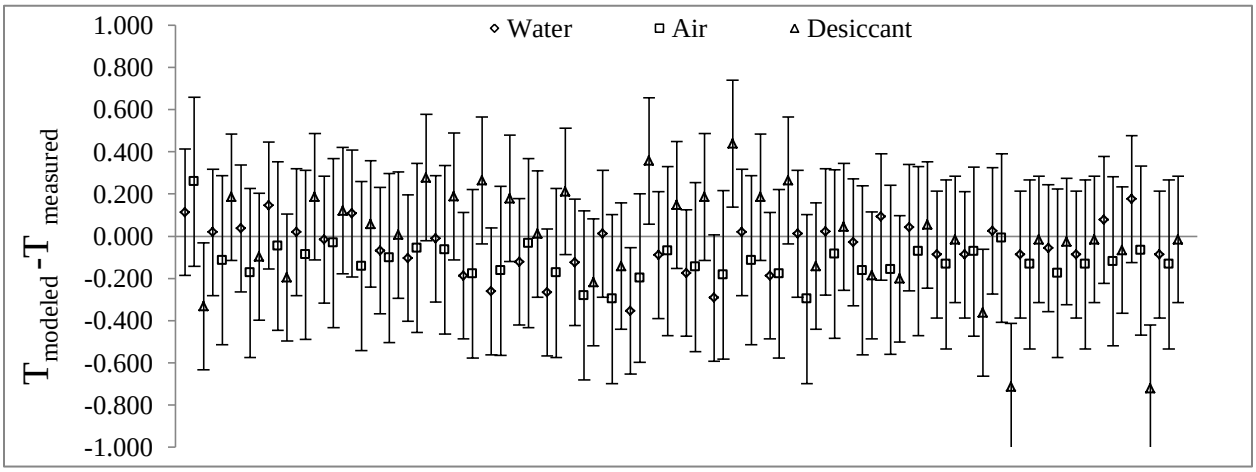

Figure E4. Discrepancy between modeled and measured outlet temperatures of three fluids. Error bars represent precision of measuring instruments

Regenerator Model Comparison and Empirical Formulation

As expected, the regenerator modeling presented more challenges than the absorber, as it had for previous researchers. The model compared poorly with the measured rates (measured performance was roughly 40% less than modeled) as shown in Figure E5. Because this design for the regenerator is shown to be performing poorly and

because it is being replaced in current field demonstrations with a better performing design, no further attempt to explain this discrepancy is made here.

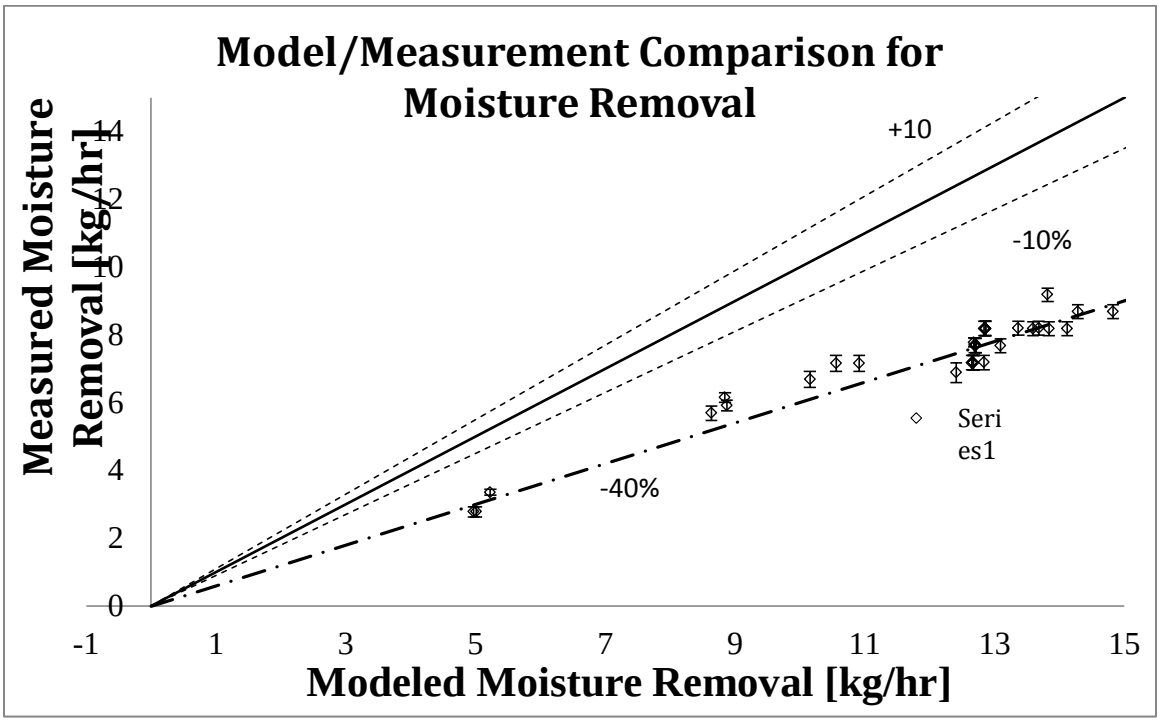

Figure E5. Comparison between model and measurement in regenerator. Error bars reflect accuracy of instruments used to measure desiccant concentration. Dotted line is 60% of modeled moisture removal rate.

An empirical correlation of the regenerator performance made from the laboratory data was used for all subsequent modeling and new designs for the regenerator are being pursued. This model consists of 5 equations relating outlet variables to inlet variables:

Eq. (2)

$\dot{Q}_{to\ air} = n_{plates} * (-3793.79139 + 5.62846 * T_{water,in} - 1.44018 * T_{air,in} + 4.10103 * T_{desiccant,in} + 4402.41865 * \dot{m}_{water}/n_{plates} + 23953.53347 * \dot{m}_{air}/n_{plates} + 30838.80248 * \dot{m}_{desiccant}/n_{plates} - 2789.89082 * x_{air} + 1707.29795 * x_{desiccant})$;

Eq. (3)

$\dot{Q}_{to\ water} = n_{plates} * (3350.00623 - 6.97888 * T_{water,in} + 0.95601 * T_{air,in} - 1.69869 * T_{desiccant,in} - 7040.46422 * \dot{m}_{water}/n_{plates} - 18134.97518 * \dot{m}_{air}/n_{plates} - 32349.13297 * \dot{m}_{desiccant}/n_{plates} + 1618.95505 * x_{air} - 1231.91233 * x_{desiccant})$;

Eq. (4)

$\dot{m}_{water\ to\ air} = n_{plates} * (-1.59745E-003 + 1.63726E-6 * T_{water,in} + 3.72626E-7 * T_{air,in} + 1.56086E-6 * T_{desiccant,in} + 1.44082E-3 * \dot{m}_{water}/n_{plates} + 5.58160E-3 * \dot{m}_{air}/n_{plates} + 0.012945 * \dot{m}_{desiccant}/n_{plates} - 1.18556E-3 * x_{air} + 7.09998E-4 * x_{desiccant})$

Eq. (5)

$\dot{Q}_{to\ water} + \dot{Q}_{to\ air} + \dot{Q}_{to\ desiccant} = 0$

$\dot{m}_{water\ to\ air} + \dot{m}_{water\ to\ desiccant} = 0$

where $\dot{Q}$ is the rate of sensible energy transfer,
$\dot{m}$ is the mass flow rate;
n_{plates} is the number of plates in the regenerator;
T is temperature;
and x is mass fraction of water.

The first three equations predict measured performance with coefficients of determination (R^2) of 0.99, 0.98 and 0.98, respectively and the last two equations ensure conservation of mass and energy. This model is valid for a 24 inch tall, 6.5 inch deep (in direction of air flow) regenerator.

Discussion and Conclusion

A first-principles physical model of the heat and mass transfer processes inside an internally cooled low-flow liquid desiccant absorber were modeled. Dehumidification was predicted with no empirical parameters and empirical heat transfer coefficients used to predict outlet temperatures changed modeled heat transfer coefficients only slightly. Model outputs compared well with experimental data. Physical modeling of regenerator performance was unsuccessful, as has been found by previous researchers. An empirical model of the regenerator is given, generated with laboratory data. With the model, analysis of design parameters was conducted.

The model developed and used herein was for a particular manufacturer and configuration. The absorber model should be robust for different operating conditions, such as varying flow rates, temperatures, etc. The use of different materials for components of either device will certainly affect performance. Specifically, a thermally conductive flocking material or a different plate material will likely affect results significantly. Analysis has begun utilizing this model which can determine the effect of different conditioner shapes, flow rates, operating temperatures, etc. on performance.

Concerns about the wisdom of using the conditioner design for regeneration purposes were deepened by the modeling effort, which showed a 40% underperformance with the current design. New designs are currently being pursued. The empirical model of the regenerator given herein is sufficient for system-level modeling and quantification of energy savings possible with the LFLD system.

Future modeling work should analyze the interactions of the conditioner and the regenerator and other components of the liquid desiccant system such as a cooling tower,

heat exchangers, boilers and storage tanks. Also interesting will be the dynamic performance of the system, and the energy savings achievable with such a system.

5. Acknowledgments

This research was funded by the American Reinvestment and Recovery Act through the National Renewable Energy Laboratory's Commercial Buildings Partnership. The authors would like to thank Andy Lowenstein of AIL Research and Greg Barker of Mountain Energy Partnership for help in coding and creating simulation tools.

6. References

1. U.S. Department of Energy (2012) *2011 Buildings Energy Data Book.* Washington, DC: U.S. Department of Energy
2. Lowenstein, A. (2008) Review of liquid desiccant technology for HVAC applications. *HVAC&R Research,* 14 (6) pp. 819
3. Lowenstein, A. et al. (2006) A zero carryover liquid-desiccant air conditioner for solar applications. *Proceedings of ISEC2006,* ISEC2006-99079
4. Lowenstein, A. (2004) *US Patent 6,745,826 B2.* Washington, DC: U.S.
5. Kessling, W; Laevemann, E; and Peltzer, M. (1998) Energy storage in open cycle liquid desiccant cooling systems. *International Journal of Refrigeration* 21 (2) 1998
6. Khan, Arshad (1998) Cooling and dehumidification performance analysis of internally-cooled liquid desiccant absorbers. *Applied Thermal Engineering* 18 (5) pp. 265-281
7. Liu, X et al. (2009) Performance analysis on the internally cooled dehumidifier using liquid desiccant *Building and Environment* 44 (2) pp. 299-308
8. Mesquita, L; Harrison, S. and Thomey, D. (2006) Modeling of heat and mass transfer in parallel plate liquid-desiccant dehumidifiers. *Solar Energy* 80 (11) 1475-1482
9. Park, M. et al. (1994) Numerical and experimental results for coupled heat and mass transfer between a desiccant film and air in cross-flow. *International Journal of Heat and Mass Transfer* 37 (1) pp. 395-402
10. Peng, C. and Howell, J. (1981) Analysis and design of efficient absorbers for low-temperature desiccant air conditioners. *Journal of Solar Energy Engineering* 103 pp. 67-74
11. Pietruschka, D et al. (2006) Experimental performance analysis and modelling of liquid desiccant cooling systems for air conditioning in residential buildings. *International Journal of Refrigeration* 29 (2006) 110-124
12. Qi, R.; Lu, L.; and Yang, H. (2013) Development of simplified prediction model for internally cooled/heated liquid desiccant dehumidification system *Energy and Buildings* 59 pp. 133-142

13. Rahamah, M; Elsayed, M. and Al-Najem, N. (1998) A numerical solution for cooling and dehumidification of air by a falling desiccant film in parallel flow. *Renewable Energy 13 (3) pp. 305-322*
14. Ren, C.; Tu, M.; and Wang, H. (2007) An analytical model for heat and mass transfer processes in internally cooled or heated liquid desiccant air-contact units. *International Journal of Heat and Mass Transfer*, 50 pp. 3545-3555
15. Saman, W. and Alizadeh, S. (2001) Modelling and performance analysis of a cross-flow type plate heat exchanger for dehumidification/cooling. *Solar Energy* 70 (4) pp. 361-372
16. Scalabrin, G. and Scaltriti, G. (1988) Modeling and experimental analysis of an efficient absorber for air dehumidification. *Warme und Stoffübertragung* 22 pp 111-124.
17. Woods, J; and Kozubal, E. (2013) A desiccant-enhanced evaporative air conditioner: Numerical model and experiments. *Energy Conversion and Management* 65 pp. 208-220
18. Yin, Y. et al. (2009) Model validation and case study on internally cooled/heated dehumidifier/regenerator of liquid desiccant systems. *International Journal of Thermal Sciences* 48 pp. 1664-1671
19. Yin, Y; Zhang, X and Lai, R. (2006) Modeling and comparative study on two types of dehumidifiers with liquid desiccant. *Journal of Chemical Industry and Engineering* 57 (12) 2828-2833
20. Bejan, A. (2004) *Convection Heat Transfer*. Hoboken, John Wiley and Sons.
21. Grossman, G. (1982). Simultaneous heat and mass transfer in film absorption under laminar flow. *International Journal of Heat and Mass Transfer*, 26 (3) pp. 357-371
22. Lund, K; Knowles, T. (2001) Enhanced laminar-flow heat transfer at fiber-flocked surfaces. *International Journal of Heat and Mass Transfer,* 44 pp. 1627-1636
23. Ganzevles, F; Gled, C. (1997) The shape factor of conduction in a multiple channel slab and the effect of non-uniform temperatures. *International Journal of Heat and Mass Transfer*, I40 (10) pp. 2493-2498
24. M. Conde Engineering. (2009) *Aqueous solutions of lithium and calcium chlorides: property formulations for use in air conditioning equipment design.* Zurich: M. Conde Engineering. Available at http://www.mrc-eng.com/Downloads/Aqueous%20LiCl&CaCl2%20Solution%20Props.pdf. Last accessed August 2013.

Appendix F: Detailed Assessment of the Energy- and Cost-Effectiveness of Low-Flow Liquid Desiccant System Retrofits in Supermarkets in the United States

Jordan Clark, Lesley Herrmann, Eric Kozubal, Atila Novoselac

Abstract

The behavior of liquid desiccant dehumidification systems is in many ways complementary to the effects that refrigeration systems have on typical supermarkets. Because of this, large energy and costs savings may be possible with liquid desiccant system retrofits in supermarkets in the United States. To investigate this possibility, a dynamic system model of a low flow liquid desiccant system with previously validated components is created in the Dymola platform. This model is attached to a reference supermarket, which is simulated in the EnergyPlus platform for several potentially applicable climates in the United States. Results show that savings of over 40% of total yearly cooling energy, 8% of total building energy, and 5% of total energy costs are achievable in hot humid climates. Mixed humid climates show lesser but substantial savings, while cold humid climates are shown to likely not benefit from these retrofits. Uncertainty in the model is quantified and found to be strongly affected by assumptions made for the amount of latent energy removed by the refrigeration system.

Introduction

Liquid desiccant (LD) systems have been gaining interest recently as a means of providing dehumidification without using the vapor compression (VC) cycle, which involves overcooling and reheating air to dehumidify. Several different types of benefits

have been demonstrated. At a basic level, desiccant systems shift dehumidification energy usage from electricity to cleaner and more efficient thermal sources, and reduce the amount of hazardous refrigerants used (Lowenstein, 2008). LDs have also been shown to reduce overall energy usage (Burns, Mitchell, & Beckman, 1985), (Dai, Wang, Zhang, & Yu, 2001), (Bergero & Chiari, 2010), (Kim, Park, & Jeong, 2013), (Kozubal, Woods, Burch, Boranian, & Merrigan, 2011); shift load profiles and reduce peak power demand (Kessling, Laevemann, & Peltzer, 1998), (Kozubal, Woods, Burch, Boranian, & Merrigan, 2011); provide more stable and deeper dehumidification of buildings (Lowenstein, 2008); and improve indoor air quality (Chung, Ghosh, Hines, & Novosel, 1993).

Supermarkets, however, may offer more applicability for these systems than any other building type, for three reasons. First, energy use in supermarkets is driven primarily by refrigeration and HVAC comprises a significant portion as well. Estimates for the percentage of whole-building energy consumed by refrigeration range from 23% to 50% and by HVAC; 5%-10% [(Kosar & Dumitrescu, 2005), (Spyrou, Shanks, Cook, Pitcher, & Lee, 2013), (Tassou, Ge, Hadawey, & Marriott, 2011)]. HVAC and refrigeration play complementary roles in supermarkets as is discussed further below.

The second way in which supermarkets differ from other building types is that supermarket space and supply conditions are different from an office building or other retail building, mainly due to the presence of large quantities of refrigeration equipment in the space. Refrigerators and freezers are strong heat sinks and provide the majority of the sensible cooling in supermarkets during the cooling season (Munters, 2005) while

adding heating loads in the heating season. This causes desirable supply conditions to be much warmer than in other building types and reduces the sensible heat ratio.

Recommendations exist for keeping space conditions at dry bulb temperatures comparable to offices or other building types (75°F (Munters, 2005), 66-77°F (Spyrou, Shanks, Cook, Pitcher, & Lee, 2013))(Point P in Figure F1) but somewhat drier. However, in reality building owners will not provide reheat required to maintain space conditions at this point during the cooling season, and spaces are much cooler (Point C in Figure F1). Because of the low sensible loads and low sensible heat ratio (depicted in lines J-C and L-P in Figure F1), space are colder in area with refrigerators and comfort is sacrificed.

Besides differing sensible conditions, drier conditions are more desirable in supermarkets than in other building types as well, especially in zones with freezers or refrigeration equipment. Munters (2005) recommends a 53°F dewpoint in the space and a 45-50°F supply dewpoint to maintain drier conditions. ASHRAE recommends a space condition less than 55% RH for proper refrigerated display case operation. This is due to the fact that refrigerator compressors work more efficiently in drier conditions and the need for heating energy for defrost and defogging of display cases is reduced. Numerous researchers have found a 3-21% reduction in compressor energy use with a 20% RH reduction in the; a 4-6% reduction in defrost energy and a 15-25% reduction in anti-sweat energy space [(Farmarzi, Sweetser, & Henninger, 2000) (Howell & Adams, 1991) (Henderson & Khattar, 1999) (Kosar & Dumitrescu, 2005)].

Because of these facets of supermarket operation, desiccant dehumidification is particularly well-suited for this application. Desiccant system operation and supermarket building operation are complementary in many ways, as shown in Figure F1. A typical vapor compression system process for an office is shown process A-B-C in Figure F1. A-B is accomplished by contact with cooling coils operating well below the dewpoint of

the air. B-C is accomplished partially with free (Green) reheat from condenser coils and partially with a secondary device. Larger sensible heat ratios in offices lead to a space line similar to C-D. Red lines depict active processes which must be paid for directly, while green lines depict passive process. For a supermarket cooled and dehumidified by a vapor compression, a similar process occurs (A-Q-J in the system, J-C in the space). However, for this process, the deeper dehumidification consumes much more energy and the space condition met without additional reheat is colder than recommended.

Adiabatic desiccant processes must involve pre-cooling and multi-stage operation in order to meet the desired humidity levels when outdoor enthalpy levels are high (depicted as process A-E-F-G-H-L in Figure F1). Internally-cooled desiccant processes, however, are great candidates for control of supermarkets as the passive process in an internally cooled desiccant absorber (A-K) is capable of bringing air very near to the desired supply condition (L), which in turn allows for a more comfortable space condition (point P).

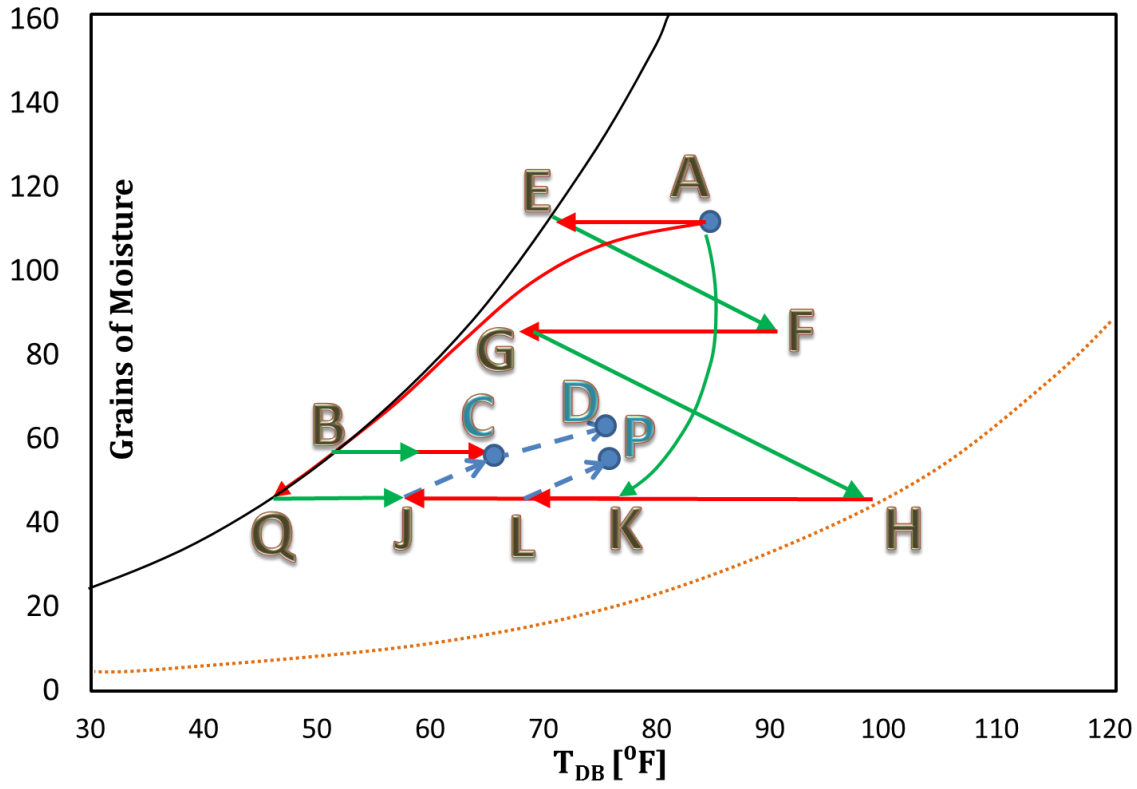

Figure F1. System and space processes in vapor compression and desiccant systems depicted in a psychrometric chart

For the reasons discussed above, desiccant systems have been shown to reduce energy use significantly in supermarkets. Lazzarin & Castellotti (2007) showed a possible 26-63% reduction in source energy use for a hybrid VC/LD system over a VC system for a single day in July. Burns showed a 50-70% reduction in air conditioning energy for a hybrid solid desiccant/VC/solar-regenerator system. Capozzoli, Mazzei, Minichiello, & Palma (2006) showed an 11-17% yearly electricity reduction and a 5-13% reduction in operating costs attributed to AC for 3 sites in Italy over the course of a year. To the authors' knowledge, however, savings possible with an internally cooled, low-flow liquid desiccant system have not been quantified. Furthermore, interaction of the

many systems within a grocery store with the desiccant system has not been conducted to any level of detail. This work seeks to fill that gap.

Objectives

The objectives of this work are to accurately model the dynamic behavior of a low-flow, internally cooled liquid desiccant (LFLD) system (Lowenstein, Slayzak, & Kozubal, 2006) and its effect on typical supermarket operation, then use this model to quantify the savings which are achievable with LD retrofits in supermarkets across the United States. A detailed error analysis is conducted to establish the precision of the models.

Energy Modeling Approach

The lack of information on desiccant performance in grocery stores is due to the complexities involved in modeling the coupled behavior of novel HVAC systems and the buildings they condition. Software is becoming available of late which allows for such a calculation and this is used in this study. The building simulation tool EnergyPlus is used to simulate building performance of a reference supermarket carefully designed to allow for benchmarking of new technologies. Through the Energy Management System interface of EnergyPlus, air boundary conditions on the existing building air handling unit are altered to reflect the conditions of the air exiting the LFLD system. The LFLD system is modeled dynamically with the system modeling software Dymola. The LFLD is modeled as a constant volume dehumidifier and ventilator (similar to Dedicated Outdoor Air System operation). Sensible control is provided by the existing system. The following sections describe the modeling assumptions.

Climate Zones

For this work, 6 representative cities (shown in Table F1 along with quantifications of sensible and latent loads) in 6 ASHRAE climate zones expected to benefit most from LFLD retrofits were tested.

Climate Zone	Representative City	Climate	Total Ventilation Load (Btu/lb-days)	Total Moisture Load (lb/lb-days)
1A	Miami, FL	Hot, Moist	8003	3.01
2A	Houston, TX	Hot, Moist	7331	2.72
3A	Atlanta, GA	Mixed, Moist	5520	2.13
4A	Baltimore, MA	Mixed, Moist	1359	0.94
5A	Chicago, IL	Cold, Moist	2144	0.92
6A	Minneapolis, MN	Cold, Moist	1791	0.79

Table F1. Relevant U.S. Climate Zones

Building

A representative supermarket retrofitted with an LFLD system was modeled. A variation of the "new construction" supermarket reference building model for EnergyPlus version 8.0 was used as the starting point for model development. This model was previously created based on 2003 CBECS data and additional research carried out by the National Renewable Energy Laboratory and Pacific Northwest National Laboratory; other inputs refer to ASHRAE Standards 90.1and 62.1 (Deru, et al., 2011). Several modifications were made for this analysis, including: (1) the refrigeration system was replaced with one based on measured data from an existing supermarket; (2) the HVAC system was replaced with one commonly used to address humidity loads; and (3) ventilation requirements and exhaust flow rates were updated to conform with ASHRAE Standard 62.1-2007 (ASHRAE, 2007). The following sections describe the building in more detail.

The supermarket model is a 45,000-ft^2 (4,186-m^2), single story, six-zone building and includes a sales floor (56% of floor area), bakery (5%), deli (5%), produce section (17%), dry storage area (15%), and office space(2%). Envelope construction and fenestration comply with ASHRAE Standard 90.1-2004 for each humid climate subcategory (ASHRAE, 2004). The produce and sales floor include 1,064 linear ft (324 linear m) of refrigerated cases; walk-in freezers are located in the dry storage area. There are a total of four racks, each including four compressors.

Baseline HVAC

In the baseline building model, each zone is equipped with a unitary packaged roof top unit, which includes an electric cooling coil and a gas heating coil. Humidity is controlled by cooling the zone supply air past saturation. Reheat energy is provided by an electric coil also included in the unitary packaged system that serves each zone. Building loads are typical of a building of this end use. Outdoor air flow and exhaust rates were calculated based on ASHRAE 62.1-2007 requirements (ASHRAE 2007); outdoor air supply and exhaust is operated during occupied hours (06:00 to 22:00). Two zones, the deli and the bakery, have exhaust requirements for cooking equipment. About 70% of the makeup air for the deli and bakery is transferred from the sales zone; the remainder is brought in through the unitary systems that serve the deli and the bakery. (This makeup air is an addition to the ventilation air provided by the unitary systems.)

Retrofit LFLD Addition

The retrofit liquid desiccant system model was simulated in the Dymola environment, which implements the object-oriented modeling language Modelica. It integrates several existing component models and control strategies, and applies fully

dynamic boundary conditions. All modeling Components of the LDAC system were either taken from the Modelica Standard Library, taken from the open source Modelica Buildings Library created by the Simulations Research Group at Lawrence Berkeley Laboratory, or created new specifically for this work. All have been previously validated. The following section describes the various components and boundary conditions and the inherent assumptions in each.

A schematic of the system level model (a screen shot of the Dymola GUI) is given in Figure F2 below. Inputs and assumptions for each component of the model are described in the following. The schematic is explained by beginning at the upper left corner and proceeding in a counter-clockwise direction.

1. Starting from the upper left corner of the schematic, TMY3 weather data is represented by the light blue box. TMY3 data is given at hourly intervals and the software interpolates between these points linearly to give fully dynamic boundary conditions.
2. Directly below, a constant flow rate scavenging air input is modeled. The air is pre-heated with an air-to-air heat exchanger with a constant effectiveness of 0.55. This effectiveness was chosen so as to prevent condensation in the heat exchanger at the worst operating conditions.
3. Directly below the air-air heat exchanger is the hot water loop which supplies heating water to the regenerator. This includes a 110kW constant-rate heat input, a hot water storage tank with a capacity of 0.25 m^3, and a controller, which maintains the temperature of the hot water between 80°C and 93°C. The boiler efficiency is assumed to be 0.8. The pump is modeled as a constant-flow rate

device. The small tank is assumed to insulated well enough to prevent appreciable heat transfer to the environment.

4. The regenerator is shown below which treats the three fluid streams (Water, Desiccant, and Air labeled with letters W, D, and A). Lab data exists (Clark et al. Under Review) for the regenerator over the entire expected range of operating conditions and an empirical correlation of the lab data was used as an input to the system level model. Firm limits on the inlet variables and operating conditions are placed in the system-level model so as to ensure extrapolation is never done for the empirical model.
5. To the right of the regenerator is an interchange heat exchanger, which exchanges sensible heat only between weak and strong desiccant streams with an assumed constant effectiveness of 0.8.
6. To the right of this is a model of a completely stratified small desiccant tank (or sump). In this model, the strong (bottom) and weak (top) desiccant regions are completely separate, with the one exception that weak desiccant is allowed to be pulled into the strong tank if the conditioner is running at a higher flow rate than the regenerator. This captures the stratification that occurs in the field due to density differences between weak and strong desiccant. This and the cooling and heating water reservoirs are the only elements whose operation is fully transient. Desiccant concentration and temperatures in the tanks are calculated continuously by application of energy and mass balances on the tank volumes.
7. In the bottom right corner is the dehumidifier (also called conditioner or absorber). The dehumidifier used for this work is the parallel-plate low-flow

liquid desiccant absorber patented by Lowenstein (2004). Its operation and performance in the laboratory is described in Lowenstein et al. (2006). A first-principles physical model validated with laboratory data was previously developed for this particular conditioner (Clark et al. Under Review) and is implemented in the current work via polynomial mapping of outlet variables to inlet variables. Air flow rate in the absorber was set to ensure maximum removal. Desiccant and water flow rates in the conditioner are set to the maximum allowable by material limitations.

8. Above the conditioner is the cooling water loop. This includes a model of a York cooling tower with a variable speed fan previously implemented in Dymola by the Simulation Research Group. The cooling tower is sized to provide a 3.89° C approach at design conditions and a 5.56° C range. Cooling tower performance is given by a performance map of the York cooling tower. A controller adjusts fan speed to one of three speeds according to delivered water temperature; natural convection operation of the cooling tower is also modeled when the fan is off. At design conditions, desired water temperature is set to be 3.89° C above the site's design dew point temperature for all sites. The pump is modeled as a constant-flow rate device.
9. The upper right corner of the schematic represents the constant supply air flow of the LDAC. Outdoor air is delivered directly to the conditioner when the conditioner is in operation. When the LDAC conditioner is shut off, outdoor air is sent through a bypass valve to either a secondary sensible device or directly to the building (neither of which are modeled as part of this work).

10. (not shown) A new class was implemented for the Lithium Chloride solution used as the liquid desiccant in this system which extends the Partial Medium model included in the Modelica Standard Library. This model implements all properties contained in (Conde, 2009)with two exceptions: specific heat capacity is modeled as constant value rather than a function of temperature, which results in less than 5% discrepancy at the extremes of the operating range, and density is modeled as a function of concentration only (not temperature) resulting in negligible discrepancy with the Conde (2009) relations. Specific enthalpy is also modeled with correlations developed by AIL Research.

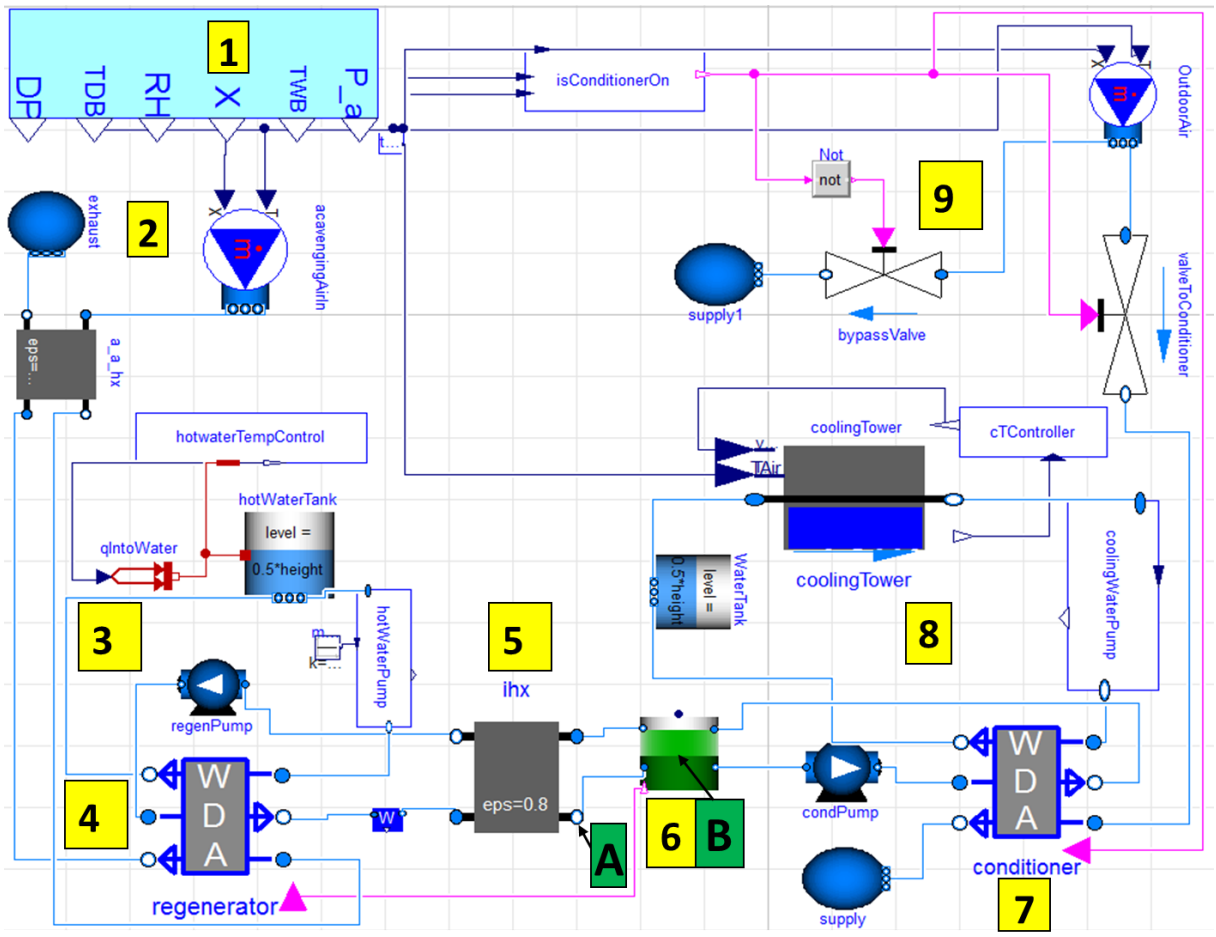

Figure F2. Schematic of LDAC system-level model

The LFLD system was bypassed when outdoor conditions did not require dehumidification (i.e., when the ambient dry bulb temperature was less than 41°F or relative humidity was less than 15%). The conditioner fan and pump did not operate during this time. The regenerator was controlled separately; this component shut off when desiccant concentration reached 0.42 kg of salt per kg of solution. Control strategies were implemented which represented the likely mode of operation, rather than strategies which created space conditions identical to the baseline model. For this reason, space DBT and RH often differ slightly from the baseline to the LDAC-assisted

simulation, as they would in an actual retrofit situation. In nearly all situations, this leads to a more comfortable space in the LDAC-retrofitted model, in addition to the energy and cost savings demonstrated below.

Interface with Building Model

Output values from the Dymola simulation for the processed air conditions (dry-bulb and wet-bulb temperature) were fed into the building simulation model using the Energy Management System (EMS). The processed air temperatures replaced the outdoor air node temperatures for the roof top units (RTUs) serving the produce and the sales zones. The reheat coils and humidistats were removed, as the LDAC was used to provide all of the latent cooling.

Economics

Energy and economic assessments of the LDAC were conducted by combining model results with pricing data. Utility tariffs used were based on the average national monthly rates from January 2010 through September 2012 for electricity (EIA, Average Price of Natural Gas Sold to Commercial Consumers, by State, 2010-2012, 2013) and from January 2010 through July 2012 for natural gas (EIA, Average Retail Price of Electricity to Ultimate Consumers, 2013). This strategy rather than referring to last year's average is used to account for price volatility.

Uncertainty Analysis

Uncertainty is often not quantified for whole-building energy simulations, as the number of inputs is great enough to make this a very difficult task. However, in this study a few inputs were not known very precisely and yet had a disproportionate effect on final outputs and for this reason an attempt was made to bound the uncertainty in the model.

Uncertainty in the model outputs was quantified by perturbing the input values of the four inputs having the greatest effect on model outputs: case runtime fraction (analogous to the size of the refrigeration cases and thus the sensible cooling done by the refrigeration systems); latent heat ratio (relative amount of latent/sensible cooling done by refrigerators); total amount of refrigeration equipment present; and infiltration rate. These four inputs were perturbed to a best estimate for ± two standard deviation and their individual effect on the output variables quantified. Assumed average values and standard deviations for these four quantities are given in Table F2.

Perturbation was done for the climate with the greatest energy savings in the baseline model and that with the least energy savings. It is assumed that uncertainty in the other climates can be interpolated from these. Ranges given on the output variables in the results section are calculated by standard error propagation analysis on these four variables and should be considered a ±one standard deviation range on the output variables. Interesting effects of the individual perturbations are discussed below as well.

Variable	**Low**	**Baseline**	**High**
Case runtime fraction	0.6	0.75	0.9
Latent Heat Ratio			
Open Refrigerator	0.15	0.3	0.33
Freezer w/ Doors	0.05	0.12	0.30
Coffins	0.05	0.1	0.030
Infiltration rate	-50% of baseline		+ 50% of baseline

Table F2. Variables Perturbed to Quantify Uncertainty

Results

End-use resolved energy analysis and cost analyses were conducted based on model results. Results are presented below

HVAC Energy Savings Available with Low Flow Liquid Desiccant Additions

Figure F3 shows cooling energy use calculated in the baseline and retrofit models. Cooling energy is greatly reduced as a result of the elimination of the need for overcooling with the vapor compression system. This is done by removing the latent load from the ventilation air upstream of the VC system, which now only handles sensible loads. Reheat energy is completely eliminated. The majority of the compressor electricity is shifted to thermal sources with the addition of the new LFLD system. It should be noted that this energy often may be available in the form of solar thermal energy or waste heat. Heating and fan energy savings are within the uncertainty of the model outputs. While some small benefit may be gained by adding complicated control strategies which take advantage of the latent heat of vaporization generated in the LDAC conditioner during the heating season, this was not modeled in this work and thus heating savings are minimal.

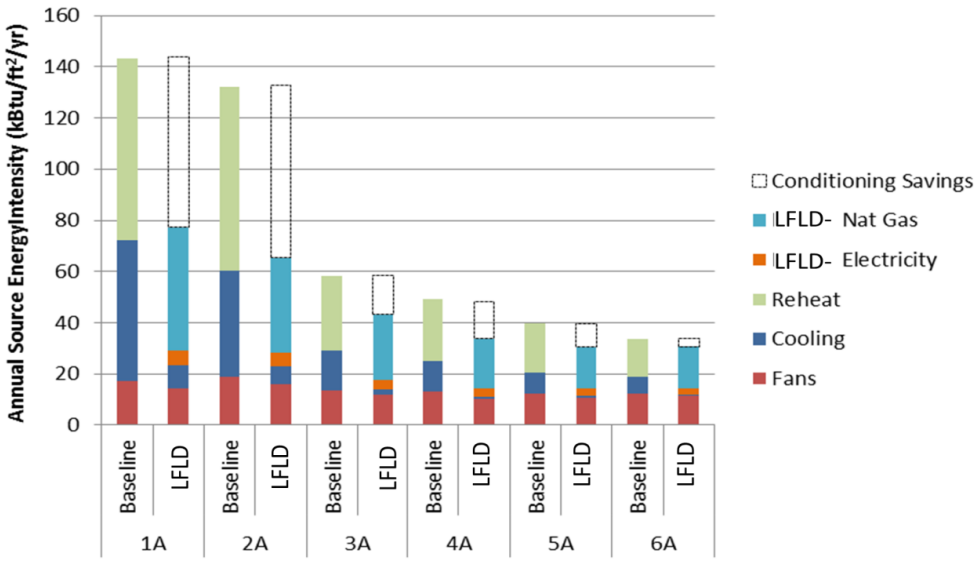

Figure F3. HVAC energy use with baseline (DX only) and LFLD retrofit

Refrigeration Energy Savings Available with Low Flow Liquid Desiccant Additions

Table F3 shows the refrigeration savings demonstrated in this study. Overall refrigeration energy savings as a percentage of baseline energy usage are small, but often significant in the whole-building energy consumption because of the large portion of building energy dedicated to refrigeration. Significant savings are demonstrated for the defrost and anti-sweat functions of the refrigerator. The defrost heaters remove frost buildup on display cases by heating and melting it, while the anti-frost heaters or anti-sweat heaters remove condensation from glass doors, also by providing electrical resistance heating. These savings are comparable to those demonstrated in previous studies [(Farmarzi, Sweetser, & Henninger, 2000) (Howell & Adams, 1991) (Henderson & Khattar, 1999) (Kosar & Dumitrescu, 2005)].

City	Climate	Zone	Defrost	Anti-sweat Heater	Compressor	Condenser Fan	Total Refrigeration
Miami	**Hot-Humid**	**1A**	12%	6%	-1%	-1%	~ 0%
Houston	**Hot-Humid**	**2A**	14%	7%	0%	0%	1%
Atlanta	**Mixed-Humid**	**3A**	17%	8%	1%	3%	2%
Baltimore	**Mixed-Humid**	**4A**	15%	7%	3%	11%	4%
Chicago	**Cold-Humid**	**5A**	17%	8%	1%	4%	2%
Minneapolis	**Cold-Humid**	**6A**	16%	6%	1%	4%	2%

Table F3. Refrigerator Energy Usage in Baseline and Retrofit Models

Total Energy Savings

Table F4 shows a summary of the relative performance of the LFLD system as modeled. As expected, the highest source energy savings are seen in the hot humid

climate zones (1A and 2A). The model shows whole building energy savings with the LFLD retrofit across all humid climates, suggesting the LFLD is most applicable in climates with large latent loads. Ranges given for values in Miami and Minneapolis represent a ±two standard deviation range calculated with the perturbation analysis discussed in Chapter 4. Uncertainty as a portion of building energy savings is significant and is discussed further below.

Energy Savings (kBtu/ft^2)	**1A**	**2A**	**3A**	**4A**	**5A**	**6A**
Total Electricity	113 [41 to 197]	108	49	16	32	22 [10 to 46]
Total Natural Gas	-48 [-48 to -46]	-36	-20	-26	-16	-16 [-16 to -16]
Source Energy Savings	66 [3 to 156]	72	32	28	16	5.2 [-4.5 to 30]
	8% [0% to 20%]	9%	4%	4%	2%	1% [-1% to 5%]

Table F4. Normalized Annual Source End Use Energy (kBtu/ft^2/yr)

Cost Savings

Table F5 shows the yearly cost savings achievable with an LFLD retrofit. Two distinct benefits are gained. First, reduction in overall energy expenditure, shown in Table F4 reduces overall cost. Second, shift in energy usage from electricity to natural gas also results in some benefit. Cost savings in Miami and Houston are 5% of total building energy costs for the year. This is achieved completely with natural gas, rather than taking advantage of any "free" heating for regeneration on site such as solar thermal or waste heat. Colder climates such as Chicago and Minneapolis show energy savings of only 1% of building energy costs.

Yearly Cost Savings ($1000/yr)	1A Miami, FL	2A Houston, TX	3A Atlanta, GA	4A Baltimore, MD	5A Chicago, IL	6A Minneapolis, MN
Electricity Cost	46 [21 to 80]	39.9	19.2	18.1	12.0	8 [5 to 18]
Natural Gas Cost	-17 [-17 to -17]	-13.0	-8.9	-7.2	-5.8	-6 [-6 to -6]
Total Energy Cost	29 [4 to 63]	26.9	10.3	11.0	6.3	2.6 [-1 to 12.1]

Table F5. Cost savings available with liquid desiccant retrofits

Uncertainty Analysis

As can be seen above in Tables F4 and F5, overall uncertainty as compared to energy savings is considerable. For climates with small savings, total uncertainty in energy usage at two standard deviations is equal to or greater than total building energy savings. The analysis found that around 60% of this uncertainty is attributable to the input for latent heat ratio (LHR) in the refrigeration systems and the majority of the rest is attributable to the uncertainty in infiltration rate. The other perturbed variables had little effect on overall uncertainty.

While infiltration will always be difficult to know precisely, latent heat ratio is a quantity that should be relatively predictable. However, there is only one instance (Farmarzi, Sweetser, & Henninger, 2000) where this quantity was actually measured, to the author's knowledge, and this used equipment and assumed operating patterns that cannot be assumed general for all supermarkets. The input for LHR strongly affects the current simulations in three ways. First, increasing the amount of dehumidification done by the refrigerators (proportional to LHR) removes latent load on the HVAC system and causes the LFLD to be relatively less beneficial, and vice versa. Secondly, decreasing sensible cooling done by the refrigerator (inversely proportional to LHR) increases the

sensible load on the HVAC system and causes the VC system to be more useful and the LFLD to be relatively less useful. Furthermore, increasing LHR on the refrigerator increases the overall dehumidification capacity of the (HVAC + Refrigeration) system and allows for lower space humidity levels, which in turn reduces overall refrigerator energy usage. More research is needed in this area to provide for more accurate simulations of supermarkets.

Summary of Results

Overall applicability of the LDAC for a particular climate can be understood as one of four situations:

- In hot, humid climates, baseline cooling energy is dominated by latent loads, including a large penalty for reheat (over 40% of HVAC energy). In these climates, the LFLD is particularly well-suited. Refrigeration savings are small. Because such a great quantity of energy usage is shifted from electricity to gas in these climates, large cost savings are achievable: roughly 5% of the yearly energy cost expenditure of the whole building.
- In mixed, humid climates such as 3A and 4A, reheat still comprises over 20% of total HVAC energy usage and this is completely eliminated by the LFLD. Again, cooling and dehumidification savings are great enough to offset additional energy expenditure for desiccant regeneration and HVAC savings of over 10% are achievable. Additional refrigeration savings are similar to hot humid climates and

contribute to a whole-building energy savings of 3-4% and cost savings of 2-3%.

- Cold, humid climates such as 5A and 6A are less applicable for the LDAC as the sensible heating dominates the HVAC energy expenditure. The LDAC retrofitted system was, however, shown to minimally improve energy usage and costs.
- The LFLD system is not expected to provide a cost or energy benefit in marine or dry climates where most of the cooling need is sensible.

At this time, the market cost for LDAC systems of this type are unavailable so a more in-depth economic analysis is not available. However, there are some general economic considerations that should be mentioned:

- The cost savings from reduced coiling coil sizes and the elimination of reheat coils can offset the capital cost of the LDAC system.
- The additional maintenance costs associated with the LDAC are expected to be minimal. Under normal operating conditions, maintenance will be limited to filter replacement and desiccant concentration monitoring, which can be simplified with hydrometers. In cold climates, winterization of the system is limited to draining the desiccant from the piping and draining the cooling tower water if such equipment is used. Additional costs associated with maintaining the cooling tower will exist.

Overall, the LFLD showed significant potential, especially in humid climates, although perturbation of model inputs had a significant effect on results, particularly in the case of latent heat ratio. However, even when this is taken into account, when control strategies are optimized and alternative thermal sources included, the LFLD system promises to greatly reduce supermarket energy usage and provide substantial cost savings in many climates.

Acknowledgments

This research was made possible through funding from the American Recovery and Reinvestment Act via the National Renewable Energy Laboratory.

References

ASHRAE. (2004). *Energy Standard for Buildings Except Low-Rise Residential Buildings-ANSI/ASHRAE/IESNA Standard 90.1-2004.* Atlanta, GA: American Society of Heating Refrigeration and Air-Conditioning Engineers.

ASHRAE. (2007). *Ventilation for Acceptable Indoor Air Quality- ANSI/ASHRAE Standard 62.1-2007.* Atlanta, GA: American Society of Heating, REfrigeration and Air-Conditioning Engineers.

Bergero, S., & Chiari, A. (2010). Performance of a liquid desiccant and membrane contactor hybrid air-conditioning system. *Energy and Buildings*, 1976-1986.

Burns, P., Mitchell, J., & Beckman, W. (1985). Hybrid desiccant cooling systems in supermarket applications. *ASHRAE Transactions*, 457-468.

Capozzoli, A., Mazzei, P., Minichiello, F., & Palma, D. (2006). Hybrid HVAC systems with chemical dehumidification for supermarket applications. *Applied Thermal Engineering*, 795-805.

Chung, T., Ghosh, T., Hines, A., & Novosel, D. (1993). Removal of selected pollutants from air during dehumidification by lithium chloride and triethylene glycol solutions. *Proceedings of the 1993 Winter Meeting of ASHRAE* , 834-841.

Conde, M. (2009). *Aqueous solutions of lithium and calcium chlorides: Property formulations for use in air conditioning equipment design.* Retrieved from Conde Engineering: http://www.mrc-eng.com/Downloads/Aqueous%20LiCl&CaCl2%20Solution%20Props.pdf

Dai, Y., Wang, R., Zhang, H., & Yu, J. (2001). Use of liquid desiccant cooling to improve the performance of vapor compression air conditioning. *Applied Thermal Engineering*, 1185-1202.

Deru, M., Field, K., Studer, D., Benne, K., Griffith, B., & Torcellini, P. (2011). *U.S, Department of Energy Commercial Reference Building Models of the National Building Stock.* NREL/TP-5500-46861.

EIA. (2013, August). *Average Price of Natural Gas Sold to Commercial Consumers, by State, 2010-2012.* Retrieved from http://www.eia.gov/naturalgas/monthly/pdf/table_21.pdf

EIA. (2013, August). *Average Retail Price of Electricity to Ultimate Consumers.* Retrieved from Electric Power Monthly: http://www.eia.gov/electricity/monthly/epm_table_grapher.cfm?t=epmt_5_03

Faramarzi, R., Sarhadian, R., & Sweetser, R. (2000). *Assessment of indoor relative humidity variations on the energy use and thermal performance of supermarkets' refrigerated display cases.*

Farmarzi, R., Sweetser, R., & Henninger, R. (2000). *Investigation of relative humidity impacts on the performance and energy use of refrigerated display cases.* Gas Research Institute GRI-00/0084.

Henderson, H., & Khattar, M. (1999). Measured Impacts of Supermarket Humidity Level on Defrost Performance and Refrigerating System Energy Use. *ASHRAE Transactions*.

Howell, R., & Adams, P. (1991). *Effects of indoor space conditions on refrigerated display case performance, Final Report, ASHRAE 596-RP.* Atlanta: AASHRAE.

Kessling, W., Laevemann, E., & Peltzer, M. (1998). Energy storage in open cycle liquid desiccant cooling systems. *International Journal of Refrigeration*, 150-156.

Khattar, M., & Henderson, H. (1999). Impact of HVAC Control Improvements on Supermarket Humidity Levels. *ASHRAE Transactions*.

Kim, M.-H., Park, J.-S., & Jeong, J.-W. (2013). Energy savings potential of liquid desiccant in evaporative-cooling-assistend 100% outdoor air system. *Energy*, 726-736.

Kosar, D., & Dumitrescu, O. (2005). Hunidity Effects on Supermarket Refrigerated Case Energy Performance: A Database Review. *ASHRAE Transactions*, 1051-1061.

Kozubal, E., Woods, J., Burch, J., Boranian, A., & Merrigan, T. (2011). *Desiccant-Enhanced Evaporative Air-Conditioning.* Golden, CO: NREL.

Lazzarin, R., & Castellotti, F. (2007). A new heat pump desiccant dehumidifier for supermarket applicaiton. *Energy and Buildings*, 59-65.

Lowenstein, A. (2008). Review of liquid desiccant technology for HVAC Applications. *HVAC&R Research*, 819-839.

Lowenstein, A., Slayzak, S., & Kozubal, E. (2006). A zero carryover liquid desiccant air conditioner for solar applications. *Proceedings of ASME International Solar Energy Conference*.

Munters. (2005). *Supermarket Air Conditioning.* Retrieved from http://www.munters.us/upload/External%20website/Commercial%20Products%20rev%2001/Supermarket%20Air%20Conditioning.pdf

Spyrou, M., Shanks, K., Cook, M., Pitcher, J., & Lee, R. (2013). An empirical study of electricity and gas demand drivers in large food retail buildings of a national organisation. *Energy and Buildings*.

Tassou, S., Ge, Y., Hadawey, A., & Marriott, D. (2011). Energy consumption and conservation in food retailing. *Applied Thermal Engineering*, 147-156.

Appendix G: The Effects of Component-Level and System-Level Variables on the Operation and Performance of Low Flow Liquid Desiccant Systems

Jordan Clark, Jason Woods

Introduction

Liquid desiccant systems dehumidify air by utilizing chemical potential differences between air near a hygroscopic fluid and process air. Water is absorbed into the solution, increasing the water content of the solution and decreasing the humidity of the process air. The solution must then be regenerated by heating it to a temperature great enough to cause a sufficient amount of moisture to be transferred from the solution to a scavenging air stream. A review of available Liquid desiccant air conditioning (LDAC) technologies is given in Lowenstein (2008). LDAC systems are gaining interest for use in dehumidification of buildings because of their many advantages over an electrically driven vapor compression cycle, including a decrease in electrical energy consumption in favor of an increase in more sustainable thermal sources such as natural gas and solar thermal; elimination of hazardous refrigerants; elimination of the wasteful overcool-reheat process through which vapor compression systems dehumidify air; introduction of the ability of air conditioning systems to shift energy usage to times of the day when energy is cheaper or more available by delaying the time between dehumidification and regeneration; and more stable and deeper dehumidification of buildings which has many secondary benefits for buildings and occupants.

Previous Work

The creation of models of LD system components has allowed for analyses of the impact of variables affecting component performance. In general, desiccant systems operate on the principle that lower desiccant temperatures and higher concentrations in the absorber lead to lower outlet humidities, documented by (Abdel-Salam, Ge, & Simonson, 2013), (Yin Y. , Zhang, Wang, & Luo, 2008), (Saman & Alizadeh, 2001), (Katejanekarn & Kumar, 2008), (Rahamah, Elsayed, & Al-Najem, 1998) and higher regeneration temperatures lead to more concentrated desiccants out of the regenerator, as shown by (Abdel-Salam, Ge, & Simonson, 2013). The following section describes some other general trends witnessed in the parametric analyses of components available in the literature. The effect of most variables is presented as a moisture transfer effectiveness, which can be thought of as the amount of moisture transferred divided by the maximum amount that could be transferred in an infinitely large component with identical boundary conditions.

Air Flow Rate

The variable most often pointed to as having the greatest effect on absorber or absorber performance is the air flow rate. A lower air flow rate increases residence time in the component, while a higher air flow rate may increase transfer coefficients in some cases. Nearly all researchers who explicitly report the relationship between flow rate and report a decrease in moisture removal effectiveness with an increase in flow rate (Yin Y. , Zhang, Peng, & Li, 2009), (Tu, Ren, Long-Ai, & Shao, 2009), (Liu, Jiang, & Qu, 2007), (Rahamah, Elsayed, & Al-Najem, 1998), (Katejanekarn & Kumar, 2008). This same phenomena is often presented in terms of one of several definitions of "number of transfer units" (NTUs), which is inversely proportional to air flow rate. (Abdel-Salam, Ge, & Simonson, 2013), (Ge, Moghaddam, Namvar, Simonson, & Besant, 2013) and

(Saman & Alizadeh, 2001) found removal effectiveness to increase with increased NTU's, implying an inverse relationship between air flow rate and effectiveness. (Katejanekarn & Kumar, 2008) found that the air flow rate was much less important in the regenerator than in the absorber, likely owing to the fact that the scavenging air is not the fluid of interest in the regenerator and transfer rate was limited by the desiccant rather than the air flow. (Saman & Alizadeh, 2001) found an absolute maximum efficiency at an intermediate flow rate, but the flow rates they investigated included those high enough to induce a transition to turbulence. For the purposes of the current work, in which low flow conditions are maintained to prevent desiccant carryover, it is safe to assume that absorber effectiveness will decrease with increased air flow rate and scavenging air flows should be set to the maximum for which entrainment does not occur.

Desiccant Flow Rate

Desiccant flow rate was also shown to effect performance of the absorber and regenerator. (Katejanekarn & Kumar, 2008) showed that varying desiccant flow rate over an order of magnitude in the absorber can increase moisture transfer effectiveness by 12%. (Saman & Alizadeh, 2001) showed that increasing desiccant flow rate increases effectiveness substantially up to a point, until the internal processes become limited by mass transfer rates and the desiccant can be considered to be at a constant concentration. (Katejanekarn & Kumar, 2008) also showed that in the regenerator, increasing desiccant flow rate increases the mass flux of moisture but can decrease the overall removal rate, and thus an optimum flow rate exists in this component.

Minor Variables

Other variables have been shown to have small or no effects on component moisture transfer performance. (Liu, Chang, & Jiang, 2009) showed that, as in the case

of sensible heat exchangers, a counter-flow LD heat and mass exchanger is more effective than a cross-flow exchanger, which is in turn more effective than a parallel flow exchanger. (Rahamah, Elsayed, & Al-Najem, 1998) and (Saman & Alizadeh, 2001) showed that inlet air temperature has little to no effect on transfer effectiveness. (Bergero & Chiari, 2011) and (Rahamah, Elsayed, & Al-Najem, 1998) report a significant decrease in transfer effectiveness with an increase in inlet humidity. This is a general trend observed in the current work as well, owing most likely to the simple need for more mass to be transferred when inlet conditions are more humid. (Rattner, Nagavarapu, Garimella, & Fuller, 2011) found that the aspect ratio of individual plates in an air-gap membrane regenerator had an insignificant effect on its performance. His setup included only two fluids, though; a separate cooling fluid was not included.

Component and system-level models have been used to determine the effect of certain variables on LD system energy usage. First and second law analyses have been conducted for this purpose. Energy efficiency of the system has, in general, been shown to increase when latent loads increase. (Bergero & Chiari, 2011) showed that power savings increase over a VC system with increases in latent loads. (Kinsara, Al-Rabghi, & Elsayed, 1997) showed a decrease in COP with an increase in sensible heat ratio. (Zhang, Liu, & Jiang, 2012) and (Ahmed, Gandhidasan, & Al-Farayedhi, 1997) show a decrease in COP with entering air humidity, but this is not compared with a VC system and for this reason may not be contradictory to the findings of (Bergero & Chiari, 2011) and (Kinsara, Al-Rabghi, & Elsayed, 1997).

The effect of other variables on energy efficiency has been investigated as well. (Rattner, Nagavarapu, Garimella, & Fuller, 2011) found a decrease in system COP with

an increase in desiccant concentration into the regenerator and (Tu, Ren, Long-Ai, & Shao, 2009) corroborated this finding. (Tu, Ren, Long-Ai, & Shao, 2009) also found an increase in COP with increasing air/desiccant flow rate ratios, and with ambient air temperature. (Bergero & Chiari, 2010) found that increasing the size of the regenerator for the same absorber resulted in a greater COP.

Some second law analysis on LD systems has been conducted as well. (Tu, Ren, Long-Ai, & Shao, 2009) found that 2nd Law efficiency decreased with desiccant temperature into the regenerator, increased with air/desiccant flow rate ratio into both the regenerator and absorber , increased with absorber inlet humidity up to relative humidity of 50%, at which point it leveled off, and was highest when scavenging air temperature was near the temperature of the desiccant in the regenerator. (Wang, Li, & Zhao, 2010) found that second law efficiency decreased with increasing desiccant temperature.

A few interesting general trends can be pulled from the previous observations. First, as expected, nearly all trends can be attributed to the size of gradients across which heat and mass transfer processes occur. It is well established that entropy generation, and thus loss of efficiency, is proportional to the size of the gradients across which transport occurs, and this is witnessed in nearly all the trends in the results described above. Next, some opportunity for control strategies are suggested by analysis of the trends, including modulation of controllable variables such as desiccant temperature and scavenging air temperature and flow rate.

While a great deal of work has been done on optimization of desiccant systems, low flow internally cooled systems present unique challenges which must be accounted

for in new optimization work. First, three streams exist in each of the main components, presenting a multitude of complex interactions which often can't be predicted intuitively. Second, the low flow system has strict bounds on the flow rates which can be used, in order to prevent desiccant entrainment into the air stream. This precludes simpler formulations for design and optimization. Lastly, the sheer number of interacting components creates the need for a fully dynamic system model to understand system operation. This work attempts to create new correlations between performance and controllable factors by leveraging existing models of a low flow system.

Objectives

The objectives of the current work are as follows:

1. Clark et al. (Under Review) and Clark et al. (Under Review) developed models of both the LFLD components and the entire LFLD system. Use these models to determine operating conditions and to size the LDAC conditioner and auxiliary components in order to provide the most energy-efficient, compact and simple design. Specifically, two goals are pursued:
    a. Optimization of the size, shape, and air flow rate of the absorber for maximum performance within practical limitations
    b. Lowenstein (2008) identified the inclusion of a cooling tower as a barrier to market acceptance owing to the cooling tower's high maintenance costs. This work seeks to identify operating regimes in which an air-cooled device could be employed, or the extent to which performance would be reduced if an air-to-liquid heat exchanger replaced the cooling tower.

2. Given this starting point, what regenerator size, what amount of desiccant, and what amount of heating water should be chosen to maximize efficiency, minimize capital costs, and deliver an effective system?

Analysis for Sizing and Design

With the existing model, the effect of design parameters canbe determined and operating conditions optimized in order to provide for a compact, effective and efficient system. Selection of auxiliary components was also made possible through analysis of the modeling outputs. The following sections look at four particular design considerations which affect performance and system size:

1. The shape of the LFLDA was analyzed to determine the most effective shape within practical bounds. These bounds included maintaining desiccant and air flow rates below the levels at which desiccant carryover may occur and water pressures below those dictated by the strength of the extruded CPVC plates.
2. The effect of air flow rate per plate was analyzed to understand tradeoffs between system size (number of plates) and dehumidification effectiveness
3. Water flow rate was analyzed to determine what flow rate was necessary for removing enough energy from the system to provide for effective dehumidification while minimizing pumping costs.
4. The effect of inlet water temperature was analyzed in conjunction with a cooling tower model to understand whether a cooling tower was necessary for all climates.

The effects of the four independent variables mentioned above were quantified by modeling the effect of each variable on moisture removal effectiveness, defined as:

$$\varepsilon_R = \frac{(\omega_{inlet} - \omega_{outlet})}{(\omega_{inlet} - \omega_{eq,desiccant})} \qquad \textbf{Eq. 1}$$

The definition of $\omega_{eq,desiccant}$ was chosen so as to provide a tangible metric which would correspond to the physics of the process and provide useful information for analysis. For these reasons $\omega_{eq,desiccant}$ was defined to be the humidity ratio of air in equilibrium with a desiccant solution at the concentration of the entering desiccant and the temperature of the *entering cooling water*. This corresponds to the driest air which could conceivably exit the absorber, which keeps effectiveness values below unity at all times and allows for appreciation of the physics of the problem.

Table G1 shows the correlation between independent variables and removal effectiveness. In general, inlet air conditions (temperature and humidity) were weaker predictors of performance than controllable factors such as geometry and flow rates and performance decreased slightly with entering air humidity. For this reason, the operation was investigated at design conditions only, with the assumption that a conditioner which was designed well for design conditions would be able to efficiently handling less demanding conditions. Miami was used as a representative city because of its high latent loads and applicability of the LFLDA, and its design conditions were assumed for all investigations.

Factor	R	Factor	R
mass flow rate of air	*-0.85*	temperature of inlet air	-0.12
form factor	*-0.47*	temperature of inlet water	-0.12
mass flow rate of water	*0.42*	inlet relative humidity	-0.09
		inlet humidity ratio	-0.04

Table G1. Correlation between independent variables and removal effectiveness. Controllable variables are in italics. Correlations provided are over all of expected operating range. Form factor is Depth/Height of conditioner at equal face velocity.

In order to isolate the effect of the variable of interest, assumptions were made for the other variables. Inlet cooling water temperature was assumed to be 3°C above the wet bulb temperature of the entering air unless otherwise noted. Desiccant and water flow rates were set at the maximum dictated by the material strength and plate capacity unless otherwise noted. Air flow rate was set at 53% of its maximum allowable value unless otherwise noted, which corresponds to a flow rate used in the field. This provides a face velocity of 4.2 feet per second. Desiccant inlet temperatures were estimated as the temperature which would result when regeneration was conducted at 90°C, an interchange heat exchanger with an effectiveness of 0.8 was used between regenerator and conditioner, and desiccant left the conditioner at 3.5°C above the entering cooling water temperature- the average observed in previous laboratory experiments.

Optimization of Shape and Flow Rate

Performance of the LFLDA is very sensitive to the shape of the absorber and the air flow rate through it as shown in Table G1. Among the reasons are the increased residence time of the air in the system and thus increased removal effectiveness resulting from either a lower flow rate or a longer absorber (increased L in Figure G1), the decrease in concentration drop the desiccant and thus greater effectiveness resulting from

a shorter system (decreased H in Figure G1), and decreased water residence time and thus water temperature increase resulting from decreases in dimensions L and H. These two variables are interrelated in several ways. A shorter system will need either an increased face velocity or an increased W dimension (greater number of plates) in order to handle the same amount of air. A longer system will require greater fan power to move the same amount of air as a shorter system.

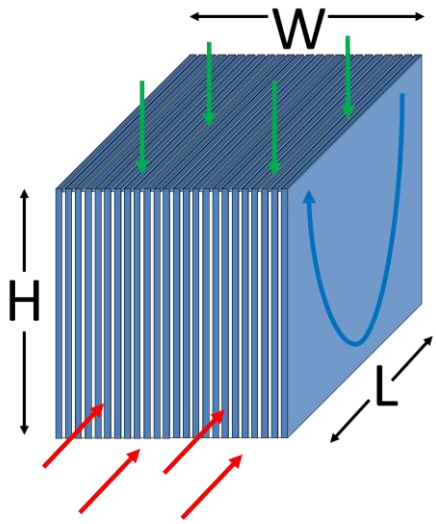

Figure G1. Schematic of LFLDA plates with dimension names. Red arrows show air flow direction; green arrows desiccant flow direction; blue arrow water flow.

This section examines the tradeoffs between these four variables (L,H,W, face velocity of air). The effect of these variables is investigated by looking at the design of a 4,000 scfm absorber. Dimensions and face velocities of the absorber were varied and the resulting effectiveness at design conditions calculated. Results are shown in Figure G2, given in terms of normalized area A* and normalized velocity, V*. A* is the total 2-dimensional area of all plates in the absorber divided by the total plate area of a *cubic* absorber operating at the maximum face velocity allowable. V* is the face velocity

divided by the maximum allowable face velocity. The term A*/V* is similar to the term NTU in NTU-effectiveness relations traditionally given for sensible heat exchangers. Dimensions given in the legend are in the form height, H, x length, L. Dimension W is fixed by the air flow rate and the other two dimensions. As was expected, removal effectiveness increases as air flow rate is decreased and as height, H, is decreased or length, L, is increased. Note that very small values of A*/V* are not possible for very short (small H) absorbers.

One can see the change in effectiveness with shape and operation is significant. As a concrete example, one may consider a baseline system which has a height H of 48", a length L of 24" and 188 plates, corresponding to a nearly square face. Air flow rates in this absorber are 53% of the maximum allowable, resulting in a removal effectiveness of 0.91. If the absorber height were to be decreased by 33% with a corresponding increase in width W and the same face velocity (32" H x 72"W x 24" L), effectiveness would be increased by 4% with the same fan power, approaching the maximum effectiveness achievable. Alternatively, if the height were decreased by 33% and the flow rate increased to 80% of the maximum flow rate (32" H x 48"W x 24" L) the resulting system would have an identical effectiveness, but achieve this effectiveness in 2/3 of the volume occupied by the baseline system, albeit with a 125% increase in fan power. However, fan power in the LFLDA has been shown to be a minor contributor to the overall energy use of the low flow liquid desiccant system. If volume were not a concern, the original volume could be maintained by adding the volume removed from the top of the system to the end of the system (making the system longer, 32" H x 48"W x 36" L)) while achieving an efficiency approaching the maximum, with a 240% increase in fan power.

Alternatively, the same size system could be constructed by putting two 32” H x 48”W x 18” L absorbers in series, achieving an effectiveness approaching 100% for the same fan power. Any increase in the number of plates, whether by increasing W or by putting two absorbers in series, would have a corresponding increase in capital costs due to the need for additional distribution systems for the desiccant and water..

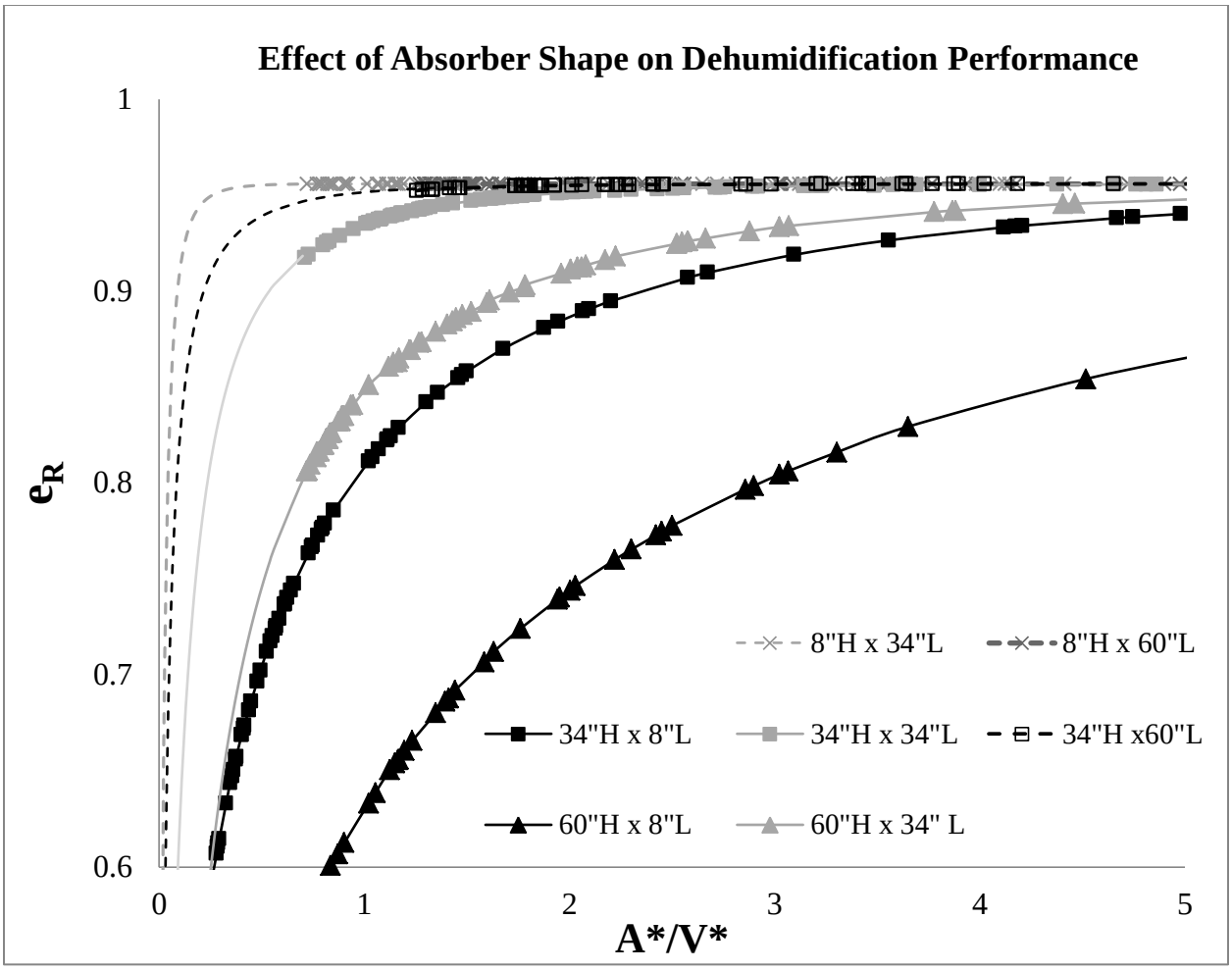

Figure G2. Graph showing the effect of absorber shape and air flow rate on performance at design conditions.

Effect of Water Flow Rate and Temperature on Performance

As shown in Table G1, cooling water flow rate and temperature have a substantial effect on the performance of the absorber. In this section, this effect is studied further and an optimal configuration is discussed. One major concern in this section is to determine which conditions might allow for the removal of any evaporative or electrical cooling device. This is desirable as it could reduce capital costs and considerably reduce maintenance required in the case of a cooling tower, thus likely increasing market acceptance.

Figure G3 shows the relationship between inlet water temperature, water flow rate, and delivered absolute humidity. The embedded graph shows the relationship between flow rate and removal effectiveness for a single temperature, 3°C above design wet bulb temperature in Miami. As can be seen, performance decreases rather quickly for entering water temperatures of greater than 25-30°C or for flow rates less than about half of the maximum allowable flow rate. These are attributable to the lack of the cooling fluid's ability to perform its function because of either insufficient driving force for heat transfer or insufficient capacity in the case of low flow rates. When the absorber is operating properly, the cooling water maintains the desiccant temperature, and thus its equilibrium vapor pressure, at a level low enough to allow for adequate moisture transfer from the process air stream. As equilibrium vapor pressure is an exponential function of desiccant temperature, small changes in cooling water temperature may have profound effects on dehumidification performance.

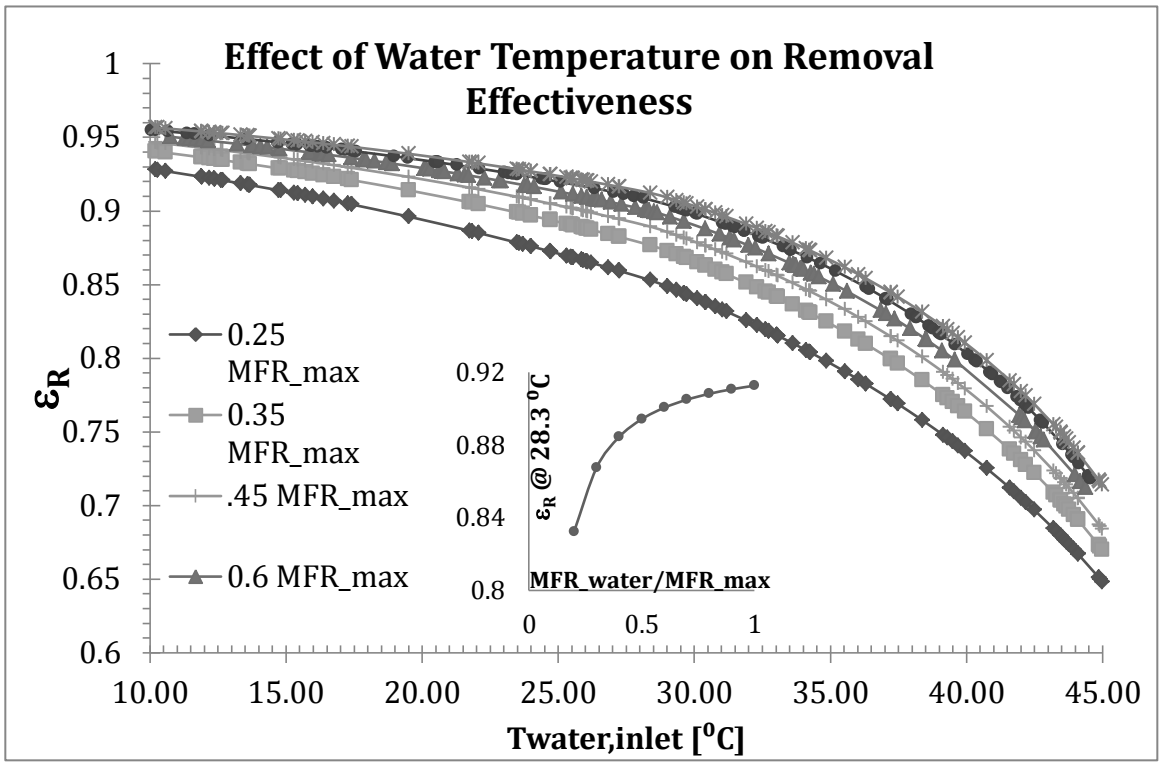

Figure G3. Graph showing relationship between entering cooling water temperature, cooling water flow rate, and absorber performance

The information in Figure G3 can be used to determine under what conditions a cooling tower could be replaced with an air-to-water heat exchanger, thus removing the cooling tower and its required maintenance from the system. Table G2 shows the conditions under which this is possible for a design day in Miami. For each desired supply humidity ratio (1st column), a necessary temperature (Column 3) for the water entering the absorber is calculated for each water flow rate (Column 2). The temperature of the water leaving the absorber is given for these conditions in Column 4. The last 5 columns show the minimum achievable temperature under the given conditions for a cooling tower and an air-to-water heat exchanger with a water-side effectiveness of 0.25, 0.3. 0.35 and 0.4, respectively. Heat exchanger calculations assume outdoor air at design

conditions is used to sensibly cool the water. Cooling tower calculations use an Energy Plus® model of a York® cooling tower, sized to give a 3.9°C approach temperature and 5.6°C range at design conditions and maximum flow rate, a common design approach.

Desired Humidity Ratio	$\dot{m}_{water}$ / $\dot{m}_{max}$	**Inlet Water Temperature Needed [°C]**	**Modeled Outlet Temperature [°C]**	**Inlet Water Temperature [°C] Achievable With:**				
				Cooling Tower	**Air-Water Heat Exchanger with Water-Side Effectiveness of:**			
					0.25	*0.3*	*0.35*	*0.4*
0.0071	0.6	33.0	36.6	28.2	34.6	34.2	33.8	33.4
0.0071	0.7	33.7	36.5	28.7	34.5	34.1	33.7	33.3
0.0071	0.8	34.2	36.4	29.2	34.4	34.0	33.7	33.3
0.0071	0.9	34.5	36.3	29.7	34.4	34.0	33.6	33.2
0.0071	1.0	34.7	36.2	30.0	34.3	33.9	33.5	33.1
0.0057	0.6	28.5	33.6	26.3	32.3	32.1	31.8	31.6
0.0057	0.7	29.6	33.9	26.8	32.5	32.3	32.0	31.7
0.0057	0.8	30.4	34.0	27.2	32.7	32.4	32.1	31.8
0.0057	0.9	30.8	34.0	27.6	32.6	32.3	32.1	31.8
0.0057	1.0	30.8	33.7	27.8	32.4	32.1	31.9	31.6
0.0045	0.6	23.0	29.1		29.0	29.0	28.9	28.9
0.0045	0.7	24.5	29.6		29.3	29.2	29.2	29.1
0.0045	0.8	25.6	30.0	25.6	29.6	29.5	29.4	29.4
0.0045	0.9	26.4	30.2	26.0	29.8	29.7	29.6	29.5
0.0045	1.0	26.9	30.3	26.3	29.8	29.7	29.7	29.6

Table G2. Table showing the ability of heat exchangers of different effectiveness and a cooling tower to meet inlet requirements needed for different delivered humidity values in Miami under design conditions.

A few trends can be noticed in Table G2. First, the driest air achievable, with a humidity ratio of 0.0045 kg/kg, is only achievable with a cooling tower sized for the greatest flow rate possible, in order to minimize water temperature change across the absorber. However, if a slightly less effective absorber (ω_{out}=0.0057 kg/kg) were acceptable, the cooling of the water could be achieved with a cooling tower at low water

flow rates (and thus reduced pumping costs and lower internal pressures). An outlet humidity ratio of 0.0071 kg/kg at design conditions can be achieved with mid-range heat exchanger at the highest flow rates and an excellent heat exchanger at 80% of the maximum flow rate. Given the desirability of elimination of the cooling tower, the additional cost of a good heat exchanger and the added fan power (which will likely be more than compensated for by the reduced pumping power), will often be worth the expense. It should be noted also that a very effective heat exchanger with a high mass flow rate would likely be very large, and thus the least effective system acceptable would be selected if doing so was deemed more desirable than keeping a cooling tower.

3. Sizing

With a validated model, the system components may be sized. The following section looks at the tradeoffs between different sizing configurations and develops a procedure for selecting the best system.

3.1 Regenerator Sizing

The first concern when selecting system components is capacity. For this reason, design conditions at steady state will first be looked at in a representative climate, Miami. A 4,000 cfm system is analyzed. The size and configuration of the conditioner is fixed at 32” high x 24” long with 283 plates, shown in Clark and O.D. to give an effectiveness approaching the theoretical maximum for this amount of supply air. The second concern is efficiency. This is quantified through the amount of energy necessary to remove a certain quantity of moisture, Regeneration-Specific Heat Input (RSHI), which is defined as:

RSHI= $\frac{\dot{m}_{water\ removed}}{\dot{Q}_{regenerator\ water}}$

where $\dot{m}_{water\ removed}$ is the steady state rate of water removed from the supply air stream [kg/s];
$\dot{Q}_{regenerator\ water}$ is the energy removed from the regenerator water at steady state [kW];

Figure G4 shows the relationship between delivered humidity ratio at design conditions in Miami and relative regenerator size. Red points represent conditions at which desiccant concentration may increase beyond the limit to prevent crystallization. The concentration limit for crystallization was taken to be 0.01 $kg_{salt}/kg_{solution}$ less than the solubility limit at a given temperature in order to account for non-uniform distribution of desiccant in the system. Two points in the system were checked: desiccant exiting the interchange heat exchanger (desiccant is most concentrated here but also is hotter than in the sump, and thus has a higher solubility); and desiccant in the tank (weaker concentration, but colder temperature). Desiccant exiting the heat exchanger was found to control in all situations. The dashed line corresponds to a 42^0F dewpoint, which is suggested in ASHRAE (2008) and in Section 4.2 as a good candidate for a choice of a lower bound for dehumidification.

One can see in Figure G4 that there exists an inverse relationship between system efficiency and effectiveness although RSHI changes only 10% over the interesting range. Spot checks of different absolute values of regenerator size show that these trends hold generally for other sizes as well. For some applications, such as in grocery stores, energy savings within the building continue to increase as humidity decreases and thus the largest regenerator which does not cause crystallization would be selected (0.97 regenerator plates for every conditioner plate). This point is above the minimum

recommended humidity level as can be seen. In other applications, a greater supply humidity would be acceptable in favor of lower regeneration energy savings, and the regenerator would be sized to produce this humidity at design conditions. For example, if a 0.008 humidity ratio at the supply were acceptable, a regenerator with 0.75 plates per conditioner plate could be selected, decreasing RSHI 4% from the maximum.

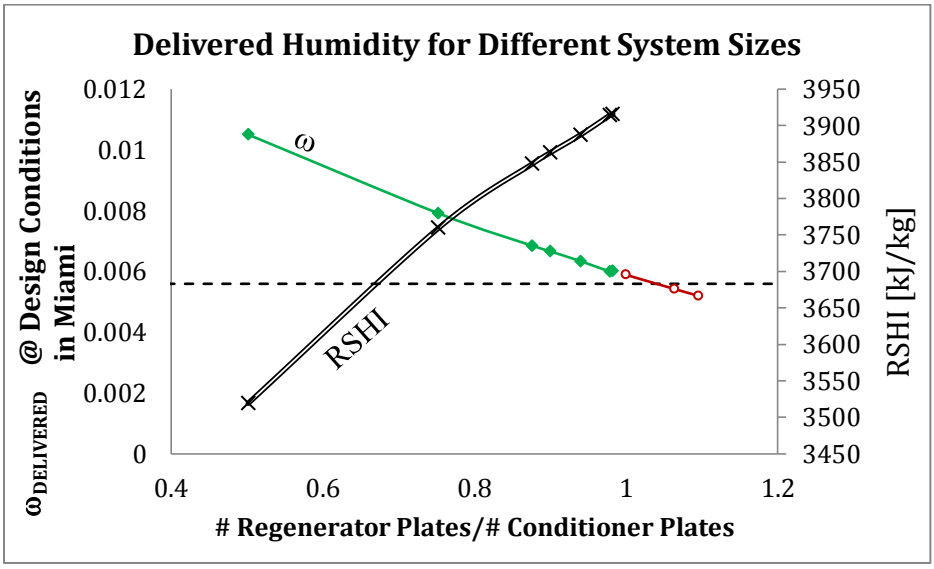

Figure G4. Relationship between relative regenerator size, regenerator-specific heat input (RSHI) and delivered humidity ratio at design conditions in Miami

3.2 Desiccant and Water Tank Sizing

With the regenerator and conditioner sized, the amount of desiccant and heating water in the system can be optimized. The primary concerns in this exercise are preventing excessive cycling of the regenerator or boiler, preventing crystallization of the desiccant system and delivering desired humidity levels. At the same time, overall system size should be minimized to allow for a smaller packaged unit and market acceptance. A control strategy is implemented in this section which maintains humidity

levels at desired points, described later in more detail in Se. March through June in Miami were analyzed to capture the performance under a variety of operating conditions. All outlet humidities calculated fell within the desired output band, described in Section 4.1. Figure G5 shows the relationship between minimum cycling time and the amount of desiccant in the system. The effect of desiccant amount was analyzed with a 32 gallon hot water tank. If a maximum of 2 cycles per hour is desired, a system with 125 gallons of desiccant would be chosen. The X's show the effect of varying the water tank size with 125 gallons of desiccant in the system.

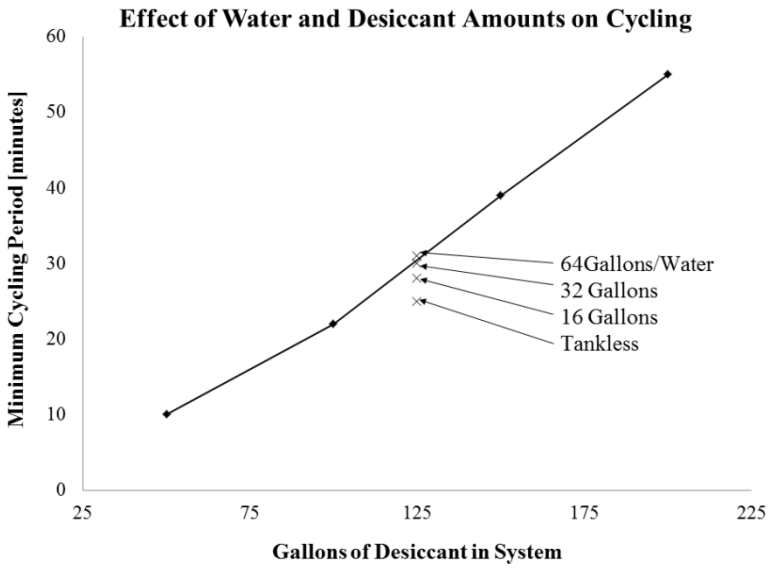

Figure G5. Graph showing relationship between amount of desiccant and water in the system and minimum cycling time observed

It can be seen that the amount of desiccant in the system greatly affects the operation of the system, while the water tank size does not. Changing the amount of water in the system was shown to only change the period of the fluctuation in the water temperature and only change the temperature itself by less than 4^0F. Water was maintained between 174^0F and 182^0F in all cases. Similarly, desiccant concentrations in

the tank also changed little for all cases analyzed, with concentrations supplied to the conditioner between 0.38kg/kg and 0.40 kg/kg in all cases. Changes in total regeneration energy for the period were less than 1% as the same amount of water was removed and the RSHI is dictated by the regenerator design. If a small system were desired, one would chose the least amount of desiccant which gave an acceptable cycling period, and then implement a tankless water heater.

Conclusions

Many improvements and optimizations to the low flow liquid desiccant system have been suggested. It is clear that simpler methods for correlating system variables to performance, such as the NTU-effectiveness method, are not sufficient for a three fluid system with unique constraints. Methods were put forward to improve and optimize such as a system and it was shown that some a few of the larger components of the system, the cooling tower and any hot water storage device, could be eliminated if desired. Sizing of system components was shown to require considerations of several interactions between systems. With the improvements suggested herein, the LFLD system may move closer to a state in which large market acceptance is possible.

References

Abdel-Salam, A., Ge, G., & Simonson, C. (2013). Performance analysis of a membrane liquid desiccant air-conditioning system. *Energy and Buildings*, 559-569.

Ahmed, C., Gandhidasan, P., & Al-Farayedhi, A. A. (1997). Simulation of a hybrid liquid desiccant based air-conditioning system. *Applied Thermal Engineering*, 125-134.

Bergero, S., & Chiari, A. (2010). Performance of a liquid desiccant and membrane contactor hybrid air-conditioning system. *Energy and Buildings*, 1976-1986.

Bergero, S., & Chiari, A. (2011). On the performances of a hybrid air-conditioning system in different climatic conditions. *Energy*, 5261-5273.

Ge, G., Moghaddam, D. G., Namvar, R., Simonson, C. J., & Besant, R. W. (2013). Analytical model based performance evaluation. sizing and coupling flow

optimization of liquid desiccant run-around membrane energy exchanger systems. *Energy and Buildings*, 248-257.

Katejanekarn, T., & Kumar, S. (2008). Performance of a solar-regenerated liquid desiccant ventilation pre-conditioning system. *Energy and Buildings*, 1252-1267.

Kinsara, A., Al-Rabghi, O. M., & Elsayed, M. M. (1997). Parametric study of an energy efficient air conditioning system using liquid desiccant. *Applied Thermal Engineering*, 327-335.

Liu, X., Chang, J., & Jiang, Y. (2009). Performance analysis on the internally cooled dehumidifier using liquid desiccant. *Building and Environment*, 299-308.

Liu, X., Jiang, Y., & Qu, K. (2007). Heat and mass transfer model of cross flow liquid desiccant air dehumidifier/regenerator. *Energy Conversion and Management*.

Lowenstein, A. (2008). Review of liquid desiccant technology for HVAC Applications. *HVAC&R Research*, 819-839.

Rahamah, A., Elsayed, M., & Al-Najem, N. (1998). A numerical solution for cooling and dehumidification of air by a falling desiccant film in parallel flow. *Renewable Energy* , 305-322.

Rattner, A. S., Nagavarapu, A. K., Garimella, S., & Fuller, T. (2011). Modeling of a plate membrane-distillation system for liquid desiccant regeneration in air-conditioning applications. *International Journal of Refrigeration*, 3650-3660.

Saman, W., & Alizadeh, S. (2001). Modeling and performance analysis of a cross-flow type plate heat exchanger for dehumidification/cooling. *Solar Energy*, 361-372.

Tu, M., Ren, C.-Q., Long-Ai, Z., & Shao, J.-W. (2009). Simulation and analysis of a novel liquid desiccant air-conditioning system. *Applied Thermal Engineering*, 2417-2425.

Wang, L., Li, N., & Zhao, B. (2010). Exergy performance and thermodynamic properties of the ideal liquid desiccant dehumidification system. *Energy and Buildings*, 2437-2444.

Yin, Y., Zhang, X., Peng, D., & Li, X. (2009). Model validation and case study on internally cooled/heated dehumidifier/regenerator of liquid desiccant systems. *International Journal of Thermal Sciences*, 1664-1671.

Yin, Y., Zhang, X., Wang, G., & Luo, L. (2008). Experimental study on a new internally cooled/heated dehumidifier/regenerator of liquid desiccant systems. *International Journal of Refrigeration*, 857-866.

Zhang, L., Liu, X.-H., & Jiang, Y. (2012). Ideal efficiency analysis and comparison of condensing and liquid desiccant dehumidification. *Energy and Buildings*, 575-583.

References

Abdalla, K., & Ahmed, A. (2011). Experimental investigation of moisture removal rate and dehumidification effectiveness of an internally cooled liquid desiccant air dehumidifier. *University of Khartoum Engineering Journal*, 25-31.

Abdel-Salam, A., Ge, G., & Simonson, C. (2013). Performance analysis of a membrane liquid desiccant air-conditioning system. *Energy and Buildings*, 559-569.

Abdulhadi, R., & Pederson, C. (1971). The behavior of a downward-directed heated wall jet. *ASHRAE Transactions*, 222-229.

Ahmed, C., Gandhidasan, P., & Al-Farayedhi, A. A. (1997). Simulation of a hybrid liquid desiccant based air-conditioning system. *Applied Thermal Engineering*, 125-134.

Alamdari, F., Hammond, G., & Melo, C. (1984). Appropriate calculation methods for convective heat transfer from building surfaces. *Proceedings of the 1st U.K. National Conference on Heat Transfer*, 1201-1211.

Alamdari, F., Hammond, G., & Melo, C. (1984). Appropriate calculation methods for convective heat transfer from building surfaces. *Proc. 1st U.K.: National Conference on Heat Transfer*(2), 1201-1211.

Andrusiak, M., Harrison, S., & Mesquita, L. (2010). Modeling of a solar thermally-driven liquid-desiccant air conditioning system. *Solar 2010 Conference Proceedingsa*.

ASHRAE. (2000). *Engineering Analysis of Experimental Data. Guideline-2.* Atlanta: ASHRAE.

ASHRAE. (2004). *Energy Standard for Buildings Except Low-Rise Residential Buildings-ANSI/ASHRAE/IESNA Standard 90.1-2004.* Atlanta, GA: American Society of Heating Refrigeration and Air-Conditioning Engineers.

ASHRAE. (2007). *Ventilation for Acceptable Indoor Air Quality- ANSI/ASHRAE Standard 62.1-2007.* Atlanta, GA: American Society of Heating, REfrigeration and Air-Conditioning Engineers.

Avedissian, T., & Naylor, D. (2008). Free convective heat transfer in an enclosure with and internal louvered blind. *International Journal of Heat and Mass Transfer*, 283-293.

Awbi, H. B. (1998). Calculation of convective heat transfer coefficients of room surfaces for natural convection. *Energy and Buildings*, 219-227.

Awbi, H., & Hatton, A. (1999). Natural convection from heated room surfaces. *Energy and Buildings*, 233-244.

Awbi, H., & Hatton, A. (2000). Mixed convection from heated room surfaces. *Energy and Buildings*, 153-166.

Bahman, A., Rosario, L., & Rahman, M. (2012). Analysis of energy savings in a supermarket refrigeration/HVAC system. *Applied Energy*, 11-21.

Beausoleil-Morrison, I. (2001). An algorithm for calculating convection coefficients for internal building surfaces for the case of mixed flow in rooms. *Energy and Buildings*(33), 351-361.

Beausoleil-Morrison, I., & Strachan, P. (2001). On the significance of modeling internal convection in dynamic whole-building simulation programs. *ASHRAE Transactions*, 929-939.

Bejan, A. (2004). *Convection Heat Transfer.* Hoboken, NJ: John Wiley and Sons.

Bergero, S., & Chiari, A. (2010). Performance of a liquid desiccant and membrane contactor hybrid air-conditioning system. *Energy and Buildings*, 1976-1986.

Bergero, S., & Chiari, A. (2011). On the performances of a hybrid air-conditioning system in different climatic conditions. *Energy*, 5261-5273.

Bird, B. R., Stewart, W. E., & Lightfoot, E. N. (2007). *Transport Phenomena.* New York: John Wiley and Sons.

Burns, P., Mitchell, J., & Beckman, W. (1985). Hybrid desiccant cooling systems in supermarket applications. *ASHRAE Transactions*, 457-468.

Cano-Ruiz, e. (1993). Removal of reactive gases at indoor surfaces combining mass transport and surface kinetics. *Atmospheric Environment*, 2039-2050.

Cao, G., Kurnitski, J., Ruponen, M., & Seppanen, O. (2009). Experimental investigation and modeling of the attached plane jet velocity development characteristics in the transition process in a room. *HVAC&R Research, 15*(3), 489-508.

Cao, G., Kurnitski, J., Ruponen, M., Mustakallio, P., & Seppanen, O. (2009). Plane-air-jet corner zone modelling in a room ventilated by an active chilled beam. *International Journal of Ventilation, 7*(4), 287-298.

Capozzoli, A., Mazzei, P., Minichiello, F., & Palma, D. (2006). Hybrid HVAC systems with chemical dehumidification for supermarket applications. *Applied Thermal Engineering*, 795-805.

Chung, T., Ghosh, T., Hines, A., & Novosel, D. (1993). Removal of selected pollutants from air during dehumidification by lithium chloride and triethylene glycol solutions. *Proceedings of the 1993 Winter Meeting of ASHRAE* , 834-841.

Churchill, S., & Chu, H. (1975). Correlating equations for laminar and turbulent free convection from a vertical plate. *International Journal of Heat and Mass Transfer, 18*, 1323-1329.

Churchill, S., & Usagi, R. (1972). A general expression for the correlation of rates of transfer and other phenomena. *AIChE Journal, 18*(6), 1121-1128.

Clark, J., & Novoselac, A. (n.d.). Experimental study of convective heat transfer from windows with Venetian blinds. *Building and Environment*.

Collins. (2004). Convective heat transfer coefficients from an internal window surface and adjacent sunlit Venetian blind. *Energy and Buildings, 36*(3).

Collins, M., Harrison, S., Naylor, D., & Oosthuizen, P. H. (2002). Heat transfer from an isothermal vertical surface with adjacent heated horizontal louvers: numerical analysis. *Journal of Heat Transfer, 124*(6), 1072-1077.

Collins, M., Tasnim, S., & Wright, J. (2008). Determination of convective heat transfer for fenestration with between-the-glass louvered shades. *International Journal of Heat and Mass Transfer, 51*(11-12), 2742-2751 .

Colomina, M. (1982). Vapour pressures and enthalpies of sublimation of naphthalene and benzoic acid. *The Journal of Chemical Thermodynamics*, 779-784.

Conde, M. (2009). *Aqueous solutions of lithium and calcium chlorides: Property formulations for use in air conditioning equipment design.* Retrieved from Conde Engineering: http://www.mrc-eng.com/Downloads/Aqueous%20LiCl&CaCl2%20Solution%20Props.pdf

Dai, Y., Wang, R., Zhang, H., & Yu, J. (2001). Use of liquid desiccant cooling to improve the performance of vapor compression air conditioning. *Applied Thermal Engineering*, 1185-1202.

Dalal, R., Naylor, D., & Roeleveld, D. (2009). A CFD study of convection in a double glazed window with an enclosed pleated blind. *Energy and Buildings, 41*(11), 1256-1262.

Deru, M., Field, K., Studer, D., Benne, K., Griffith, B., & Torcellini, P. (2011). *U.S, Department of Energy Commercial Reference Building Models of the National Building Stock.* NREL/TP-5500-46861.

Diaz, G. (2010). Numerical investigation of transient heat and mass transfer in a parallel-flow liquid-desiccant absorber. *Heat Mass Transfer*, 1335-1344.

EIA. (2013, August). *Average Price of Natural Gas Sold to Commercial Consumers, by State, 2010-2012.* Retrieved from http://www.eia.gov/naturalgas/monthly/pdf/table_21.pdf

EIA. (2013, August). *Average Retail Price of Electricity to Ultimate Consumers.* Retrieved from Electric Power Monthly: http://www.eia.gov/electricity/monthly/epm_table_grapher.cfm?t=epmt_5_03

Faramarzi, R., Sarhadian, R., & Sweetser, R. (2000). *Assessment of indoor relative humidity variations on the energy use and thermal performance of supermarkets' refrigerated display cases.*

Farmarzi, R., Sweetser, R., & Henninger, R. (2000). *Investigation of relative humidity impacts on the performance and energy use of refrigerated display cases.* Gas Research Institute GRI-00/0084.

Fisher, D., & Pederson, C. (1997). Convective heat transfer in building energy and thermal load calculations. *ASHRAE Transactions, 103*(2), 137-148.

Gandhidasan, P., Al-Farayedhi, A., & Antar, M. (2002). Investigation of heat and mass transfer in a gauze-type structured packaging. *International Journal of Energy Research*, 1035-1044.

Ganzevles, F., & Gled, C. (1997). The shape factor of conduction in a multiple channel slab and the effect of non-uniform temperatures. *International Journal of Heat and Mass Transfer*, 2493-2498.

Ge, G., Moghaddam, D. G., Namvar, R., Simonson, C. J., & Besant, R. W. (2013). Analytical model based performance evaluation. sizing and coupling flow optimization of liquid desiccant run-around membrane energy exchanger systems. *Energy and Buildings*, 248-257.

Ge, G., Xiao, F., & Niu, X. (2011). Control strategies for a liquid desiccant air-conditioning system. *Energy and Buildings*, 1499-1507.

Ge, G., Xiao, F., & Xu, X. (2011). Model-based optimal control of a dedicated outdoor air-chilled ceiling system using liquid desiccant and membrane-based total heat recovery. *Applied Energy*, 4180-4190.

Gill, A. E. (1966). The boundary layer regime for convection in a rectangular cavity. *Journal of Fluid Mechanics, 23*, 515-536.

Goldman, D., & Jaluria, Y. (1986). Effect of buoyancy on the flow in free and wall jets. *Journal of Fluid Mechanics, 166*, 41-56.

Goldstein, K., & Novoselac, A. (2010). Convective Heat Transfer in Rooms with Ceiling Slot Diffusers. *HVAC&R Research*, 629-655.

Grossman, G. (1982). Simultaneous heat and mass transfer in film absorption under laminar flow. *International Journal of Heat and Mass Transfer*, 357-371.

He, S., Xu, Z., & Jackson, J. (2002). An experimental investigation of buoyancy-opposed wall jet flow. *International Journal of Heat and Fluid Flow, 23*, 487-496.

Henderson, H., & Khattar, M. (1999). Measured Impacts of Supermarket Humidity Level on Defrost Performance and Refrigerating System Energy Use. *ASHRAE Transactions*.

Howell, R., & Adams, P. (1991). *Effects of indoor space conditions on refrigerated display case performance, Final Report, ASHRAE 596-RP.* Atlanta: AASHRAE.

Jain, S., Dhar, P., & Kaushik, S. (2000). Experimental studies on the dehumidifier and regenerator of a liquid desiccant cooling system. *Applied Thermal Engineering*, 253-267.

Kapoor, K., & Jaluria, Y. (1988). Heat transfer from a negatively buoyant wall jet. *International Journal of Heat and Mass Transfer*, 697-709.

Kapoor, K., & Jaluria, Y. (1993). Penetrative convection of a plane turbulent wall jet in a two-layer thermally stable environment: a problem in enclosure fires. *International Journal of Heat and Mass Transfer, 36*(1), 155-167.

Katejanekarn, T., & Kumar, S. (2008). Performance of a solar-regenerated liquid desiccant ventilation pre-conditioning system. *Energy and Buildings*, 1252-1267.

Kessling, W., Laevemann, E., & Peltzer, M. (1998). Energy storage in open cycle liquid desiccant cooling systems. *International Journal of Refrigeration*, 150-156.

Keumnam, C. e. (1992). Measurement of the diffusion coefficient of naphthalene into air. *International Journal of Heat and Mass transfer*, 957-966.

Khalifa, A. (1989). *Heat transfer processes in buildings.* Cardiff, U.K.: University of Wales College of Cardiff.

Khan, A. (1998). Cooling and dehumidification performance analysis of internally-cooled liquid desiccant absorbers. *Applied Thermal Engineering*, 265-281.

Khattar, M., & Henderson, H. (1999). Impact of HVAC Control Improvements on Supermarket Humidity Levels. *ASHRAE Transactions*.

Kim, M.-H., Park, J.-S., & Jeong, J.-W. (2013). Energy savings potential of liquid desiccant in evaporative-cooling-assistend 100% outdoor air system. *Energy*, 726-736.

Kinsara, A., Al-Rabghi, O. M., & Elsayed, M. M. (1997). Parametric study of an energy efficient air conditioning system using liquid desiccant. *Applied Thermal Engineering*, 327-335.

Kinsara, A., Elsayed, M., & Al-Rabghi, O. M. (1996). Proposed energy-efficient air-conditioning system using liquid desiccant. *Applied Thermal Engineering*, 791-806.

Kosar, D., & Dumitrescu, O. (2005). Hunidity Effects on Supermarket Refrigerated Case Energy Performance: A Database Review. *ASHRAE Transactions*, 1051-1061.

Kozubal, E., Herrmann, L., Deru, M., Lowenstein, A., & Clark, J. (Under Review). *Liquid Desiccant Air-Conditioning: Demonstrated Performance and Cost Implications.*

Kozubal, E., Woods, J., Burch, J., Boranian, A., & Merrigan, T. (2011). *Desiccant-Enhanced Evaporative Air-Conditioning.* Golden, CO: NREL.

Lazzarin, R., & Castellotti, F. (2007). A new heat pump desiccant dehumidifier for supermarket applicaiton. *Energy and Buildings*, 59-65.

Liu, X., Chang, J., & Jiang, Y. (2009). Performance analysis on the internally cooled dehumidifier using liquid desiccant. *Building and Environment*, 299-308.

Liu, X., Jiang, Y., & Qu, K. (2007). Heat and mass transfer model of cross flow liquid desiccant air dehumidifier/regenerator. *Energy Conversion and Management*.

Lomas, K. J. (1996). The U.K. applicability study: an evaluation of thermal simulation programs for solar passive house design. *Building and Environment, 31*(3), 197-206.

Lowenstein, A. (2004). *Patent No. 6,745,826 B2.* U.S.

Lowenstein, A. (2008). Review of liquid desiccant technology for HVAC Applications. *HVAC&R Research*, 819-839.

Lowenstein, A., Slayzak, S., & Kozubal, E. (2006). A zero carryover liquid desiccant air conditioner for solar applications. *Proceedings of ASME International Solar Energy Conference*.

Lund, K., & Knowles, T. (2001). Enhanced laminar-flow heat transfer at fiber-flocked surfaces. *International Journal of Heat and Mass Transfer*, 1627-1636.

Machin, A., Harrison, S., Naylor, D., & Oosthuizen, P. (1998). Experimental Study of Free Convection at an Indoor Glazing Surface with a Venetian Blind. *HVAC&R Research, 4*(2), 153-166.

Mahmoud, K. G., & Ball, H. D. (1992). Liquid-desiccant systems simulation. *International Journal of Refrigeration*, 74-80.

Mendes, P. (1991). The naphthalene sublimation technique. *Experimental Thermal and Fluid Science*, 510-523.

Mesquita, L., Harrison, S., & Thomey, D. (2006). Modeling of heat and mass transfer in parallel plate liquid-desiccant dehumidifiers. *Solar Energy*, 1475-1482.

Miller, D., & Comings, E. (1960). Force momentum fields in a dual-jet flow. *Journal of Fluid Mechanics, 7*(2), 237.

Morrison, G. (2003). Rapid measurements of indoor mass transfer coefficients. *Atmospheric Environment*, 5611-5619.

Morrison, G., & Wiseman, D. (2006). Temporal considerations in the measurements of indoor mass transfer coefficients. *Atmospheric Environment*, 3389-3395.

Munters. (2005). *Supermarket Air Conditioning.* Retrieved from http://www.munters.us/upload/External%20website/Commercial%20Products%20rev%2001/Supermarket%20Air%20Conditioning.pdf

Nasr, A., & Lai, C. (1998). A turbulent plane offset jet with small offset ratio. *Experiments in Fluids*(24), 47-57.

Nazaroff, W., Gadgil, A., & Weschler, C. (1993). Critique of the use of deposition velocity in modeling indoor air quality. In *Modeling of Indoor Air Quality and Exposure* (pp. 81-104). Philadelphia: ASTM.

Nozaki, T. (1983). Reattachment flow issuing from a finite width nozzle. *Bulletin of the JSME, 26*(221), 1884-1890.

Park, M., Howell, J., Vliet, G. C., & Peterson, J. (1994). Numerical and experimental results for coupled heat and mass transfer between a desiccant film and air in cross-flow. *International Journal of Heat and MAss Transfer*, 395-402.

Peng, C., & Howell, J. (1981). Analysis and design of efficient absorbers for low-temperature desiccant air conditioners. *Journal of Solar Energy Engineering*, 67-74.

Peng, S., & Pan, Z. (2009). Heat and mass transfer in liquid desiccant air-conditioning process at low flow conditions. *Communications in Nonlinear Science and Numerical Simulation*, 3599-3607.

Pietruschka, D., Eicker, U., Huber, M., & Schumacher, J. (2006). Experimental performance analysis and modelling of liquid desiccant cooling systems for air conditioning in residential buildings. *International Journal of Refrigeration*, 110-124.

Qi, R., Lu, L., & Yang, H. (2013). Development of simplified prediction model for internally cooled/heated liquid desiccant dehumidification system. *Energy and Buildings*, 133-142.

Rahamah, A., Elsayed, M., & Al-Najem, N. (1998). A numerical solution for cooling and dehumidification of air by a falling desiccant film in parallel flow. *Renewable Energy* , 305-322.

Raja, K. K., Das, M. K., & Kanna, P. R. (2009). Numerical study of mixed convection in a two-dimensional laminar incompressible offset jet flow. *International Journal of Heat and Mass Transfer*(52), 1023-1035.

Rajaratnam, N. (1976). *Turbulent Jets.* Amsterdam: Elsevier.

Rattner, A. S., Nagavarapu, A. K., Garimella, S., & Fuller, T. (2011). Modeling of a plate membrane-distillation system for liquid desiccant regeneration in air-conditioning applications. *International Journal of Refrigeration*, 3650-3660.

Ren, C. Q., Tu, M., & Wang, H. (2007). An analytical model for heat and mass transfer processes in internally cooled or heated liquid desiccant air contact units. *International Journal of Heat and Mass Transfer*, 3545-3555.

Saman, W., & Alizadeh, S. (2001). Modeling and performance analysis of a cross-flow type plate heat exchanger for dehumidification/cooling. *Solar Energy*, 361-372.

Scalabrin, G., & Scaltriti, G. (1988). Modeling and experimental analysis of an efficient absorber for air dehumidification. *Heat and Mass Transfer*, 111-124.

Shahid, & Naylor. (2005). Energy performance assessment of a window with a horizontal Venetian blind. *37*(8).

Siegel, R., & Howell, J. (2002). *Thermal Radiation Heat Transfer.* New York: Taylor and Francis.

Smith, T., & Duck, P. (1977). Seperation of jets or thermal boundary layers from a wall. *Quarterly Journal of Mechanics and Applied Mathematics*, 143-156.

Song, H. B., Soon, H. Y., & Lee, D. H. (2000). Flow and heat transfer characteristics of a two-dimensional oblique wall attaching offset jet. *International Journal of Heat and Mass Transfer*(43), 2395-2404.

Sparks, L. (1991). Exposure version 2, a computer model for analyzing the effects of indoor air pollutant sources on individual exposure. *EPA-600/8/91/013*.

Spitler, J., Pederson, C., & Fisher, D. (1991). Interior convective heat transfer in buildings with large ventilative flow rates. *AHSRAE Transactions, 97*(1), 505-515.

Spyrou, M., Shanks, K., Cook, M., Pitcher, J., & Lee, R. (2013). An empirical study of electricity and gas demand drivers in large food retail buildings of a national organisation. *Energy and Buildings*.

Tassou, S., Ge, Y., Hadawey, A., & Marriott, D. (2011). Energy consumption and conservation in food retailing. *Applied Thermal Engineering*, 147-156.

Tiller, M. (2001). *Introduction to physical modeling with modelica.* Norwell, MA: Kluwer Academic Publishers.

Tu, M., Ren, C.-Q., Long-Ai, Z., & Shao, J.-W. (2009). Simulation and analysis of a novel liquid desiccant air-conditioning system. *Applied Thermal Engineering*, 2417-2425.

U.S. Department of Energy. (2012). *2011 Buildings Energy Data Book.* Washington, D.C.: U.S. Department of Energy.

Wang, L., Li, N., & Zhao, B. (2010). Exergy performance and thermodynamic properties of the ideal liquid desiccant dehumidification system. *Energy and Buildings*, 2437-2444.

Wang, X., Cai, W., Lu, J., Sun, Y., & Ding, X. (2013). A hybrid dehumidifier model for real-time performance monitoring, control and optimization in liquid desiccant dehumidification system. *Applied Energy*, 449-455.

Waters, J. (1980). The experimental verification of a computerised thermal model for buildings. *Building Services Engineering Research and Technology, 1*(2), 76-82.

Wilcox, S., & Marion, W. (2008, May). *Users Manual for TMY3 Data Sets NREL/TP-581-43156.* Golden, CO: National Renewable Energy Laboratory. Retrieved from National renewable Energy Laboratory.

Woods, J., & Kozubal, E. (2013). A desiccant-enhanced evaporative air conditioner: Numerical model and experiments. *Energy Conversion and Management*, 208-220.

Wright, J. L., Collins, M. R., Kotey, N. A., & Barnaby, C. S. (2009). *Improving cooling load calculations for fenestration with shading devices.* Atlanta, GA: ASHRAE.

Xiao, F., Ge, G., & Niu, X. (2011). Control performance of a dedicated outdoor air system adopting liquid desiccant dehumidification. *Applied Energy*, 143-149.

Yamaguchi, S., Jeong, J., Saito, K., Miyauchi, H., & Harada, M. (2011). Hybrid liquid desiccant air-conditioning system: Experiments and simulations. *Applied Thermal Engineering*, 3741-3747.

Yao, e. (2008). Evaluating fabric fuzziness using laser range sensing. *Optical Engineering*, 47.

Yin, Y., Zhang, X., Peng, D., & Li, X. (2009). Model validation and case study on internally cooled/heated dehumidifier/regenerator of liquid desiccant systems. *International Journal of Thermal Sciences*, 1664-1671.

Yin, Y., Zhang, X., Wang, G., & Luo, L. (2008). Experimental study on a new internally cooled/heated dehumidifier/regenerator of liquid desiccant systems. *International Journal of Refrigeration*, 857-866.

Zhang, L., Liu, X.-H., & Jiang, Y. (2012). Ideal efficiency analysis and comparison of condensing and liquid desiccant dehumidification. *Energy and Buildings*, 575-583.

Zhang, T., Liu, X., Jiang, J., Chang, X., & Jiang, Y. (2013). Experimental analysis of an internally-cooled liquid desiccant dehumidifier. *Building and Environment*, 1-10.

Vita

Jordan Clark began his life a few miles outside a village of 1200 souls in the foothills of the Appalachian Mountains, on the banks of the mighty Muskingum River. Here he was nurtured by an extremely patient mother and spurred along by a boisterous father. He graduated high school at the turn of the century, then headed East. There he received a thorough education in the ways of the world, along with a B.Eng. in Civil Engineering, and a B.A. in Philosophy. After a brief stint below the Mason-Dixon Line, he found his home in Rocky Mountains, where he now resides with his beautiful, talented, and long-suffering wife, and his trusty, fluffy sidekick, Fozzie. He considers it a great privilege to have studied at the University of Texas at Austin and hopes to use the knowledge he acquired there to fight the good fight with tooth and nail until he can fight no more.

Permanent email address: jdclark34@gmail.com

This thesis was typed by Jordan Douglas Clark.